

**DI(HYDROPEROXY)ALKANE ADDUCTS OF PHOSPHINE OXIDES:
SAFE, SOLID, STOICHIOMETRIC AND SOLUBLE OXIDIZING AGENTS**

A Dissertation

by

SHIN HYE AHN

Submitted to the Office of Graduate and Professional Studies of
Texas A&M University
in partial fulfillment of the requirements for the degree of

DOCTOR OF PHILOSOPHY

| | |
|---------------------|----------------|
| Chair of Committee, | Janet Bluemel |
| Committee Members, | Simon North |
| | Kim Dunbar |
| | Hae-Kwon Jeong |
| Head of Department, | Simon North |

December 2017

Major Subject: Chemistry

Copyright 2017 Shin Hye Ahn

ABSTRACT

Despite its importance and wide use as oxidizing agent, aqueous H_2O_2 has disadvantages. It easily decomposes, and when the substrates are not water-soluble, biphasic reaction mixtures are required. Thus, oxidizing agents that are anhydrous and soluble in organic solvents are desired. To this purpose, several H_2O_2 adducts of phosphine oxides, for example $[\text{tBu}_3\text{PO}\cdot\text{H}_2\text{O}_2]_2$ and $[\text{Ph}_3\text{PO}\cdot\text{H}_2\text{O}_2]_2\cdot\text{H}_2\text{O}_2$, have been synthesized and characterized. These adducts represent an extension to the adducts previously reported by the Bluemel group, and display comparable physical properties.

Furthermore, di(hydroperoxy)alkane adducts, $\text{R}_3\text{PO}\cdot(\text{HOO})_2\text{CR}'\text{R}''$ ($\text{R}, \text{R}', \text{R}'' =$ alkyl, aryl), were synthesized and fully characterized. These adducts can be constructed using a wide variety of alkanes and phosphine oxides. All di(hydroperoxy)alkane adducts are structurally well defined as proven by single crystal X-ray analysis, and they contain two active oxygen atoms per assembly.

These adducts of the type $\text{R}_3\text{PO}\cdot(\text{HOO})_2\text{CR}'\text{R}''$ are highly soluble in organic solvents, allowing for oxidation reactions to occur in one phase. Moreover, there are many beneficial features to be harvested from their well-defined molecular structure and relatively anhydrous character. For example, selective and fast oxidation of dialkylsulfides to corresponding sulfoxides can be accomplished, without overoxidation to sulfones, because the solid oxidizing agents can easily be administered stoichiometrically. The adducts can also successfully oxidize substrates sensitive to hydrolysis, such as $\text{Ph}_2\text{P}-\text{PPh}_2$, without cleaving the P-P bond.

The $R_3PO \cdot (HOO)_2CR'R''$ adducts are robust and practically no decomposition is found after storing the solids for 100 days at 4 °C. At room temperature, the adducts slowly decompose over time, via the release of oxygen gas. When exposed to higher temperatures or mechanical stress such as hammering or grinding, no sudden release of energy and/or oxygen was observed, attesting to the stability of the adducts. In the presence of catalytic amounts of acid, adducts with di(hydroperoxy)*cycloalkane* moieties decompose by undergoing a Baeyer-Villiger oxidation, and the di(hydroperoxy)cycloalkanes are transformed into the corresponding lactones.

The $R_3PO \cdot (HOO)_2CR'R''$ adducts are stable, solid, stoichiometric and soluble materials, and can serve as an excellent complement to aqueous H_2O_2 as oxidizing agents.

ACKNOWLEDGEMENTS

First and foremost, thank you Dr. Janet Bluemel for the countless hours of help and guidance throughout the past 5 years. I genuinely appreciate all of your advice, pertaining to both chemistry and life in general.

Thanks also to my committee members, Dr. Simon North, Dr. Kim Dunbar and Dr. Hae-Kwon Jeong for attending my seminars and for the helpful questions and suggestions.

I would like to sincerely thank Dr. Nattamai Bhuvanesh, for that very first X-ray crystal structure you solved for me, which gave birth to this project. And thank you for the many more excellent crystal structures that followed. Your emails were the highlight of my days in lab.

I am indebted to the Bluemel group members for their help. Thank you for listening to all my talks so many times, for giving me helpful ideas, and encouraging me during the stressful job hunt process. I would like to especially thank Joe for being such a dependable friend and colleague. Passing the multiple hurdles of PhD was much more fun, since we were going through it together.

Finally, I would like to thank my family for their support and prayers. I am especially grateful to Melody for being an awesome sister, my best friend, personal secretary, chauffeuse, chef and housekeeper. I could not possibly have done this without your help.

CONTRIBUTORS AND FUNDING SOURCES

Contributors

This work was supervised by a dissertation committee consisting of the chair, Professor Dr. Janet Bluemel, and Professors Dr. Simon North and Dr. Kim Dunbar of the Department of Chemistry, and Professor Dr. Hae-Kwon Jeong of the Department of Chemical Engineering.

All work for the dissertation was completed by the student, under the advisement of Professor Dr. Janet Bluemel of the Department of Chemistry.

Funding Sources

This work was made possible in part by the Robert A. Welch Foundation under grant number A-1706, and the National Science Foundation under grant numbers CHE-1300208 and CHE-0840464.

NOMENCLATURE

| | |
|------------------|---|
| δ | chemical shift in ppm |
| λ | wavelength |
| ^{13}C | carbon nucleus (NMR) |
| ^2H | deuterium nucleus (NMR) |
| ^1H | proton nucleus (NMR) |
| ^{31}P | phosphorus nucleus (NMR) |
| { ^1H } | proton decoupled (NMR) |
| \AA | \AA ngstrom |
| br | broad |
| Bu | butyl |
| COSY | Correlation SpectroscopY (2D NMR) |
| CP | cross-polarization |
| CP/MAS | cross-polarization/magic angle spinning |
| CSA | chemical shift anisotropy |
| Cy | cyclohexyl |
| d | doublet (NMR), days |
| D | deuterium (^2H) atom |
| DCM | dichloromethane |
| dppm | bis(diphenylphosphino)methane |
| dppe | bis(diphenylphosphino)ethane |

| | |
|------------------|--|
| dppp | bis(diphenylphosphino)propane |
| D ₂ O | deuterium oxide |
| eq | equivalents, equatorial (NMR) |
| FID | free induction decay (NMR) |
| FT | Fourier Transformation |
| h | hours |
| HSQC | heteronuclear single quantum coherence spectroscopy (2D NMR) |
| Hz | Hertz |
| <i>i</i> | ipso |
| <i>J</i> | scalar coupling constant (NMR) |
| IR | infrared |
| m | multiplet (NMR) |
| <i>m</i> | meta |
| MAS | magic angle spinning |
| Me | methyl |
| NMR | nuclear magnetic resonance |
| <i>o</i> | ortho |
| <i>p</i> | para |
| Ph | phenyl |
| ppm | parts per million |
| R | alkyl, aryl group |
| RT | room temperature |

| | |
|-------------------|-----------------------------|
| s | singlet (NMR) |
| sept | septet (NMR) |
| t | triplet (NMR) |
| <i>t</i> | tertiary |
| T | temperature, time |
| <i>tert</i> | tertiary |
| THF | tetrahydrofuran |
| $\Delta\nu_{1/2}$ | signal width at half height |
| xs | excess |

TABLE OF CONTENTS

| | Page |
|---|------|
| ABSTRACT | ii |
| ACKNOWLEDGEMENTS | iv |
| CONTRIBUTORS AND FUNDING SOURCES..... | v |
| NOMENCLATURE..... | vi |
| TABLE OF CONTENTS | ix |
| LIST OF FIGURES..... | xi |
| LIST OF SCHEMES | xix |
| LIST OF TABLES | xx |
| CHAPTER I INTRODUCTION | 1 |
| CHAPTER II HYDROGEN PEROXIDE ADDUCTS OF PHOSPHINE OXIDES | 4 |
| Introduction | 4 |
| Results and Discussions | 6 |
| Conclusion..... | 9 |
| Experimental | 10 |
| CHAPTER III SYNTHESIS OF DI(HYDROPEROXY)ALKANE ADDUCTS OF PHOSPHINE OXIDES | 12 |
| Introduction | 12 |
| Results and Discussion..... | 13 |
| Conclusion..... | 17 |
| Experimental | 17 |
| CHAPTER IV CHARACTERIZATION OF THE ADDUCTS $R_3PO \cdot (HOO)_2CR'R''$... | 28 |
| Introduction | 28 |
| Results and Discussion..... | 29 |
| Conclusion..... | 41 |

| | |
|--|-----|
| CHAPTER V SOLUBILITY STUDY | 43 |
| Introduction | 43 |
| Results and Discussion..... | 43 |
| Conclusion..... | 45 |
| CHAPTER VI SHELF LIFE AND DECOMPOSITION STUDY | 46 |
| Introduction | 46 |
| Results and Discussion..... | 53 |
| Conclusion..... | 60 |
| Experimental | 61 |
| CHAPTER VII APPLICATIONS IN OXIDATION REACTIONS..... | 62 |
| Introduction | 62 |
| Results and Discussion..... | 65 |
| Conclusion..... | 75 |
| Experimental | 76 |
| CHAPTER VIII MISCELLANEOUS RESULTS | 82 |
| Introduction | 82 |
| Results and Discussion..... | 83 |
| Conclusion..... | 88 |
| Experimental | 88 |
| CHAPTER IX SUMMARY | 91 |
| REFERENCES | 95 |
| APPENDIX A NMR SPECTRA..... | 103 |
| APPENDIX B FT-IR SPECTRA | 164 |
| APPENDIX C DECOMPOSITION DATA..... | 175 |

LIST OF FIGURES

| | Page |
|--|------|
| Figure 2.1. Single crystal X-ray structure of $[\text{Cy}_3\text{PO}\cdot\text{H}_2\text{O}_2]_2$. ⁶ | 4 |
| Figure 2.2. Single crystal X-ray structure of $(\text{Ph}_3\text{PO})_2\cdot\text{H}_2\text{O}_2$. ¹⁹ | 5 |
| Figure 2.3. Single crystal X-ray structures of 1 (left) ^{18,20} and 2 (right). ^{18,22} | 7 |
| Figure 2.4. ¹ H NMR spectrum of 3 (top) and ² H NMR spectrum of partially deuterated 3 (bottom). | 8 |
| Figure 2.5. Solubilities of 2 and 3 in representative solvents | 9 |
| Figure 4.1. Large single crystals of (a) 4 , (b) 9 , (c) 10 , and (d) 11 | 29 |
| Figure 4.2. Single crystal X-ray structures of adducts 4-15 . ²⁸⁻⁴⁰ | 30 |
| Figure 4.3. X-ray structure of 13 with corresponding bond distances. | 32 |
| Figure 4.4. ¹³ C NMR spectrum of $\text{Ph}_3\text{PO}\cdot(\text{HOO})_2\text{CMe}_2$ in CDCl_3 | 34 |
| Figure 4.5. ³¹ P CP wideline NMR spectrum of polycrystalline 4 | 36 |
| Figure 4.6. ³¹ P CP NMR spectra of a large single crystal of 4 at different random orientations with respect to the external magnetic field..... | 37 |
| Figure 4.7. ¹ H NMR spectrum of 5 in CDCl_3 , with complete signal assignment | 38 |
| Figure 4.8. Representative IR spectra of adduct 4 (top) and 5 (bottom)..... | 40 |
| Figure 5.1. Solubilities of adducts 4-11 in common organic solvents. | 44 |
| Figure 6.1. ³¹ P NMR spectrum obtained following the partial oxidation of an excess of PPh_3 with 5 | 48 |
| Figure 6.2. Capillary insert with ClPPh_2 centered inside a 5 mm NMR tube | 48 |
| Figure 6.3. Point display of the ³¹ P NMR signals obtained after the partial oxidation of PPh_3 with 5 | 50 |
| Figure 6.4. Three different positions of the 5 mm NMR tube inside the sample gauge, representing the probehead dimensions | 51 |

| | |
|---|-----|
| Figure 6.5. ^{31}P NMR spectra obtained following the oxidation of an excess of PPh_3 with 5 | 52 |
| Figure 6.6. Thermogravimetric analysis (TGA) of 5 | 54 |
| Figure 6.7. Oxidative power of 5 after being stored at the indicated conditions | 56 |
| Figure 6.8. Large crystals (left) and single crystal X-ray structure (right) of 16 . ⁵³ | 57 |
| Figure 6.9. Solubility of cyclic adducts 9-11 and “half-adduct” 16 | 59 |
| Figure 8.1. Single crystal X-ray structure of material 18 . ⁷⁴ | 84 |
| Figure 8.2. Single crystal X-ray structure of a single molecule of 19 (left) and 19 in the unit cell (right). ⁷⁶ | 86 |
| Figure 8.3. Single crystal X-ray structure of a single molecule of 20 (left) and 20 in the unit cell (right). ⁷⁷ | 87 |
| Figure 8.4. Potential products from reaction of acetylacetone with aq. H_2O_2 | 87 |
| Figure A.1. ^1H NMR spectrum of 1 in CDCl_3 | 103 |
| Figure A.2. $^{13}\text{C}\{^1\text{H}\}$ NMR spectrum of 1 in CDCl_3 | 103 |
| Figure A.3. $^{31}\text{P}\{^1\text{H}\}$ NMR spectrum of 1 in CDCl_3 | 104 |
| Figure A.4. ^1H NMR spectrum of 1 in acetone- d_6 | 104 |
| Figure A.5. $^{13}\text{C}\{^1\text{H}\}$ NMR spectrum of 1 in acetone- d_6 | 105 |
| Figure A.6. $^{31}\text{P}\{^1\text{H}\}$ NMR spectrum of 1 in acetone- d_6 | 105 |
| Figure A.7. ^1H NMR spectrum of 4 in CDCl_3 | 106 |
| Figure A.8. $^{13}\text{C}\{^1\text{H}\}$ NMR spectrum of 4 in CDCl_3 | 106 |
| Figure A.9. Expansion of aryl region of $^{13}\text{C}\{^1\text{H}\}$ NMR spectrum of 4 in CDCl_3 | 107 |
| Figure A.10. $^{31}\text{P}\{^1\text{H}\}$ NMR spectrum of 4 in CDCl_3 | 107 |
| Figure A.11. ^1H NMR spectrum of 4 in acetone- d_6 | 108 |
| Figure A.12. $^{13}\text{C}\{^1\text{H}\}$ NMR spectrum of 4 in acetone- d_6 | 108 |
| Figure A.13. $^{13}\text{C}\{^1\text{H}\}$ NMR spectrum of 4 in acetone- d_6 , aryl region expansion | 109 |

| | |
|--|-----|
| Figure A.14. $^{31}\text{P}\{^1\text{H}\}$ NMR spectrum of 4 in acetone- d_6 | 109 |
| Figure A.15. ^1H NMR spectrum of 5 in CDCl_3 (top), alkyl region expansion (bottom)..... | 110 |
| Figure A.16. $^{13}\text{C}\{^1\text{H}\}$ NMR spectrum of 5 in CDCl_3 | 111 |
| Figure A.17. $^{13}\text{C}\{^1\text{H}\}$ NMR spectrum of 5 in CDCl_3 , alkyl region expansion. | 111 |
| Figure A.18. ^{13}C , ^1H COSY NMR spectrum of 5 in CDCl_3 | 112 |
| Figure A.19. $^{31}\text{P}\{^1\text{H}\}$ NMR spectrum of 5 in CDCl_3 | 113 |
| Figure A.20. ^1H NMR spectrum of 5 in acetone- d_6 | 113 |
| Figure A.21. ^1H NMR spectrum of 5 in acetone- d_6 , alkyl region expansion..... | 114 |
| Figure A.22. $^{13}\text{C}\{^1\text{H}\}$ NMR spectrum of 5 in acetone- d_6 | 114 |
| Figure A.23. $^{13}\text{C}\{^1\text{H}\}$ NMR spectrum of 5 in acetone- d_6 , alkyl region expansion..... | 115 |
| Figure A.24. $^{31}\text{P}\{^1\text{H}\}$ NMR spectrum of 5 in acetone- d_6 | 115 |
| Figure A.25. ^1H NMR spectrum of 6 in CDCl_3 | 116 |
| Figure A.26. $^{13}\text{C}\{^1\text{H}\}$ NMR spectrum of 6 in CDCl_3 | 116 |
| Figure A.27. $^{31}\text{P}\{^1\text{H}\}$ NMR spectrum of 6 in CDCl_3 | 117 |
| Figure A.28. ^1H NMR spectrum of 6 in C_6D_6 | 117 |
| Figure A.29. $^{13}\text{C}\{^1\text{H}\}$ NMR spectrum of 6 in C_6D_6 | 118 |
| Figure A.30. $^{31}\text{P}\{^1\text{H}\}$ NMR spectrum of 6 in C_6D_6 | 118 |
| Figure A.31. ^1H NMR spectrum of 7 in CDCl_3 (top), alkyl region expansion (bottom)..... | 119 |
| Figure A.32. $^{13}\text{C}\{^1\text{H}\}$ NMR spectrum of 7 in CDCl_3 | 120 |
| Figure A.33. $^{13}\text{C}\{^1\text{H}\}$ NMR spectrum of 7 in CDCl_3 , alkyl region expansion..... | 120 |
| Figure A.34. $^{31}\text{P}\{^1\text{H}\}$ NMR spectrum of 7 in CDCl_3 | 121 |
| Figure A.35. ^1H NMR spectrum of 8 in CDCl_3 | 122 |
| Figure A.36. ^1H NMR spectrum of 8 in CDCl_3 , alkyl region expansion | 122 |

| | |
|--|-----|
| Figure A.37. $^{13}\text{C}\{^1\text{H}\}$ NMR spectrum of 8 in CDCl_3 . | 123 |
| Figure A.38. $^{13}\text{C}\{^1\text{H}\}$ NMR spectrum of 8 in CDCl_3 , alkyl region expansion | 123 |
| Figure A.39. $^{31}\text{P}\{^1\text{H}\}$ NMR spectrum of 8 in CDCl_3 . | 124 |
| Figure A.40. ^1H NMR spectrum of 9 in CDCl_3 | 125 |
| Figure A.41. ^1H NMR spectrum of 9 in CDCl_3 , alkyl region expansion | 125 |
| Figure A.42. $^{13}\text{C}\{^1\text{H}\}$ NMR spectrum of 9 in CDCl_3 . | 126 |
| Figure A.43. $^{13}\text{C}\{^1\text{H}\}$ NMR spectrum of 9 in CDCl_3 , alkyl region expansion | 126 |
| Figure A.44. $^{31}\text{P}\{^1\text{H}\}$ NMR spectrum of 9 in CDCl_3 . | 127 |
| Figure A.45. ^1H NMR spectrum of 10 in CDCl_3 | 128 |
| Figure A.46. ^1H NMR spectrum of 10 in CDCl_3 , alkyl region expansion | 128 |
| Figure A.47. $^{13}\text{C}\{^1\text{H}\}$ NMR spectrum of 10 in CDCl_3 | 129 |
| Figure A.48. $^{13}\text{C}\{^1\text{H}\}$ NMR spectrum of 10 in CDCl_3 , alkyl region expansion | 129 |
| Figure A.49. $^{31}\text{P}\{^1\text{H}\}$ NMR spectrum of 10 in CDCl_3 . | 130 |
| Figure A.50. ^1H NMR spectrum of 11 in CDCl_3 | 131 |
| Figure A.51. ^1H NMR spectrum of 11 in CDCl_3 , alkyl region expansion | 131 |
| Figure A.52. $^{13}\text{C}\{^1\text{H}\}$ NMR spectrum of 11 in CDCl_3 . | 132 |
| Figure A.53. $^{13}\text{C}\{^1\text{H}\}$ NMR spectrum of 11 in CDCl_3 , alkyl region expansion | 132 |
| Figure A.54. $^{31}\text{P}\{^1\text{H}\}$ NMR spectrum of 11 in CDCl_3 . | 133 |
| Figure A.55. ^1H NMR spectrum of 12 in CDCl_3 | 134 |
| Figure A.56. ^1H NMR spectrum of 12 in CDCl_3 , alkyl region expansion | 134 |
| Figure A.57. $^{13}\text{C}\{^1\text{H}\}$ NMR spectrum of 12 in CDCl_3 . | 135 |
| Figure A.58. $^{13}\text{C}\{^1\text{H}\}$ NMR spectrum of 12 in CDCl_3 , alkyl region expansion | 135 |
| Figure A.59. $^{31}\text{P}\{^1\text{H}\}$ NMR spectrum of 12 in CDCl_3 . | 136 |
| Figure A.60. ^1H NMR spectrum of 13 in CDCl_3 | 137 |

| | |
|---|-----|
| Figure A.61. ^1H NMR spectrum of 13 in CDCl_3 , aryl region expansion..... | 137 |
| Figure A.62. $^{13}\text{C}\{^1\text{H}\}$ NMR spectrum of 13 in CDCl_3 | 138 |
| Figure A.63. $^{13}\text{C}\{^1\text{H}\}$ NMR spectrum of 13 in CDCl_3 , aryl region expansion..... | 138 |
| Figure A.64. $^{31}\text{P}\{^1\text{H}\}$ NMR spectrum of 13 in CDCl_3 | 139 |
| Figure A.65. ^1H NMR spectrum of 13 in acetone- d_6 | 139 |
| Figure A.66. ^1H NMR spectrum of 13 in acetone- d_6 , aryl region expansion..... | 140 |
| Figure A.67. $^{13}\text{C}\{^1\text{H}\}$ NMR spectrum of 13 in acetone- d_6 , aryl region expansion | 140 |
| Figure A.68. $^{13}\text{C}\{^1\text{H}\}$ NMR spectrum of 13 in acetone- d_6 , aryl region expansion | 141 |
| Figure A.69 $^{31}\text{P}\{^1\text{H}\}$ NMR spectrum of 13 in acetone- d_6 , aryl region expansion..... | 141 |
| Figure A.70. ^1H NMR spectrum of 14 in CDCl_3 | 142 |
| Figure A.71. $^{13}\text{C}\{^1\text{H}\}$ NMR spectrum of 14 in CDCl_3 | 142 |
| Figure A.72. $^{13}\text{C}\{^1\text{H}\}$ NMR spectrum of 14 in CDCl_3 , aryl region expansion..... | 143 |
| Figure A.73. $^{31}\text{P}\{^1\text{H}\}$ NMR spectrum of 14 in CDCl_3 | 143 |
| Figure A.74. ^1H NMR spectrum of 15 in CDCl_3 | 144 |
| Figure A.75. ^1H NMR spectrum of 15 in CDCl_3 , aryl region expansion..... | 144 |
| Figure A.76. $^{13}\text{C}\{^1\text{H}\}$ NMR spectrum of 15 in CDCl_3 | 145 |
| Figure A.77. $^{13}\text{C}\{^1\text{H}\}$ NMR spectrum of 15 in CDCl_3 , aryl region expansion..... | 145 |
| Figure A.78. $^{31}\text{P}\{^1\text{H}\}$ NMR spectrum of 15 in CDCl_3 | 146 |
| Figure A.79. ^{13}C NMR spectrum of 4 in benzene after heating at 90 °C for 3 days. | 147 |
| Figure A.80. ^1H NMR spectrum of 16 in CDCl_3 | 148 |
| Figure A.81. ^1H NMR spectrum of 16 in CDCl_3 , alkyl region expansion | 148 |
| Figure A.82. $^{13}\text{C}\{^1\text{H}\}$ NMR spectrum of 16 in CDCl_3 | 149 |
| Figure A.83. $^{13}\text{C}\{^1\text{H}\}$ NMR spectrum of 16 in CDCl_3 , alkyl region expansion..... | 149 |
| Figure A.84. $^{31}\text{P}\{^1\text{H}\}$ NMR spectrum of 16 in CDCl_3 | 150 |

| | |
|---|-----|
| Figure A.85. ^1H NMR spectrum of 1,1,2,2-tetraphenyldiphosphine in CDCl_3 | 151 |
| Figure A.86. ^1H NMR spectrum of 1,1,2,2-tetraphenyldiphosphine in CDCl_3 , aryl region expansion | 151 |
| Figure A.87. $^{13}\text{C}\{^1\text{H}\}$ NMR spectrum of 1,1,2,2-tetraphenyldiphosphine in CDCl_3 | 152 |
| Figure A.88. $^{13}\text{C}\{^1\text{H}\}$ NMR spectrum of 1,1,2,2-tetraphenyldiphosphine in CDCl_3 , aryl region expansion | 152 |
| Figure A.89. ^{13}C , ^1H HSQC NMR spectrum of 1,1,2,2-tetraphenyldiphosphine in CDCl_3 | 153 |
| Figure A.90. ^{13}C , ^1H HMBC NMR spectrum of 1,1,2,2-tetraphenyldiphosphine in CDCl_3 | 154 |
| Figure A.91. $^{31}\text{P}\{^1\text{H}\}$ NMR spectrum of 1,1,2,2-tetraphenyldiphosphine in CDCl_3 | 155 |
| Figure A.92. Oxidation of 1,1,2,2-tetraphenyldiphosphine in air over a period of 5 days..... | 156 |
| Figure A.93. Stoichiometric oxidation of 1,1,2,2-tetraphenyldiphosphine with 5 as oxidant; starting diphosphine in C_6D_6 (bottom), product 1,1,2,2-tetraphenyldiphosphine dioxide and consumed adduct in C_6D_6 (middle), and 1,1,2,2-tetraphenyldiphosphine dioxide isolated via simple filtration and dissolved in CDCl_3 (top)..... | 157 |
| Figure A.94. ^1H NMR spectrum of 1,1,2,2-tetraphenyldiphosphine dioxide (17) in CDCl_3 | 158 |
| Figure A.95. ^1H NMR spectrum of 17 in CDCl_3 , aryl region expansion..... | 158 |
| Figure A.96. $^{13}\text{C}\{^1\text{H}\}$ NMR spectrum of 17 in CDCl_3 | 159 |
| Figure A.97. $^{13}\text{C}\{^1\text{H}\}$ NMR spectrum of 17 in CDCl_3 , aryl region expansion..... | 159 |
| Figure A.98. $^{31}\text{P}\{^1\text{H}\}$ NMR spectrum of 17 in CDCl_3 | 160 |
| Figure A.99. ^1H NMR spectrum of 18 in CDCl_3 | 161 |
| Figure A.100. ^1H NMR spectrum of 18 in CDCl_3 , alkyl region expansion..... | 161 |
| Figure A.101. ^1H NMR spectrum of 18 in CDCl_3 , aryl region expansion..... | 162 |
| Figure A.102. $^{13}\text{C}\{^1\text{H}\}$ NMR spectrum of 18 in CDCl_3 | 162 |

| | |
|---|-----|
| Figure A.103. $^{13}\text{C}\{^1\text{H}\}$ NMR spectrum of 18 in CDCl_3 , aryl region expansion..... | 163 |
| Figure A.104. $^{31}\text{P}\{^1\text{H}\}$ NMR spectrum of 18 in CDCl_3 | 163 |
| Figure B.1. IR spectra of aqueous H_2O_2 in 35 wt% (top) and 17 wt% (bottom). | 164 |
| Figure B.2. IR spectrum of 1 | 165 |
| Figure B.3. IR spectrum of 2 | 165 |
| Figure B. 4 IR spectra of 3 before (bottom) and after (top) deuteration | 166 |
| Figure B.5. IR spectrum of 4 | 167 |
| Figure B.6. IR spectrum of 5 | 167 |
| Figure B.7. IR spectrum of 6 | 168 |
| Figure B.8. IR spectrum of 7 | 168 |
| Figure B.9. IR spectrum of 8 | 169 |
| Figure B.10. IR spectrum of 9 | 169 |
| Figure B.11. IR spectrum of 10 | 170 |
| Figure B.12. IR spectrum of 1,1-di(hydroperoxy)cyclohexane | 170 |
| Figure B.13. IR spectrum of 11 | 171 |
| Figure B.14. IR spectrum of 1,1-di(hydroperoxy)heptanes. | 171 |
| Figure B.15. IR spectrum of 12 | 172 |
| Figure B.16. IR spectrum of 13 | 172 |
| Figure B.17. IR spectrum of 14 | 173 |
| Figure B.18. IR spectrum of 15 | 173 |
| Figure B.19. IR spectrum of 16 | 174 |
| Figure B.20. IR spectrum of 18 | 174 |
| Figure C.1. Oxidizing power of 3 after being stored at the indicated conditions. | 175 |
| Figure C.2. Oxidizing power of 4 after being stored at the indicated conditions. | 176 |

Figure C.3. Oxidizing power of **6** after being stored at the indicated conditions.177

LIST OF SCHEMES

| | Page |
|---|------|
| Scheme 3.1. (HOO) ₂ CR'R" adducts of phosphine oxides 4-12 and diphosphine dioxides 13-15 | 14 |
| Scheme 3.2. General synthesis routes for R ₃ PO•(HOO) ₂ CR'R" adducts (R, R', R" = alkyl, aryl) | 15 |
| Scheme 3.3. Suggested mechanism for the formation of R ₃ PO•(HOO) ₂ CMe ₂ (R, R', R" = alkyl, aryl)..... | 16 |
| Scheme 7.1. Oxidation of HD to HD-sulfoxide and HD-sulfone in the presence of excess oxidant | 63 |
| Scheme 7.2. Oxidation of 1,1,2,2-tetraphenyldiphosphine in dry air | 64 |
| Scheme 7.3. Stoichiometric oxidation of THT with R ₃ PO•(HOO) ₂ CR'R" (4-8, 12)..... | 65 |
| Scheme 7.4. Oxidation of Ph ₂ S with R ₃ PO•(HOO) ₂ CR'R" (4, 5, 7, 8)..... | 67 |
| Scheme 7.5. Oxidation of thiophene with the R ₃ PO•(HOO) ₂ CR'R" adduct 7 | 69 |
| Scheme 7.6. Epoxidation attempts with R ₃ PO•(HOO) ₂ CR'R" adducts | 70 |
| Scheme 7.7. Stoichiometric oxidation of 1,1,2,2-tetraphenyldiphosphine with Cy ₃ PO•(HOO) ₂ CMe ₂ (5) in benzene..... | 71 |
| Scheme 7.8. Formation of lactones from the cycloalkane adducts Cy ₃ PO•(HOO) ₂ C(CH ₂) _n in the presence of trace amounts of acid..... | 72 |
| Scheme 7.9. Oxidation of cyclopentanone to δ-valerolactone and di(hydroperoxy)-cyclopentane in the presence of 3 and trace amounts of acid. | 74 |
| Scheme 7.10. δ-Valerolactone (left) and ε-caprolactone (right), numbered for the purpose of NMR signal assignment. | 79 |
| Scheme 8.1. Attempted synthesis of the shown desired adduct..... | 85 |
| Scheme 8.2. Synthesis of cyclic di(hydroxy)peroxide | 86 |

LIST OF TABLES

| | Page |
|---|------|
| Table 4.1. Comparison of the P=O bond lengths of the pure phosphine oxides Ph ₃ PO, Cy ₃ PO, Ph ₂ P(O)CH ₂ P(O)Ph ₂ and Ph ₂ P(O)CH ₂ CH ₂ P(O)Ph ₂ with the adducts 4-15 | 33 |
| Table 4.2. ¹³ C NMR Chemical shifts of the quaternary carbon signals of the adducts R ₃ PO•(HOO) ₂ CR'R" in CDCl ₃ | 34 |
| Table 4.3. ³¹ P NMR chemical shifts for the adducts R ₃ PO•(HOO) ₂ CR'R" and the corresponding neat R ₃ PO in CDCl ₃ | 35 |
| Table 4.4. ¹ H chemical shifts of the peroxide protons of the adducts 4-15 | 38 |
| Table 4.5. Stretching bands ν(O-H), ν(C-O), ν(O-O) and comparison of the ν(P=O) IR values of the pure phosphine oxides with those of the adducts 4-15 , given as Δν(P=O)..... | 39 |
| Table 6.1. Comparison of experimental and theoretical yields of OPPh ₃ , expressed as %, following the oxidation of PPh ₃ with freshly synthesized 5 | 55 |
| Table 6.2. Comparison of IR and X-ray crystallographic data of Cy ₃ PO, 16 and 10 | 58 |
| Table 6.3. Comparison of ¹³ C and ³¹ P NMR chemical shifts of Cy ₃ PO, 16 and 10 | 59 |
| Table 7.1. Selective and complete oxidation of THT to tetramethylene sulfoxide..... | 66 |
| Table 7.2. Yields (%) of oxidized products Ph ₂ SO and Ph ₂ SO ₂ after reacting Ph ₂ S with selected adducts R ₃ PO•(HOO) ₂ CR'R"..... | 67 |
| Table 7.3. Yields (%) of the oxidation products Ph ₂ SO and Ph ₂ SO ₂ after reaction of Ph ₂ S with selected adducts R ₃ PO•(HOO) ₂ CR'R", with and without catalytic amounts of SiO ₂ and Br ₂ | 68 |
| Table 7.4. Product yields (%) after oxidation of thiophene with 7 | 69 |
| Table 7.5. Baeyer-Villiger oxidation of substrate ketone and (HOO) ₂ C(CH ₂) _n moieties in the presence of a drop (< 1 mg) of H ₂ SO ₄ | 73 |
| Table C.1. Decomposition temperature of adducts 4-15 | 177 |

CHAPTER I

INTRODUCTION

H_2O_2 is an immensely important reagent for oxidation reactions in organic syntheses.¹ For example, Baeyer-Villiger oxidations^{2,3} and sulfide oxidation processes,⁴ as well as epoxidation reactions,⁵ are mainly performed using H_2O_2 . Most importantly, since the rise of the new propylene oxide processes that use aqueous H_2O_2 as the oxidant, it has turned into a commodity with world capacities well above 2 million tons per year.^{1a} The reactions with H_2O_2 are very selective and efficient, with fast and quantitative reactions taking place at low temperatures. Additionally, many oxidation reactions with H_2O_2 , for example, the transformation of phosphines to their oxides,⁶ do not need any catalyst.

Aqueous H_2O_2 is an enticing oxidizing agent in industrial settings because it is cheap, available on a large scale and it can be applied in concentrations up to 85 wt%. Its major drawback, however, remains the water byproduct. Aqueous H_2O_2 solutions used in modern industrial processes are very pure and stable, with typical decomposition rates of 1% per year. On the other hand, in academic settings 30 wt% aqueous solutions are usually purchased as a compromise between potency and safety regulations. In practice, with many users, aqueous H_2O_2 decomposes at unpredictable rates, and the solutions have to be titrated⁷ prior to each application when exact stoichiometry is needed. Furthermore, in case the reagents are not soluble in water, the oxidation has to be

performed in a biphasic system, which entails a slow reaction at the phase boundary and a phase separation requirement in the workup.

Different formulations of H_2O_2 are also in use, for example, urea hydrogen peroxide (UHP) adducts.⁸ However, the UHP adducts are not stoichiometric in nature, and urea and water have to be removed after the reaction. Alternatively, alkali metal peroxocarbonates have been applied,^{9,10} but like UHP, they are caustic. Unfortunately, H_2O_2 is much less stable under basic conditions. Additionally, many oxidations performed with H_2O_2 are co-catalyzed by acids.^{1a} Besides these materials, encapsulated¹¹ and immobilized versions of hydrogen peroxide are known.^{12,13} Again, the stoichiometry of these materials is not very well defined. Furthermore, H_2O_2 adducts of metal complexes have been characterized.¹⁴ Organic and silicon-containing peroxides are important, but can be difficult to synthesize and remove from reaction mixtures.¹⁵

The ideal oxidizing agent is an easy to synthesize, solid and molecular H_2O_2 adduct of reproducible stoichiometry that is soluble in organic solvents. This thesis describes the discovery of two different peroxide containing adducts of phosphine oxides as oxidizing agents – the H_2O_2 and the di(hydroperoxy)alkane adducts of phosphine oxides. In contrast to urea hydrogen peroxide or peroxocarbonates, phosphine oxides are only moderate Lewis bases, and they could also function as ligands for Mo or W centers in oxidation reactions,¹⁶ therewith playing a dual role.

For both types of adducts, once all active peroxide is consumed during an oxidation reaction, the remaining phosphine oxide can easily be removed from the reaction mixture via reversible adsorption on solid oxide materials, such as silica or

molecular sieves.⁶ Once the phosphine oxides are retrieved from the support by washing with polar solvents,¹⁷ they can undergo the synthetic procedure to regenerate the adduct.

In the following chapters, the synthetic methods of each type of adduct are described in detail and full characterization data are provided. Furthermore, the potential of each type of adduct as stoichiometric oxidizing agent for different oxidation reactions is explored.

CHAPTER II

HYDROGEN PEROXIDE ADDUCTS OF PHOSPHINE OXIDES*

Introduction

H₂O₂ adducts of phosphine oxides, such as [Cy₃PO•H₂O₂]₂,⁶ have been described by the Blümel group as stoichiometric, well-defined molecules with high melting points that are stable over months on the shelf and can easily be crystallized.^{6,18} Previously, a single crystal X-ray structure of [Cy₃PO•H₂O₂]₂ had been obtained, where the two H₂O₂ molecules bridge the two phosphine oxides to form a chair-like structure (Figure 2.1).⁶ This well-defined molecular structure of [Cy₃PO•H₂O₂]₂ allows for exact stoichiometric determination of peroxy groups and active oxygen atoms.

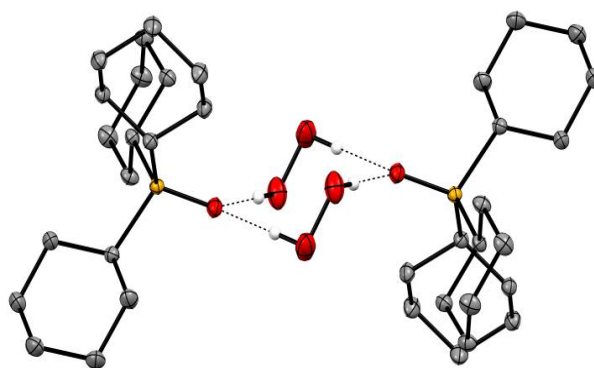


Figure 2.1. Single crystal X-ray structure of [Cy₃PO•H₂O₂]₂.⁶

* Reproduced with permission from “Hydrogen Peroxide and Di(hydroperoxy)propane Adducts of Phosphine Oxides as Stoichiometric and Soluble Oxidizing Agents” Ahn, S. H.; Cluff, K. J.; Bhuvanesh, N.; Blümel, J. *Angew. Chem.* **2015**, *127*, 13539-13543. Copyright Wiley-VCH Verlag GmbH & Co. KGaA.

On the other hand, the structural data of $(\text{Ph}_3\text{PO})_2\cdot\text{H}_2\text{O}_2$ have been known for decades,¹⁹ where two phosphine oxide molecules are bridged by a single H_2O_2 molecule (Figure 2.2). Although H_2O_2 adducts of other phosphine oxide molecules have been reported,⁶ single crystal X-ray data have only been obtained for $[\text{Cy}_3\text{PO}\cdot\text{H}_2\text{O}_2]_2$ ⁶ and $(\text{Ph}_3\text{PO})_2\cdot\text{H}_2\text{O}_2$ ¹⁹ when the work on this thesis was started. Therefore, it was difficult to determine the ratio $\text{R}_3\text{PO} : \text{H}_2\text{O}_2$ for a H_2O_2 adduct of any given phosphine oxide. Moreover, adducts of phosphine oxides with less steric bulk are often viscous oils.

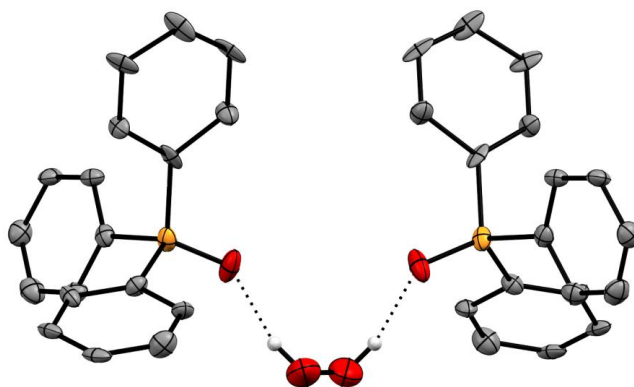


Figure 2.2. Single crystal X-ray structure of $(\text{Ph}_3\text{PO})_2\cdot\text{H}_2\text{O}_2$.¹⁹

The synthetic method described previously⁶ was applied to various different phosphine oxides in an attempt to crystallize another adduct and determine whether the chair-like structure found in $[\text{Cy}_3\text{PO}\cdot\text{H}_2\text{O}_2]_2$ ⁶ is unique to Cy_3PO , or if this is a general motif for trialkylphosphine oxides.

Previously, ³¹P NMR and IR spectroscopy have been used to confirm the presence of H_2O_2 and the absence of H_2O in adduct molecules.⁶ In the ³¹P NMR

spectrum, the phosphorus peak of an adduct $(R_3PO)_x \cdot (H_2O_2)_y$ is downfield shifted compared to the neat R_3PO , as electron density is removed to form the P=O group by hydrogen bonding, and phosphorus is deshielded. In the IR spectrum, the O-H band for H_2O_2 appears as a broad band around 3200 cm^{-1} , distinct from the O-H band of H_2O at 3400 cm^{-1} (Figure B.1).

For the newly synthesized H_2O_2 adducts, both ^{31}P NMR and IR spectroscopy were performed, and the solubilities of these adducts in common organic solvents were measured.

Results and Discussions

In order to probe whether $[R_3PO \cdot H_2O_2]_2$ represents a general composition of hydrogen peroxide adducts of phosphine oxides, analogous compounds with different substituents ($R = ^t\text{Bu}, \text{Ph}$) have been synthesized following the previously described method.⁶ Indeed, the adduct $[^t\text{Bu}_3\text{PO} \cdot \text{H}_2\text{O}_2]_2$ (**1**) crystallized as a dimer with two H_2O_2 molecules hydrogen-bonded between two phosphine oxide groups in a chair conformation (Figure 2.3).^{18,20} The tendency of P=O groups to eagerly form hydrogen bonds to H_2O_2 molecules,⁶ H_2O ¹⁷ and silanols¹⁷ has been described. Recently, hydrogen bonding between P=O and phenol -OH groups has also been used to create dimeric motifs.²¹

Many triarylphosphine oxides do not follow this structural trend, and they can even lead to different adduct structures and stoichiometries for one given

triarylphosphine oxide. For example, an adduct of Ph_3PO has been described earlier and its composition has been determined as $(\text{Ph}_3\text{PO})_2\cdot\text{H}_2\text{O}_2$ with H_2O_2 bridging two Ph_3PO molecules.¹⁹ Two separate attempts to reproduce this result led to $(\text{Ph}_3\text{PO})_2\cdot\text{H}_2\text{O}_2$ (Figure 2.2)¹⁹ and a new adduct $[\text{Ph}_3\text{PO}\cdot\text{H}_2\text{O}_2]_2\cdot\text{H}_2\text{O}_2$ (**2**) (Figure 2.3).^{18,22} Most probably, due to the rigid nature and sterics of the phenyl groups, additional H_2O_2 molecules can be accommodated in the space between the dimers, depending on the reaction conditions.

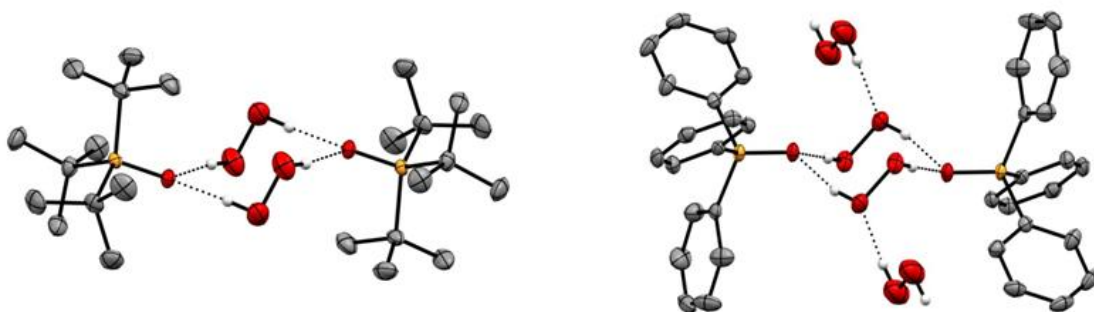


Figure 2.3. Single crystal X-ray structures of **1** (left)^{18,20} and **2** (right).^{18,22}

The crystalline adduct $[\text{Cy}_3\text{PO}\cdot\text{H}_2\text{O}_2]_2$ (**3**) was easily reproduced in high yield following the previously reported synthetic method.⁶ The absence of bulk water molecules was confirmed via NMR and IR spectroscopy.

When solubilized, the hydrogen bond between H_2O_2 and R_3PO reversibly forms, and proton exchange can occur between H_2O_2 and protic solvents. This exchange was observed when adduct **3** was dissolved in a $\text{CDCl}_3/\text{D}_2\text{O}$ (6:1) mixture and stirred overnight. The resulting product was precipitated, and analyzed with ^2H NMR and IR

spectroscopy. In the ^2H NMR spectrum, a broad peak is observed at 10.51 ppm, corresponding to the peroxide-bound deuterium (Figure 2.4).

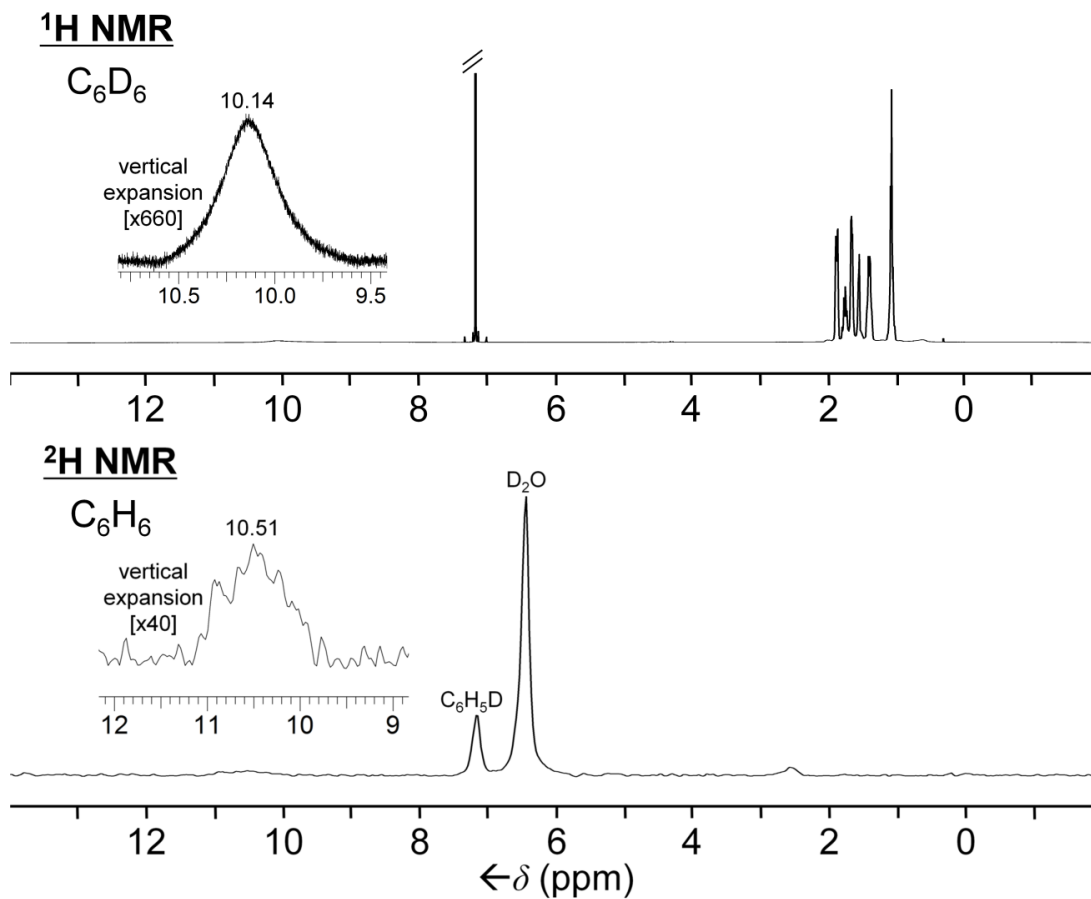


Figure 2.4. ^1H NMR spectrum of **3** (top) and ^2H NMR spectrum of partially deuterated **3** (bottom).

In the ^1H NMR spectrum of a non-deuterated sample, the -OOH proton peak occurs in the same region, at 10.14 ppm. The IR spectrum shows signs of residual H_2O_2 (3165.2 cm^{-1}) as well as the exchanged D_2O_2 (2358.9 cm^{-1}) (Figure B. 4).

One of the most important advantages of the hydrogen peroxide adducts of phosphine oxides with respect to their application as oxidizing agents is that they are very soluble in organic solvents, rendering biphasic reaction mixtures obsolete. The solubilities of **2** and **3** in representative organic solvents have been quantified (Figure 2.5).¹⁸ They are substantially higher in polar solvents, with adduct **3** displaying remarkably high solubility especially in chlorinated solvents.

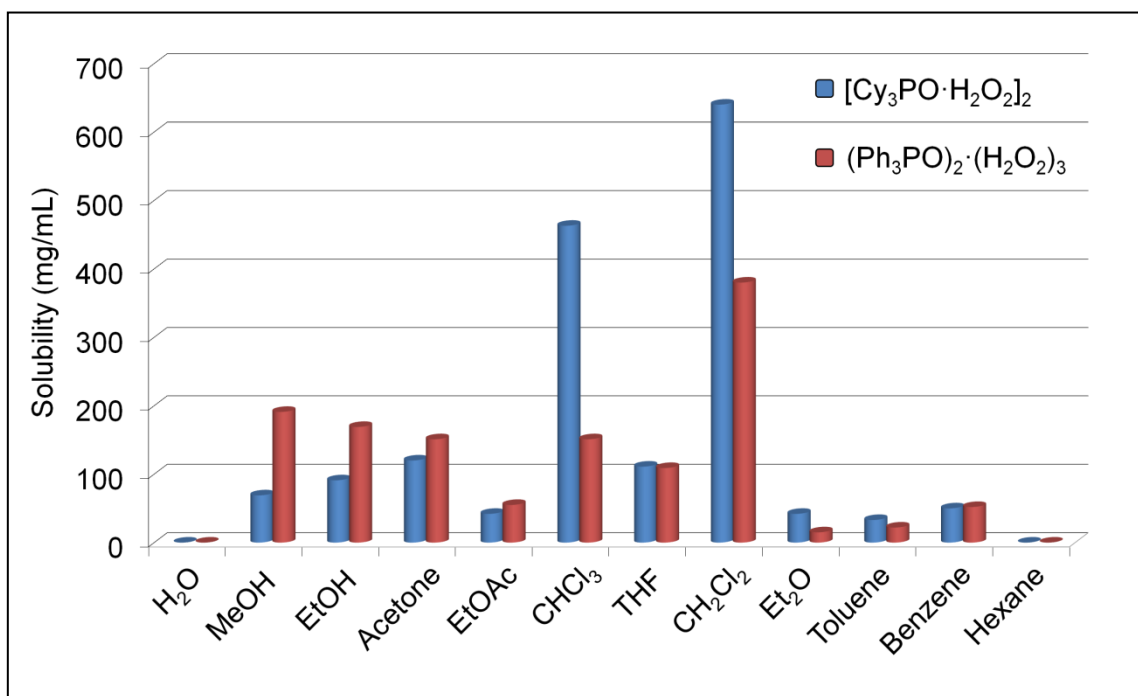


Figure 2.5. Solubilities of **2** and **3** in representative solvents.

Conclusion

In this chapter it has been demonstrated that the H₂O₂ adducts of trialkylphosphine oxides crystallize readily and reproducibly in a dimer structure with a

chair-type arrangement of the H₂O₂ moieties. Triarylphosphine oxides can lead to different H₂O₂ contents, and therefore quantification of the ratio R₃PO : H₂O₂ is necessary for each new batch. The described adducts do not contain an excess of water molecules and are very soluble in representative organic solvents, allowing oxidation reactions in a single organic phase.

Experimental

[^tBu₃PO•H₂O₂]₂ (1)

^tBu₃P (20 mg, 0.099 mmol) is weighed into a Schlenk flask inside a glove box. The flask is then sealed, brought outside, and acetone (40 mL) is added under a nitrogen stream. Once the phosphine is dissolved, aqueous H₂O₂ (1.0 mL, 10 mmol) is added and the reaction mixture is stirred for 1 h. 100 mL of EtOH is then added to the flask, and the azeotropic mixture of EtOH and H₂O is removed *in vacuo* at ambient temperature. The resulting viscous material is washed with toluene and left to crystallize. The adduct [^tBu₃PO•H₂O₂]₂ is obtained in the form of white rhombic crystals (19 mg, 0.075 mmol, 76% yield).

NMR (δ , CDCl₃), ³¹P{¹H} 43.16 (s); ¹H 9.10 (br. s, H₂O₂), 1.41 (d, ³J(³¹P-¹H) = 12.5 Hz, -CH₃); ¹³C{¹H} 39.17 (d, ¹J(³¹P-¹³C) = 49.6 Hz, PC), 29.00 (s, -CH₃).

NMR (δ , (CD₃)₂CO), ³¹P{¹H} 65.61 (s); ¹H 1.34 (d, ³J(³¹P-¹H) = 12.0 Hz, -CH₃); ¹³C{¹H} 40.35 (d, ¹J(³¹P-¹³C) = 51.1 Hz, PC), 30.08 (s, -CH₃). mp 122-125 °C.

[Ph₃PO•H₂O₂]₂•H₂O₂ (**2**)

Ph₃P (150 mg, 0.572 mmol) is weighed into a Schlenk flask flushed with nitrogen gas. CH₂Cl₂ (150 mL) is added under a nitrogen stream. Once the phosphine is dissolved, aqueous H₂O₂ (1.0 mL, 10 mmol) is added and the reaction mixture is stirred for 30 min. The organic layer is collected via separation funnel, and the solvent is removed *in vacuo*. The resulting white precipitate is dissolved in acetone (60 mL), and after the addition of H₂O₂ (0.1 mL, 1 mmol), the sample is allowed to crystallize. [Ph₃PO•H₂O₂]₂•H₂O₂ is obtained in the form of colorless needles (286 mg, 0.434 mmol, 76% yield).

NMR (δ , CDCl₃), ³¹P{¹H} 32.84 (s); ¹H 11.24 (br. s, H₂O₂), 8.93 (br. s, H₂O₂), 7.67-7.62 (m, 6H, H_o), 7.58-7.55 (m, 3H, H_p), 7.49-7.45 (m, 6H, H_m); ¹³C{¹H} 132.43 (s, C_p), 132.04 (d, ²J(³¹P-¹³C) = 10.2 Hz, C_o), 130.71 (d, ¹J(³¹P-¹³C) = 108.8 Hz, C_i), 128.69 (d, ³J(³¹P-¹³C) = 12.1 Hz, C_m). mp 143-155 °C.

Deuteration of [Cy₃PO•H₂O₂]₂ (**3**)

0.5 mL of D₂O was added to a solution of 50 mg (0.08 mmol) of [Cy₃PO•H₂O₂]₂, dissolved in 3 mL of CDCl₃, and the mixture was stirred vigorously for 24 h. The remaining CDCl₃ and D₂O were removed via slow evaporation, and the deuterated adduct was obtained as white crystalline powder. A sample was prepared for ²H NMR by dissolving the product in C₆H₆.

CHAPTER III
SYNTHESIS OF DI(HYDROPEROXY)ALKANE ADDUCTS OF PHOSPHINE
OXIDES*

Introduction

In an attempt to control the $R_3PO : H_2O_2$ ratio in H_2O_2 adducts of triarylphosphine oxides, and to be able to work in one organic phase, the solvent for the reaction was changed from CH_2Cl_2 to acetone. Contrary to anticipation, a new class of adducts was discovered, with the molecular formula $R_3PO \cdot (HOO)_2CR'R''$ ($R, R', R'' =$ alkyl, aryl). For these di(hydroperoxy)alkane adducts the number of active peroxide groups is even higher than for H_2O_2 adducts, as two peroxy groups are bound to one phosphine oxide group. The high tendency of these adducts to crystallize makes them an ideal source for stoichiometric active peroxides.

While di(hydroperoxy)alkanes have been known for a long time,²³ the only preceding report of this class of phosphine oxide adduct was made when H_2O_2 and bis(diphenylphosphino)ethane (dppe) were reacted in acetone in the presence of R_2SnCl_2 ($R = Me$ or nBu) as catalyst to form $(Ph_2P(O)CH_2CH_2P(O)Ph_2) \cdot ((HOO)_2CMe_2)_2$.²⁴ The authors proposed that this adduct could only form with a chelating phosphine that has two methylene carbons in the chain between the two P atoms.

* Reproduced with permission from "Hydrogen Peroxide and Di(hydroperoxy)propane Adducts of Phosphine Oxides as Stoichiometric and Soluble Oxidizing Agents" Ahn, S. H.; Cluff, K. J.; Bhuvanesh, N.; Blümel, J. *Angew. Chem.* **2015**, *127*, 13539-13543. Copyright Wiley-VCH Verlag GmbH & Co. KGaA.

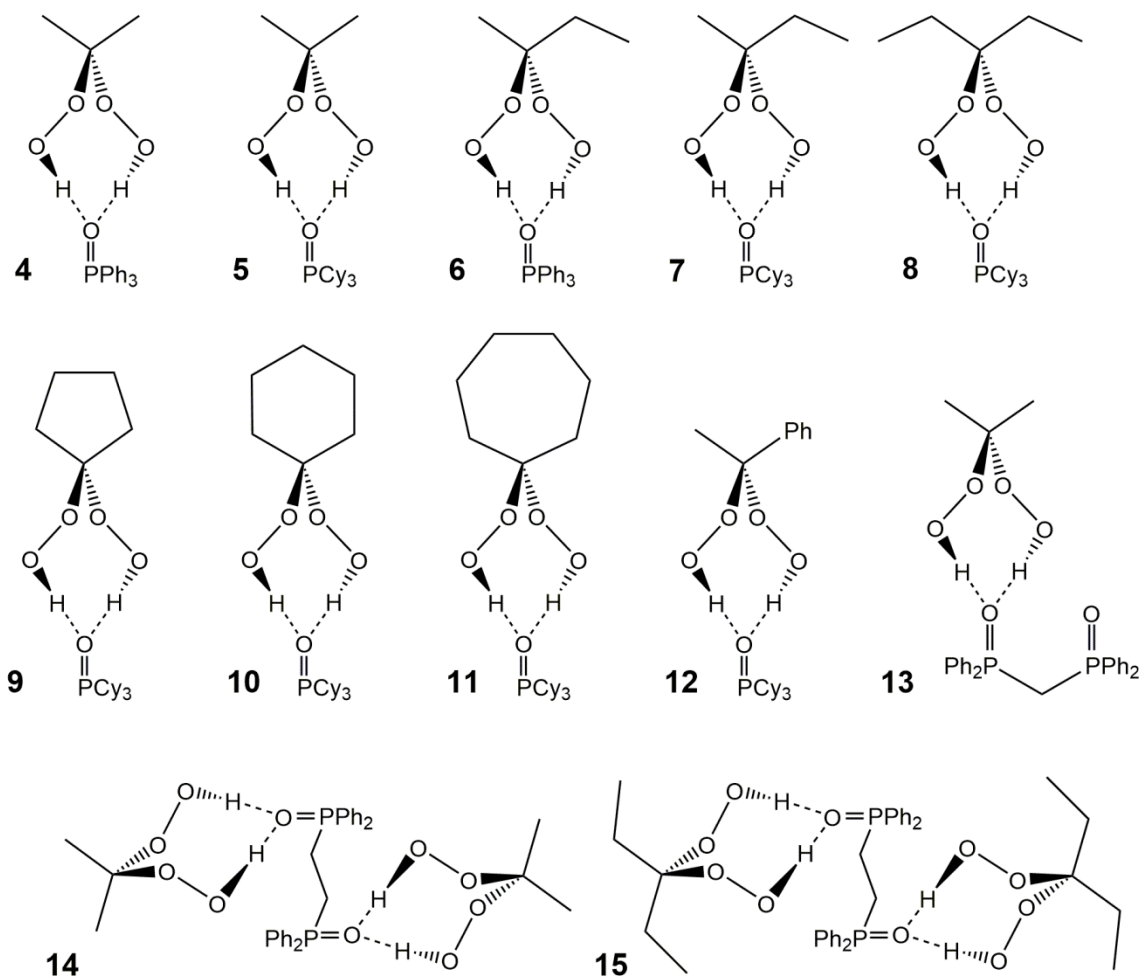
Here, it will be demonstrated that di(hydroperoxy)alkane adducts of phosphine oxides are actually easy to synthesize with a large variety of alkane moieties. Moreover, the active oxygen content and the structural mode remain the same for different phosphine oxides. A description of the general synthetic method and its mechanism are provided in this chapter.

Results and Discussion

Di(hydroperoxy)alkane adducts of various phosphine oxides and alkanes (**4-15**) were successfully synthesized and obtained in nearly quantitative yields as giant crystals (Scheme 3.1). Adducts of the bulky Cy_3PO crystallize especially readily, and thus Cy_3PO was used most often in adduct syntheses. In order to improve the atom economy of active oxygen, and to probe the general structure of the di(hydroperoxy)alkane adducts, 1,2-bis(diphenylphosphino)ethane (dppe) and 1,2-bis(diphenylphosphino)methane (dppm) were treated with acetone and aqueous H_2O_2 . While dppm dioxide only formed the adduct with one molecule of $(\text{HOO})_2\text{CMe}_2$, dppe dioxide formed hydrogen bonds with $(\text{HOO})_2\text{CMe}_2$ at both $\text{P}=\text{O}$ groups. Encouraged by this success, the dppe dioxide adduct synthesis was repeated with 3-pentanone to produce $(\text{Ph}_2\text{P}(\text{O})\text{CH}_2\text{CH}_2\text{P}(\text{O})\text{Ph}_2)\cdot((\text{HOO})_2\text{CEt}_2)_2$ (**15**). The discrepancy in the ratio of dppm dioxide and $(\text{HOO})_2\text{CMe}_2$ is studied in detail in the following chapter.

It is important to note that the di(hydroperoxy)alkane adducts can be generated at room temperature and without addition of a strong acid or catalyst.^{18,23a,25} This prevents the formation of potentially dangerous cyclic peroxide trimers.²⁶ In fact, none of the

adducts **4-15** displayed any violent release of energy when being ground, hammered, stored over months, or heated up.

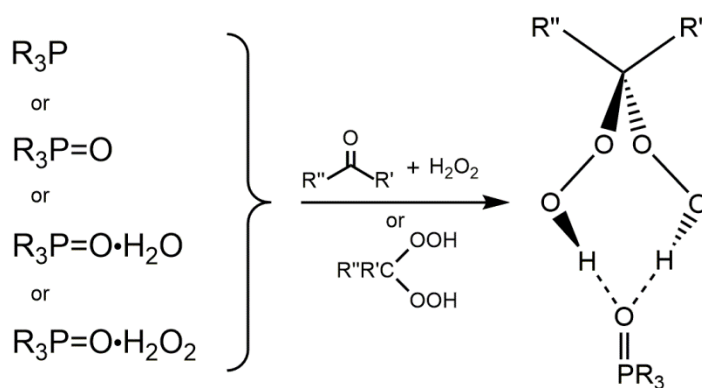


Scheme 3.1. (HOO)₂CR'R'' adducts of the phosphine oxides **4-12** and the diphosphine dioxides **13-15**.

The adducts can be synthesized in a variety of ways (Scheme 3.2). One option is to start from the phosphine oxides or their corresponding H₂O or H₂O₂ adducts.

Alternatively, the phosphines can be used as educts. When starting from the phosphine oxides, exclusion of air is not necessary during the adduct synthesis. However, starting from the phosphines entails the risk of formation of other unwanted products from oxygen insertion into the P-C bonds, and thus the synthesis must be performed in inert atmosphere.⁶

For all starting materials, the adduct formation can be achieved by adding the corresponding ketone and H₂O₂, or the pre-formed di(hydroperoxy)alkane moiety,^{23a} if available in stable form. The ketone can serve a dual role as the reaction solvent, or CH₂Cl₂ can be used instead, as the phosphines and phosphine oxides are highly soluble in polar chlorinated solvents.

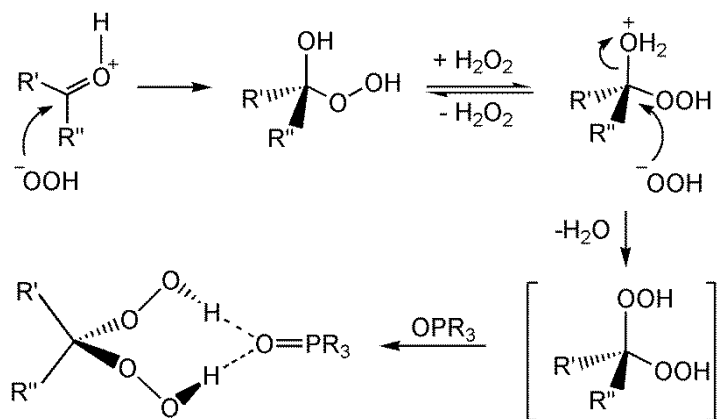


Scheme 3.2. General synthesis routes for the adducts R₃PO•(HOO)₂CR'R'' (R, R', R'' = alkyl, aryl).

The mechanism for the formation of the adducts is suggested in Scheme 3.3.¹⁸

Two hydroperoxides perform a nucleophilic attack on the carbonyl carbon atom to form

the di(hydroperoxy)alkane, which then attaches to the phosphine oxide *via* hydrogen bonds.



Scheme 3.3. Suggested mechanism for the formation of adducts $R_3PO \cdot (HOO)_2CR'R''$ ($R, R', R'' = \text{alkyl, aryl}$).

In order to remove excess water from the solution without decomposing the peroxide groups, ethanol is used to form an azeotropic mixture with water. This mixture is then removed in a mild vacuum at room temperature, and the adduct is crystallized from the remaining solution. Starting from larger ketones, the ensuing $(HOO)_2CR'R''$ molecule can be safely isolated and dried,^{23a} and combined with pure phosphine oxide at a later time to form the adduct. Thus, an azeotropic mixture is unnecessary. Excess solvent is removed *in vacuo* at room temperature, as the peroxide functionality can decompose at higher temperatures. The adduct is obtained in the form of crystals from the concentrated solution.

The general synthetic routes outlined in Scheme 3.2 allow for easy recycling of the adducts. Once the peroxide oxygen atoms are consumed in the course of an oxidation

reaction, the remaining phosphine oxide can be removed and the adduct is regenerated by stirring the phosphine oxide in a solution of excess H_2O_2 together with the corresponding ketone.

Conclusion

Di(hydroperoxy)alkane adducts of phosphine oxides are successfully synthesized at room temperature, without the use of acid or metal catalysts. Phosphine, phosphine oxide, and H_2O or H_2O_2 adducts of phosphine oxides can be used as the starting materials. While the high solubility of these starting materials make CH_2Cl_2 an attractive solvent, the corresponding ketone can be used as the solvent instead. This one-pot, general synthetic approach can be applied to a wide variety of phosphine oxides and ketones, and the resulting adducts can be safely and easily isolated in the form of large crystals.

Experimental

$\text{Ph}_3\text{PO}\cdot(\text{HOO})_2\text{CMe}_2$ (**4**)

Ph_3P (200 mg, 0.762 mmol) is weighed into a Schlenk flask flushed with nitrogen gas. Acetone (100 mL) is added under a nitrogen flow. Once the phosphine is all dissolved, H_2O_2 (1.0 mL, 10 mmol) is added and the reaction mixture is stirred for 3 h. The sample is concentrated *in vacuo* to 5 mL, then allowed to crystallize.

(Ph₃PO)•(HOO)₂CMe₂ (**4**) is obtained as colorless rectangular crystals (243 mg, 0.629 mmol, 82.5% yield).

NMR (δ , CDCl₃), ³¹P{¹H} 34.74 (s); ¹H 11.29-10.90 (br. s, -OOH), 7.68-7.61 (m, 6H, *H_o*), 7.60-7.55 (m, 3H, *H_p*), 7.51-7.46 (m, 6H, *H_m*), 1.47 (m, 6H, *CH₃*); ¹³C{¹H} 132.57 (s, *C_p*), 132.10 (d, ²*J*(³¹P-¹³C) = 10.7 Hz, *C_o*), 130.56 (d, ¹*J*(³¹P-¹³C) = 106.07 Hz, *C_i*), 128.77 (d, ³*J*(³¹P-¹³C) = 12.6 Hz, *C_m*), 109.28 (s, *CH₃C*), 20.64 (s, *CH₃*).

NMR (δ , (CD₃)₂CO), ³¹P{¹H} 31.21 (s); ¹H 10.97 (br. s, -OOH), 7.76-7.68 (m, 6H, *H_o*), 7.67-7.62 (m, 3H, *H_p*), 7.60-7.53 (m, 6H, *H_m*), 1.35 (m, *CH₃*); ¹³C{¹H} 133.14 (d, ⁴*J*(³¹P-¹³C) = 2.3 Hz, *C_p*), 132.58 (d, ²*J*(³¹P-¹³C) = 10.2 Hz, *C_o*), 132.51 (d, ¹*J*(³¹P-¹³C) = 104.7 Hz, *C_i*), 129.52 (d, ³*J*(³¹P-¹³C) = 12.1 Hz, *C_m*), 109.03 (s, *CH₃C*), 20.97 (s, *CH₃*). IR: ν (PO) = 1152 cm⁻¹. mp (decomp.) 75 °C.

Cy₃PO•(HOO)₂CMe₂ (**5**)

Cy₃P (100 mg, 0.357 mmol) is weighed into a Schlenk flask inside a glove box. The flask is then sealed, brought outside, and acetone (60 mL) is added under a nitrogen flow. Once the phosphine is all dissolved, H₂O₂ (0.5 mL, 5.1 mmol) is added and the reaction mixture is stirred for 1 h. 100 mL of EtOH is then added to the flask, and the azeotropic mixture of EtOH and H₂O is removed *in vacuo* at ambient temperature. (Cy₃PO)•(HOO)₂CMe₂ (**5**) is obtained as colorless hexagonal crystals (126 mg, 0.327 mmol, 91.6% yield)

NMR (δ , CDCl₃), ³¹P{¹H} 55.59 (s); ¹H 1.97-1.80 (m, 15H, PCH_{ax}CH_{eq}CH_{eq}), 1.77-1.70 (s, 3H, PCH(CH₂)₂CH_{eq}), 1.49-1.36 (s, 12H, PCHCH_{ax}, CH₃), 1.36-1.21(m, 9H, PCHCH₂CH_{ax}CH_{ax}); ¹³C{¹H} 108.91 (s, CH₃C), 34.79 (d, ¹J(³¹P-¹³C) = 60.9 Hz, PCH), 26.74 (d, ³J(³¹P-¹³C) = 12.7 Hz, PCHCH₂CH₂), 25.98 (d, ²J(³¹P-¹³C) = 3.6 Hz, PCHCH₂), 25.92 (d, ⁴J(³¹P-¹³C) = 1.8 Hz, PCH(CH₂)₂CH₂), 20.63 (s, CH₃).

NMR (δ , (CD₃)₂CO), ³¹P{¹H} 56.44 (s); ¹H 11.45 (br. s, -OOH), 2.02-1.89 (m, 9H, PCH_{ax}CH_{eq}), 1.86-1.76 (m, 6H, PCHCH₂CH_{eq}), 1.74-1.66 (m, 3H, PCH(CH₂)₂CH_{eq}), 1.52-1.38 (m, 6H, PCHCH_{ax}), 1.37-1.19 (m, 9H, PCHCH₂CH_{ax}CH_{ax}), 1.30 (s, CH₃); ¹³C{¹H} 108.61 (s, (CH₃)₂C(OOH)₂), 35.53 (d, ¹J(³¹P-¹³C) = 61.0 Hz, PCH), 27.36 (d, ³J(³¹P-¹³C) = 12.1 Hz, PCHCH₂CH₂), 26.74 (s, PCH(CH₂)₂CH₂), 26.73 (d, ²J(³¹P-¹³C) = 2.8 Hz, PCHCH₂). IR: ν (PO) = 1125 cm⁻¹. mp (decomp.) 70 °C.

Ph₃PO•(HOO)₂CMeEt (**6**)

Ph₃P (300 mg, 1.1 mmol) was placed in a round bottom flask and dissolved in toluene (40 mL). 2-Butanone (0.12 mL, 1.3 mmol) and H₂O₂ (0.5 mL, 5 mmol) were added, and the reaction mixture was stirred overnight. The solution was concentrated to approximately 3 mL *in vacuo* and the product was allowed to crystallize. Adduct **6** was obtained in the form of colorless crystals (294 mg, 0.71 mmol, 65% yield).

NMR (δ , CDCl₃), ³¹P{¹H} 30.52 (s); ¹H 11.38 (s, 2H, OOH), 7.69-7.64 (m, 6H, H_o), 7.60-7.55 (m, 3H, H_p), 7.51-7.46 (m, 6H, H_m), 1.79 (q, ³J(¹H-¹H) = 7.6 Hz, 2H,

CH₂CH₃), 1.41 (s, 3H, CCH₃), 1.01 (t, ³J(¹H-¹H) = 7.6 Hz, 3H, CH₂CH₃); ¹³C{¹H} 132.32 (d, ⁴J(³¹P-¹³C) = 2.7 Hz, C_p), 132.08 (d, ²J(³¹P-¹³C) = 10.0 Hz, C_o), 131.29 (d, ¹J(³¹P-¹³C) = 105.4 Hz, C_i), 128.66 (d, ³J(³¹P-¹³C) = 12.3 Hz, C_m), 111.56 (s, CH₃C), 26.09 (s, CH₂CH₃), 17.46 (s, CCH₃), 8.38 (s, CH₂CH₃).

NMR (δ, C₆D₆), ³¹P{¹H} 31.42 (s); ¹H 11.95 (s, 2H, OOH), 7.62-7.56 (m, 6H, H_o), 7.03-6.98 (m, 3H, H_p), 6.96-6.91 (m, 6H, H_m), 2.09 (q, ³J(¹H-¹H) = 7.6 Hz, 2H, CH₂CH₃), 1.65 (s, 3H, CCH₃), 1.11 (t, ³J(¹H-¹H) = 7.6 Hz, 3H, CH₂CH₃); ¹³C{¹H} 132.32 (d, ²J(³¹P-¹³C) = 10.4 Hz, C_o), 132.11 (d, ¹J(³¹P-¹³C) = 104.0 Hz, C_i), 132.10 (d, ⁴J(³¹P-¹³C) = 3.2 Hz, C_p), 128.72 (d, ³J(³¹P-¹³C) = 12.3 Hz, C_m), 111.70 (s, CH₃C), 26.94 (s, CH₂CH₃), 18.16 (s, CCH₃), 8.78 (s, CH₂CH₃). IR: ν(PO) = 1142 cm⁻¹. mp (decomp.) 54 °C.

Cy₃PO•(HOO)₂CMeEt (**7**)

[Cy₃PO•H₂O₂]₂ (300 mg, 0.91 mmol) was placed in a round bottom flask and dissolved in 30 mL of butanone (0.33 mol). After addition of H₂O₂ (0.5 mL, 5 mmol) the solution was stirred overnight. Excess butanone was removed *in vacuo* until a precipitate appeared. Subsequently, 50 mL of EtOH was added to the flask, and the azeotropic mixture of EtOH and H₂O was removed *in vacuo* at ambient temperature to give white crystals of **7** (345 mg, 0.82 mmol, 90% yield).

NMR (δ , CDCl₃), ³¹P{¹H} 58.77 (s); ¹H 11.47 (s, 2H, OOH), 1.97-1.80 (m, 15H, PCHCH_{eq}CH_{eq}), 1.73 (q, ³J(¹H-¹H) = 7.6 Hz, 2H, CH₂CH₃), 1.76-1.72 (m, 3H, PCH(CH₂)₂CH_{eq}), 1.48-1.39 (m, 6H, PCHCH_{ax}), 1.38 (s, 3H, CCH₃), 1.29-1.23 (m, 9H, PCHCH₂CH_{ax}CH_{ax}), 0.97 (t, ³J(¹H-¹H) = 7.6 Hz, 3H, CH₂CH₃); ¹³C{¹H} 111.26 (s, CH₃C), 34.72 (d, ¹J(³¹P-¹³C) = 60.5 Hz, PC), 26.72 (d, ³J(³¹P-¹³C) = 12.1 Hz, PCHCH₂CH₂), 26.02 (s, CH₂CH₃), 25.96 (d, ²J(³¹P-¹³C) = 2.8 Hz, PCHCH₂), 25.91 (d, ⁴J(³¹P-¹³C) = 1.4 Hz, PCH(CH₂)₂CH₂), 17.41 (s, CCH₃), 8.36 (s, CH₂CH₃). IR: ν (PO) = 1124 cm⁻¹. mp (decomp.) 108 °C.

Cy₃PO•(HOO)₂CET₂ (**8**)

[Cy₃PO•H₂O₂]₂ (330 mg, 1.0 mmol) was placed in a round bottom flask and combined with 3-pentanone (0.4 mL, 2 mmol) and H₂O₂ (0.2 mL, 2 mmol). The mixture was stirred for 1 h, then left to crystallize by slow evaporation of solvent. Cy₃PO•(HOO)₂CET₂ (**8**) was obtained in the form of white, rod-shaped crystals (425 mg, 1.0 mmol, 98% yield).

NMR (δ , CDCl₃), ³¹P{¹H} 58.35 (s); ¹H 10.82 (br. s, 2H, OOH), 1.96-1.81 (m, 15H, PCH_{ax}CH_{eq}CH_{eq}), 1.76-1.71 (m, 3H, PCH(CH₂)₂CH_{eq}), 1.81 (t, ³J(¹H-¹H) = 6.4 Hz, 4H, CCH₂), 1.68 (q, ³J(¹H-¹H) = 7.6 Hz, 4H, CCH₂), 1.47-1.37 (m, 8H, PCHCH_{ax}, CCH₂CH₂CH₂), 1.30-1.22 (m, 9H, PCHCH₂CH_{ax}CH_{ax}), 0.94 (t, ³J(¹H-¹H) = 7.6 Hz, 6H, CCH₂CH₃); ¹³C{¹H} 113.76 (s, CCH₃), 34.64 (d, ¹J(³¹P-¹³C) = 60.5 Hz, PC), 26.68 (d, ³J(³¹P-¹³C) = 11.6 Hz, PCHCH₂CH₂), 25.93 (d, ²J(³¹P-¹³C) = 3.3 Hz, PCHCH₂), 25.87 (d,

$^4J(^{31}\text{P}-^{13}\text{C}) = 0.9 \text{ Hz}$, $\text{PCH}(\text{CH}_2)_2\text{CH}_2$, 21.64 (s, CH_2CH_3), 7.91 (s, CH_2CH_3). IR: $\nu(\text{PO}) = 1126 \text{ cm}^{-1}$. mp 138 °C.

$\text{Cy}_3\text{PO}\cdot(\text{HOO})_2\text{C}(\text{CH}_2)_4$ (**9**)

In a round bottom flask $[\text{Cy}_3\text{PO}\cdot\text{H}_2\text{O}_2]_2$ (996 mg, 3 mmol) is dissolved in cyclopentanone (4.6 mL, 52 mmol). H_2O_2 (1 mL, 10 mmol) is added to the flask, the contents is stirred for 1 h, then left to crystallize by slow evaporation of the solvent. $\text{Cy}_3\text{PO}\cdot(\text{HOO})_2\text{C}(\text{CH}_2)_4$ (**9**) is obtained in the form of colorless, cubic crystals (1049 mg, 2.3 mmol, 76% yield).

NMR (δ , CDCl_3), $^{31}\text{P}\{^1\text{H}\}$ 57.14 (s); ^1H 11.61 (br. s, 2H, OOH), 1.93 (t, 4H, $^3J(^1\text{H}-^1\text{H}) = 7.58 \text{ Hz}$, CCH_2), 1.95-1.81 (m, 15H, $\text{PCH}_{\text{ax}}\text{CH}_{\text{eq}}\text{CH}_{\text{eq}}$), 1.75-1.71 (m, 3H, $\text{PCH}(\text{CH}_2)_2\text{CH}_{\text{eq}}$), 1.70 (t, 4H, $^3J(^1\text{H}-^1\text{H}) = 7.58 \text{ Hz}$, CCH_2CH_2), 1.47-1.37 (m, 6H, PCHCH_{ax}), 1.31-1.21 (m, 9H, $\text{PCHCH}_2\text{CH}_{\text{ax}}\text{CH}_{\text{ax}}$); $^{13}\text{C}\{^1\text{H}\}$ 120.92 (s, CCH_3), 34.80 (d, $^1J(^{31}\text{P}-^{13}\text{C}) = 60.5 \text{ Hz}$, PC), 33.14 (s, CCH_2), 26.76 (d, $^3J(^{31}\text{P}-^{13}\text{C}) = 11.6 \text{ Hz}$, $\text{PCHCH}_2\text{CH}_2$), 26.01 (d, $^2J(^{31}\text{P}-^{13}\text{C}) = 3.3 \text{ Hz}$, PCHCH_2), 25.95 (d, $^4J(^{31}\text{P}-^{13}\text{C}) = 1.4 \text{ Hz}$, $\text{PCH}(\text{CH}_2)_2\text{CH}_2$), 24.66 (s, CCH_2CH_2). IR: $\nu(\text{PO}) = 1123 \text{ cm}^{-1}$. mp 152 °C.

$\text{Cy}_3\text{PO}\cdot(\text{HOO})_2\text{C}(\text{CH}_2)_5$ (**10**)

0.3 mL of H_2SO_4 (5 mmol) and 13.5 mL of H_2O_2 (0.135 mol) were combined with THF (25 mL) in a round bottom flask. Cyclohexanone (1.00 mL, 9.7 mmol) was added dropwise over a period of 15 min, while stirring vigorously. After 5 h, 10 mL of

CH₂Cl₂ was added, and NaHCO₃ was used to neutralize the mixture to pH 7. The organic layer was collected, washed with H₂O (4x3 mL) and dried with MgSO₄. Solvent from the filtrate was removed *in vacuo*, to produce (HOO)₂C(CH₂)₅. The ¹H and ¹³C NMR spectra of (HOO)₂C(CH₂)₅ matched those in the literature.^{23a} [Cy₃PO•H₂O₂]₂ (297 mg, 0.9 mmol) was dissolved in 5 mL of benzene and added to the flask. The mixture was stirred for 2 h and subsequently concentrated *in vacuo* to about 2 mL at ambient temperature. Cy₃PO•(HOO)₂C(CH₂)₅ (**10**) was obtained as clear, hexagonal crystals (235 mg, 0.53 mmol, 59% yield).

NMR (δ, CDCl₃), ³¹P{¹H} 58.01 (s); ¹H 10.66 (br. s, 2H, OOH), 1.97-1.79 (m, 15H, PCH_{ax}CH_{eq}CH_{eq}), 1.81 (t, ³J(¹H-¹H) = 6.4 Hz, 4H, CCH₂), 1.75-1.71 (m, 3H, PCH(CH₂)₂CH_{eq}), 1.58 (quin, ³J(¹H-¹H) = 6.4 Hz, 4H, CCH₂CH₂), 1.47-1.37 (m, 8H, PCHCH_{ax}, CCH₂CH₂CH₂), 1.31-1.22 (m, 9H, PCHCH₂CH_{ax}CH_{ax}); ¹³C{¹H} 109.52 (s, CCH₃), 34.67 (d, ¹J(³¹P-¹³C) = 60.5 Hz, PC), 29.68 (s, CCH₂), 26.69 (d, ³J(³¹P-¹³C) = 12.1 Hz, PCHCH₂CH₂), 25.94 (d, ²J(³¹P-¹³C) = 3.3 Hz, PCHCH₂), 25.89 (d, ⁴J(³¹P-¹³C) = 0.9 Hz, PCH(CH₂)₂CH₂), 25.55 (s, CCH₂CH₂CH₂), 22.53 (s, CCH₂CH₂). IR: ν(PO) = 1123 cm⁻¹. mp 121 °C.

Cy₃PO•(HOO)₂C(CH₂)₆ (**11**)

[Cy₃PO•H₂O₂]₂ (831 mg, 2.5 mmol), dissolved in cycloheptanone (3.0 mL, 25 mmol), is placed into a round bottom flask. H₂O₂ (1 mL, 10 mmol) is added to the flask,

the contents is stirred for 1 h, and then left to crystallize. $\text{Cy}_3\text{PO}\cdot(\text{HOO})_2\text{C}(\text{CH}_2)_6$ (**11**) is obtained in the form of colorless, cubic crystals (1067 mg, 2.2 mmol, 88% yield).

NMR (δ , CDCl_3), $^{31}\text{P}\{^1\text{H}\}$ 56.63 (s); ^1H 11.57 (br. s, 2H, OOH), 1.93-1.81 (m, 19H, $\text{PCH}_{\text{ax}}\text{CH}_{\text{eq}}\text{CH}_{\text{eq}}$, CCH_2), 1.75-1.71 (m, 3H, $\text{PCH}(\text{CH}_2)_2\text{CH}_{\text{eq}}$), 1.61-1.53 (m, $\text{CCH}_2\text{CH}_2\text{CH}_2$), 1.47-1.36 (m, 6H, PCHCH_{ax}), 1.31-1.21 (m, 9H, $\text{PCHCH}_2\text{CH}_{\text{ax}}\text{CH}_{\text{ax}}$); $^{13}\text{C}\{^1\text{H}\}$ 114.33 (s, CCH_3), 34.80 (d, $^1J(^{31}\text{P}-^{13}\text{C}) = 60.9$ Hz, PC), 32.36 (s, CCH_2), 30.23 (s, CCH_2CH_2), 26.75 (d, $^3J(^{31}\text{P}-^{13}\text{C}) = 11.6$ Hz, $\text{PCHCH}_2\text{CH}_2$), 26.00 (d, $^2J(^{31}\text{P}-^{13}\text{C}) = 2.7$ Hz, PCHCH_2), 25.95 (d, $^4J(^{31}\text{P}-^{13}\text{C}) = 0.9$ Hz, $\text{PCH}(\text{CH}_2)_2\text{CH}_2$), 22.84 (s, $\text{CCH}_2\text{CH}_2\text{CH}_2$). IR: $\nu(\text{PO}) = 1123$ cm^{-1} . mp 138 °C.

$\text{Cy}_3\text{PO}\cdot(\text{HOO})_2\text{CMePh}$ (**12**)

$[\text{Cy}_3\text{PO}\cdot\text{H}_2\text{O}_2]_2$ (425 mg, 1.30 mmol) was dissolved in 3 mL of acetophenone (25.7 mmol) in a round bottom flask. Then, H_2O_2 (1.3 mL, 130 mmol) was added, and the solution was stirred for 4 h. The solution was concentrated *in vacuo* to about 3 mL, then allowed to crystallize. $\text{Cy}_3\text{PO}\cdot(\text{HOO})_2\text{CMePh}$ (**12**) was obtained in the form of colorless crystals (327 mg, 0.70 mmol, 54%).

$^{31}\text{P}\{^1\text{H}\}$ NMR (δ , CDCl_3), ^{31}P 58.31 (s); ^1H 11.89 (br. s, 2H, OOH), 7.59-7.56 (m, 2H, H_o), 7.38-7.33 (m, 2H, H_m), 7.31-7.27 (m, 1H, H_p), 1.94-1.80 (m, 15H, $\text{PCH}_{\text{ax}}\text{CH}_{\text{eq}}\text{CH}_{\text{eq}}$), 1.75-1.71 (m, 3H, $\text{PCH}(\text{CH}_2)_2\text{CH}_{\text{eq}}$), 1.66 (s, 3H, CH_3), 1.47-1.37 (m, 6H, PCHCH_{ax}), 1.30-1.20 (m, 9H, $\text{PCHCH}_2\text{CH}_{\text{ax}}\text{CH}_{\text{ax}}$); $^{13}\text{C}\{^1\text{H}\}$ 140.09 (s, C_i), 127.98 (s, C_o), 127.82 (s,

C_p), 125.94 (s, C_m), 110.18, (S, CCH_3), 34.68 (d, $^1J(^{31}P-^{13}C) = 60.5$ Hz, PC), 26.70 (d, $^3J(^{31}P-^{13}C) = 12.1$ Hz, PCHCH₂CH₂), 25.95 (d, $^2J(^{31}P-^{13}C) = 3.3$ Hz, PCHCH₂), 25.89 (d, $^4J(^{31}P-^{13}C) = 1.4$ Hz, PCH(CH₂)₂CH₂), 23.40 (CCH_3). IR: $\nu(PO) = 1123$ cm⁻¹. mp (decomp.) 100 °C.

Ph₂P(O)CH₂P(O)Ph₂•(HOO)₂CMe₂ (13)

In a round bottom flask Ph₂PCH₂PPh₂ (384 mg, 1 mmol) was dissolved in 60 mL of CH₂Cl₂. Then H₂O₂ (0.5 mL, 5 mmol) was added, and the solution was stirred for 1 h. The organic layer was collected in a separation funnel, and the solvent was removed *in vacuo*. The resulting white precipitate (Ph₂P(O)CH₂P(O)Ph₂) was dissolved in 5 mL of acetone, and after the addition of another 0.5 mL of H₂O₂, the sample was allowed to crystallize *via* slow evaporation of the solvent. Adduct **14** was obtained in the form of white, needle-like crystals (364 mg, 0.76 mmol, 76% yield).

NMR (δ , CDCl₃), $^{31}P\{^1H\}$ 30.33 (s); 1H 11.01 (br. s, 2H, OOH), 7.72-7.66 (m, 8H, H_o), 7.47-7.42 (m, 4H, H_p), 7.38-7.33 (m, 8H, H_m), 3.62 (t, $^3J(^{31}P-^1H) = 14.7$ Hz, 2H, PCH₂), 1.48 (s, 6H, CCH_3); $^{13}C\{^1H\}$ 132.21 (s, C_p), 131.07 (d, $^1J(^{31}P-^{13}C) = 107.0$ Hz, C_i), 130.86 (virtual quintet, $J(^{31}P-^{13}C) = 5.1$ Hz, C_o), 128.64 (virtual quintet, $J(^{31}P-^{13}C) = 6.1$ Hz, C_m), 109.21 (s, CCH_3), 21.26 (PCH₂), 20.63 (s, CCH_3).

NMR (δ , (CD₃)₂CO), $^{31}P\{^1H\}$ 26.63 (s); 1H 10.49 (br. s, OOH), 7.87-7.81 (ddd, $^3J(^{31}P-^1H) = 12.2$ Hz, $^3J(^1H-^1H) = 8.3$ Hz, $^4J(^1H-^1H) = 1.2$ Hz, H_o), 7.52-7.47 (td $^3J(^1H-^1H) =$

7.3 Hz, ${}^4J(^1\text{H}-^1\text{H}) = 1.2$ Hz, H_p), 7.43-7.38 (td ${}^3J(^1\text{H}-^1\text{H}) = 8.3$ Hz, ${}^3J(^1\text{H}-^1\text{H}) = 7.3$ Hz, H_m), 3.99 (t, ${}^2J(^{31}\text{P}-^1\text{H}) = 13.9$ Hz, $-\text{CH}_2-$), 1.36 (s, $-\text{CH}_3$); ${}^{13}\text{C}\{^1\text{H}\}$ 133.46 (d, ${}^1J(^{31}\text{P}-^{13}\text{C}) = 106.2$ Hz, C_i), 131.74 (s, C_p), 130.89 (virtual quintet 29.3 Hz, C_o), 128.38 (virtual quintet, 30.5 Hz, C_m), 108.34 (s, CH_3C), 20.43 (s, PCH_2), 20.25 (s, $-\text{CH}_3$). IR: $\nu(\text{PO}) = 1163.1$ cm^{-1} . mp (decomp.) 120 °C.

($\text{Ph}_2\text{P}(\text{O})\text{CH}_2\text{CH}_2\text{P}(\text{O})\text{Ph}_2$)•((HOO) $_2\text{CMe}_2$) $_2$ (**14**)

$\text{Ph}_2\text{P}(\text{O})\text{CH}_2\text{CH}_2\text{P}(\text{O})\text{Ph}_2$ (20 mg, 0.05 mmol) was dissolved in 0.5 mL of acetone (6.8 mmol) in a round bottom flask. Subsequently, H_2O_2 (0.1 mL, 1 mmol) was added and the solution was stirred for 1 h, then left to crystallize *via* slow evaporation of the solvent. Adduct **14** crystallized in the form of colorless, needle-like crystals (27 mg, 0.04 mmol, 84% yield).

NMR (δ , CDCl_3), ${}^{31}\text{P}\{^1\text{H}\}$ 38.78 (s); ^1H 11.34 (s, 2H, OOH), 7.71 (dd, 8H, ${}^3J(^{31}\text{P}-^1\text{H}) = 11.5$ Hz, ${}^3J(^1\text{H}-^1\text{H}) = 7.3$ Hz, H_o), 7.52 (t, 4H, ${}^3J(^1\text{H}-^1\text{H}) = 7.3$ Hz, H_p), 7.45 (dd, 8H, ${}^3J(^1\text{H}-^1\text{H}) = 11.5$ Hz, ${}^3J(^1\text{H}-^1\text{H}) = 7.3$ Hz, H_m), 2.52 (d, 4H, ${}^2J(^{31}\text{P}-^1\text{H}) = 2.5$ Hz, PCH_2-), 1.51 (s, 12H, $-\text{CH}_3$); ${}^{13}\text{C}\{^1\text{H}\} = 132.70$ (s, C_p), 130.68 (virtual triplet, $J(^{31}\text{P}-^{13}\text{C}) = 4.9$ Hz, C_o), 129.86 (d, ${}^1J(^{31}\text{P}-^{13}\text{C}) = 100.0$ Hz, C_i), 129.21 (virtual triplet, $J(^{31}\text{P}-^{13}\text{C}) = 6.1$ Hz, C_m), 109.38 (s, CH_3C), 21.08 (virtual triplet, $J(^{31}\text{P}-^{13}\text{C}) = 33.0$ Hz, PCH_2), 20.68 (s, $-\text{CH}_3$). IR: $\nu(\text{PO}) = 1148$ cm^{-1} . mp (decomp.) 80 °C.

(Ph₂P(O)CH₂CH₂P(O)Ph₂)•((HOO)₂CEt₂)₂ (**15**)

Ph₂P(O)CH₂CH₂P(O)Ph₂ (20 mg, 0.05 mmol) was dissolved in 0.3 mL of pentanone (2.8 mmol) in a round bottom flask. Subsequently, H₂O₂ (0.1 mL, 1 mmol) was added and the solution was stirred for 1 h, then left to crystallize *via* slow evaporation of the solvent. Adduct **15** crystallized in the form of colorless, needle-like crystals (22 mg, 0.04 mmol, 78% yield).

NMR (δ , CDCl₃), ³¹P{¹H} 39.42 (s); ¹H 10.81 (virtual doublet, $J(^{31}\text{P}-^1\text{H}) = 82.2$ Hz, 2H, OOH), 7.81-7.75 (m, 8H, H_o), 7.58-7.53 (m, 4H, H_p), 7.51-7.46 (m, 8H, H_m), 2.66 (d, $^3J(^{31}\text{P}-^1\text{H}) = 2.7$ Hz, 2H, PCH₂), 1.75 (q, $^3J(^1\text{H}-^1\text{H}) = 7.6$ Hz, 8H, CH₂CH₃), 1.00 (t, $^3J(^1\text{H}-^1\text{H}) = 7.6$ Hz, 12H, CH₂CH₃); ¹³C{¹H} 132.74 (s, C_p), 130.67 (virtual quintet, $J(^{31}\text{P}-^{13}\text{C}) = 5.1$ Hz, C_o), 129.61 (d, $^1J(^{31}\text{P}-^{13}\text{C}) = 102.8$ Hz, C_i), 129.23 (virtual quintet, $J(^{31}\text{P}-^{13}\text{C}) = 6.1$ Hz, C_m), 114.13 (s, CCH₃), 21.81 (s, CH₂CH₃), 21.05 (virtual triplet, $J(^{31}\text{P}-^{13}\text{C}) = 33.0$ Hz, PCH₂), 7.99 (s, CH₃). IR: $\nu(\text{PO}) = 1150$ cm⁻¹. mp (decomp.) 82 °C.

CHAPTER IV

CHARACTERIZATION OF THE ADDUCTS $R_3PO \cdot (HOO)_2CR'R''^*$

Introduction

It is known that acetone and hydrogen peroxide can form triacetone triperoxide (TATP) and other oligomers in the presence of acid, which can be explosive in the solid form.²⁶⁻²⁷ Because both acetone and hydrogen peroxide are involved in the synthesis of the first few adducts, it was important to have analytical tools for determining the identity of the product in solution, prior to crystallization. NMR spectroscopy is especially useful in this respect, and attention is given to some of these characterization data, as they can be used diagnostically during the synthesis, prior to isolation of the product.

In an FT-IR spectrum, the characteristic peroxide band $\nu(O-H)$ is easily differentiable from the broad water band $\nu(O-H)$. Therefore, IR spectroscopy can be used as a quick analytical check for confirming the absence of water in the material prior to applying the adduct in organic reactions.

Single crystal X-ray crystallography allows for exact structural determination of these adducts, as well as providing information regarding the phosphine oxide to

* Reproduced with permission from "Hydrogen Peroxide and Di(hydroperoxy)propane Adducts of Phosphine Oxides as Stoichiometric and Soluble Oxidizing Agents" Ahn, S. H.; Cluff, K. J.; Bhuvanesh, N.; Blümel, J. *Angew. Chem.* **2015**, *127*, 13539-13543. Copyright Wiley-VCH Verlag GmbH & Co. KGaA.

(HOO)₂CR'R" ratio. A trend with respect to the elongation of the P=O bond length is also observed with the increase of the number of hydrogen bonds and their strengths.

The characteristic signals in each of these analytical methods are unique to the R₃PO•(HOO)₂CR'R" adducts. Thus, the properties of the newly discovered adducts are studied *via* multinuclear NMR spectroscopy, single crystal X-ray crystallography and IR spectroscopy, and the results of these analyses are described in detail.

Results and Discussion

All adducts **4-15** have been obtained in the form of large single crystals, and they have been characterized with single crystal X-ray crystallography (Figure 4.1, Figure 4.2).

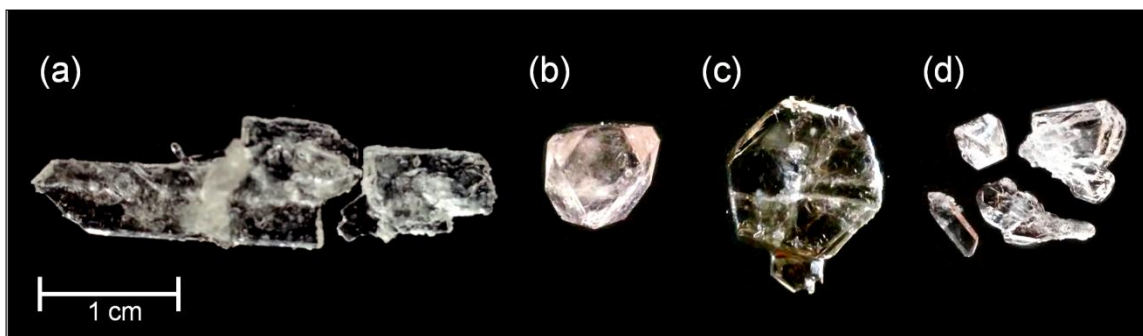


Figure 4.1. Large single crystals of (a) **4**, (b) **9**, (c) **10**, and (d) **11**.

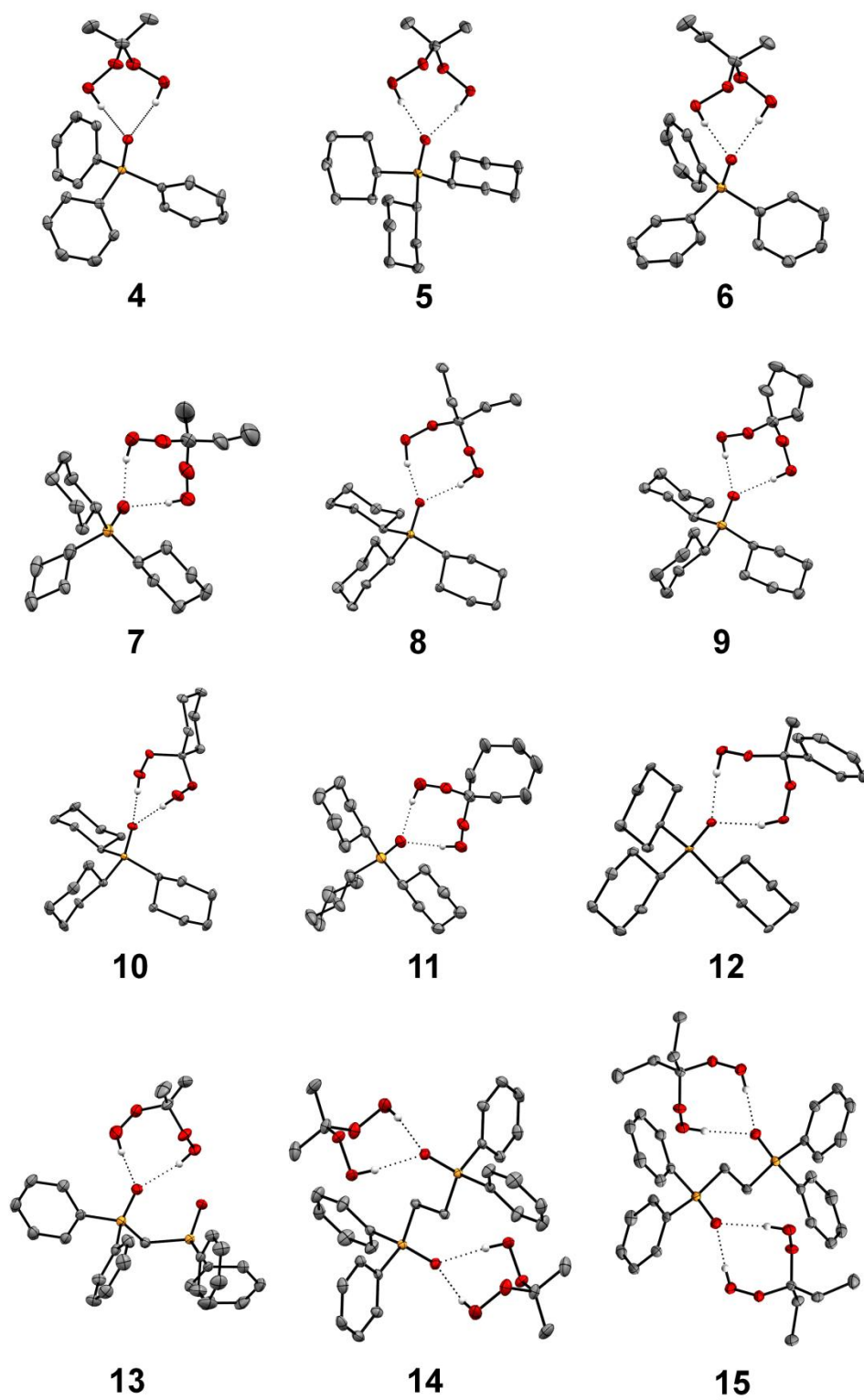


Figure 4.2. Single crystal X-ray structures of adducts **4-15**.²⁸⁻⁴⁰

For monodentate phosphine oxides, X-ray structures of the adducts **4-12**²⁸⁻³⁷ confirm that each P=O group forms two hydrogen bridges to one (HOO)₂CR'R" moiety. This means that there are two active oxygen atoms per P=O group, and thus the molar ratio of active peroxide is twice as high as for the H₂O₂ adducts presented previously.^{6,18} This is also true for the bidentate dppe dioxide. Each P=O group forms two hydrogen bonds, with both (HOO)₂CMe₂ (**14**)³⁸ and (HOO)₂CEt₂ (**15**).³⁹

Regarding the dppm dioxide, however, only one of the two P=O groups is bonded to the (HOO)₂CMe₂ moiety (**13**).⁴⁰ The two P=O groups are only separated by one methylene group, and thus the interaction with a second (HOO)₂CMe₂ unit may be sterically hindered. The distances between the two P=O oxygen atoms and the terminal oxygen atom of one OOH group are practically identical with 2.816 and 2.817 Å (Figure 4.3). Therefore, one could imagine that the hydrogen atom interacts with both P=O oxygen atoms equally.

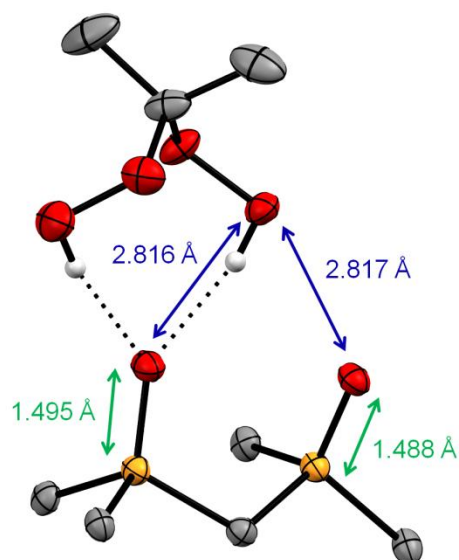


Figure 4.3. X-ray structure of **13** with corresponding bond distances. Only the hydrogen-bonded H atoms and *ipso* carbon atoms of the phenyl rings are shown for clarity.⁴⁰

However, the P=O bond lengths differ. The P=O bond of the group carrying the adduct is lengthened to 1.495 Å, while the free P=O bond remains in the typical range of undisturbed P=O bond lengths with 1.488 Å, and thus the interaction of the proton with both P=O groups is not likely in the solid state.¹⁷ As for adducts **4-12** and **14-15**, a significant elongation of the P=O bond is observed between neat phosphine oxide and adducts as a result of hydrogen bonding (Table 4.1).

Table 4.1. Comparison of the P=O bond lengths of the pure phosphine oxides Ph₃PO, Cy₃PO, Ph₂P(O)CH₂P(O)Ph₂ and Ph₂P(O)CH₂CH₂P(O)Ph₂ with the adducts **4-15**.

| Species | P=O bond length (Å) | Δ Bond length |
|---|-------------------------------|---------------|
| 4 | 1.502 | +0.023 |
| 5 | 1.507 | +0.017 |
| 6 | 1.507/1.505 | +0.017/0.015 |
| 7 | 1.510 | +0.020 |
| 8 | 1.508 | +0.018 |
| 9 | 1.513 | +0.023 |
| 10 | 1.512 | +0.022 |
| 11 | 1.505 | +0.015 |
| 12 | 1.510 | +0.020 |
| 13 | 1.488/1.495 average: 1.492 | +0.001 |
| 14 | 1.505 | +0.015 |
| 15 | 1.501 | +0.011 |
| Ph ₃ PO | 1.479 ⁴¹ | - |
| Cy ₃ PO | 1.490 ⁴² | - |
| Ph ₂ P(O)CH ₂ P(O)Ph ₂ | 1.491 ⁴³ | - |
| Ph ₂ P(O)CH ₂ CH ₂ P(O)Ph ₂ | average: 1.490 ⁴⁴ | - |

In determining whether the reaction product is safe to isolate and crystallize, ¹³C NMR spectroscopy is especially useful, as the signal of the quaternary carbon nucleus in the (HOO)₂CR'R'' moieties occurs in a narrow range and unique region (108-120 ppm) of the carbon spectrum and can therefore be used as a diagnostic signal (Figure 4.4,

Table 4.2).¹⁸ In the case of shock-sensitive DADP (diacetone diperoxide) or TATP, the quaternary peak appears more upfield shifted, at about 105 ppm.²⁶

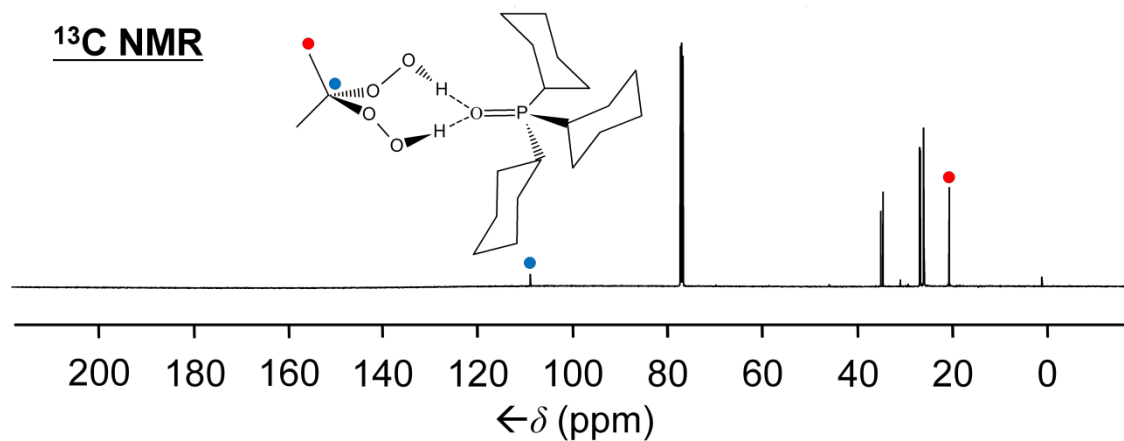


Figure 4.4. ¹³C NMR spectrum of Ph₃PO•(HOO)₂CMe₂ in CDCl₃.

Table 4.2. ¹³C NMR Chemical shifts of the quaternary carbon signals of the adducts R₃PO•(HOO)₂CR'R'' in CDCl₃.

| Adduct | C _q (ppm) | Adduct | C _q (ppm) |
|----------|----------------------|-----------|----------------------|
| 4 | 109.28 | 10 | 109.52 |
| 5 | 108.91 | 11 | 114.34 |
| 6 | 111.56 | 12 | 110.18 |
| 7 | 111.26 | 13 | 109.21 |
| 8 | 113.76 | 14 | 109.38 |
| 9 | 120.92 | 15 | 114.13 |

The ^{31}P NMR signals of the adducts $\text{R}_3\text{PO}\cdot(\text{HOO})_2\text{CR}'\text{R}''$ are shifted downfield as compared to the neat phosphine oxides R_3PO (Table 4.3).¹⁸ This downfield shift is caused by the decrease in electron density around the phosphorus nucleus of the $\text{P}=\text{O}$ group, as the electrons get pulled towards the oxygen atom to support the hydrogen bonds. The change in the ^{31}P chemical shift is most significant for Cy_3PO , with $\Delta\delta$ being larger than 6 ppm in most cases.

Table 4.3. ^{31}P NMR chemical shifts for the adducts $\text{R}_3\text{PO}\cdot(\text{HOO})_2\text{CR}'\text{R}''$ and the corresponding neat R_3PO in CDCl_3 . The differences are given as $\Delta\delta$ (ppm).

| Adduct | $\delta(^{31}\text{P})$ (ppm) | $\Delta\delta$ (ppm) |
|--|-------------------------------|----------------------|
| 4 | 34.74 | 5.64 |
| 5 | 55.59 | 5.68 |
| 6 | 30.52 | 1.42 |
| 7 | 58.77 | 8.86 |
| 8 | 58.35 | 8.44 |
| 9 | 57.14 | 7.23 |
| 10 | 58.01 | 8.10 |
| 11 | 56.63 | 6.72 |
| 12 | 58.31 | 8.40 |
| 13 | 30.33 | 5.47 |
| 14 | 38.78 | 6.10 |
| 15 | 39.42 | 6.74 |
| Ph_3PO | 29.16 | - |
| Cy_3PO | 49.91 | - |
| $\text{Ph}_2\text{P}(\text{O})\text{CH}_2\text{P}(\text{O})\text{Ph}_2$ | 24.86 | - |
| $\text{Ph}_2\text{P}(\text{O})\text{CH}_2\text{CH}_2\text{P}(\text{O})\text{Ph}_2$ | 32.68 | - |

Many of these adducts could easily be obtained as large single crystals (Figure 4.1). This rare opportunity could be seized to perform single crystal solid-state NMR measurements of **4**. The chemical shift anisotropy (CSA) obtained from the span of the ^{31}P wideline NMR spectrum of polycrystalline **4** amounts to 166 ppm (Figure 4.5).¹⁸

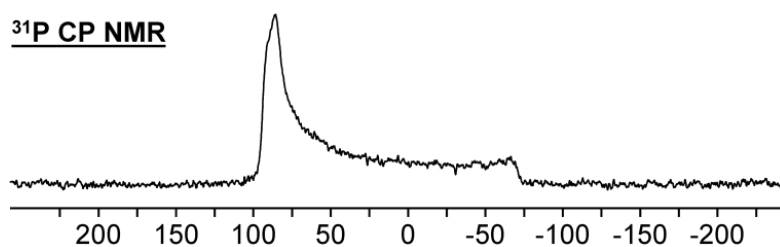


Figure 4.5. ^{31}P CP wideline NMR spectrum of polycrystalline **4**. The CSA, defined as the span of the signal, $\delta_{11}-\delta_{33}$, amounts to 166.3 ppm. $\delta_{11} = 95.4$, $\delta_{22} = 85.0$, $\delta_{33} = -70.9$, $\delta_{\text{iso}} = 36.5$ ppm.¹⁸

Figure 4.6 displays the ^{31}P CP spectra of a single crystal of **4** recorded with different random orientations. The random orientations were obtained by ejecting and reinserting the rotors into the probehead. Two resonances, corresponding to two magnetically inequivalent ^{31}P nuclei in the unit cell, are obtained in most cases. The two resonances can overlap by accident, but this event is statistically less favored. The chemical shift changes of the two signals with the orientation of the crystal in the external magnetic field are different, as expected and described for other cases.^{17,45}

³¹P NMR (161.976 MHz)

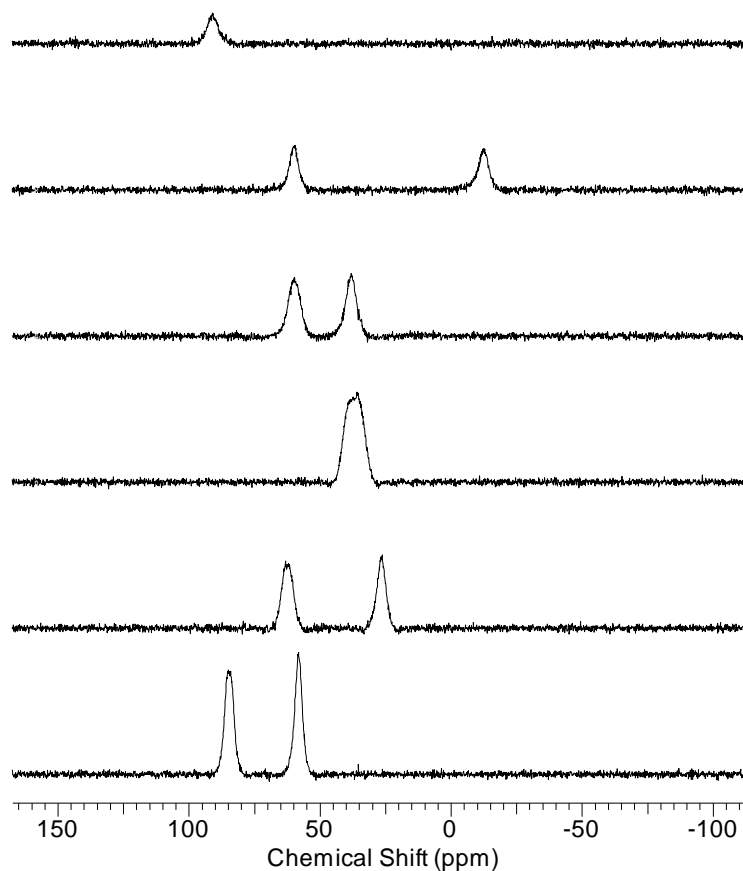


Figure 4.6. ³¹P CP NMR spectra of a large single crystal of **4** at different random orientations with respect to the external magnetic field.

For adduct **5**, all protons of the adducts are accounted for in the ¹H NMR spectra, and all signals have been successfully assigned with the help of 2-dimensional ¹³C,¹H COSY NMR spectroscopy (Figure 4.7, Figure A.18). While the peroxide protons appear downfield shifted to about 11.5 ppm (Table 4.4), the absence of any obvious water signal corroborates the assumption that the sample is water-free (Figure 4.7).

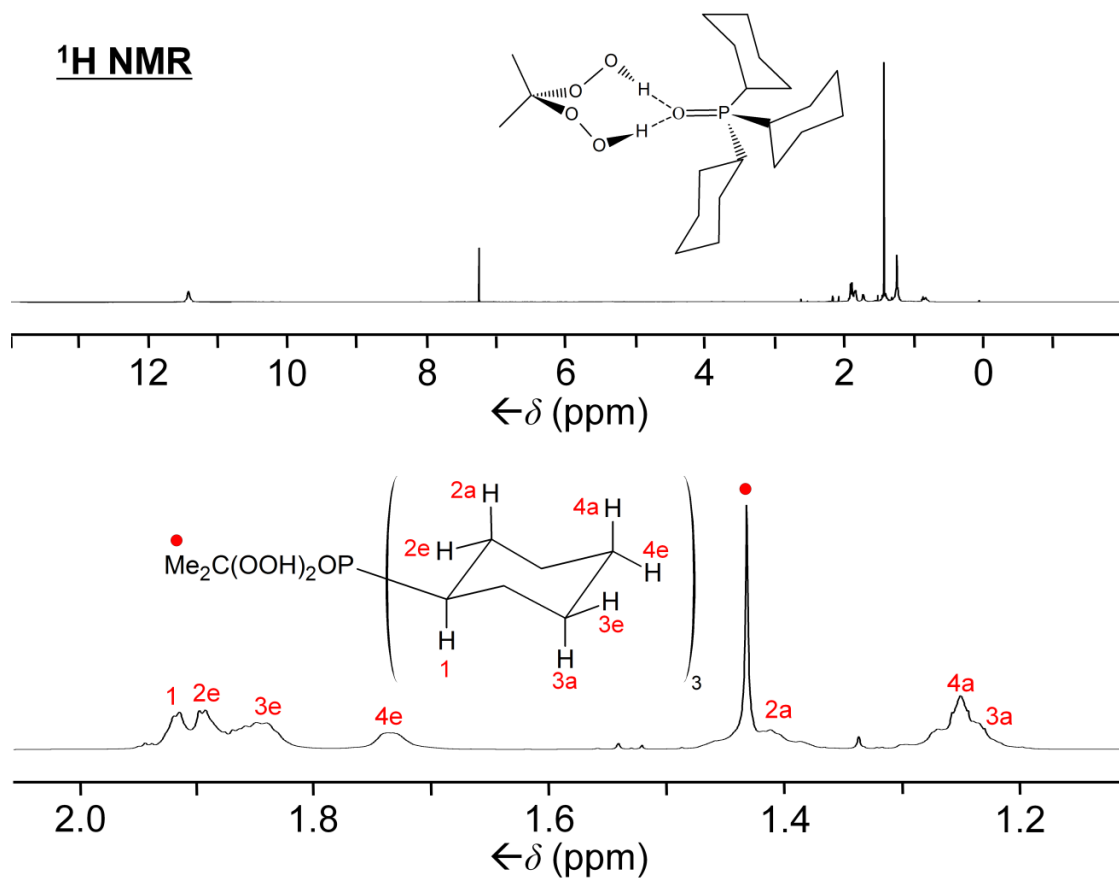


Figure 4.7. ¹H NMR spectrum of **5** in CDCl₃, with complete signal assignment. The peroxide proton peak is visible at 11.45 ppm.

Table 4.4. ¹H Chemical shifts of the peroxide protons of the adducts **4-15**.

| Adduct | $\delta(^1\text{H})$ OOH (ppm) | Adduct | $\delta(^1\text{H})$ OOH (ppm) |
|----------|--------------------------------|-----------|--------------------------------|
| 4 | 11.15 | 10 | 10.66 |
| 5 | 11.45 | 11 | 11.57 |
| 6 | 11.38 | 12 | 11.89 |
| 7 | 10.90 | 13 | 10.73 |
| 8 | 10.82 | 14 | 11.28 |
| 9 | 11.61 | 15 | 10.81 |

Additionally, the IR spectra of **4-15** show no H₂O hydroxyl stretching band at 3400 cm⁻¹ (Figure B.5-Figure B.18), and thus it can be confirmed that no water is present in these adducts.⁶ Instead, all adducts display a broad band around 3200 cm⁻¹, corresponding to the hydroperoxy stretching band $\nu(\text{O-H})$ (Table 4.5).

Table 4.5. Stretching bands $\nu(\text{O-H})$, $\nu(\text{C-O})$, $\nu(\text{O-O})$ and comparison of the $\nu(\text{P=O})$ IR values of the pure phosphine oxides with those of the adducts **4-15**, given as $\Delta\nu(\text{P=O})$.

| Species | $\nu(\text{O-H})$ (cm ⁻¹) | $\nu(\text{P=O})$ (cm ⁻¹) | $\nu(\text{C-O})$ (cm ⁻¹) | $\nu(\text{O-O})$ (cm ⁻¹) ⁴⁶ | $\Delta\nu(\text{P=O})$ (cm ⁻¹) |
|---|--|--|--|--|--|
| 4 | 3256 | 1152 | 1118 | 885 | 30 |
| 5 | 3192 | 1125 | 1099 | 891, 856 | 32 |
| 6 | 3250 | 1142 | 1118 | 889, 851 | 40 |
| 7 | 3196 | 1124 | 1101 | 893, 854 | 33 |
| 8 | 3194 | 1126 | 1103 | 891, 858 | 31 |
| 9 | 3167 | 1123 | 1101 | 891, 860 | 34 |
| 10 | 3196 | 1123 | 1103 | 893, 860 | 34 |
| 11 | 3186 | 1123 | 1101 | 891, 856 | 34 |
| 12 | 3176 | 1123 | 1101 | 889, 851 | 34 |
| 13 | 3291 | 1163 | 1099 | 871 | 25 |
| 14 | 3242 | 1148 | 1097 | 872 | 24 |
| 15 | 3275 | 1150 | 1097 | 858 | 22 |
| Ph ₃ PO | - | 1182 | - | - | - |
| Cy ₃ PO | - | 1157 ¹ | - | - | - |
| Ph ₂ P(O)CH ₂ P(O)Ph ₂ | - | 1188 | - | - | - |
| Ph ₂ P(O)CH ₂ CH ₂ P(O)Ph ₂ | - | 1172 | - | - | - |

Representative FT-IR spectra of **6** and **7** are shown in Figure 4.8. In general, the P=O band is observed around 1150 cm^{-1} for aryl phosphine oxide adducts and 1120 cm^{-1} for Cy_3PO adducts (Table 4.5).

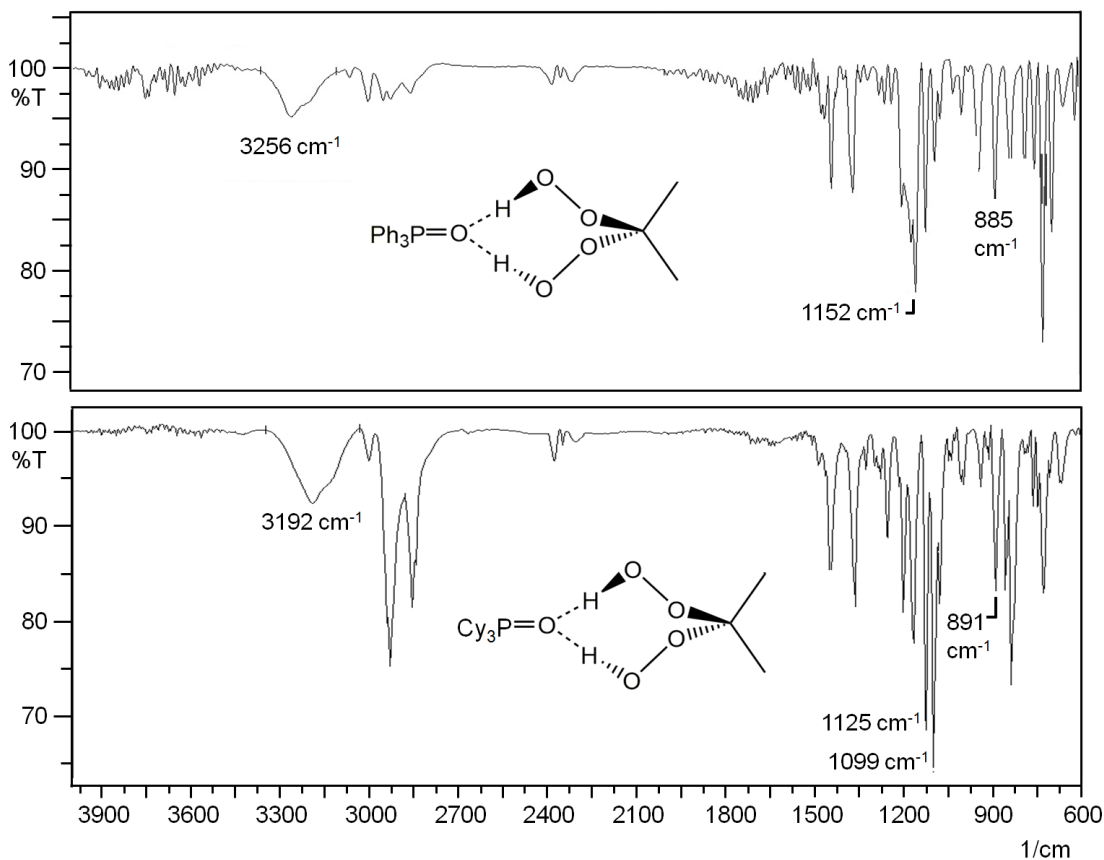


Figure 4.8. Representative IR spectra of adduct **4** (top) and **5** (bottom).

The $\nu(\text{P}=\text{O})$ bands of the adducts **4-15** are lower in frequency as compared to the neat R_3PO analogs, due to the P=O bond strength being weakened by the hydrogen bonds. The change in wavenumber is similar for most of the R_3PO adducts incorporating one PO group, with a shift of $30\text{-}34\text{ cm}^{-1}$. The red shift is less significant for the adducts

13-15 with two PO bonds each, which agrees with the smaller change in P=O bond lengths of the adducts **13-15** (Table 4.1). The $\nu(\text{P}=\text{O})$ stretching bands for Cy_3PO adducts often overlap with strong $\nu(\text{C}-\text{O})$ bands that occur around 1101 cm^{-1} . Finally, the $\nu(\text{O}-\text{O})$ stretching frequency can be observed as sharp signals around 890 and 860 cm^{-1} , as expected (Table 4.5), the only problem being potential overlap with other fingerprint IR absorptions in this region.⁴⁶⁻⁴⁷

Conclusion

^{13}C NMR spectroscopy is an excellent tool for confirming the synthesis of a new adduct prior to its isolation. The diagnostic signal at $108\text{-}120\text{ ppm}$ in CDCl_3 is unique to a quaternary carbon bound to two peroxide functionalities, and yet is different enough from the quaternary carbon of the shock-sensitive oligomers DADP or TATP. At this point, no specific trend is observed between the changing R' and R'' groups of the moiety $(\text{HOO})_2\text{CR}'\text{R}''$ and the shift in the quaternary signal.

Single crystal X-ray crystallography provides indisputable proof that the adducts are systematic molecule-type assemblies with an exact ratio between the phosphine oxide groups and the $(\text{HOO})_2\text{CR}'\text{R}''$ moieties. Significant P=O bond elongation is observed in connection with the formation of multiple hydrogen bonds.

The weakened P=O bond strength is also observed in the IR spectra, as the $\nu(\text{P}=\text{O})$ bands undergo red shifts of around 30 cm^{-1} . Along with the ^1H NMR peaks at

10-11 ppm, the peroxide $\nu(\text{O-H})$ stretching bands around 3200 cm^{-1} in the IR spectra confirm the presence of peroxide protons in the adduct molecules.

CHAPTER V

SOLUBILITY STUDY*

Introduction

In Chapter II, it was mentioned that one of the most important advantages of the hydrogen peroxide adducts $[R_3PO \cdot H_2O_2]_2$ with respect to their application as oxidizing agents is that they are very soluble in organic solvents, rendering biphasic reaction mixtures obsolete. The same is true for the adducts $R_3PO \cdot (HOO)_2CR'R''$ (R, R', R'' = alkyl, aryl), and therefore the solubilities of selected adducts in common organic solvents were quantified.

Results and Discussion

The solubilities of the adducts in organic solvents are measured by dissolving 20 mg of each adduct in the determined minimum amount of solvent, and measuring the mass of the solvent upon complete solvation. The results of the solubility tests for the representative adducts **4-11** are summarized in Figure 5.1. The solubilities are remarkably high in chloroform and dichloromethane, but even in aromatic solvents such as toluene and benzene, the solubilities are substantial.

* Reproduced with permission from "Hydrogen Peroxide and Di(hydroperoxy)propane Adducts of Phosphine Oxides as Stoichiometric and Soluble Oxidizing Agents" Ahn, S. H.; Cluff, K. J.; Bhuvanesh, N.; Blümel, J. *Angew. Chem.* **2015**, *127*, 13539-13543. Copyright Wiley-VCH Verlag GmbH & Co. KGaA.

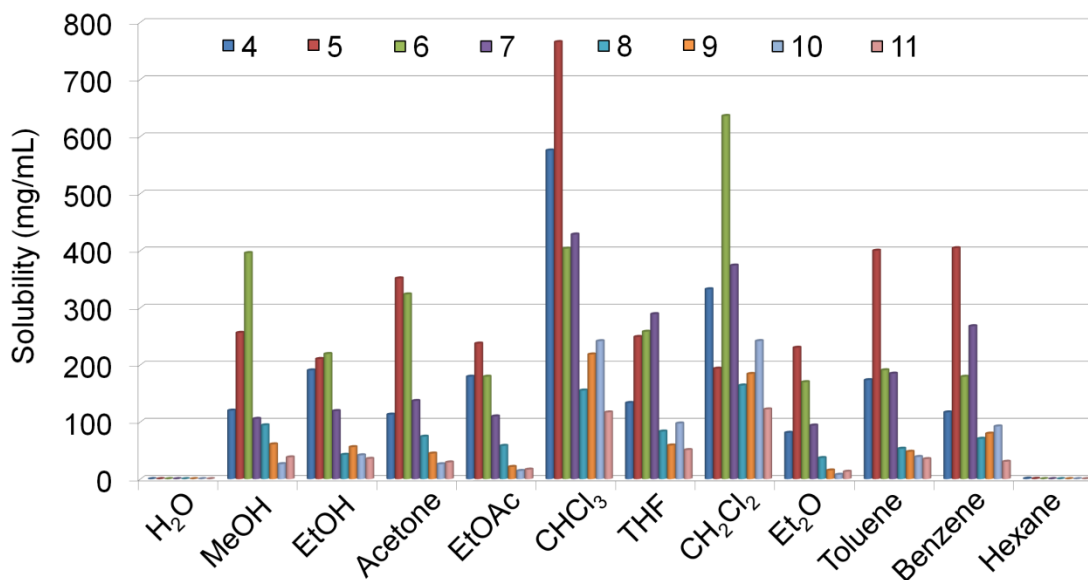


Figure 5.1. Solubilities of the adducts **4-11** in common organic solvents.

The total concentration of active peroxide in a sample solution can be increased even more by dissolving two or more adducts with different phosphine oxides in the same solution. For instance, 20 mg of **6** and 20 mg of **7** were both dissolved together in a minimum amount of CH₂Cl₂ (84 mg, 0.063 mL). Therefore, in this mixture, **6** and **7** each display a solubility of 317 mg/mL, for a total of 3.0 M concentration of active peroxide in CH₂Cl₂. When compared to the individual solubilities of 636 mg/mL of **6** and 374 mg/mL of **7** in CH₂Cl₂ (Figure 5.1), the solubilities of the mixture of **6** and **7** appear reduced. However, the 3.0 M concentration of active peroxide is comparable to that of **7** (3.18 M in CH₂Cl₂), and significantly increased compared to **6** (1.79 M in CH₂Cl₂). Therefore, the mixture contains overall a much higher concentration of peroxide than each single component by itself.

In an analogous experiment, 19 mg of **7** were dissolved in a minimum amount of CH₂Cl₂ (27 mg, 0.05 mL). To this completely saturated solution, a powder sample of **6** was added in very small portions and the mixture was swirled to facilitate dissolution. The process was continued until the powder did not dissolve anymore, at which point a total of 17 mg of **6** had been added. In this mixture, the solubility of **6** was 333 mg/mL and **7** was 374 mg/mL, for a combined concentration of 3.4 M active peroxide in CH₂Cl₂. This is in the same order of magnitude as the 35 wt% aqueous H₂O₂, with a 10 M concentration of active peroxide.

As evidenced from these two tests, the saturation with one adduct does not completely prohibit the dissolution of another adduct in the same sample, although the solubility of the second adduct may be decreased as compared with its solubility in pristine solvent.

Conclusion

Similar to the H₂O₂ adducts of phosphine oxides, the adducts of the type R₃PO•(HOO)₂CR'R'' (R, R', R'' = alkyl, aryl) display high solubility in common organic solvents. The concentration of active peroxide can be increased even more by combining adducts of multiple different phosphine oxides. When applied to organic reactions, these adducts are very appealing, as the reactions can be performed in one phase, and the volume of solvent can be decreased to reduce costs.

CHAPTER VI

SHELF LIFE AND DECOMPOSITION STUDY*

Introduction

Aqueous H₂O₂ gradually decomposes to form oxygen gas and H₂O. Therefore, aqueous H₂O₂ is often administered in excess because the oxidant decomposes at unpredictable rates, and thus the concentration at any given time is unknown. For applications requiring exact stoichiometry, the solution has to be titrated prior to use.⁷

In the case of the adducts R₃PO•(HOO)₂CR'R" (R, R', R" = alkyl, aryl) the hydrogen bonds between the peroxide and the phosphine oxide groups do not break easily, and therefore the phosphine oxides act as stable, solid carriers of the peroxide. However, in order to ensure accurate stoichiometry at the time of use, the study of stability and shelf life of the adducts is essential. Decomposition of these adducts occurs *via* the release of oxygen gas from the peroxide functionality.^{8c,48} In addition to shelf life, the safety of these adducts during decomposition was of interest, and thus the adducts were exposed to mechanical and thermal stress on a small scale.

In this chapter, the results of the decomposition tests are reported, and a quantitative NMR (QNMR) method is described in which ³¹P NMR spectroscopy is utilized to determine the % decomposition of active peroxide in the adducts over time.⁴⁹

* Reproduced with permission from "Hydrogen Peroxide and Di(hydroperoxy)propane Adducts of Phosphine Oxides as Stoichiometric and Soluble Oxidizing Agents" Ahn, S. H.; Cluff, K. J.; Bhuvanesh, N.; Blümel, J. *Angew. Chem.* **2015**, *127*, 13539-13543. Copyright Wiley-VCH Verlag GmbH & Co. KGaA.

In order to determine the number of active peroxide groups remaining in a sample of $R_3PO \cdot (HOO)_2CR'R''$, a known mass of the adduct was used as an oxidant for PPh_3 , and the degree of its oxidation was observed through NMR spectroscopy. Oxidation of PPh_3 was chosen for strategic reasons: PPh_3 is solid and air-stable even in most solvents, and therefore it is easy to handle and any oxidation is not due to admission of air, but only to the oxidant. When dissolved in a solvent together with the above adduct, oxidation of PPh_3 occurs immediately, with $OPPh_3$ being the sole product. PPh_3 and $OPPh_3$ display two far apart, distinct peaks in the ^{31}P NMR spectrum which are easy to identify and integrate.^{49a-c}

A series of ^{31}P NMR spectra is collected following the addition of adduct to a weighed excess of PPh_3 . The samples are carefully prepared so that the concentration of each analyte exceeds 20 mM.⁵⁰ The proton decoupler is turned off, because the Nuclear Overhauser Effect (NOE) can alter the peak intensities.^{49d} Three peaks occur in the spectrum, belonging to the carrier phosphine oxide of the spent adduct, $OPPh_3$ and the remaining PPh_3 (Figure 6.1). A capillary insert with neat $ClPPh_2$ as the chemical shift standard is centered in the NMR tube (Figure 6.2).^{6,50-51} $ClPPh_2$ is an ideal standard, as its peak occurs at 81.92 ppm, clear of the region of interest.^{6,49a,52}

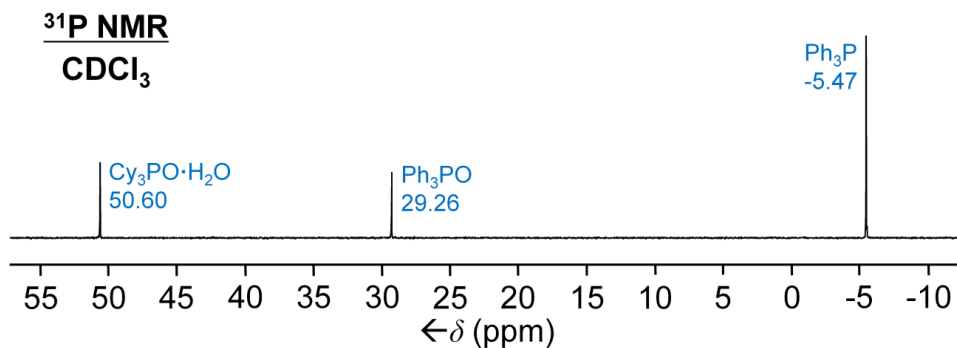


Figure 6.1. ³¹P NMR spectrum obtained following the partial oxidation of an excess of PPh₃ with **5**.



Figure 6.2. Capillary insert with ClPPh₂ centered inside a 5 mm NMR tube.

By integrating the OPPh₃ and PPh₃ peaks, one can calculate what percentage of the original PPh₃ has been oxidized. The number of moles of oxidized PPh₃ corresponds to the number of moles of active peroxide groups that remain in the applied adduct after long term storage. Comparison of this number with the mole of peroxide that the

measured amount of pristine adduct contains, provides the degree of decomposition of the adduct.

For an accurate determination of the integrals it is important that the signals are defined by a sufficient number of data points. A representative ^{31}P NMR point spectrum of a sample after PPh_3 oxidation (Figure 6.3) shows that the signals are defined by a sufficient number of data points, ensuring the quality of the integration. Since the intensity of a signal, and therewith the integral, when comparing the intensities of different signals, is calculated by adding the discrete height values of the data points, it is important that each peak incorporates a sufficient number of data points.^{49d} The digital resolution used typically for determining the integrals in this project is 0.56 Hz per point (65536 data points for a sweep width of 36764.71 Hz). Furthermore, it is important to allow for enough area around the signals when choosing the boundaries for their integration. Figure 6.3 shows representative signals with a sufficient number of data points and ample space around them. The integration extends 100 Hz in each direction from the center of PPh_3 and OPPh_3 peaks. It has been previously reported that integration should be performed over an area of 20-30 times the linewidth of the signal of interest for accurate analysis.^{49a,49d}

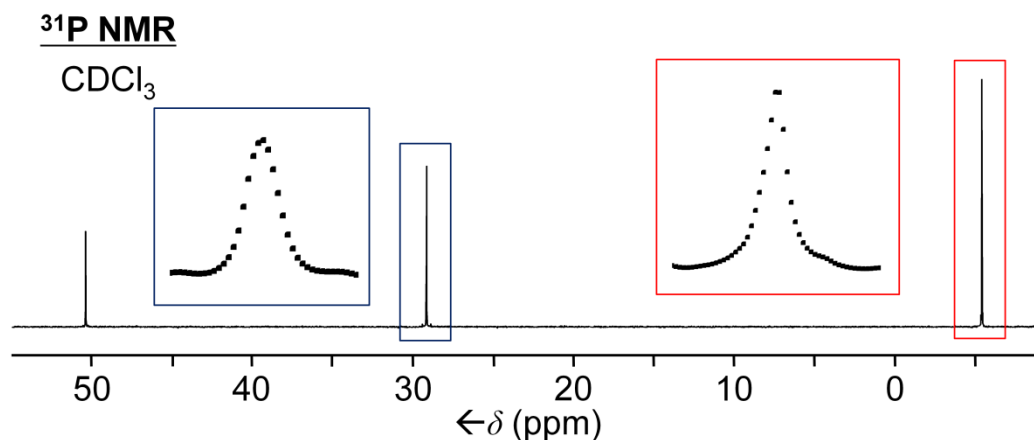


Figure 6.3. Point display of the ³¹P NMR signals obtained after the partial oxidation of PPh₃ with **5**.

This quantitative NMR method was furthermore tested against multiple criteria to validate its consistency. Specifically, it was tested whether the following factors influenced the integration of the signals: (1) the depth of insertion of the sample into the probehead, (2) the spectral range or sweep width, and (3) the applied relaxation delay. For checking factor (1), the sample is placed in three different positions within the probehead so that the bottom of the NMR tube would be 1.5 cm (A), 1.0 cm (B), and 0.5 cm (C) below the region with the optimal RF (radio frequency) coil transmission and reception. Figure 6.4 indicates the bottom of the NMR tube in the sample gauge with a red line, and the area that the coil would stretch over in the probehead with a blue rectangle. The same sample was placed at the different positions into the probehead and ³¹P NMR spectra were measured with varying spectral windows and relaxation delays ranging from 1 to 40 seconds.

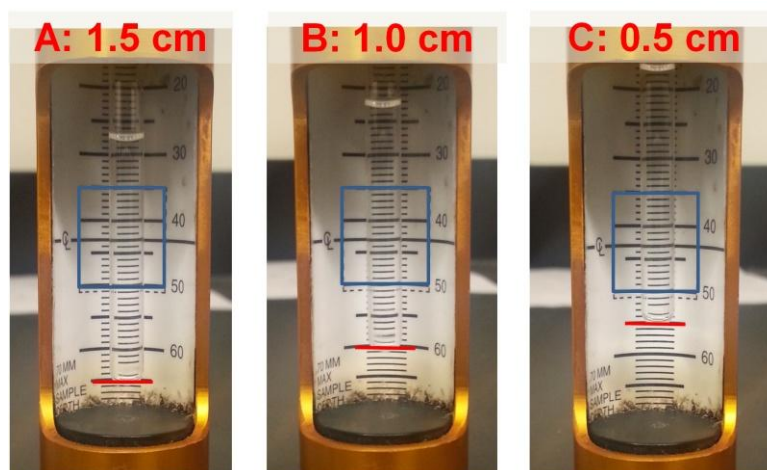


Figure 6.4. Three different positions of the 5 mm NMR tube inside the sample gauge, representing the probehead dimensions. For detailed description see text.

Collecting NMR spectra of the sample at different positions within the probehead tests for equal RF homogeneity for the solubilized adduct, the initial PPh_3 and the product OPPh_3 . Theoretically, if all components are homogeneously dispersed throughout the CDCl_3 solution, changing the extent of the sample tube that is exposed to the region with optimal RF homogeneity should not change the ratio between PPh_3 and OPPh_3 . However, the response of the various substances to the RF excitation could be different, thus leading to a deviating integral.

When the spectral window is changed by moving it, the maximal intensity of the excitation pulse, which is in the center of the spectrum, is also moved. The closer the maximal intensity of the excitation pulse is to a signal of the sample, the more intense it will be in the spectrum (Figure 6.5).^{49a}

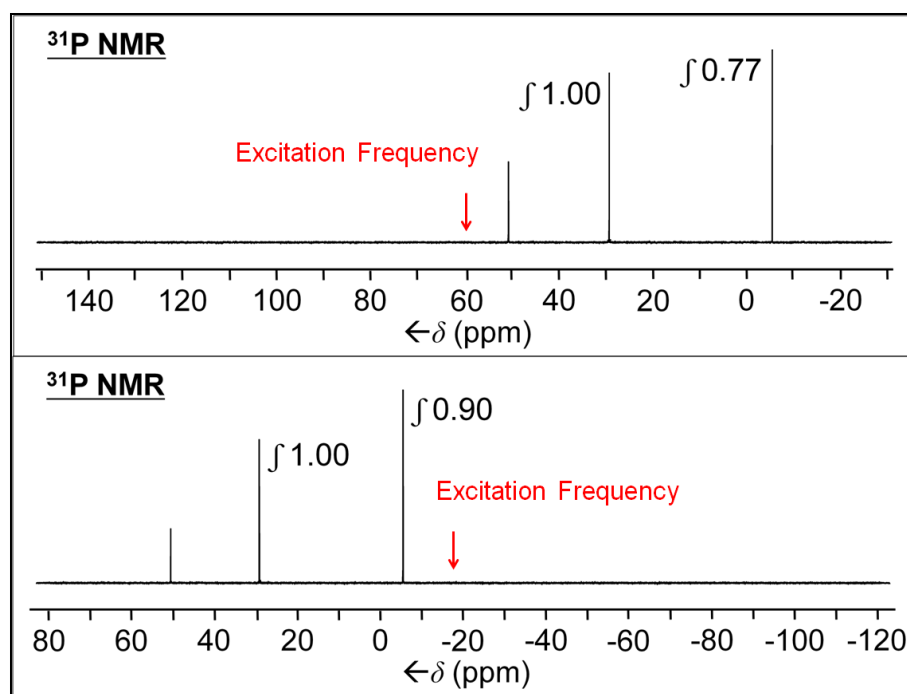


Figure 6.5. ^{31}P NMR spectra obtained following the oxidation of an excess of PPh_3 with **5**. The change in the integrals with the change of the center of the excitation pulse is demonstrated.

The different ^{31}P nuclei in a sample require different relaxation times after a RF pulse is applied. Optimally, a subsequent pulse would not be applied until each nucleus is fully relaxed again. In case the next pulse is applied before the magnetization of one sort of nuclei is returned to the Boltzmann distribution equilibrium, it would reach eventually a steady state situation where the intensity of the signal does not show to its full extent. For maximum integration accuracy, all magnetizations of all species need to entirely return to equilibrium. Therefore, in order to obtain correct integral ratios between the PPh_3 and OPPh_3 peaks, it is paramount that the relaxation delay chosen is longer than the relaxation time that the involved nuclei require.^{49a,49d,52}

Results and Discussion

The decomposition temperatures of neat $(\text{HOO})_2\text{CR}'\text{R}''$ adducts range from 70 to 150 °C (Table C.1). Prior to recording the actual melting points, the adducts have been tested regarding their thermal stability by exposing them to gradually increasing temperatures in an oil bath to expedite decomposition. It should be noted that no explosive TATP or other explosive oligomers are formed during this process. The representative adducts **4** and **5** have also been tested by applying mechanical stress. No sudden release of oxygen occurred during forceful grinding or hammering of the pure powders. This may be due to the low weight% of active oxygen in the molecules, which is 7.9% for $\text{Cy}_3\text{PO}\cdot(\text{HOO})_2\text{CMe}_2$ and 8.3% for $\text{Ph}_3\text{PO}\cdot(\text{HOO})_2\text{CMe}_2$. The ^{31}P NMR spectra before and after the grinding only show the starting materials. Thermogravimetric analyses (TGA) of **4** and **5** indicated that the $(\text{HOO})_2\text{CMe}_2$ moiety, as a whole or in fragments, is lost upon heating (80-110 °C), and this is followed by the loss of H_2O_2 molecules at 150 °C, leaving the phosphine oxides behind (Figure 6.6).

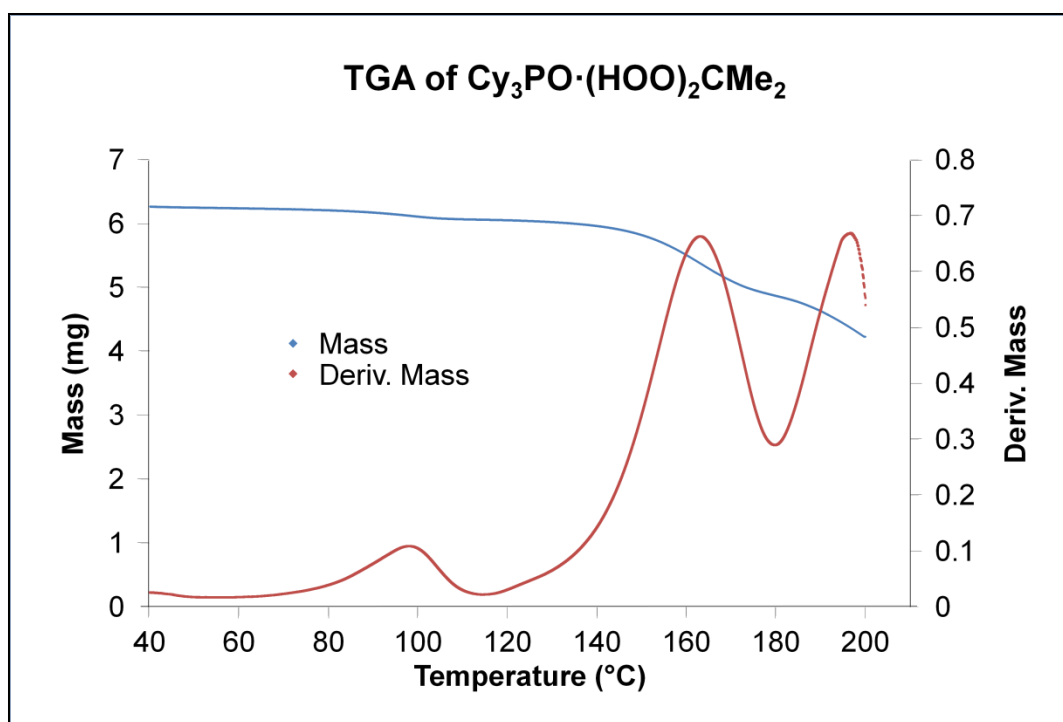


Figure 6.6. Thermogravimetric analysis (TGA) of **5**.

Even in solution, the $\text{R}_3\text{PO}\cdot(\text{HOO})_2\text{CR}'\text{R}''$ adducts are remarkably stable in the absence of a reducing agent. For example, heating a benzene solution of **4** to 90 °C and monitoring the solution with ^{13}C NMR showed that three days were needed to decompose about 80% of **4**. The main products remaining in solution were $\text{Ph}_3\text{PO}\cdot\text{H}_2\text{O}$ ^{6,17} and acetone, besides traces of isopropanol, formic acid, and acetic acid (Figure A.79).

Next, a QNMR method was developed to observe the shelf life of the representative adducts. The oxidation yields from the integrals of PPh_3 and OPPh_3 under varying factors, as described above, are summarized in Table 6.1. Comparing the results of *A*, *B* and *C*, the position of the NMR tube within the probe does not exhibit a

significant influence on the integral ratio. This was expected, since both the phosphine and the phosphine oxide are dispersed homogeneously in the NMR sample. On the other hand, changing the spectral ranges and therefore the point of irradiation with maximal intensity, shows a definite trend. As the excitation pulse frequency with maximal intensity moves closer, the OPPh₃ peak intensity grows for all constellations A, B and C. Finally, the relaxation delay has to be longer than 35 seconds, in order for the phosphine oxide to relax completely.

Table 6.1. Comparison of experimental and theoretical yields of OPPh₃, expressed as %, following the oxidation of PPh₃ with freshly synthesized **5**. Experimental yields were calculated from the integral ratio of OPPh₃ and PPh₃ peaks in the ³¹P NMR spectra.

| A (1.5 cm) | | [Measured yield]/[Theoretical yield](%), at specified Delay | | | | | |
|-------------------|-----|---|-----|-----|-----|-----|-----|
| SW (range in ppm) | 1s | 5s | 10s | 20s | 30s | 35s | 40s |
| 150 to -30 | 139 | 123 | 114 | 108 | 105 | 105 | 104 |
| 150 to -50 | 137 | 123 | 114 | 105 | 103 | 103 | 102 |
| 100 to -100 | 130 | 120 | 112 | 103 | 102 | 101 | 101 |
| 80 to -120 | 127 | 120 | 111 | 103 | 101 | 99 | 99 |

| B (1.0 cm) | | [Measured yield]/[Theoretical yield](%), at specified Delay | | | | | |
|-------------------|-----|---|-----|-----|-----|-----|-----|
| SW (range in ppm) | 1s | 5s | 10s | 20s | 30s | 35s | 40s |
| 150 to -30 | 132 | 121 | 111 | 106 | 104 | 102 | 102 |
| 150 to -50 | 127 | 123 | 111 | 106 | 103 | 101 | 101 |
| 100 to -100 | 126 | 118 | 110 | 102 | 98 | 99 | 99 |
| 80 to -120 | 128 | 118 | 111 | 102 | 98 | 99 | 99 |

| C (0.5 cm) | | [Measured yield]/[Theoretical yield](%), at specified Delay | | | | | |
|-------------------|-----|---|-----|-----|-----|-----|-----|
| SW (range in ppm) | 1s | 5s | 10s | 20s | 30s | 35s | 40s |
| 150 to -30 | 130 | 116 | 112 | 105 | 103 | 103 | 103 |
| 150 to -50 | 130 | 122 | 113 | 105 | 103 | 103 | 103 |
| 100 to -100 | 127 | 120 | 112 | 103 | 100 | 100 | 100 |
| 80 to -120 | 124 | 118 | 109 | 102 | 101 | 99 | 99 |

Ph₃P oxidation was performed with representative adducts after they have been stored in polycrystalline form under different conditions. The adducts were exposed to the atmosphere at room temperature with and without light, and at -4 °C and -20 °C in the dark. At regular intervals aliquots were removed from the stored samples and the described Ph₃P oxidation test was performed. ³¹P NMR spectra were recorded with a spectral range from 100 to -100 ppm and a relaxation delay of 35 seconds. In this way the oxidative power of the adducts was monitored for up to 100 days (Figure 6.7, Figure C.1-Figure C.3).

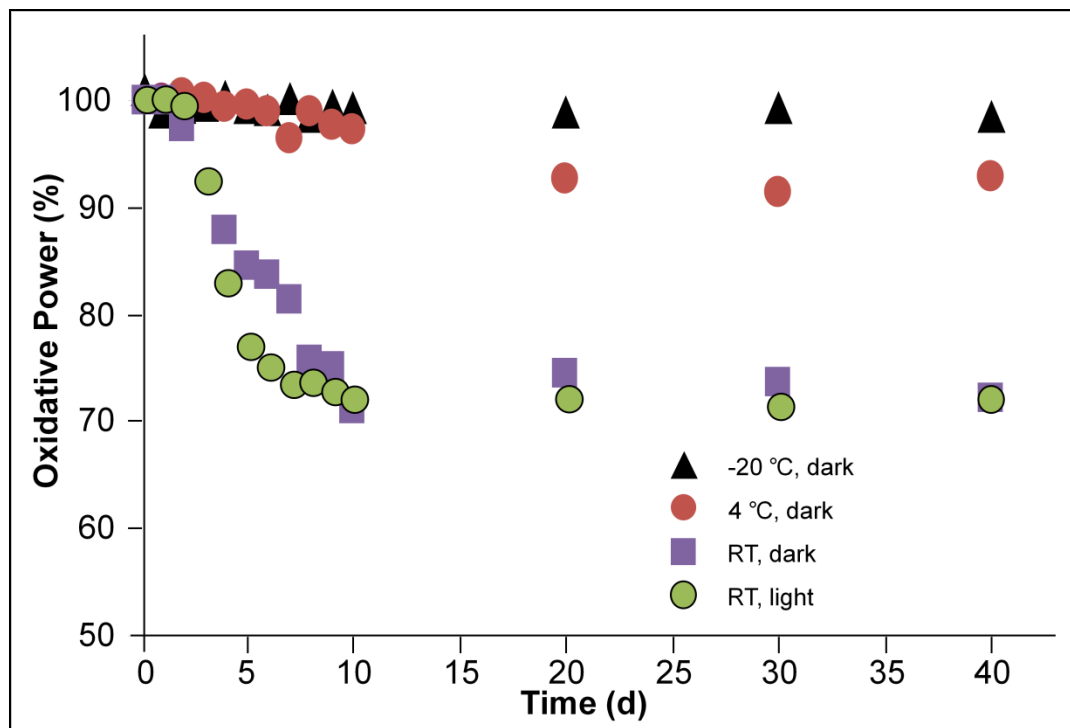


Figure 6.7. Oxidative power of **5** after being stored at the indicated conditions. 100% equals to two moles of active oxygen per mole of **5**.

At -20 and 4 °C the adducts retain most of their oxidative power over months. Exposure to light did not influence the decomposition, while the temperature played a dominant role. Furthermore, the exposed surface area of the materials made a difference. For example, large crystals ($3 \times 3 \times 1 \text{ mm}^3$) of **4-7**, **9** and **10** retained 99% oxidative power after 100 days of being exposed to the ambient atmosphere and light at room temperature. Under the same conditions, the polycrystalline materials retain 60 to 70% of their oxidative power in the course of months. It is possible that the peroxides on the surface of the adduct are decomposing while the shielded molecules in the interior of the crystals remain unchanged.

Decomposition may also occur in a stepwise manner, in which only one of the peroxide groups loses an oxygen atom, to initially form $\text{R}_3\text{PO}\cdot(\text{HOO})(\text{HO})\text{CR}'\text{R}''$. Indeed, a single crystal X-ray structure obtained from large crystals of $\text{Cy}_3\text{PO}\cdot(\text{HOO})(\text{HO})\text{C}(\text{CH}_2)_5$ (**16**) (Figure 6.8)⁵³ demonstrates that such a molecule is stable enough to assemble systematically and it might slow down decomposition.



Figure 6.8. Large crystals (left) and single crystal X-ray structure (right) of **16**.⁵³

Since this hydroperoxy(hydroxy)alkane adduct (**16**) is stable and melts without decomposition at 33 °C, it was possible to perform full characterization. In the IR spectrum two distinct stretching bands are observed, one each for the hydroxy O-H and the hydroperoxy O-H group (Figure B.19). In comparison to the di(hydroperoxy)-cyclohexane adduct **10**, the P=O bond is stronger, as evidenced from the frequency of P=O stretching band $\nu(\text{P=O})$, which lies in between the values of neat Cy_3PO and adduct **10** (Table 6.2). The stronger P=O bond of **16** as compared to **10** can also be assumed due to the shorter bond length of the P=O group in the X-ray structure.

Table 6.2. Comparison of IR and X-ray crystallographic data of Cy_3PO , **16** and **10**.

| Species | $\nu(\text{O-H})$ (cm^{-1}) | $\nu(\text{P=O})$ (cm^{-1}) | $\Delta \nu(\text{P=O})$ (cm^{-1}) | P=O (\AA) | Δ Bond length |
|------------------------|---|---|--|----------------------|----------------------|
| Cy_3PO | - | 1157 | - | 1.490 ⁴² | - |
| 16 | 3323/ 3246 | 1144 | 13 | 1.509 | +0.019 |
| 10 | 3196 | 1123 | 24 | 1.512 | +0.022 |

The trend is continued in ^{31}P NMR spectroscopy. Less electron density is removed from the P=O bond, and thus the phosphorus nucleus is more shielded than **10**, and the signal for **16** appears more upfield shifted and closer to Cy_3PO , with a $\Delta\delta$ value of approximately half of that of **10**. The quaternary carbon on the $(\text{HOO})(\text{HO})\text{C}(\text{CH}_2)_5$ moiety is also observed more upfield shifted compared to **10** (Table 6.3). Nonetheless, this monoperoxy adduct **16** is still capable of stoichiometrically oxidizing Ph_3P to Ph_3PO .

Table 6.3. Comparison of ^{13}C and ^{31}P NMR chemical shifts of Cy_3PO , **16** and **10**.

| Adduct | $\delta(^{13}\text{C}) \text{C}_q$ (ppm) | $\delta(^{31}\text{P}) \text{P=O}$ (ppm) | $\delta(^{31}\text{P})$ neat R_3PO (ppm) | $\Delta\delta$ (ppm) |
|-----------|---|---|---|----------------------|
| 16 | 102.65 | 53.34 | 49.91 | 3.43 |
| 10 | 109.52 | 58.01 | | 8.10 |

Finally, the solubility of **16** was compared with those of the cyclic adducts **9-11** (Figure 6.9). Adduct **16** shows slightly higher solubility than **9-11** in most solvents with the exception of chlorinated solvents, benzene, and THF.

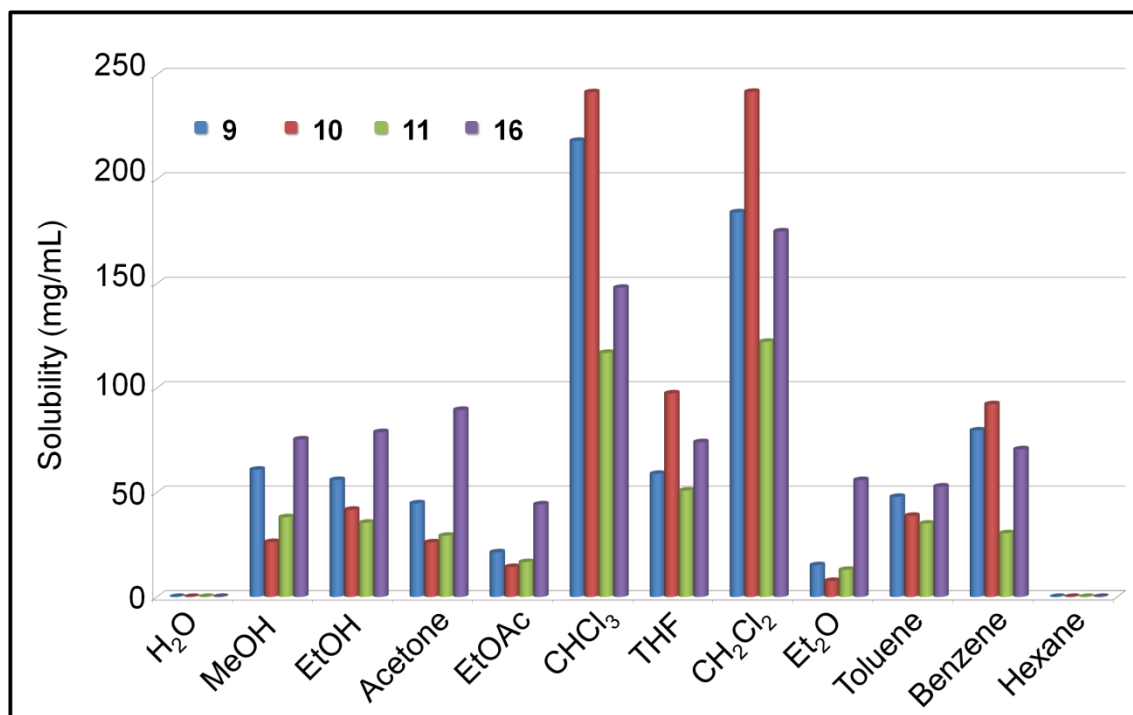


Figure 6.9. Solubility of the cyclic adducts **9-11** and “half-adduct” **16**.

Conclusion

The decomposition of the adducts of the type $R_3PO\cdot(HOO)_2CR'R''$ was studied from multiple perspectives. The adducts were first exposed to thermal and mechanical stress, during which sudden release of energy was never observed, once again confirming the safety of these adducts.

Next, the decomposition rate of these adducts was studied under various storage conditions to test for their shelf life. In order to quantify the rate of decomposition, a quantitative NMR method was developed, involving the use of precise ^{31}P NMR peak integration. Using this method, it was shown that the adducts decompose over time to about 70% when stored at room temperature in powder form. However, when the powder is stored at decreased temperatures of $-4\text{ }^\circ\text{C}$, there is essentially no decomposition even after months. Moreover, when the adducts are stored as large single crystals, the decomposition is insignificant even at room temperature.

Since the adducts decompose much faster as powders than in the form of large crystals, it is hypothesized that the surface area plays a role in the decomposition of the peroxide groups. This decomposition can occur simultaneously at both peroxide positions, or it could take place in a stepwise manner, to form $R_3PO\cdot(HOO)(HO)CR'R''$ as an intermediate. The latter assumption is supported by successful characterization of $Cy_3PO\cdot(HOO)(HO)C(CH_2)_5$ *via* single crystal X-ray crystallography, NMR and IR spectroscopy.

Experimental

Cy₃PO•(HOO)(HO)C(CH₂)₅ (**16**)

300 mg of [Cy₃PO•H₂O₂]₂ (0.45 mmol) was dissolved in 10 mL of cyclohexanone (97 mmol) in a 20 mL vial. 1.5 mL aqueous H₂O₂ (15 mmol) was added to the vial, and the solution was stirred vigorously overnight, then left to crystallize via slow evaporation. Colorless rhombic crystals appeared after three days (327 mg, 0.76 mmol, 84% yield).

NMR (δ , CDCl₃), ³¹P{¹H} 53.34 (s); ¹H 10.37 (s, 1H, OOH), 9.51 (s, 1H, OH), 1.95-1.78 (m, 17H, PCH_{ax}CH_{eq}CH_{eq}, OCCH) 1.74-1.68 (m, 3H, PCH(CH₂)₂CH_{eq}), 1.67-1.60 (m, 2H, CCH), 1.58-1.52 (m, 4H, CCH₂CH₂), 1.47-1.34 (m, 8H, PCHCH_{ax}, CCH₂CH₂CH₂), 1.31-1.19 (m, 9H, PCHCH₂CH_{ax}CH_{ax}); ¹³C{¹H} 102.65 (s, COO), 35.01 (d, ¹J(³¹P-¹³C) = 60.6 Hz, PC), 34.15 (s, CCH₂), 26.80 (d, ³J(³¹P-¹³C) = 11.8 Hz, PCHCH₂CH₂), 26.11 (d, ²J(³¹P-¹³C) = 3.4 Hz, PCHCH₂), 26.00 (d, ⁴J(³¹P-¹³C) = 1.7 Hz, PCH(CH₂)₂CH₂), 25.40 (s, CCH₂CH₂CH₂), 22.93 (s, CCH₂CH₂). IR: ν (PO) = 1143 cm⁻¹.

CHAPTER VII

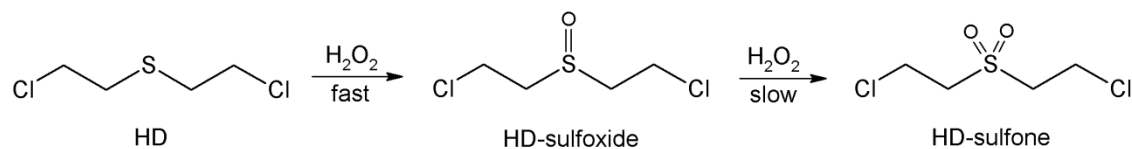
APPLICATIONS IN OXIDATION REACTIONS*

Introduction

The ultimate objective of this project is to apply the adducts of the type $R_3PO \cdot (HOO)_2CR'R''$ ($R, R', R'' = \text{alkyl, aryl}$) as stoichiometric and soluble oxidizing agents in organic reactions. In the previous chapter, it was demonstrated that these adducts are capable of oxidizing PPh_3 to $OPPh_3$ selectively and stoichiometrically. The well-defined and reproducible composition of the adducts allows for stoichiometric application in reactions that are sensitive to overoxidation. This property of the adducts also makes them an attractive option in reactions such as sulfoxidations,^{4b,4c,54} where the sulfoxide (R_2SO) is preferred to the sulfone (R_2SO_2).

One particular example where selective oxidation to the sulfoxide is desired is in the neutralization of the chemical warfare agent mustard gas (bis(2-chloroethyl)sulfide, codename HD). Upon contact with an oxidant, the sulfide in HD is initially oxidized to the harmless HD-sulfoxide. However, overoxidation to the vesicant HD-sulfone occurs over time in the presence of excess oxidizing agent (Scheme 7.1).⁵⁵

* Reproduced with permission from "Hydrogen Peroxide and Di(hydroperoxy)propane Adducts of Phosphine Oxides as Stoichiometric and Soluble Oxidizing Agents" Ahn, S. H.; Cluff, K. J.; Bhuvanesh, N.; Blümel, J. *Angew. Chem.* **2015**, *127*, 13539-13543. Copyright Wiley-VCH Verlag GmbH & Co. KGaA.

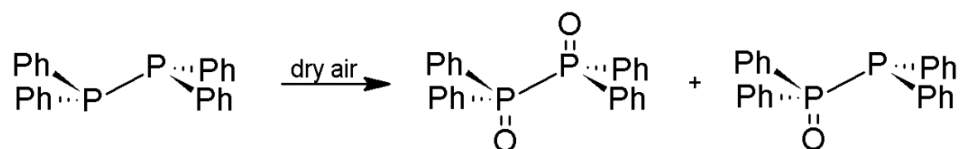


Scheme 7.1. Oxidation of HD to HD-sulfoxide and HD-sulfone in the presence of excess oxidant.

Because the adducts $\text{R}_3\text{PO}\cdot(\text{HOO})_2\text{CR}'\text{R}''$ ($\text{R}, \text{R}', \text{R}'' = \text{alkyl, aryl}$) are stored in solid form, it is relatively easy to use them in reactions that require air- and moisture-free conditions. Moreover, due to their high solubility in organic solvents, the oxidation reaction can occur in one phase, eliminating the need for phase transfer agents. The oxidation of PPh_3 is relatively easy, as PPh_3 is not air-sensitive in the solid state and in most solvents, and OPPh_3 is the sole product with no occurrence of overoxidation. In the case of alkyl- and other phosphines which are sensitive to overoxidation and hydrolysis,⁶ it is interesting to probe whether oxidation with the adducts of the type $\text{R}_3\text{PO}\cdot(\text{HOO})_2\text{CR}'\text{R}''$ can proceed in a stoichiometric manner, and whether the reaction conditions would remain sufficiently anhydrous to prevent hydrolysis.⁵⁶

For instance, 1,1,2,2-tetraphenyldiphosphine dioxide, $\text{Ph}_2\text{P}(\text{O})\text{-P}(\text{O})\text{Ph}_2$, is a species of interest because of its structural similarity to hypophosphoric acid, $(\text{RO})_2\text{P}(\text{O})\text{-P}(\text{O})(\text{OR})_2$, which exhibits anti-tumor activity.^{56a} The oxidation of 1,1,2,2-tetraphenyldiphosphine, $\text{Ph}_2\text{P-PPh}_2$, to the dioxide is traditionally performed in dry solvents with oxygen gas, as the P-P bond is sensitive to hydrolysis. In the presence of moisture, the P-P bond is cleaved to produce a mixture of oxidized species, including $\text{Ph}_2\text{P}(\text{O})\text{H}$ and $\text{Ph}_2\text{P}(\text{O})\text{OH}$.⁵⁷ Therefore, this method of oxidation is inconvenient, also

because it involves the use of an oxygen gas cylinder. When exposed to dry air at merely atmospheric pressure, the oxidation is extremely slow and incomplete, with a mixture of diphosphine dioxide and diphosphine monoxide in the product mixture (Scheme 7.2, Figure A.92).^{56a}



Scheme 7.2. Oxidation of 1,1,2,2-tetraphenyldiphosphine in dry air.

More recent approaches to the 1,1,2,2-tetraphenyldiphosphine dioxide involve 1) the reaction between an electrophilic $R_2P(O)X$ ($X = Cl, Br$) and deprotonated R_2POH , 2) an alkali metal reduction of $R_2P(O)X$, or 3) the reaction of R_2PCl with $R_2P(O)H$ and oxygen gas in anhydrous conditions.^{56a} However, all of these methods result in a mixture of products, including $R_2P(O)-P(O)R_2$ and $R_2P(O)-O-PR_2$. On the other hand, $R_3PO \cdot (HOO)_2CR'R''$ adducts are dry, solid materials that can simply be weighed in and administered in a stoichiometric manner. If successful, this provides a new and efficient way of selectively oxidizing 1,1,2,2-tetraphenyldiphosphine to the diphosphine dioxide.

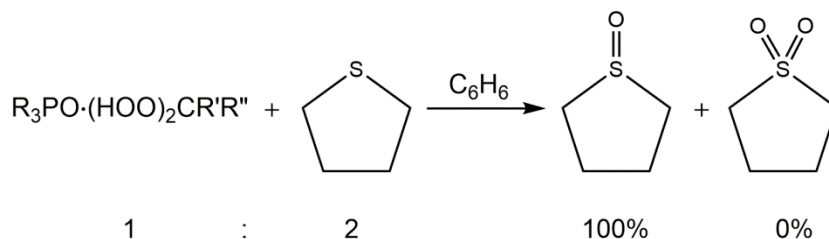
Additionally, the potency of the adducts as oxidants in epoxidation reactions is studied. On one hand, the anhydrous properties of the adducts make them desirable, as the absence of water molecules should prevent the hydrolysis of the generated epoxide. However, the adducts are milder oxidants than aqueous H_2O_2 , and thus may not be strong enough to activate all types of olefins.^{8b,33}

Finally, the reactivity of the di(hydroperoxy)cycloalkane adducts **9-11** under Baeyer-Villiger reaction conditions is explored.^{2,58} Baeyer-Villiger oxidations are used to transform a cyclic ketone to its corresponding lactone. In the case of the adducts **9-11**, a cyclic ketone is already used to generate the adduct molecule, which incorporates two moles of peroxides as potent oxidants. In this chapter, the transformation of the moiety $(\text{HOO})_2\text{C}(\text{CH}_2)_n$ ($n = 4-6$) in the adducts to the corresponding lactone, with and without offering additional ketone, is studied in detail.

Results and Discussion

Sulfoxidation

To study the application of the adducts $\text{R}_3\text{PO}\cdot(\text{HOO})_2\text{CR}'\text{R}''$ as oxidants for reactands that are air-sensitive and prone to overoxidation, tetrahydrothiophene (THT) oxidation was selected.^{4b,4c,54} When **3** or **4** was combined with THT in a 1 : 2 molar ratio in benzene, it was selectively and quantitatively oxidized to tetramethylene sulfoxide at ambient temperatures within two hours (Scheme 7.3)



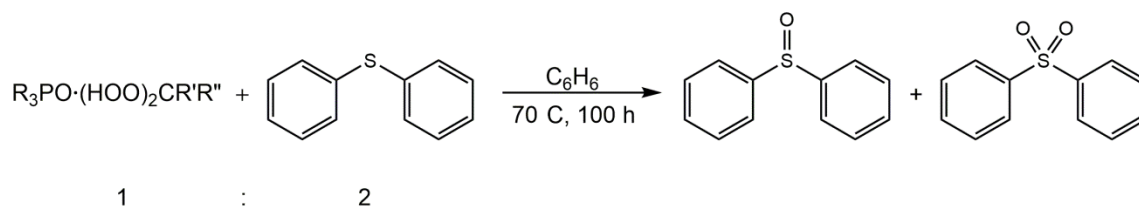
Scheme 7.3. Stoichiometric oxidation of THT with $\text{R}_3\text{PO}\cdot(\text{HOO})_2\text{CR}'\text{R}''$ (**4-8**, **12**).

Generally, with adducts incorporating sterically more shielding substituents, the reaction times were increased (Table 7.1). However, the sulfoxide was still produced selectively, with the only other reaction products being the corresponding phosphine oxide carriers and the regenerated ketones. The resulting water molecule remains hydrogen bonded to the phosphine oxide group.¹⁷ This fast and clean reaction in one organic phase compares favorably to earlier studies which required biphasic mixtures and added catalysts.^{4b,4c,54}

Table 7.1. Selective and complete oxidation of THT to tetramethylene sulfoxide.

| Adduct | Reaction Time at Different Temperatures (h) | | |
|-----------|---|-------|-------|
| | 23 °C | 50 °C | 60 °C |
| 4 | 2 | 0.5 | 0.4 |
| 5 | 2 | 0.5 | 0.4 |
| 6 | 5 | 2 | 1 |
| 7 | 8 | 3 | 1 |
| 8 | 8 | 7 | 2 |
| 12 | 6 | 1 | 0.5 |

While the challenge regarding the oxidation of dialkyl sulfides lies in the selective oxidation to sulfoxides, oxidations of diaryl sulfides and thiophenes are intrinsically difficult due to low reactivity in the absence of a catalyst.^{4a-c,4e,54,59} Following the successful selective oxidation of THT to tetramethylene sulfoxide, oxidation of diphenylsulfide was attempted using the adducts **4**, **5**, **7** and **8** (Scheme 7.4).



Scheme 7.4. Oxidation of Ph_2S with $\text{R}_3\text{PO}\cdot(\text{HOO})_2\text{CR}'\text{R}''$ (**4**, **5**, **7**, **8**).

Upon addition of the adduct and SPh_2 in a 1 : 2 ratio in benzene at room temperature, no oxidation occurred even after a prolonged time period of 100 hours. When the reaction temperature was increased to 70 °C, conversion to the corresponding sulfoxide took place, with some overoxidation to the sulfone in two cases (Table 7.2).

Table 7.2. Yields (%) of oxidized products Ph_2SO and Ph_2SO_2 after reacting Ph_2S with selected adducts $\text{R}_3\text{PO}\cdot(\text{HOO})_2\text{CR}'\text{R}''$.

| Adduct | Ph_2SO | Ph_2SO_2 |
|----------|------------------------|--------------------------|
| 4 | 60 | 11 |
| 5 | 61 | 8 |
| 7 | 40 | 0 |
| 8 | 30 | 0 |

Adducts **4** and **5** exhibited the highest activities, oxidizing Ph_2S in moderately high yields to Ph_2SO without any catalyst, albeit extended reaction times of 100 h were required and some overoxidation to Ph_2SO_2 occurred. To increase the sulfoxide yield and minimize overoxidation to the sulfone, the oxidation reaction was repeated with adduct **7** at room temperature, in the presence of catalytic amounts of silica and Br_2 , which have

been shown to be useful by another group previously.⁶⁰ With the addition of silica and Br₂, the sulfoxide yield remained 43% in acetonitrile and 47% in benzene, both after 100 h of stirring (Table 7.3 entries 6 and 7). When silica was added without Br₂, diphenylsulfoxide and diphenylsulfone are produced in almost equal amounts (Entries 3 and 4). When Br₂ is added without silica, the sulfoxide is obtained as the only product; however, the yield is decreased (Entry 5). Increasing the reaction temperature to 50 °C resulted in a high conversion of 86% after only one day of stirring. However, the major product was diphenylsulfone (53%), and the yield of diphenylsulfoxide was merely 33% (Entry 8).

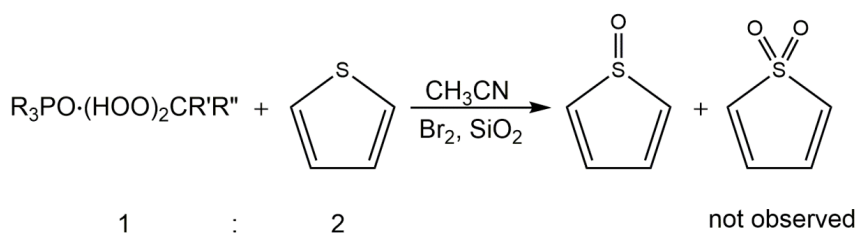
Table 7.3. Yields (%) of the oxidation products Ph₂SO and Ph₂SO₂ after reaction of Ph₂S with selected adducts R₃PO•(HOO)₂CR'R", with and without catalytic amounts of SiO₂ and Br₂.

| Entry | Adduct | SiO ₂ (g) | Br ₂ | Ph ₂ SO | Ph ₂ SO ₂ | |
|-------|----------|----------------------|-----------------|--------------------|---------------------------------|---|
| 1 | 7 | - | - | 0 | 0 | |
| 2 | | - | | 40 ^[a] | 0 | |
| 3 | | 0.5 | | 25 | 25 | |
| 4 | | 2.0 | | 24 | 18 | |
| 5 | | - | 1 drop | 29 | 0 | |
| 6 | | 0.5 | | 43 | 0 | |
| 7 | | 0.5 | | 47 ^[b] | 0 | |
| 8 | | 0.5 | | 33 ^[c] | 53 ^[c] | |
| 9 | | 5 | | 0.5 | 49 | 0 |
| 10 | | 10 | | 0.5 | 46 | 0 |

[a] Reaction temperature 70 °C; [b] Reaction was performed in benzene; [c] Reaction temperature 50 °C.

Assured that conducting the oxidation reaction at room temperature does not yield the sulfone, the sulfoxidation was attempted with adducts **5** and **10**, using the same reaction conditions. In both cases, no overoxidation to the sulfone was observed, in contrast to previous results. The yields for the sulfoxide were similar to the ones obtained with adduct **7**, with 49% for **5** and 46% for **10** (Table 7.3, entries 9 and 10).

Finally, the oxidation of thiophene was attempted using the adducts. Thiophene and adduct **7** were combined in a 2 : 1 ratio, and dissolved in acetonitrile (Scheme 7.5). After stirring for 4 days at room temperature, no oxidation occurred without silica and Br₂ (Table 7.4, entry 1). With addition of catalytic amounts of silica and Br₂, 41% conversion was observed, with thiophene oxide being the only product (Entry 2). No overoxidation was detected.



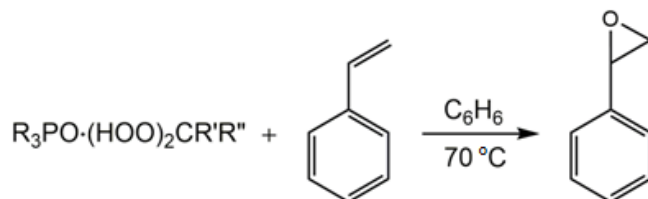
Scheme 7.5. Oxidation of thiophene with the R₃PO·(HOO)₂CR'R'' adduct **7**.

Table 7.4. Product yields (%) after oxidation of thiophene with **7**.

| Entry | SiO ₂ / Br ₂ | Thiophene 1-oxide | Thiophene 1,1-dioxide |
|-------|------------------------------------|-------------------|-----------------------|
| 1 | - / - | 0 | 0 |
| 2 | 0.5 g / 1 drop | 41 | 0 |

Epoxidation

Epoxidations of styrene and cyclohexene were attempted using the adducts **4-8** (Scheme 7.6) in benzene.^{8b,48d,61}



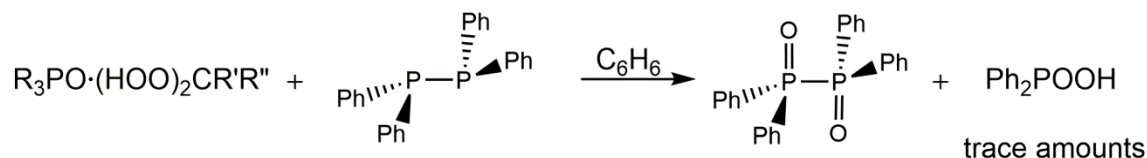
Scheme 7.6. Epoxidation attempts with $R_3PO \cdot (HOO)_2CR'R''$ adducts.

In the absence of any catalyst, no reaction occurs, even at elevated temperatures ($70\text{ }^\circ\text{C}$). This is plausible, as the adducts are milder oxidants than aqueous H_2O_2 . When 0.01 mol% of methyltrioxo rhenium (MTO) is added to the reaction mixture, 100% conversion is achieved, but the product is fully hydrolyzed to trans-1,2-cyclohexanediol.^{5c,61-62} Further epoxidation attempts were discontinued due to time constraints.

Phosphine oxidation

When $Cy_3PO \cdot (HOO)_2CMe_2$ (**5**) and $Ph_2P \cdot PPh_2$ were added in a 1 : 1 ratio to dry benzene, the diphosphine dioxide was obtained as the main product (Scheme 7.7). While the resulting water adduct of the phosphine carrier, $Cy_3PO \cdot H_2O$, is highly soluble in benzene, 1,1,2,2,-tetraphenyldiphosphine dioxide (**17**) is insoluble and precipitates out of the solution, allowing for easy separation from the reaction mixture (Figure A.93). In the

solid form, **17** is air-stable and can be stored for weeks without P-P bond cleavage due to hydrolysis or oxygen insertion.



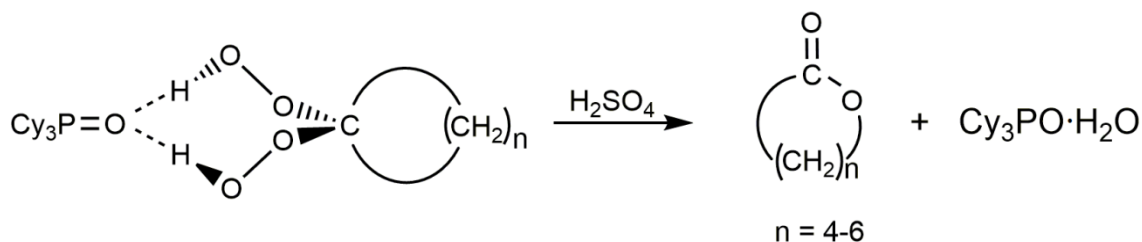
Scheme 7.7. Stoichiometric oxidation of 1,1,2,2-tetraphenyldiphosphine with $\text{Cy}_3\text{PO}\cdot(\text{HOO})_2\text{CMe}_2$ (**5**) in benzene.

17 was intended to serve as a diphosphine dioxide carrier for di(hydroperoxy)alkanes. The interest was to extend the known diphosphine dioxide adducts from those with two methylene groups between the P atoms (**14**, **15**), via the one with one CH_2 group (**13**) to an adduct with no carbon between the two PO groups. Therefore, an adduct synthesis with **17** as a new diphosphine dioxide carrier was attempted. However, when **17** was brought in contact with equal molar amounts of $(\text{HOO})_2\text{C}(\text{CH}_2)_5$ crystals, the P-P bond was immediately hydrolyzed to the phosphinic acid $\text{Ph}_2\text{P}(\text{O})\text{OH}$ even in the absence of any solvent.

Baeyer-Villiger oxidation

For each cycloalkane adduct $\text{Cy}_3\text{PO}\cdot(\text{HOO})_2\text{C}(\text{CH}_2)_n$ ($n = 4-6$) there is a cyclic ketone inherently present, arranged favorably with respect to its oxidation with two active peroxide groups attached to the quaternary carbon. In the presence of a catalytic

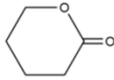
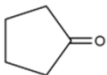
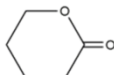
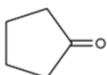
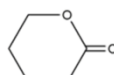
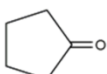
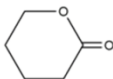
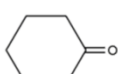
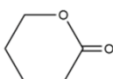
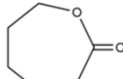
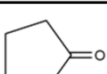
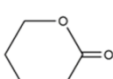
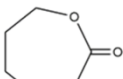
amount of H_2SO_4 , these $(\text{HOO})_2\text{C}(\text{CH}_2)_n$ moieties immediately form the corresponding free lactones in quantitative yields (Scheme 7.8).



Scheme 7.8. Formation of lactones from the cycloalkane adducts $\text{Cy}_3\text{PO} \cdot (\text{HOO})_2\text{C}(\text{CH}_2)_n$ in the presence of trace amounts of acid.

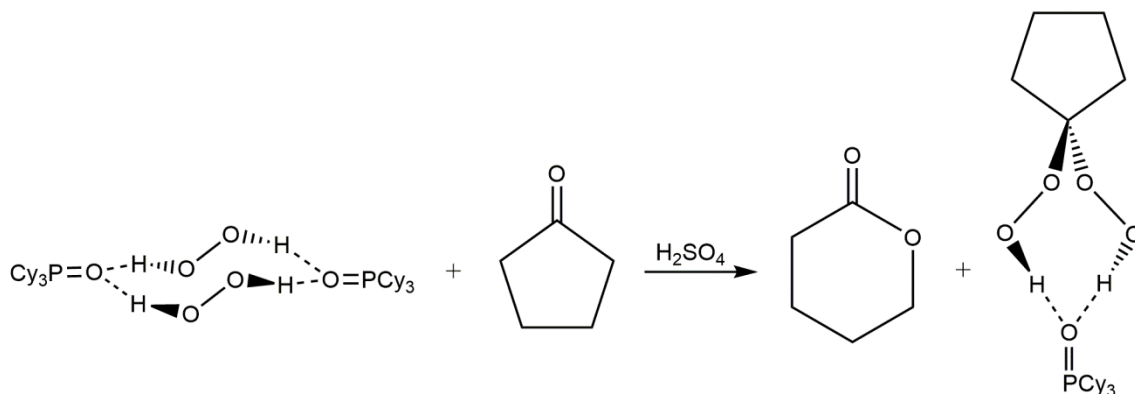
It is not yet clear whether the oxidation takes place while the di(hydroperoxy)cycloalkanes are still attached to the phosphine oxide carriers, or whether they are released from the phosphine oxides prior to the oxidation. Even though there are two peroxy groups per $(\text{HOO})_2\text{C}(\text{CH}_2)_n$ moiety, no further oxidation of the lactones is observed, and the only other product remaining in the reaction mixture is $\text{Cy}_3\text{PO} \cdot \text{H}_2\text{O}$ (Table 7.5, entry 1).

Table 7.5. Baeyer-Villiger oxidation of substrate ketone and (HOO)₂C(CH₂)_n moieties in the presence of a drop (< 1 mg) of H₂SO₄.

| Entry | Adduct | Substrate | Product |
|-------|--------|---|--|
| 1 | 9 | - |  100% |
| 2 | 9 |  (1 eq) |  58% |
| 3 | 3 |  (2 eq) |  55% |
| 4 | 3 |  (1 eq) | 9 +  5% 52% |
| 5 | 9 |  (1 eq) |  +  21% 23% |
| 6 | 10 |  (1 eq) |  +  24% 22% |

For comparison, the Baeyer-Villiger oxidation was attempted with cyclopentanone and the hydrogen peroxide adduct [Cy₃PO•H₂O₂]₂ in a 2 : 1 molar ratio, again with only a trace amount of H₂SO₄. The corresponding δ -valerolactone is the only product, however, the yield is decreased to 55% (Table 7.5, entry 3). When the molar ratio of adduct to substrate is increased to 1 : 1, such that there are two active peroxide

groups per cyclopentanone, a mixture of δ -valerolactone and adduct **9** is obtained (Scheme 7.9, Table 7.5, entry 4).



Scheme 7.9. Oxidation of cyclopentanone to δ -valerolactone and di(hydroperoxy)-cyclopentane in the presence of **3** and trace amounts of acid.

In order to test whether the peroxy groups show selectivity with the attached cycloalkyl group over freshly added cyclic ketone, adduct **9** was reacted with cyclohexanone, and adduct **10** was reacted with cyclopentanone in a 1 : 1 molar ratio. In both cases, mixtures of δ -valerolactone and ϵ -caprolactone (Table 7.5, entries 5 and 6) are obtained, in approximately 1 : 1 molar ratio. Therefore, one can conclude that there is no preference for the oxidation of phosphine oxide-bound di(hydroperoxy)cycloalkanes over the lactone formation from added free ketones.

Conclusion

The anhydrous and stoichiometric character of the di(hydroperoxy)alkane adducts $R_3PO \cdot (HOO)_2CR'R''$ ($R, R', R'' = \text{alkyl, aryl}$) places them in a unique position in organic oxidation reactions. As demonstrated by the successful selective oxidation of tetrahydrothiophene and 1,1,2,2-tetraphenyldiphosphine, these adducts can be applied as oxidants in reactions that require air- and water-free conditions, as well as reactions with desired products that are sensitive to overoxidation.

The selectivity of these adducts stems from their exact stoichiometry and their mild oxidizing power, relative to aqueous H_2O_2 . In the case of reluctant reactions such as diarylsulfide oxidation, a catalyst or initiator can be used in combination with the adducts to push the reaction forward. Overoxidation to $R'R''SO_2$ does not occur under optimized reaction conditions, and the corresponding sulfoxide $R'R''SO$ is obtained as the only product in good yields. In the presence of trace amounts of H_2SO_4 , the di(hydroperoxy)cycloalkane moieties of **9-11** produce the corresponding lactones, leaving the phosphine oxide carriers behind.

While reactions such as epoxidations, which involve the activation of $C=C$ bonds, are possible with the adducts $R_3PO \cdot (HOO)_2CR'R''$ in the presence of a catalyst like MTO, the adducts are most favorable for reactions that require mild oxidants, such as the oxidation of 1,1,2,2-tetraphenyldiphosphine. Because the oxidizing power of the adducts is mild, the P-P bond is not cleaved and the diphosphine dioxide **17** is obtained quantitatively. However, the scope of applications of these adducts is still being

expanded in every direction, including oxidations of substrates that contain sensitive functional groups.

Experimental

Tetrahydrothiophene (THT) oxidation

46 mg (0.1 mmol) of $\text{Cy}_3\text{PO}\cdot(\text{HOO})_2\text{C}(\text{CH}_2)_4$ (**9**) and 9 mg (0.1 mmol) of THT are weighed into a 20 mL vial inside a glove box and dissolved in 0.6 mL of C_6D_6 . The vial is capped, and the contents are stirred. Every 10 minutes, an aliquot is transferred to an NMR tube, and the product identity and yield are determined by ^1H and ^{13}C NMR analyses.

Tetrahydrothiophene NMR (δ , C_6D_6), ^1H 2.55-2.42 (m, 4H, SCH_2), 1.48-1.36 (m, 4H, SCH_2CH_2); ^{13}C 31.37 (s, SC), 30.85 (s, SCH_2C).⁶³

Tetramethylene sulfoxide NMR (δ , C_6D_6), ^1H 2.89-2.74 (m, 4H, SCH_2), 2.47-2.04 (m, 4H, SCH_2CH_2); ^{13}C 53.98 (s, SC), 25.02 (s, SCH_2C).⁶⁴

SPh₂ oxidation

In a representative reaction, 84 mg (0.2 mmol) of **7** and 78 mg (0.4 mmol) of Ph_2S are weighed into a 20 mL vial. The mixture is then dissolved in 3 mL of distilled acetonitrile. Finally, 0.5 g of dry SiO_2 and 1 drop (less than 1 mg) of Br_2 are added to the vial, and the contents is stirred for 4 days. The reaction progress is monitored every 12 hours via ^1H and ^{13}C NMR spectroscopy.

Ph₂S NMR (δ , C₆D₆), ¹H 7.47-7.26 (m, 10H); ¹³C 135.83 (s, C_i), 131.00 (s, C_o), 129.11 (s, C_m), 126.94 (s, C_p).⁶³

Ph₂SO NMR (δ , C₆D₆), ¹H 7.71-7.63 (m, 4H, H_o), 7.50-7.46 (m, 2H, H_p), 7.45-7.41 (m, 4H, H_m); ¹³C 145.76 (s, C_i), 130.96 (s, C_p), 129.25 (s, C_m), 124.67 (s, C_o).⁶⁴

Ph₂SO₂ NMR (δ , C₆D₆), ¹H 7.95-7.91 (m, 4H, H_o), 7.55-7.53 (m, 2H, H_m), 7.52-7.49 (m, 4H, H_p); ¹³C 141.53 (s, C_i), 133.21 (s, C_p), 129.27 (s, C_m), 127.54 (s, C_o).⁶⁴

Thiophene oxidation

84 mg (0.2 mmol) of **7** and 34 mg (0.4 mmol) of C₄H₄S are weighed into a 20 mL vial. The mixture is then dissolved in 3 mL of distilled acetonitrile. Finally, 0.5 g of dry SiO₂ and 1 drop (less than 1 mg) of Br₂ are added to the vial, and the contents is stirred for 4 days. The reaction progress is monitored every 12 hours via ¹H and ¹³C NMR spectroscopy.

Thiophene NMR (δ , C₆D₆), ¹H 7.34-7.30 (m, 2H, SCH), 7.09-7.06 (m, 2H, SCHCH); ¹³C 126.82 (s, SCC), 125.08 (s, SC).⁶⁵

Thiophene-1-oxide NMR (δ , C₆D₆), ¹H 7.34-7.30 (m, 2H, SCH), 7.09-7.06 (m, 2H, SCHCH); ¹³C 140.93 (s, SC), 126.48 (s, SCC).⁶⁵

Baeyer-Villiger oxidation

23 mg (0.05 mmol) of Cy₃PO•(HOO)₂C(CH₂)₄ is dissolved in 3 mL of benzene in a 20 mL vial, and a drop of H₂SO₄ (98 wt%) is added. The contents of the vial is

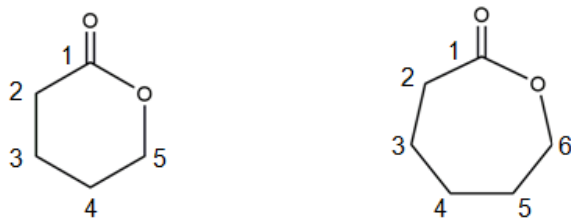
stirred for 20 min, and subsequently an NMR sample is prepared for ^1H and ^{13}C NMR analyses. δ -Valerolactone is produced in 100% yield, with respect to the di(hydroperoxy)cyclopentane moiety.

In a new vial, 92 mg (0.2 mmol) of $\text{Cy}_3\text{PO}\cdot(\text{HOO})_2\text{C}(\text{CH}_2)_4$ (**9**) and 17 mg (0.2 mmol) of cyclopentanone are dissolved in CDCl_3 (1.0 mL). 1 drop of H_2SO_4 (98 wt%) is added, and the contents is stirred for 20 min. Both $(\text{HOO})_2\text{C}(\text{CH}_2)_4$ and cyclopentanone are oxidized to δ -valerolactone (58% yield according to ^{13}C NMR).

In another 20 mL vial, $[\text{Cy}_3\text{PO}\cdot\text{H}_2\text{O}_2]_2$ (33 mg, 0.05 mmol) is reacted with 10 mg (0.12 mmol) of cyclopentanone and one drop of H_2SO_4 (98 wt%) in 1.0 mL of CDCl_3 . After stirring for 20 min, δ -valerolactone is produced in 55% yield with respect to the $(\text{HOO})_2\text{C}(\text{CH}_2)_4$ moiety, according to ^1H NMR spectroscopy.

When $[\text{Cy}_3\text{PO}\cdot\text{H}_2\text{O}_2]_2$ (**3**) (66 mg, 0.11 mmol) is reacted with 10 mg (0.12 mmol) of cyclopentanone and H_2SO_4 (98 wt%), 100% conversion occurs, but the product is a mixture of δ -valerolactone and adduct **9**.

When **9** (46 mg, 0.1 mmol) is reacted with 10 mg (0.1 mmol) of cyclohexanone and one drop of H_2SO_4 (98 wt%) in 1.0 mL of CDCl_3 , a mixture of δ -valerolactone (21% yield) and ϵ -caprolactone (23% yield) are produced. Reacting adduct **10** with cyclopentanone in a 1 : 1 ratio results in a mixture of δ -valerolactone (24% yield) and ϵ -caprolactone (22% yield) as well (Scheme 7.10).



Scheme 7.10. δ -Valerolactone (left) and ϵ -caprolactone (right), numbered for the purpose of NMR signal assignment.

δ -Valerolactone NMR (δ , CDCl_3), ^1H 4.35-4.31 (m, 2H, H_5), 2.58-2.51 (m, 2H, H_2), 2.15-1.63 (m, 4H, H_3 , H_4); ^{13}C 172.01 (s, C_1), 69.45 (s, C_5), 29.53 (s, C_2), 21.96 (s, C_4), 18.68 (s, C_3).⁶⁶

ϵ -Caprolactone NMR (δ , CDCl_3), ^1H 4.24-4.20 (m, 2H), 2.65-2.61 (m, 2H), 1.88-1.82 (m, 2H), 1.79-1.70 (m, 4H); ^{13}C 176.22 (s, C_1), 69.30 (s, C_6), 34.57 (s, C_2), 29.34 (s, C_4), 28.93 (s, C_5), 22.99 (s, C_3).⁶⁷

Styrene oxidation

In a representative styrene epoxidation attempt, 44 mg (0.1 mmol) of $\text{Cy}_3\text{PO}\cdot(\text{HOO})_2\text{CMeEt}$ (**7**) and 23 mg of styrene (0.2 mmol) are combined in a 25 mL Schlenk flask and flushed with N_2 gas. The mixture is dissolved in 3 mL of benzene and stirred overnight at each of following temperatures: room temperature, 40 $^\circ\text{C}$, 50 $^\circ\text{C}$, 60 $^\circ\text{C}$, and 70 $^\circ\text{C}$. The reaction is monitored with ^1H and ^{13}C NMR spectroscopy. No conversion of styrene is observed.

440 mg (1 mmol) of $\text{Cy}_3\text{PO}\cdot(\text{HOO})_2\text{CMeEt}$ (**7**), 230 mg (2 mmol) of styrene and 5 mg (0.02 mmol, 1 mol%) of CH_3ReO_3 (MTO) are placed in a 100 mL Schlenk flask, flushed with N_2 gas and dissolved in 40 mL of benzene. The reaction mixture is stirred for 2 h at room temperature. ^1H and ^{13}C NMR spectra show the hydrolyzed phenylethane-1,2-diol as the only product.⁶⁸

Phenylethane-1,2-diol NMR (δ , CDCl_3), ^1H 7.35-7.21 (m, 5H, aryl-*H*), 4.74-4.71 (m, 1H, PhCH), 3.69-3.57 (m, 2H, CH_2OH), 3.08 (s, 2H, OH); ^{13}C 140.55 (s, C_i), 128.42 (s, C_m), 127.78 (s, C_p), 126.09 (s, C_o), 74.71 (PhC), 67.95 (CH_2).⁶⁸

Ph₂P-PPh₂ oxidation

1,1,2,2-Tetraphenyldiphosphane $\text{Ph}_2\text{P-PPh}_2$ is synthesized according to a literature method in 83% isolated yield.⁶⁹ The ^1H and ^{13}C NMR peaks are determined using $^{13}\text{C}, ^1\text{H}$ HMBC and COSY NMR spectra. The ^1H and ^{31}P NMR signals agree with literature values,⁶⁹ and ^{13}C NMR signals agree with trends found in the literature for arylphosphines.⁶

NMR (δ , CDCl_3), ^{31}P -14.84 (s); ^1H 7.39-7.35 (m, 8H, H_o), 7.26 (m, 4H, H_p), 7.20 (m, 8H, H_m);⁶⁹ ^{13}C 135.64 (virtual t, $J(^{31}\text{P}-^{13}\text{C}) = 5.1$ Hz, C_i) 134.30 (virtual t, $J(^{31}\text{P}-^{13}\text{C}) = 12.6$ Hz, C_o), 128.66 (s, C_p), 128.20 (virtual t, $J(^{31}\text{P}-^{13}\text{C}) = 3.3$ Hz, C_m). mp 96-98 °C.

41 mg (0.11 mmol) of $\text{Ph}_2\text{P-PPh}_2$ and 47 mg (0.12 mmol) of $\text{Cy}_3\text{PO}\cdot(\text{HOO})_2\text{CMe}_2$ are filled into an NMR tube flushed with N_2 gas. When 0.4 mL of

C_6D_6 is added to the tube, it heats up immediately. Initially, the sample forms a cloudy solution. However, after a few minutes, $Ph_2P(O)-P(O)Ph_2$ precipitates as a white powder and settles at the bottom of the tube. The water adduct of the phosphine oxide carrier, $Cy_3PO \cdot H_2O$, remains dissolved in C_6D_6 , allowing for easy separation of the product $Ph_2P(O)-P(O)Ph_2$ via filtration. The solid $Ph_2P(O)-P(O)Ph_2$ is redissolved in 0.5 mL of $CDCl_3$ and characterized with 1H , ^{13}C and ^{31}P NMR spectroscopy. The 1H and ^{31}P NMR signals agree with literature values.^{56a} ^{13}C NMR signal assignment is reported for the first time in this dissertation.

NMR (δ , $CDCl_3$), ^{31}P 23.71 (s); 1H 7.93 (dd, $^3J(^{31}P-^1H) = 12.5$ Hz, $^3J(^1H-^1H) = 7.6$ Hz, 8H, H_o), 7.49 (t, $^3J(^1H-^1H) = 7.6$ Hz, 4H, H_p), 7.40 (t, $^3J(^1H-^1H) = 7.6$ Hz, 8H, H_m);^{56a} ^{13}C 132.43 (s, C_i) 131.80 (virtual t, $J(^{31}P-^{13}C) = 5.1$ Hz, C_o), 128.57 (virtual t, $J(^{31}P-^{13}C) = 6.1$ Hz, C_m), 128.32 (s, C_p).

CHAPTER VIII

MISCELLANEOUS RESULTS

Introduction

Di(hydroperoxy)alkane adducts of phosphine oxides are easily synthesized and crystallized. The synthetic method was tested across a wide scope of phosphine oxides and ketones, and all starting materials have successfully produced the expected adducts. However, in one case a completely different species was obtained as product.

In the absence of phosphine oxide, butanone is known to react with H_2O_2 to form 2,2'-peroxydi(butane-2-peroxol), $[\text{HOOCMeEtO-}]_2$, commonly referred to as methylethylketone peroxide (MEKPO).⁷⁰ This substance is used in the polymer industry as a catalyst for acrylic resins or as curing agent for unsaturated polyester resins, and is produced by addition of aqueous H_2O_2 to 2-butanone in the presence of acid.^{71,72} Regarding the previously described adducts of phosphine oxides, the strong hydrogen bond between the phosphine oxide and the 2,2-di(hydroxy)butane prevents the formation of MEKPO. However, in one case the MEKPO came into existence nonetheless, forming a network of hydrogen bonds with the phosphine oxides in the reaction mixture.

Following a similar line of thought, it was hypothesized that diketones which normally undergo cyclization upon reaction with H_2O_2 ,⁷³ could instead form di(hydroperoxy) moieties from each carbonyl group and become attached to diphosphine dioxides with a fitting distance between the PO groups, through hydrogen bonding. Surprisingly, it turned out that bidentate phosphine oxides can act as bystander

molecules, and from a series of experiments different forms of cyclized products were isolated and crystallized. In this chapter, the synthesis and characterization of these serendipitously found molecules, which do not align with the adducts **4-15**, are described in detail.

Results and Discussion

When acetone and 3-pentanone were combined with bis(diphenylphosphino)ethane dioxide (dppe dioxide), the adducts **14** and **15** were formed, respectively. However, when butanone was combined with this diphosphine dioxide and an excess of aqueous H₂O₂, the crystallized product obtained in 83% yield, poly(2,2'-peroxydi(butane-2-peroxol)-bis(diphenylphosphino)ethane dioxide) (**18**), shows a polymeric structure, consisting of dppe dioxide and MEKPO (Figure 8.1).⁷⁴ The two phosphine oxide groups point in opposite directions and form hydrogen bonds with the hydroperoxy functionalities of different MEKPO molecules.

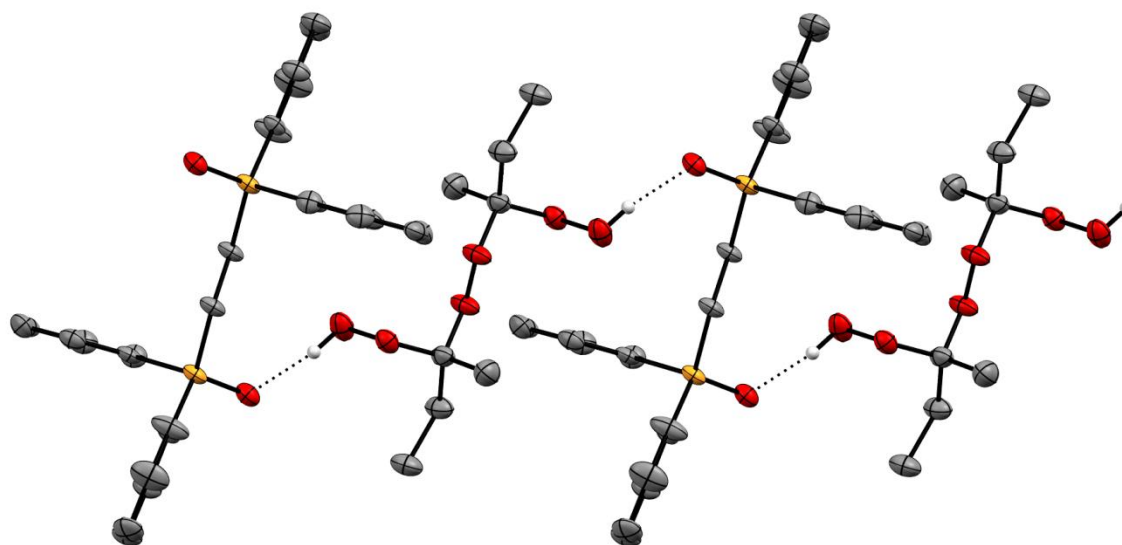
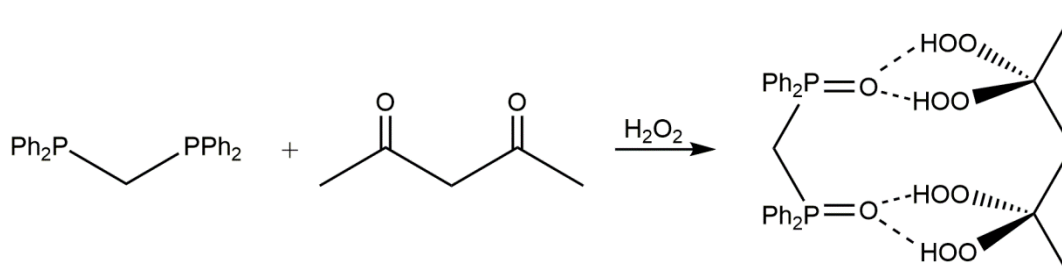


Figure 8.1. Single crystal X-ray structure of material **18**.⁷⁴

Perhaps the ideal packing of the phenyl groups in dppe dioxide promotes the formation of MEKPO as opposed to the di(hydroperoxy)butane moieties found in the adducts **6** and **7**. Another factor favoring the structure of the material is the similar lengths of the P-C-C-P and C-O-O-C units, which allow for their parallel arrangement and strainless stacking in the crystal. The slight difference in the lengths is made up for by the hydrogen bonds. It is yet to be seen whether a similar polymer forms with the cyclohexyl analog of dppe dioxide, [Cy₂P(O)CH₂]₂.

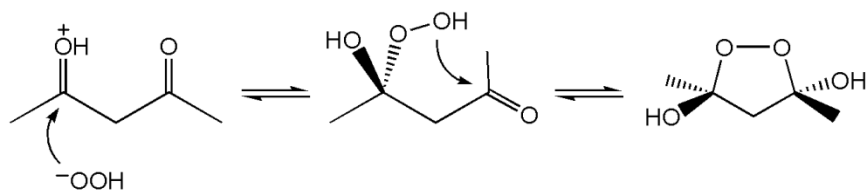
Since dppe dioxide is able to form multiple hydrogen bonds to di(hydroperoxy)alkanes, the next step in synthesis involved expanding the scope of ketones to diketones. It was interesting to see whether both carbonyl groups would undergo nucleophilic attack to each form the di(hydroperoxy)alkane moiety, and finally bind to phosphine oxides, as shown for one example in Scheme 8.1.

To test this idea, dppm dioxide and dppp dioxide were chosen as the phosphine oxides, and acetylacetone was selected as the diketone. While the two P=O groups in dppe dioxide point away from each other in the structures we have obtained so far, the P=O groups in dppm dioxide and dppp dioxide point in the same direction, and are in close enough proximity to form hydrogen bonds, should the acetylacetone successfully form di(hydroperoxy)alkane moieties at both carbonyl positions (Scheme 8.1).



Scheme 8.1. Attempted synthesis of the shown desired adduct.

Unfortunately, the two carbonyl groups in acetylacetone are so close to each other that as soon as one carbonyl group undergoes a nucleophilic attack by hydrogen peroxide, the second carbonyl group is attacked by the resulting hydroperoxide, forming a five-membered ring (Scheme 8.2).^{46,75} Unlike the cases of previous adducts, where the phosphine oxides favorably formed hydrogen bonds with the di(hydroperoxy)alkane moieties and thereby prohibited the cyclic condensation of acetone peroxide or butanone peroxide, the presence of dppm dioxide or dppp dioxide does not prevent the formation of the cycloperoxide according to the pathway displayed in Scheme 8.2 below.



Scheme 8.2. Synthesis of cyclic di(hydroxy)peroxide.

Depending on the concentration of the aqueous H_2O_2 in the reaction mixture, the 3,5-dimethyl-1,2-dioxolane-3,5-diol (**19**)⁷⁶ or the 3,5-dihydroperoxy-3,5-dimethyl-1,2-dioxolane (**20**)⁷⁷ are obtained. An orderly network of hydrogen bonds is formed for both **19** and **20**, and both crystallize easily, without any interaction with the phosphine oxide in solution (Figure 8.2, Figure 8.3). As seen from the X-ray structures, both compounds form the *trans* isomer. The same compounds could also be synthesized just as easily in the absence of chelating phosphine oxides, but with acid catalysis.⁴⁶

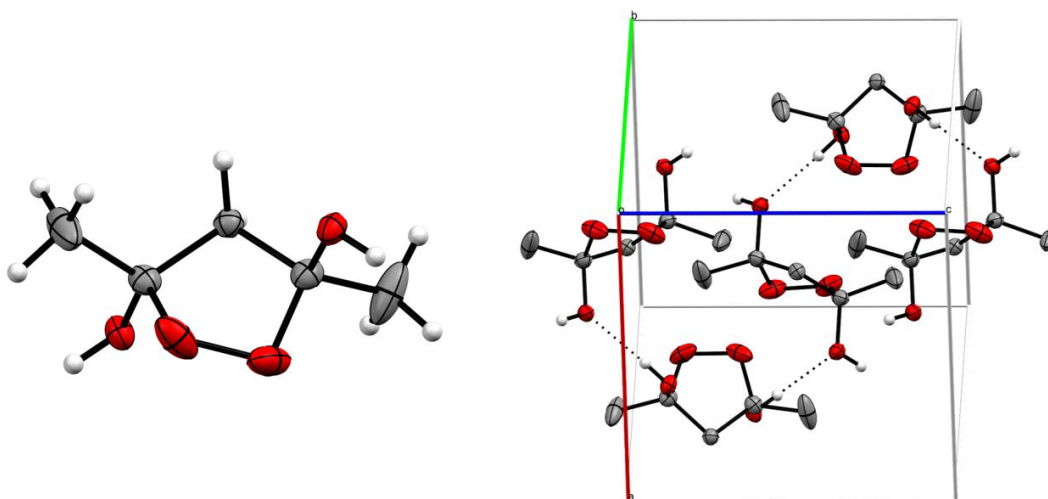


Figure 8.2. Single crystal X-ray structure of a single molecule of **19** (left) and **19** in the unit cell (right).⁷⁶

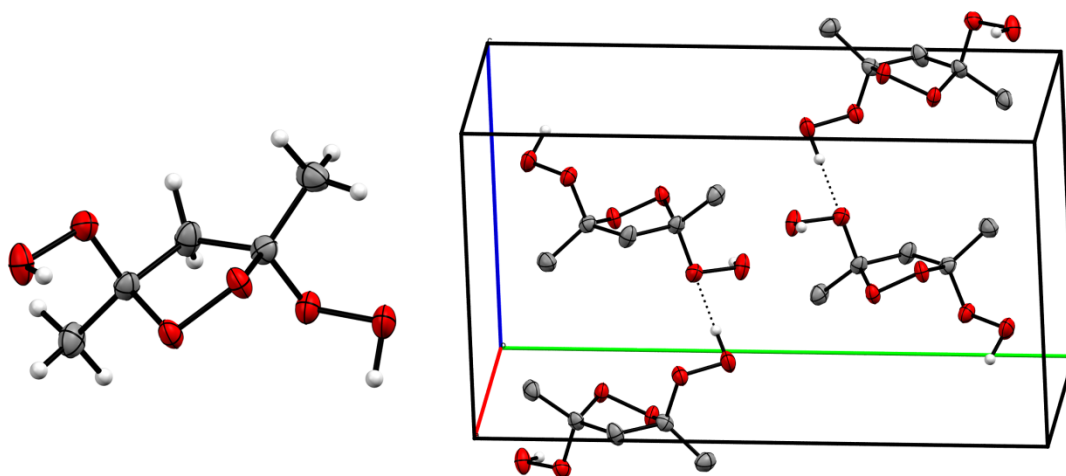


Figure 8.3. Single crystal X-ray structure of a single molecule of **20** (left) and **20** in the unit cell (right).⁷⁷

These diol and dioxolane compounds have been known for some time,^{46,73,75} but the X-ray crystal structures have not been reported yet. Previous reports state that reactions of diketones with aqueous H_2O_2 at room temperature form inseparable mixtures of the di(hydroxy)peroxide (**19**), di(hydroperoxy)peroxide (**20**), and hydroperoxyperoxides (Figure 8.4).^{46,73,75} Contrary to this, in our hands **19** and **20** were both obtained as isolated products in high yields, without the need for further purification.

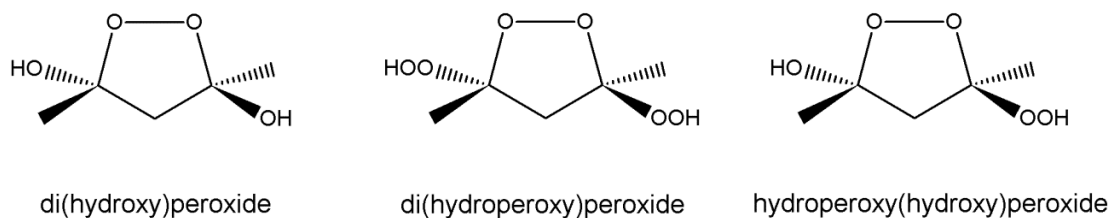


Figure 8.4. Potential products from reaction of acetylacetone with aq. H_2O_2 .

Conclusion

Unlike the cases of the adducts **6** and **7**, reacting H₂O₂ with butanone in the presence of dppe dioxide gives the methylethylketone peroxide molecule (MEKPO). The hydroperoxides at either end of the MEKPO molecule form hydrogen bonds with phosphine oxide groups of different dppe dioxide molecules, thereby generating the polymeric adduct **18**. This adduct is stable and it has been obtained in the form of large single crystals.

The presence of dppm dioxide does not prohibit the cyclization of the diketone when being treated with aqueous H₂O₂. Acetylacetone undergoes nucleophilic attack by aqueous H₂O₂ to form the *trans*-cycloperoxides **19** and **20**. These two species were successfully characterized by single crystal X-ray crystallography, and the structures show intricate networks of intermolecular hydrogen bonds.

Experimental

Poly(2,2'-peroxydi(butane-2-peroxol)-bis(diphenylphosphino)ethane dioxide) (**18**)

In a round bottom flask, dppe dioxide (103 mg, 0.24 mmol) was dissolved in 10 mL of toluene. 10 mL (112 mmol) of butanone and 0.1 mL (1 mmol) of aqueous H₂O₂ was added, and the solution was stirred overnight. The solution was concentrated in vacuum to 5 mL, then the mixture was left so that the product could crystallize. Adduct **19** was obtained in the form of large, colorless, rectangular crystals (126 mg, 0.20 mmol, 83% yield).

NMR (δ , CDCl_3), $^{31}\text{P}\{^1\text{H}\}$ 36.91 (s); ^1H 11.27 (br. s, 2H, OOH), 7.76-7.71 (m, 8H, H_o), 7.56-7.51 (m, 4H, H_p), 7.49-7.45 (m, 8H, H_m), 2.59 (d, $^2J(^{31}\text{P}-^1\text{H}) = 2.7$ Hz, 4H, PCH_2), 1.81 (q, $^3J(^1\text{H}-^1\text{H}) = 7.6$ Hz, 4H, CH_2CH_3), 1.44 (s, 6H, CCH_3), 1.03 (t, $^3J(^1\text{H}-^1\text{H}) = 7.6$ Hz, 6H, CH_2CH_3); $^{13}\text{C}\{^1\text{H}\}$ 132.49 (s, C_p), 130.73 (d, $^1J(^{31}\text{P}-^{13}\text{C}) = 102.8$ Hz, C_i), 130.70 (virtual triplet, $J(^{31}\text{P}-^{13}\text{C}) = 4.7$ Hz, C_o), 129.08 (virtual triplet, $J(^{31}\text{P}-^{13}\text{C}) = 6.1$ Hz, C_m), 111.73 (s, CCH_3), 26.15 (s, CH_2CH_3), 21.31 (t, $^3J(^{31}\text{P}-^{13}\text{C}) = 33.0$ Hz, PCH_2), 17.49 (s, CCH_3), 8.39 (s, CH_2CH_3). IR: $\nu(\text{PO}) = 1437.0$ cm^{-1} .

3,5-Dimethyl-1,2-dioxolane-3,5-diol (**19**)

Dppp (1.001 g, 2.43 mmol) is dissolved in 60 mL of CH_2Cl_2 . Aqueous H_2O_2 (5.0 mL, 0.05 mol) is added, and the solution is stirred for 1 h. The organic layer is collected using a separation funnel, and the solvent is removed *in vacuo*. The resulting white residue is dissolved in 2.5 mL (24.3 mmol) of acetylacetone, followed by the addition of excess aqueous H_2O_2 (0.1 mL, 1.0 mmol). The solution is stirred for 3 days, then the mixture is allowed to stand for crystallization. The unintentional product **19** is obtained in the form of white, crystalline needles (94 mg, 0.71 mmol, 71% yield with respect to amount of H_2O_2 added into the acetylacetone), while an oily liquid remains.

The procedure is repeated without phosphine oxide. 100 mg (1 mmol) of acetylacetone is weighed into a vial, followed by 0.15 mL (1.5 mmol) of H_2O_2 . The solution is stirred overnight, and excess water is removed with vacuum. Benzene (1.0 mL) is used to precipitate the product, which is filtered and dried *in vacuo*. (83 mg, 0.62 mmol, 62% yield). ^1H and ^{13}C NMR data match the literature values.⁴⁶

NMR (δ , CDCl_3), ^1H 2.74 (s, 2H, CH_2), 1.63 (s, 6H, CH_3); ^{13}C 105.50 (s, OC), 55.23 (CH_2), 22.59 (CH_3). mp (decomp.) 82 °C.

3,5-Dihydroperoxy-3,5-dimethyl-1,2-dioxolane (**20**)

100 mg (1 mmol) of acetylacetone is weighed into a vial and combined with 1.0 mL (10 mmol) of aqueous H_2O_2 . The solution is stirred overnight, and the excess of water is removed with vacuum. Benzene (1.0 mL) is used to precipitate the product (113 mg, 0.68 mmol, 68% yield). ^1H and ^{13}C NMR data match the literature values.⁴⁶

NMR (δ , CDCl_3), ^1H 8.54 (s, 2H, OH), 2.74 (s, 2H, CH_2), 1.63 (s, 6H, CH_3); ^{13}C 112.99 (s, OC), 51.11 (CH_2), 17.52 (CH_3). mp (decomp.) 98 °C.

CHAPTER IX

SUMMARY

Hydrogen peroxide and di(hydroperoxy)alkane adducts of phosphine oxides are presented as solid, safe, stoichiometric and soluble oxidizing agents. Structural motifs of H_2O_2 adducts with different $\text{R}_3\text{PO} : \text{H}_2\text{O}_2$ ratios are highlighted by single crystal analyses, and the physical properties of all adducts are described in detail.

Di(hydroperoxy)alkane adducts of phosphine oxides are successfully synthesized at room temperature in high yields, without the use of acid or metal catalysts. Phosphines, phosphine oxides, and H_2O or H_2O_2 adducts of phosphine oxides can be used as the starting materials. While high solubility of these starting materials in CH_2Cl_2 renders it an attractive solvent, the corresponding ketone can just as well be used as the solvent. This one-pot, general synthetic method has been applied to a wide variety of phosphine oxides and ketones, and the resulting adducts can be safely and easily isolated in the form of large crystals. The general synthetic approach also allows for easy recycling of the phosphine oxide carriers. The adducts can be regenerated by simply stirring the phosphine oxides in a solution of excess H_2O_2 and ketone.

All adducts have been fully characterized, using mostly the methods multinuclear NMR and IR spectroscopy, X-ray crystallography and melting point analyses. ^{13}C NMR spectroscopy is especially valuable as a diagnostic tool, as the quaternary carbon on the $(\text{HOO})_2\text{CR}'\text{R}''$ moiety displays a unique signal at 108-120 ppm, and the product can be identified prior to its isolation. X-Ray crystallography and IR spectroscopy show

significant elongation and weakening of the P=O bond as a result of hydrogen bonding to the $(\text{HOO})_2\text{CR}'\text{R}''$ moiety.

IR spectroscopy also confirms the absence of water molecules in the adducts. Moreover, the adducts are insoluble in H_2O , but they show high solubility in many common organic solvents. Thus, when used as oxidizing agents, the oxidation reaction can be performed in a single organic phase.

Because these adducts have a well-defined molecular structure, the exact number of active oxygen atoms can be easily calculated. The anhydrous and stoichiometric character of the adducts of the type $\text{R}_3\text{PO}\cdot(\text{HOO})_2\text{CR}'\text{R}''$ allows for their application as oxidants in reactions that require air- and water-free conditions, as well as reactions that are sensitive to overoxidation. Indeed, dialkyl sulfides were selectively oxidized to sulfoxides, and 1,1,2,2-tetraphenyldiphosphine was transformed quantitatively into the corresponding dioxide without hydrolysis of the P-P bond or oxygen insertion.

In the case of reluctant educts such as diarylsulfides, a catalyst or initiator can be used in combination with the adducts to push the reaction forward. Overoxidation to the sulfones $\text{R}'\text{R}''\text{SO}_2$ can be prevented by careful control of the reaction conditions. In the presence of acid, but no other substrate, the di(hydroperoxy)cycloalkane moieties are transformed into the corresponding free lactones and the phosphine oxide carriers.

Decomposition of the adducts $\text{R}_3\text{PO}\cdot(\text{HOO})_2\text{CR}'\text{R}''$ under thermal and mechanical stress was studied in more detail. Upon heating, hammering and grinding, no sudden release of oxygen or other sign of violent decomposition was observed, confirming the safety of these adducts. Furthermore, the long term stability and shelf life

of the adducts was studied by storing them under various conditions. A quantitative NMR method was developed to study the rate of decomposition. The oxidation capacity of the stored adducts was monitored by the oxidation of Ph_3P , and the amount of oxidized Ph_3P was calculated *via* ^{31}P NMR peak integration. This number was compared to the mass of adduct used for the oxidation to quantify the number of active peroxide groups remaining in the adduct. Using this method, it has been shown that the adducts decompose to about 70% of their original oxidative power when stored as powders at room temperature for several months. However, when the powders are stored at a lower temperature of $-4\text{ }^\circ\text{C}$, there is essentially no decomposition even after months. Moreover, when the adducts are stored as large single crystals, decomposition is insignificant even at room temperature.

In one particular case, adduct synthesis with 2-butanone in the presence of a stoichiometric amount of dppe dioxide resulted in the condensation to methylethylketone peroxide (MEKPO), which then formed hydrogen bonds to two molecules of dppe dioxide. The resulting adduct displayed a polymeric structure, as opposed to the discrete molecular structures observed for $\text{R}_3\text{PO}\cdot(\text{HOO})_2\text{CMeEt}$ ($\text{R} = \text{Cy}, \text{Ph}$). It is hypothesized that the sterics of dppe dioxide is favorable for packing with MEKPO, and thus unlike the previous adducts, condensation of 2,2-di(hydroperoxy)butane to MEKPO is not prohibited by the presence of phosphine oxide bonds.

The presence of phosphine oxide also does not interfere with cyclization of diketones with H_2O_2 . Acetylacetone undergoes nucleophilic attack by aqueous H_2O_2 to form *trans*-cycloperoxides. Depending on the concentration of H_2O_2 , either 3,5-

dimethyl-1,2-dioxolane-3,5-diol or 3,5-dihydroperoxy-3,5-dimethyl-1,2-dioxolane is isolated as the sole product. Both species form an intricate network of hydrogen bonds with neighboring molecules and crystallize easily. This might be the reason why no interactions with the offered diphosphine dioxides are observed.

REFERENCES

- (1) (a) Cavani, F.; Teles, J. H. *ChemSusChem* **2009**, *2*, 508-534; (b) Comyns, A. E. *Peroxides and Peroxide Compounds (Inorganic)* in *Van Nostrand's Encyclopedia of Chemistry*, John Wiley & Sons, Inc., **2005**.
- (2) Uyanik, M.; Nakashima, D.; Ishihara, K. *Angew. Chem. Int. Ed.* **2012**, *51*, 9093-9096.
- (3) Goodman, M. A.; Detty, M. R. *Synlett* **2006**, *2006*, 1100-1104.
- (4) (a) Habibi, D.; Zolfigol, M. A.; Safaiee, M.; Shamsian, A.; Ghorbani-Choghamarani, A. *Catal. Commun.* **2009**, *10*, 1257-1260; (b) Golchoubian, H.; Hosseinpour, F. *Molecules* **2007**, *12*, 304-311; (c) Amini, M.; Bagherzadeh, M.; Moradi-Shoeili, Z.; Boghaei, D. M.; Ellern, A.; Woo, L. K. *J. Coord. Chem.* **2013**, *66*, 464-472; (d) Selvam, J. J. P.; Suresh, V.; Rajesh, K.; Babu, D. C.; Suryakiran, N.; Venkateswarlu, Y. *Tetrahedron Lett.* **2008**, *49*, 3463-3465; (e) Chu, J.-W.; Trout, B. L. *J. Amer. Chem. Soc.* **2004**, *126*, 900-908.
- (5) (a) Markovits, I. I.; Eger, W. A.; Yue, S.; Cokoja, M.; Münchmeyer, C. J.; Zhang, B.; Zhou, M. D.; Genest, A.; Mink, J.; Zang, S. L. *Chem. Eur. J.* **2013**, *19*, 5972-5979; (b) Yao, H.; Richardson, D. E. *J. Amer. Chem. Soc.* **2000**, *122*, 3220-3221; (c) Owens, G. S.; Abu-Omar, M. M. *Chem. Commun.* **2000**, 1165-1166.
- (6) Hilliard, C. R.; Bhuvanesh, N.; Gladysz, J. A.; Blümel, J. *Dalton Trans.* **2012**, *41*, 1742-1754.
- (7) Klassen, N. V.; Marchington, D.; McGowan, H. C. *Anal. Chem.* **1994**, *66*, 2921-2925.
- (8) (a) Lin, Q.; Jiang, Y.; Geng, J.; Qian, Y. *Chem. Eng. J.* **2008**, *139*, 264-271; (b) Ji, L.; Wang, Y.-N.; Qian, C.; Chen, X.-Z. *Synth. Commun.* **2013**, *43*, 2256-2264; (c) Ball, M. C.; Massey, S. *Thermochim. Acta* **1995**, *261*, 95-106; (d) Dobado, J.; Molina, J.; Portal, D. *J. Phys. Chem. A* **1998**, *102*, 778-784; (e) Taliansky, S. *Synlett* **2005**, *2005*, 1962-1963; (f) Cooper, M. S.; Heaney, H.; Newbold, A. J.; Sanderson, W. R. *Synlett* **1990**, *1990*, 533-535.
- (9) (a) Koukabi, N. *Synlett* **2010**, *2010*, 2969-2970; (b) Pritchard, R. G.; Islam, E. *Acta Crystallogr. Sect. B: Struct. Sci.* **2003**, *59*, 596-605.

- (10) (a) McKillop, A.; Sanderson, W. R. *J. Chem. Soc., Perkin Trans. 1* **2000**, 471-476; (b) Jones, D. P.; Griffith, W. P. *J. Chem. Soc., Dalton Trans.* **1980**, 2526-2532.
- (11) Bednarz, S.; Ryś, B.; Bogdał, D. *Molecules* **2012**, *17*, 8068-8078.
- (12) Jiang, T.; Wang, W.; Han, B. *New J. Chem.* **2013**, *37*, 1654-1664.
- (13) Prakash, G. S.; Shakhmin, A.; Glinton, K. E.; Rao, S.; Mathew, T.; Olah, G. A. *Green Chem.* **2014**, *16*, 3616-3622.
- (14) (a) Mühle, C.; Peters, E.-M.; Jansen, M. *Z. Naturforsch.* **2009**, *64b*, 111-115; (b) Cho, J.; Jeon, S.; Wilson, S. A.; Liu, L. V.; Kang, E. A.; Braymer, J. J.; Lim, M. H.; Hedman, B.; Hodgson, K. O.; Valentine, J. S.; Solomon, E. I.; Nam, W. *Nature* **2011**, *478*, 502-505; (c) Schölkopf, T.; Van, N.-D.; Schleid, T. *Inorg. Chim. Acta* **2011**, *374*, 181-186; (d) Kunishita, A.; Scanlon, J. D.; Ishimaru, H.; Honda, K.; Ogura, T.; Suzuki, M.; Cramer, C. J.; Itoh, S. *Inorg. Chem.* **2008**, *47*, 8222-8232.
- (15) Arzumanyan, A. V.; Terent'ev, A. O.; Novikov, R. A.; Lakhtin, V. G.; Chernyshev, V. V.; Fitch, A. N.; Nikishin, G. I. *Eur. J. Org. Chem.* **2014**, *2014*, 6877-6883.
- (16) Schulz, M.; Teles, J. H.; Sundermeyer, J.; Wahl, G. Patent DE 19533331, **1997**.
- (17) Hilliard, C. R.; Kharel, S.; Cluff, K. J.; Bhuvanesh, N.; Gladysz, J. A.; Blümel, J. *Chem. Eur. J.* **2014**, *20*, 17292-17295.
- (18) Ahn, S. H.; Cluff, K. J.; Bhuvanesh, N.; Blümel, J. *Angew. Chem.* **2015**, *127*, 13539-13543.
- (19) (a) Temple, R.; Tsuno, Y.; Leffler, J. *J. Org. Chem.* **1963**, *28*, 2495-2495; (b) Thierbach, D.; Huber, F.; Preut, H. *Acta Crystallogr. Sect. B: Struct. Sci.* **1980**, *36*, 974-977.
- (20) CCDC 1033533 contains the supplementary crystallographic data of **1**. These data can be obtained free of charge from the Cambridge Crystallographic Data Centre via www.ccdc.cam.ac.uk/data_request/cif., C₁₂H₂₇O₁P₁·H₂O₂ unit cell parameters: a 8.266(2), b 15.032(4), c 12.467(4), P2₁/n.
- (21) Bewick, N. A.; Arendt, A.; Li, Y.; Szafert, S.; Lis, T.; Wheeler, K. A.; Young, J.; Dembinski, R. *Curr. Org. Chem.* **2015**, *19*, 469-474.

- (22) CCDC 1033531 contains the supplementary crystallographic data of **2**. These data can be obtained free of charge from the Cambridge Crystallographic Data Centre via www.ccdc.cam.ac.uk/data_request/cif., (C₁₈H₁₅O₁P₁)₂·(H₂O₂)₃ unit cell parameters: a 9.6284(3), b 16.8881(6), c 10.9317(4), P₂₁/n.
- (23) (a) Terent'ev, A.; Platonov, M.; Ogibin, Y. N.; Nikishin, G. *Synth. Commun.* **2007**, *37*, 1281-1287; (b) Terent'ev, A. O.; Kutkin, A. V.; Platonov, M. M.; Vorontsov, I. I.; Antipin, M. Y.; Ogibin, Y. N.; Nikishin, G. I. *Russ. Chem. Bull.* **2004**, *53*, 681-687; (c) Ghorai, P.; Dussault, P. H. *Org. Lett.* **2008**, *10*, 4577-4579; (d) M. C. V. Sauer, J. O. E. *J. Phys. Chem.* **1972**, *76*, 1283-1288.
- (24) Pettinari, C.; Marchetti, F.; Cingolani, A.; Drozdov, A.; Troyanov, S. *Chem. Commun.* **2000**, 1901-1902.
- (25) van Tonder, J. H. *Synlett* **2014**, *25*, 1629-1630.
- (26) Oxley, J. C.; Smith, J. L.; Bowden, P. R.; Rettinger, R. C. *Propellants Explos. Pyrotech.* **2013**, *38*, 244-254.
- (27) (a) Espinosa-Fuentes, E. A.; Pacheco-Londoño, L. C.; Hidalgo-Santiago, M.; Moreno, M.; Vivas-Reyes, R.; Hernández-Rivera, S. P. *J. Phys. Chem. A* **2013**, *117*, 10753-10763; (b) Oxley, J. C.; Smith, J. L.; Huang, J.; Luo, W. *J. Forensic Sci.* **2009**, *54*, 1029-1033; (c) Oxley, J.; Smith, J.; Brady, J.; Dubnikova, F.; Kosloff, R.; Zeiri, L.; Zeiri, Y. *Appl. Spectr.* **2008**, *62*, 906-915.
- (28) CCDC 1033532 contains the supplementary crystallographic data of **4**. These data can be obtained free of charge from the Cambridge Crystallographic Data Centre via www.ccdc.cam.ac.uk/data_request/cif., (C₁₈H₁₅O₁P₁)·(C₃H₈O₄) unit cell parameters: a 9.1646(19), b 21.719(5), c 10.053(2), P₂₁/n.
- (29) CCDC 1033530 contains the supplementary crystallographic data OF **5**. These data can be obtained free of charge from the Cambridge Crystallographic Data Centre via www.ccdc.cam.ac.uk/data_request/cif., (C₁₈H₃₃O₁P₁)·(C₃H₈O₄) unit cell parameters: a 10.158(3), b 10.645(3), c 11.169(3), P-1.
- (30) CCDC 1449060 contains the supplementary crystallographic data of **6**. These data can be obtained free of charge from the Cambridge Crystallographic Data Centre via www.ccdc.cam.ac.uk/data_request/cif., C₁₈H₁₅O₁P₁·(C₄H₁₀O₄) unit cell parameters: a 13.212(3), b 10.652(2), c 15.084(3), P_c.
- (31) CCDC 1449059 contains the supplementary crystallographic data of **7**. These data can be obtained free of charge from the Cambridge Crystallographic Data Centre via www.ccdc.cam.ac.uk/data_request/cif., C₁₈H₃₃O₁P₁·(C₄H₁₀O₄) unit cell parameters: a 10.952(5), b 18.674(0), c 11.503(1), P₂₁/c.

- (32) CCDC 1451015 contains the supplementary crystallographic data of **8**. These data can be obtained free of charge from the Cambridge Crystallographic Data Centre via www.ccdc.cam.ac.uk/data_request/cif, $C_{18}H_{33}O_1P_1 \cdot (C_5H_{12}O_4)$ unit cell parameters: a 11.000(7), b 18.599(0), c 11.828(2), $P2_1/c$.
- (33) CCDC 1451754 contains the supplementary crystallographic data of another polymorph of **8**. These data can be obtained free of charge from the Cambridge Crystallographic Data Centre via www.ccdc.cam.ac.uk/data_request/cif, $C_{18}H_{33}O_1P_1 \cdot (C_5H_{12}O_4)$ unit cell parameters: a 9.629(2), b 11.173(5), c 12.034(9), $P-1$.
- (34) CCDC 1561376 contains the supplementary crystallographic data of **9**. These data can be obtained free of charge from the Cambridge Crystallographic Data Centre via www.ccdc.cam.ac.uk/data_request/cif, $C_{18}H_{33}O_1P_1 \cdot (C_5H_{10}O_4)$ unit cell parameters: a 10.995(3), b 18.254(3), c 11.838(4), $P2_1/c$.
- (35) CCDC 1451014 contains the supplementary crystallographic data of **10**. These data can be obtained free of charge from the Cambridge Crystallographic Data Centre via www.ccdc.cam.ac.uk/data_request/cif, $C_{18}H_{33}O_1P_1 \cdot (C_6H_{12}O_4)$ unit cell parameters: a 10.874(2), b 18.629(3), c 11.959(1), $P2_1/c$.
- (36) CCDC 1561375 contains the supplementary crystallographic data of **11**. These data can be obtained free of charge from the Cambridge Crystallographic Data Centre via www.ccdc.cam.ac.uk/data_request/cif, $C_{18}H_{33}O_1P_1 \cdot (C_7H_{14}O_4)$ unit cell parameters: a 10.841(2), b 18.222(4), c 12.877(3), $P2_1/c$.
- (37) CCDC 1449062 contains the supplementary crystallographic data of **12**. These data can be obtained free of charge from the Cambridge Crystallographic Data Centre via www.ccdc.cam.ac.uk/data_request/cif, $C_{18}H_{33}O_1P_1 \cdot (C_8H_{10}O_4)$ unit cell parameters: a 19.226(0), b 10.972(3), c 25.247(4), $C2/c$.
- (38) CCDC 1044831 contains the supplementary crystallographic data of **14**. These data can be obtained free of charge from the Cambridge Crystallographic Data Centre via www.ccdc.cam.ac.uk/data_request/cif, $[(C_{26}H_{24}O_2P_2) \cdot (C_3H_8O_4)_2]$ unit cell parameters: a 10.8389(17), b 19.838(3), c 15.277(2), $P2_1/c$.
- (39) CCDC 1449063 contains the supplementary crystallographic data of **15**. These data can be obtained free of charge from the Cambridge Crystallographic Data Centre via www.ccdc.cam.ac.uk/data_request/cif, $[C_{26}H_{24}O_2P_2 \cdot (C_5H_{12}O_4)_2]$ unit cell parameters: a 8.794(4), b 12.076(3), c 17.271(4), $P2_1/n$.
- (40) CCDC 1449058 contains the supplementary crystallographic data of **13**. These data can be obtained free of charge from the Cambridge Crystallographic Data

Centre via www.ccdc.cam.ac.uk/data_request/cif., $C_{25}H_{22}O_2P_2 \cdot (C_3H_8O_4)$ unit cell parameters: a 23.661(2), b 11.106(0), c 21.401(6), *Pbcn*.

- (41) Al-Farhan, K. A. *J. Chem. Crystallogr.* **1992**, *22*, 687-689.
- (42) Davies, J. A.; Dutremez, S.; Pinkerton, A. A. *Inorg. Chem.* **1991**, *30*, 2380-2387.
- (43) Antipin, M. Y.; Struchkov, Y. T.; Pisareva, S.; Medved', T. Y.; Kabachnik, M. J. *Struct. Chem.* **1980**, *21*, 644-649.
- (44) Calcagno, P.; Kariuki, B. M.; Kitchin, S. J.; Robinson, J.; Philp, D.; Harris, K. D. *Chem. Eur. J.* **2000**, *6*, 2338-2349.
- (45) Piestert, F.; Fetouaki, R.; Bogza, M.; Oeser, T.; Blümel, J. *Chem. Commun.* **2005**, 1481-1483.
- (46) Novikov, V.; Shestak, O. *Russ. Chem. Bull.* **2013**, *62*, 2171-2190.
- (47) (a) Perkampus, H. H. *Ber. Bunsen Ges. Phys. Chem.* **1976**, *80*, 99-100; (b) Bellamy, L. J. *Advances in infrared group frequencies*; Methuen: London, 1968.
- (48) (a) Corpening, J.; Heister, S. D.; Anderson, W.; Austin, B. *J. Propul. Power* **2006**, *22*, 996-1005; (b) Cynn, H.; Yoo, C.-S.; Sheffield, S. A. *J. Chem. Phys.* **1999**, *110*, 6836-6843; (c) Lousada, C. M.; Johansson, A. J.; Brinck, T.; Jonsson, M. *J. Phys. Chem. C* **2012**, *116*, 9533-9543; (d) Rocha Gonsalves, A. A.; Johnstone, R.; Pereira, M.; Shaw, J. *J. Chem. Res., Synop.* **1991**, 208-209.
- (49) (a) Rizzo, V.; Pinciroli, V. *J. Pharm. Biomed. Anal.* **2005**, *38*, 851-857; (b) Malz, F.; Jancke, H. *J. Pharm. Biomed. Anal.* **2005**, *38*, 813-823; (c) Holzgrabe, U.; Deubner, R.; Schollmayer, C.; Waibel, B. *J. Pharm. Biomed. Anal.* **2005**, *38*, 806-812; (d) Evilia, R. F. *Anal. Lett.* **2001**, *34*, 2227-2236.
- (50) Maniara, G.; Rajamoorthi, K.; Rajan, S.; Stockton, G. W. *Anal. Chem.* **1998**, *70*, 4921-4928.
- (51) Henderson, T. J. *Anal. Chem.* **2002**, *74*, 191-198.
- (52) Saito, T.; Nakaie, S.; Kinoshita, M.; Ihara, T.; Kinugasa, S.; Nomura, A.; Maeda, T. *Metrologia* **2004**, *41*, 213-218.
- (53) CCDC 1561377 contains the supplementary crystallographic data of **16**. These data can be obtained free of charge from the Cambridge Crystallographic Data Centre via www.ccdc.cam.ac.uk/data_request/cif., $C_{18}H_{33}O_1P_1 \cdot (C_6H_{12}O_3)$ unit cell parameters: a 11.055(1), b 18.209(2), c 11.971(9), *P2₁/c*.

- (54) (a) Bayat, A.; Shakourian-Fard, M.; Hashemi, M. M. *Catal. Commun.* **2014**, *52*, 16-21; (b) Chica, A.; Gatti, G.; Moden, B.; Marchese, L.; Iglesia, E. *Chem. Eur. J.* **2006**, *12*, 1960-1967; (c) He, Y.; Ma, X.; Ji, H. F.; Zha, X. B.; Jiang, H.; Lu, M. *Phosphorus Sulfur Silicon Relat. Elem.* **2012**, *187*, 822-830; (d) Shaabani, A.; Farhangi, E.; Rahmati, A. *Phosphorus Sulfur Silicon* **2010**, *185*, 463-468.
- (55) Osovsky, R.; Kaplan, D.; Nir, I.; Rotter, H.; Elisha, S.; Columbus, I. *Environ. Sci. Technol.* **2014**, *48*, 10912-10918.
- (56) (a) Nycz, J. E.; Musiol, R. *Heteroatom Chem.* **2006**, *17*, 310-316; (b) Woźniak, L.; Kowalski, J.; Chojnowski, J. *Tetrahedron Lett.* **1985**, *26*, 4965-4968.
- (57) Blake, A.; McQuillan, G.; Oxtan, I.; Troy, D. *J. Mol. Struct.* **1982**, *78*, 265-271.
- (58) (a) Baj, S.; Chrobok, A.; Słupska, R. *Green Chem.* **2009**, *11*, 279-282; (b) Brunetta, A.; Strukul, G. *Eur. J. Inorg. Chem.* **2004**, *2004*, 1030-1038; (c) Göttlich, R.; Yamakoshi, K.; Sasai, H.; Shibasaki, M. *Synlett* **1997**, *1997*, 971-973; (d) Kirumakki, S.; Samarajeewa, S.; Harwell, R.; Mukherjee, A.; Herber, R. H.; Clearfield, A. *Chem. Commun.* **2008**, 5556-5558; (e) Kjonaas, R. A.; Clemons, A. E. *J. Chem. Ed.* **2008**, *85*, 827; (f) Ma, Q.; Xing, W.; Xu, J.; Peng, X. *Catal. Commun.* **2014**, *53*, 5-8; (g) Baj, S.; Słupska, R.; Chrobok, A.; Drożdż, A. *J. Mol. Catal. A: Chem.* **2013**, *376*, 120-126.
- (59) (a) Ali, M. H.; Hedell, J.; Wenczewicz, T. *J. Sulfur Chem.* **2009**, *30*, 160-166; (b) Ashikhmina, E.; Rubtsova, S.; Dvornikova, I.; Kuchin, A. *Russ. J. Org. Chem.* **2009**, *45*, 1509-1514; (c) Balicki, R. *Synth. Commun.* **1999**, *29*, 2235-2239; (d) Kadijani, J. A.; Narimani, E.; Kadijani, H. A. *Pet. Coal* **2014**, *56*, 116-123; (e) Lakouraj, M. M.; Hasantabar, V. *J. Sulfur Chem.* **2011**, *32*, 93-98; (f) Pires, S. M. G.; Simões, M. M. Q.; Santos, I. C. M. S.; Rebelo, S. L. H.; Paz, F. A. A.; Neves, M. G. P. M. S.; Cavaleiro, J. A. S. *Appl. Catal. B: Environ.* **2014**, *160*, 80-88; (g) Sharma, V. K.; Luther III, G. W.; Millero, F. J. *Chemosphere* **2011**, *82*, 1083-1089; (h) Vin, T. F.; Tarakanova, A.; Kostyuchenko, O.; Tarasevich, B.; Kulikov, N.; Anisimov, A. *Theor. Found. Chem. Eng.* **2008**, *42*, 636-642.
- (60) Maleki, B.; Hemmati, S.; Sedrpoushan, A.; Ashrafi, S. S.; Veisi, H. *RSC Adv.* **2014**, *4*, 40505-40510.
- (61) (a) Deubel, D. V.; Frenking, G.; Gisdakis, P.; Herrmann, W. A.; Rösch, N.; Sundermeyer, J. *Acc. Chem. Res.* **2004**, *37*, 645-652; (b) Figueras, F.; Kochkar, H. *Catal. Lett.* **1999**, *59*, 79-81; (c) Grigoropoulou, G.; Clark, J.; Elings, J. *Green Chem.* **2003**, *5*, 1-7; (d) Kamata, K.; Yonehara, K.; Sumida, Y.; Yamaguchi, K.; Hikichi, S.; Mizuno, N. *Science* **2003**, *300*, 964-966; (e) Usui, Y.; Sato, K.; Tanaka, M. *Angew. Chem. Int. Ed.* **2003**, *115*, 5781-5783.

- (62) Lane, B. S.; Burgess, K. *J. Amer. Chem. Soc.* **2001**, *123*, 2933-2934.
- (63) Enthaler, S.; Weidauer, M. *Catal. Lett.* **2011**, *141*, 833-838.
- (64) Abraham, R. J.; Byrne, J. J.; Griffiths, L. *Magn. Reson. Chem.* **2008**, *46*, 667-675.
- (65) Abraham, R. J.; Reid, M. *J. Chem. Soc., Perkin Trans. 2* **2002**, 1081-1091.
- (66) Nikishin, G. I.; Sokova, L. L.; Makhaev, V. D.; Kapustina, N. I. *Mendeleev Commun.* **2003**, *13*, 264-265.
- (67) Brodsky, B. H.; Du Bois, J. *J. Amer. Chem. Soc.* **2005**, *127*, 15391-15393.
- (68) Plietker, B.; Niggemann, M.; Pollrich, A. *Org. Biomol. Chem.* **2004**, *2*, 1116-1124.
- (69) Dodds, D. L.; Haddow, M. F.; Orpen, A. G.; Pringle, P. G.; Woodward, G. *Organometallics* **2006**, *25*, 5937-5945.
- (70) Zhang, J.; Wu, W.; Qian, G.; Zhou, X.-G. *J. Hazard. Mater.* **2010**, *181*, 1024-1030.
- (71) (a) Vaidya, U. R.; Nadkarni, V. M. *Ind. Eng. Chem. Res.* **1987**, *26*, 194-198; (b) Aslan, S.; Immirzi, B.; Laurienzo, P.; Malinconico, M.; Martuscelli, E.; Volpe, M.; Pelino, M.; Savini, L. *J. Mater. Sci.* **1997**, *32*, 2329-2336.
- (72) (a) Soulounganga, P.; Marion, C.; Huber, F.; Gerardin, P. *J. Appl. Polym. Sci.* **2003**, *88*, 743-749; (b) Zhou, Q.; Cho, D.; Song, B. K.; Kim, H.-J. *J. Therm. Anal. Calorim.* **2010**, *99*, 277-284.
- (73) Payne, G. B. *J. Org. Chem.* **1961**, *26*, 4793-4797.
- (74) CCDC 1449057 contains the supplementary crystallographic data of **18** for this paper. These data can be obtained free of charge from the Cambridge Crystallographic Data Centre via www.ccdc.cam.ac.uk/data_request/cif., [C₂₆H₂₄O₂P₂·(C₈H₁₈O₆)_n] unit cell parameters: *a* 8.635(2), *b* 9.022(9), *c* 11.547(7), *P*-1.
- (75) (a) Rieche, A.; Bischoff, C. *Eur. J. Inorg. Chem.* **1962**, *95*, 77-82; (b) Azarifar, D.; Khosravi, K. *Eur. J. Chem.* **2010**, *1*, 15-19.

- (76) CCDC 1449061 contains the supplementary crystallographic data of **19** for this paper. These data can be obtained free of charge from the Cambridge Crystallographic Data Centre via www.ccdc.cam.ac.uk/data_request/cif., C₅H₁₀O₄ unit cell parameters: *a* 8.9984(5), *b* 8.984(5), *c* 8.500(7), *P*4₃2₁2.
- (77) CCDC 1452863 contains the supplementary crystallographic data of **20** for this paper. These data can be obtained free of charge from the Cambridge Crystallographic Data Centre via www.ccdc.cam.ac.uk/data_request/cif., C₅H₁₀O₆ unit cell parameters: *a* 5.566(1), *b* 15.416(7), *c* 8.854(5), *P*2₁/n.

APPENDIX A
NMR SPECTRA

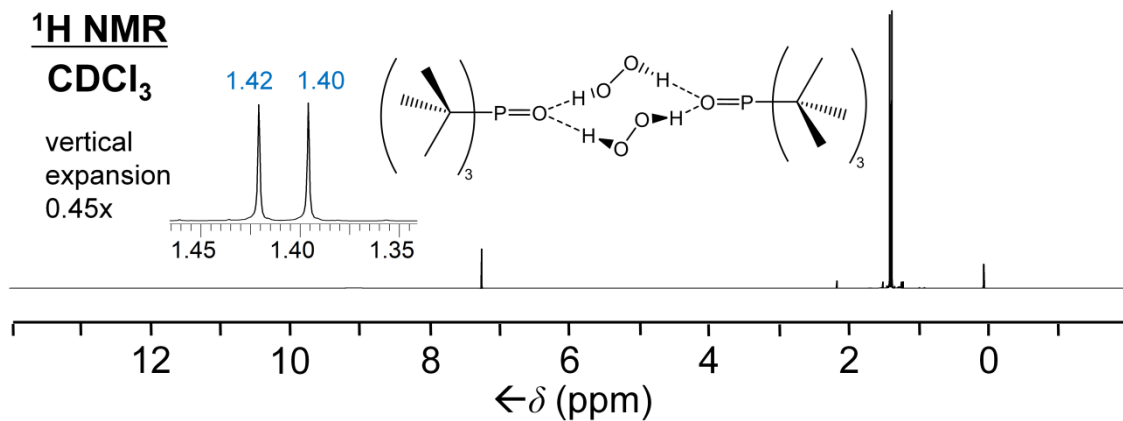


Figure A.1. ¹H NMR spectrum of **1** in CDCl₃.

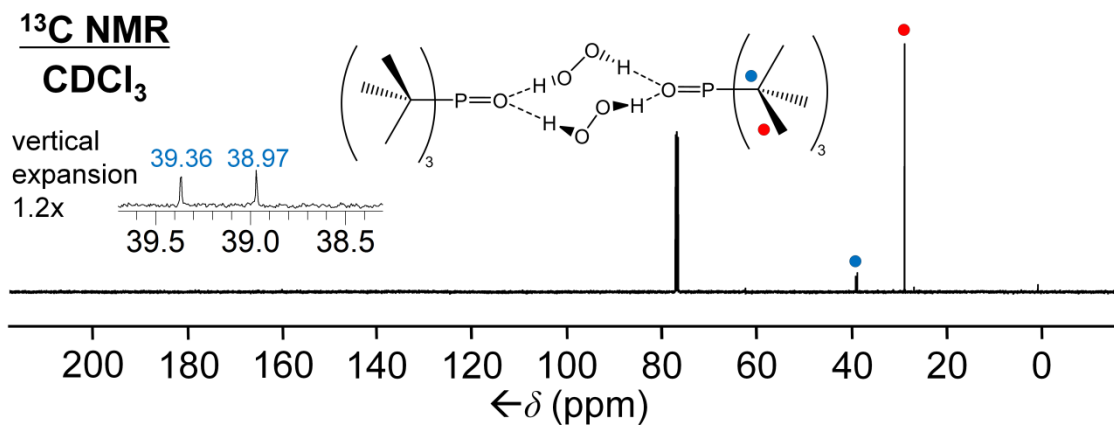


Figure A.2. ¹³C{¹H} NMR spectrum of **1** in CDCl₃.

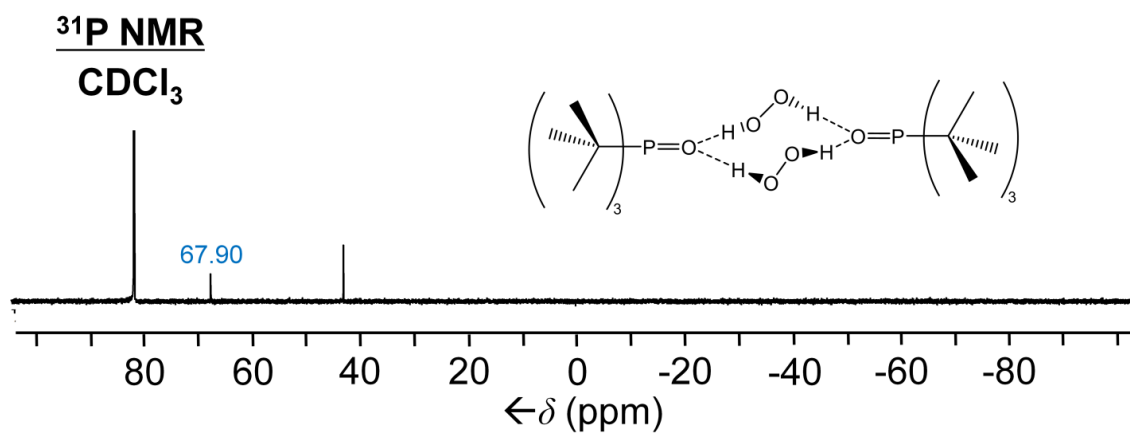


Figure A.3. ³¹P{¹H} NMR spectrum of **1** in CDCl₃.

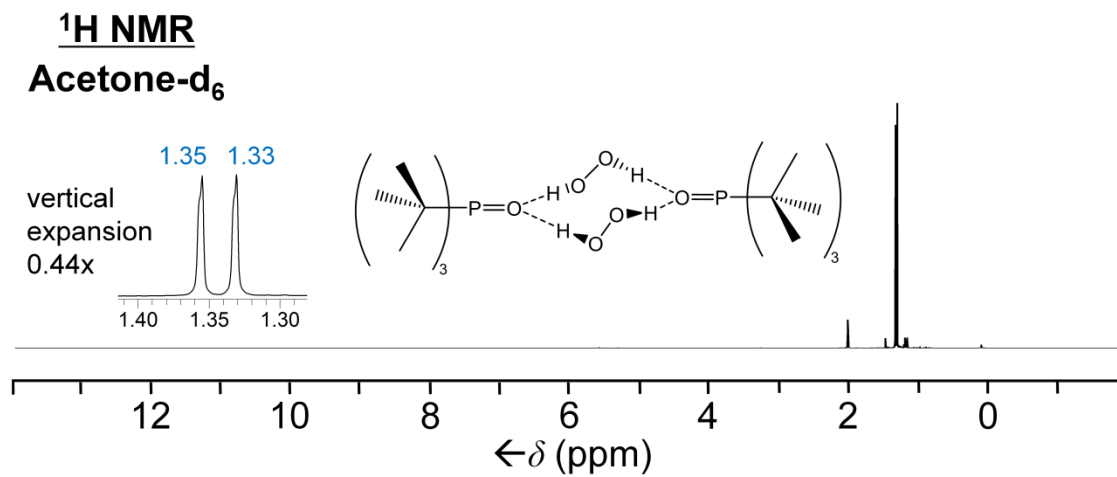


Figure A.4. ¹H NMR spectrum of **1** in acetone-d₆.

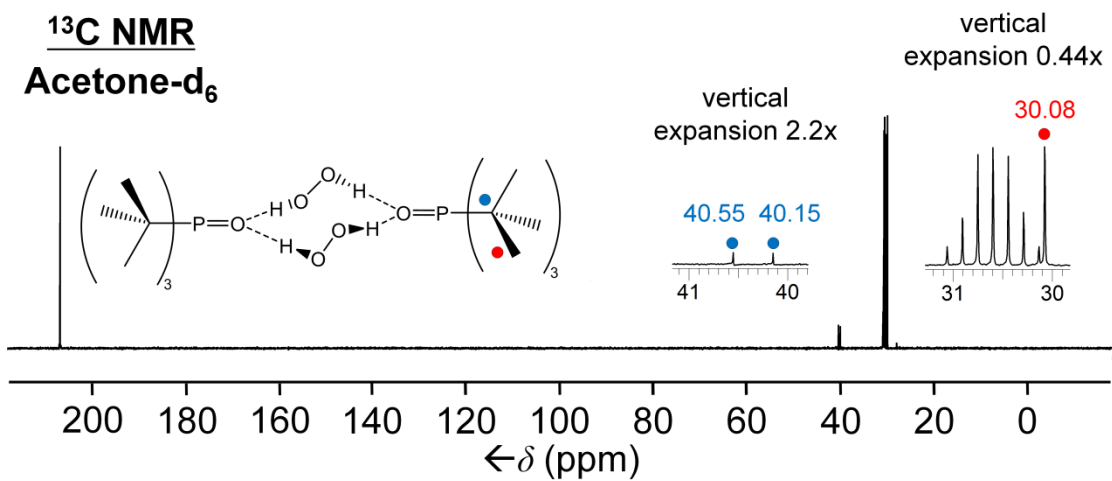


Figure A.5. $^{13}\text{C}\{^1\text{H}\}$ NMR spectrum of **1** in acetone-d₆.

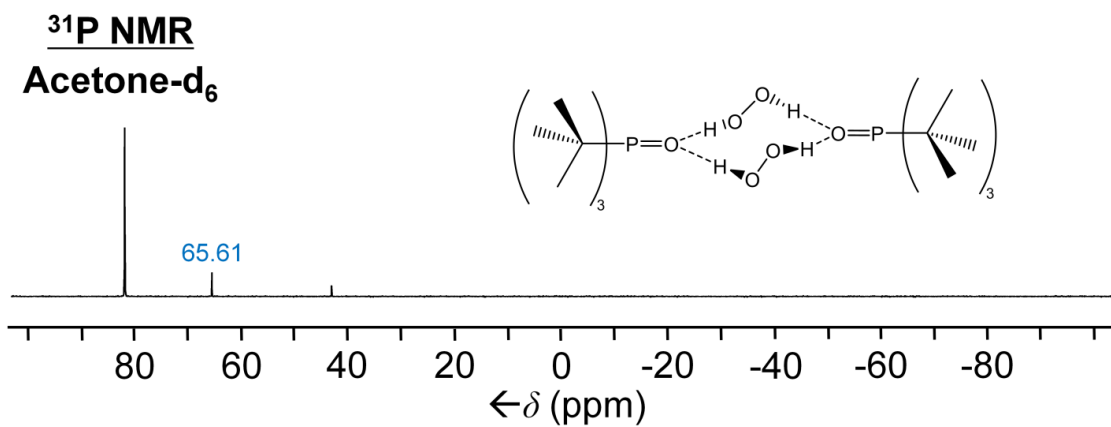


Figure A.6. $^{31}\text{P}\{^1\text{H}\}$ NMR spectrum of **1** in acetone-d₆.

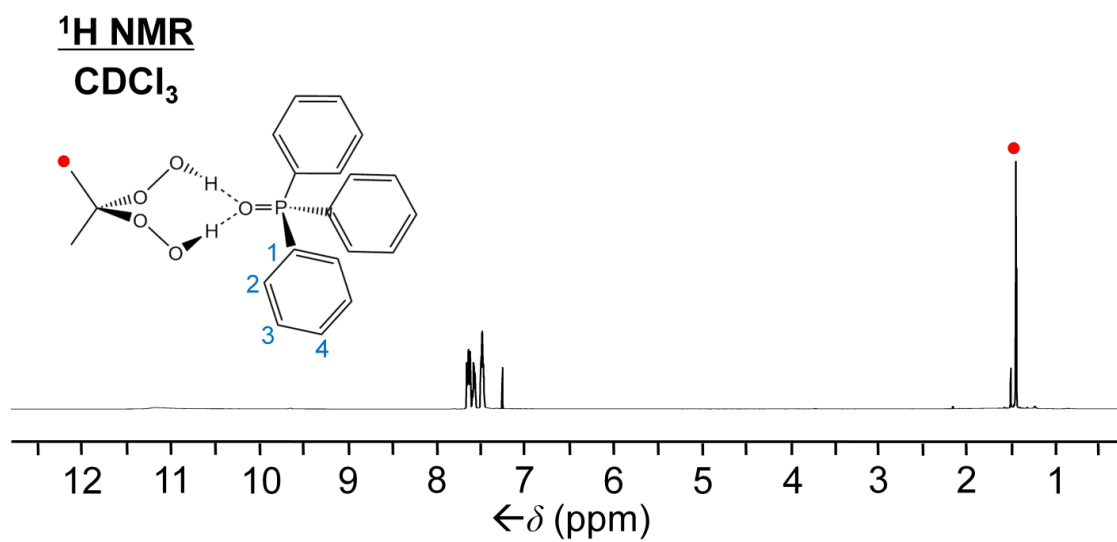


Figure A.7. ¹H NMR spectrum of **4** in CDCl₃.

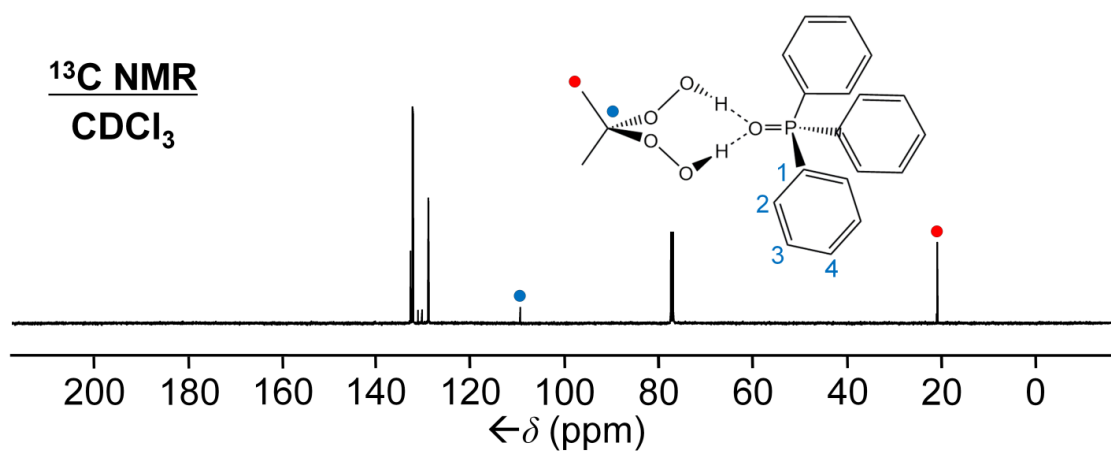


Figure A.8. ¹³C{¹H} NMR spectrum of **4** in CDCl₃.

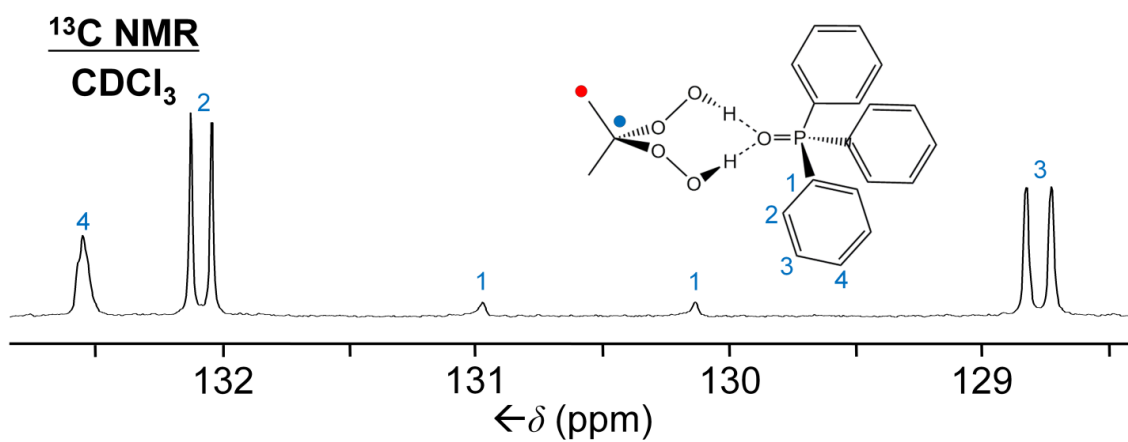


Figure A.9. Expansion of aryl region of ¹³C{¹H} NMR spectrum of **4** in CDCl₃.

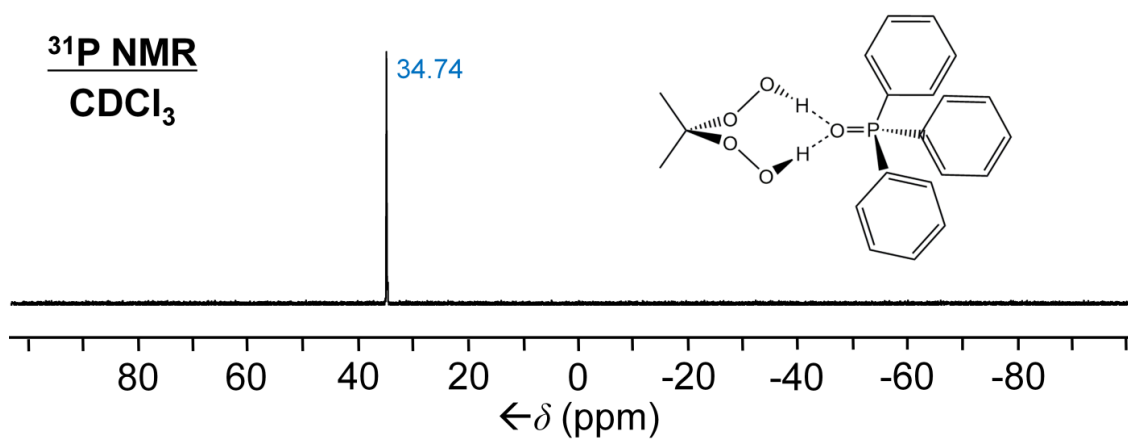


Figure A.10. ³¹P{¹H} NMR spectrum of **4** in CDCl₃.

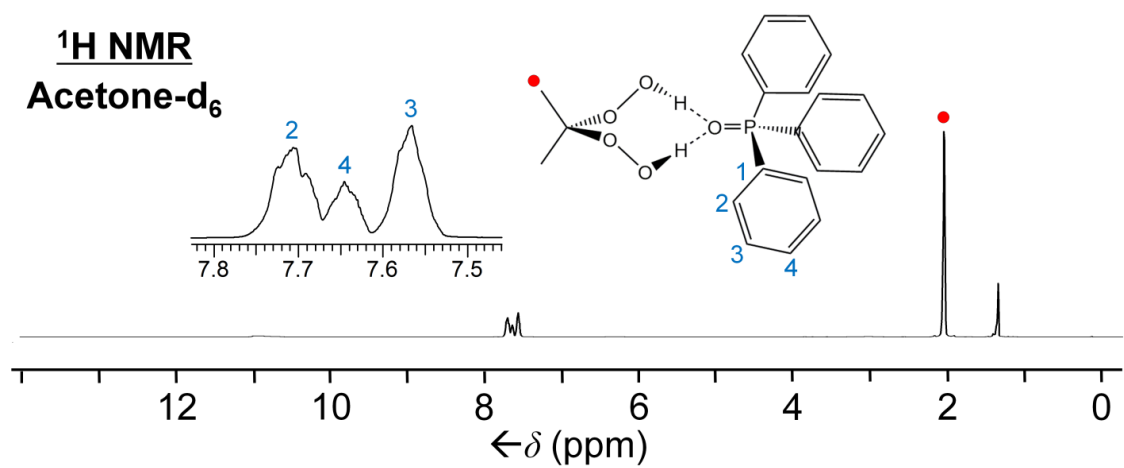


Figure A.11. ¹H NMR spectrum of **4** in acetone-d₆.

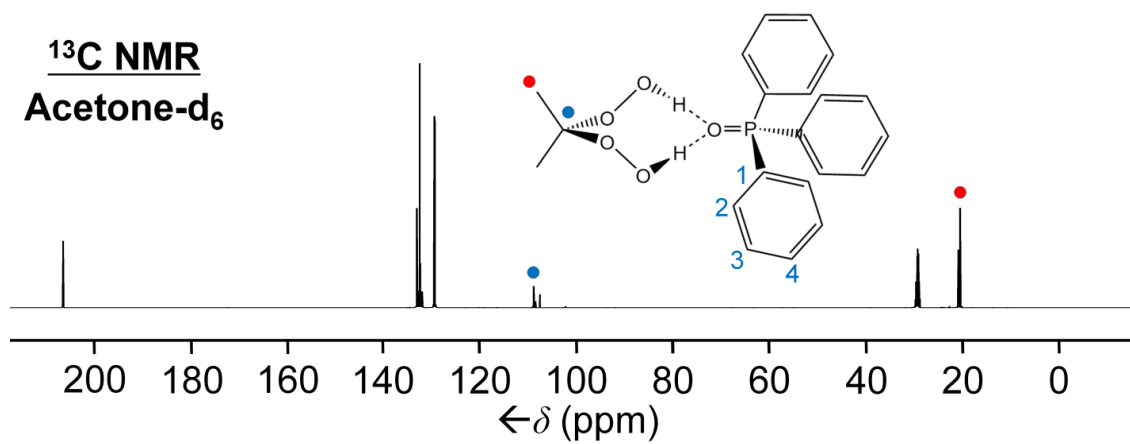


Figure A.12. ¹³C{¹H} NMR spectrum of **4** in acetone-d₆.

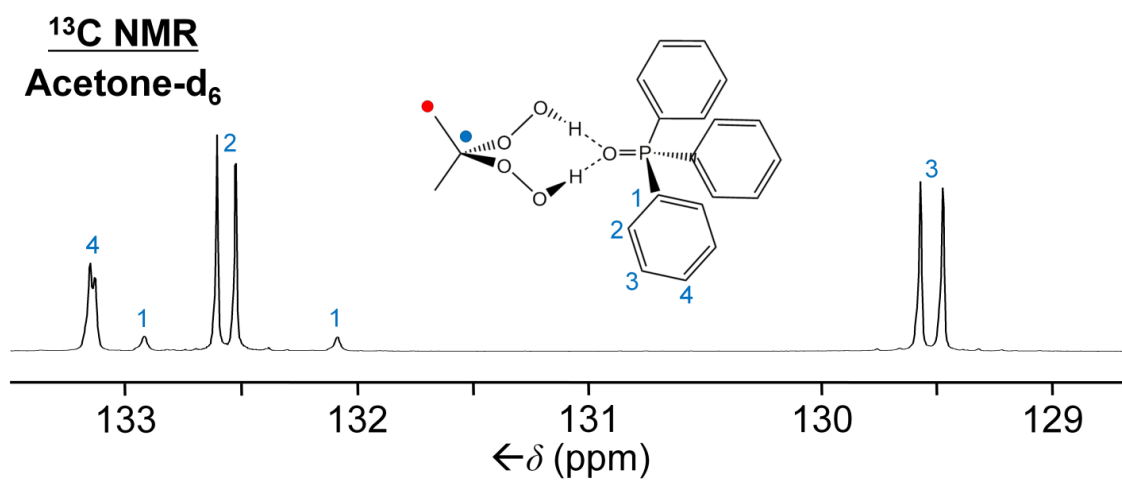


Figure A.13. $^{13}\text{C}\{^1\text{H}\}$ NMR spectrum of **4** in acetone-d₆, aryl region expansion.

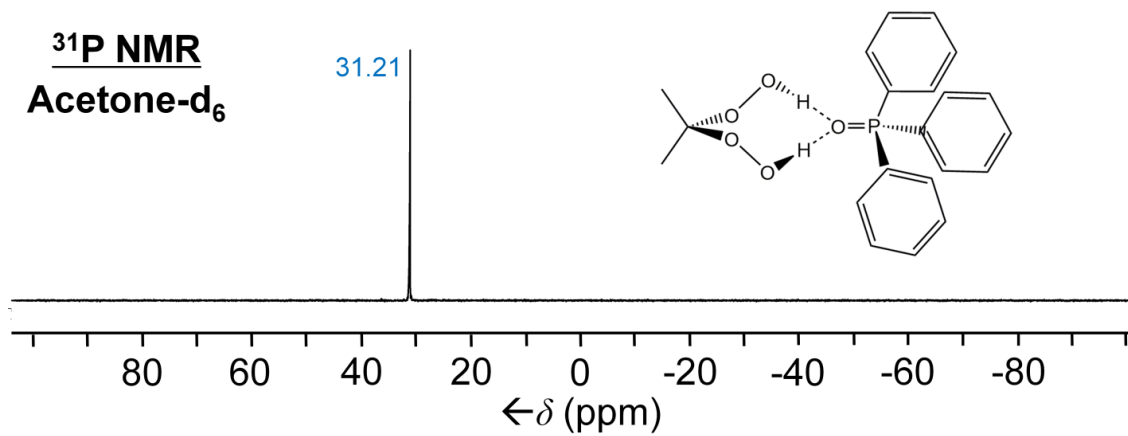


Figure A.14. $^{31}\text{P}\{^1\text{H}\}$ NMR spectrum of **4** in acetone-d₆.

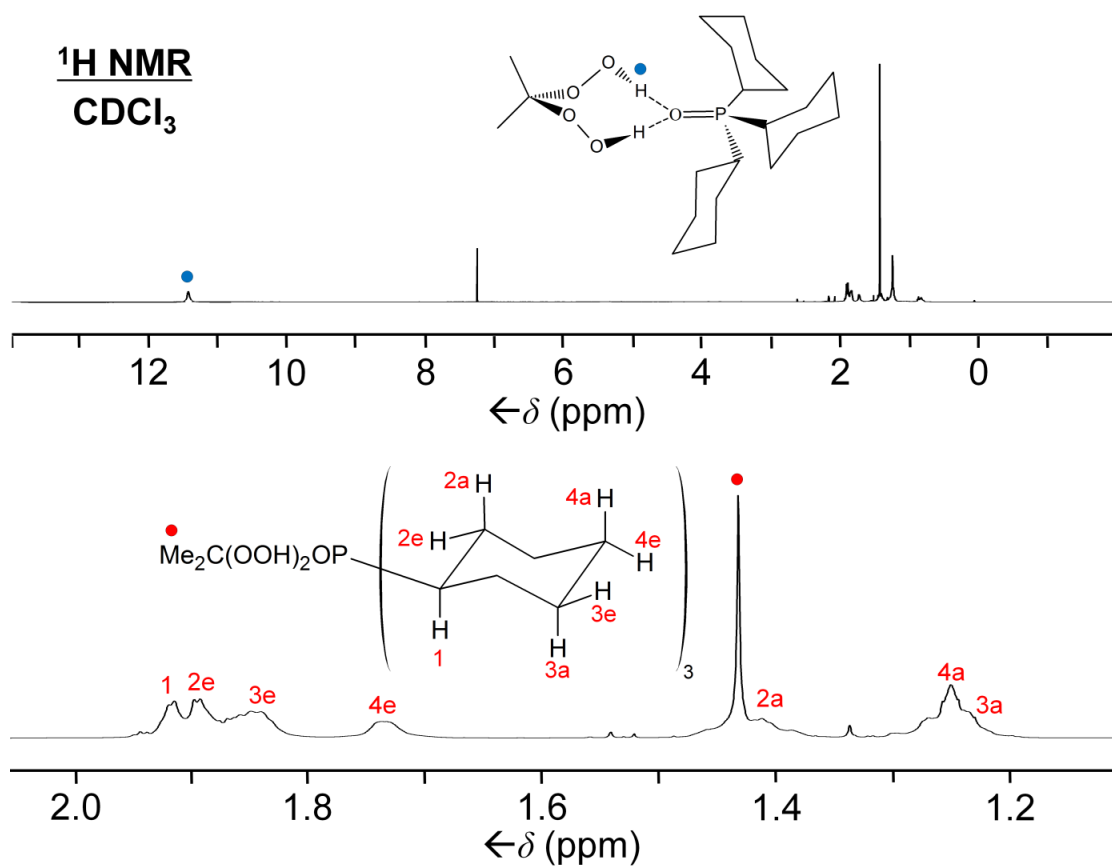


Figure A.15. ¹H NMR spectrum of **5** in CDCl₃ (top), alkyl region expansion (bottom).

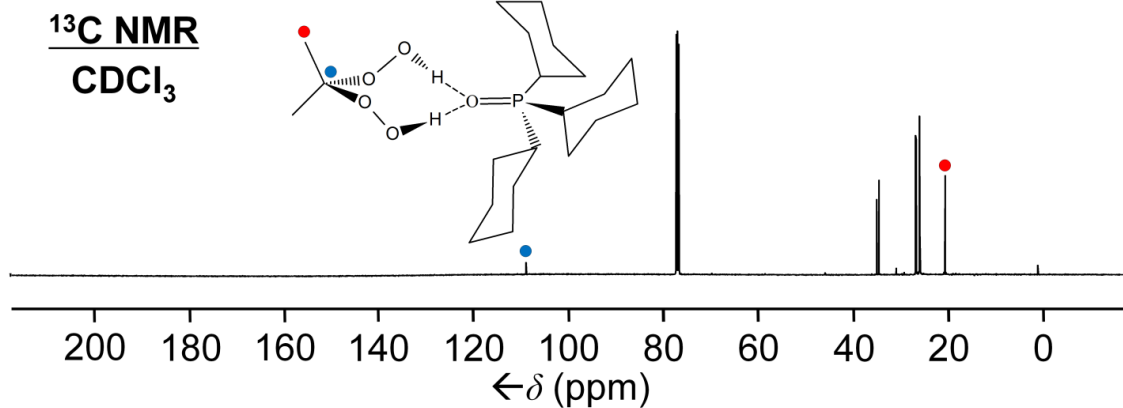


Figure A.16. $^{13}\text{C}\{^1\text{H}\}$ NMR spectrum of **5** in CDCl_3 .

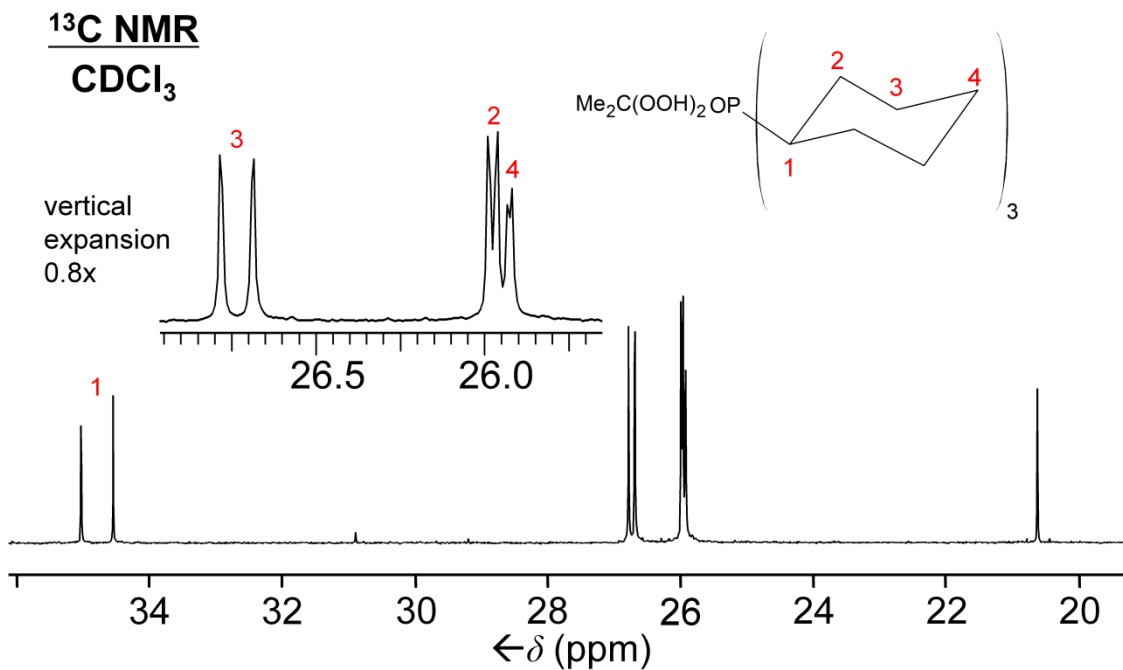


Figure A.17. $^{13}\text{C}\{^1\text{H}\}$ NMR spectrum of **5** in CDCl_3 , alkyl region expansion.

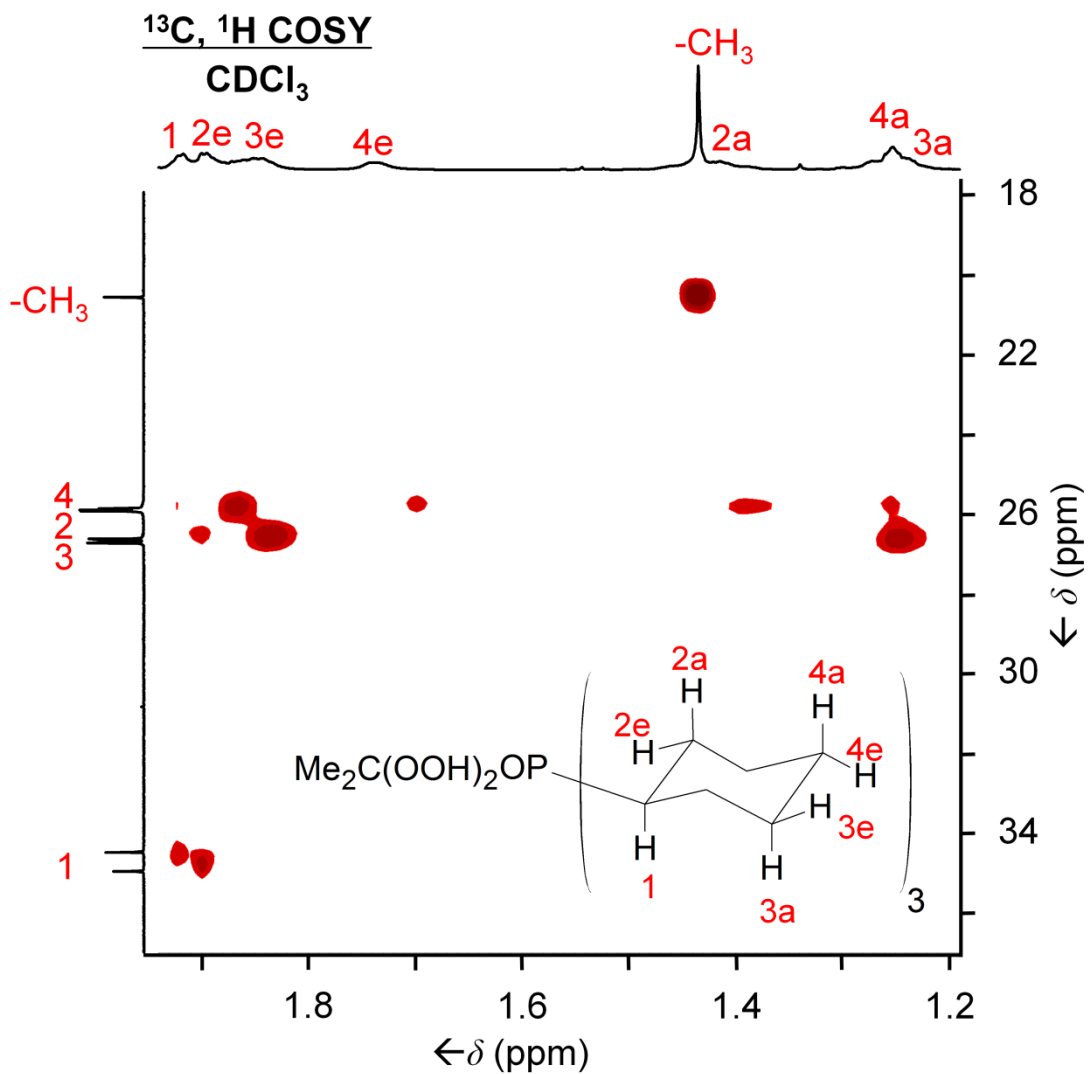


Figure A.18. ¹³C, ¹H COSY NMR spectrum of **5** in CDCl₃.

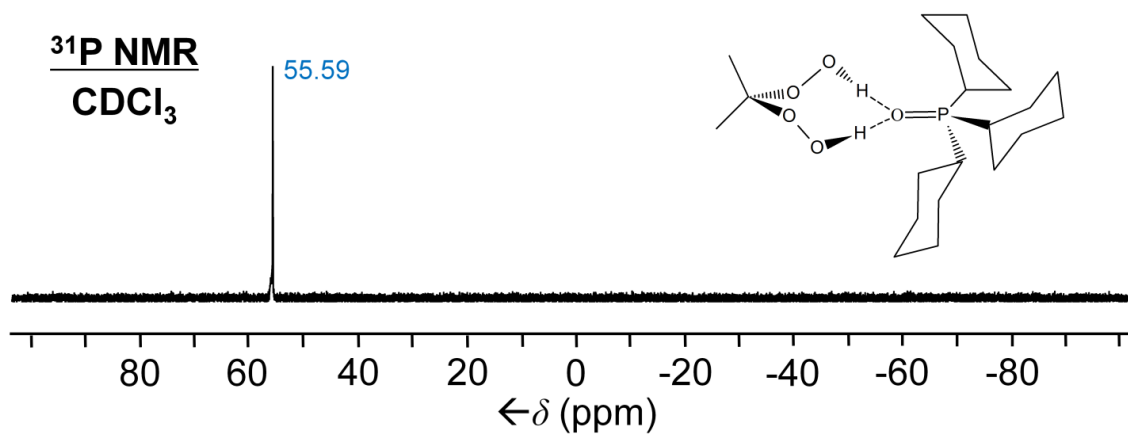


Figure A.19. ³¹P{¹H} NMR spectrum of **5** in CDCl₃.

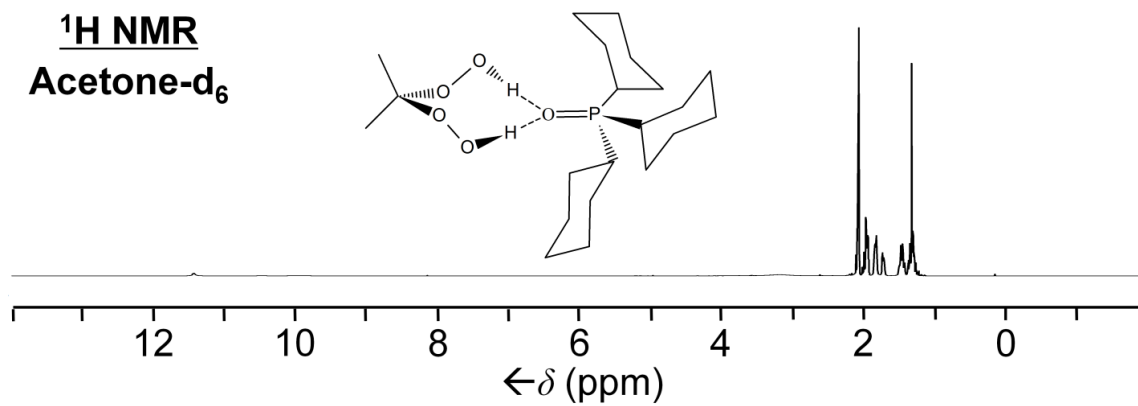


Figure A.20. ¹H NMR spectrum of **5** in acetone-d₆.

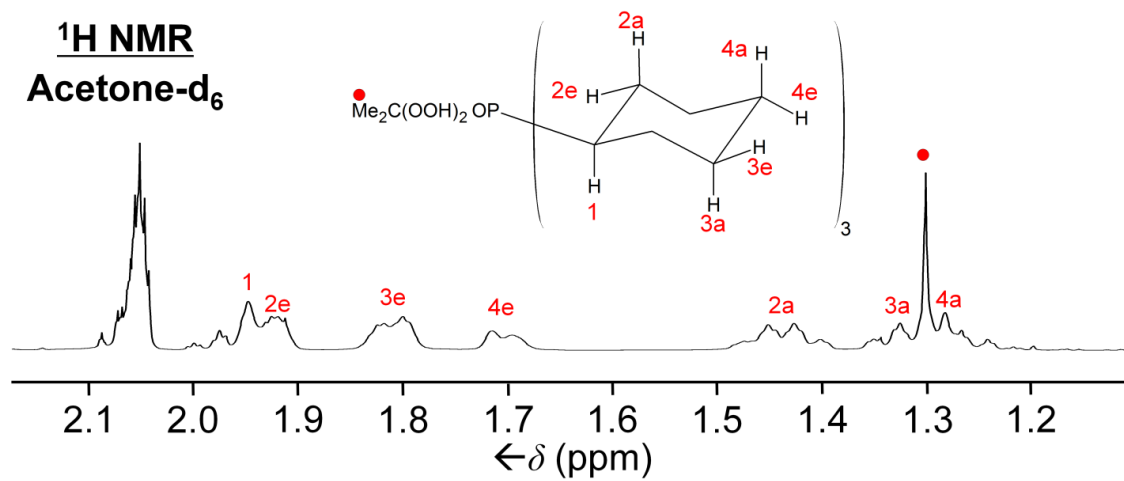


Figure A.21. ¹H NMR spectrum of **5** in acetone-d₆, alkyl region expansion.

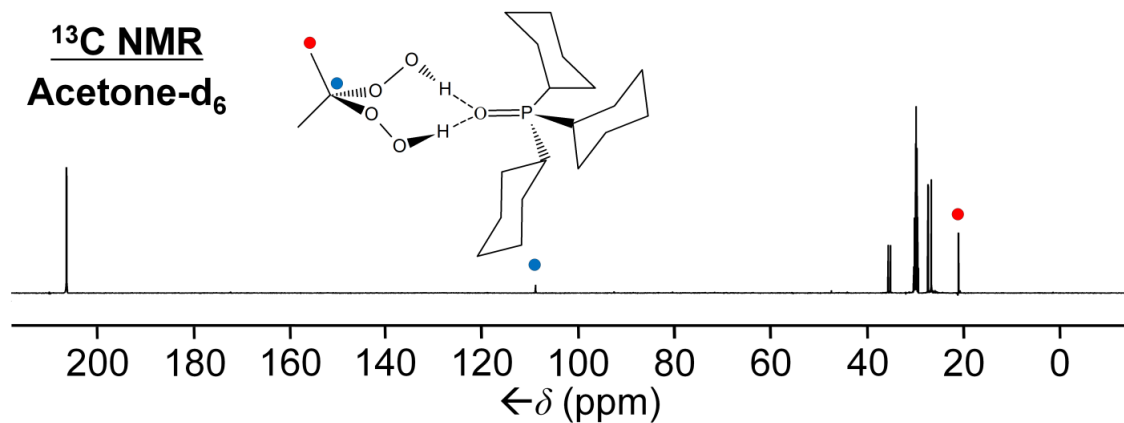


Figure A.22. ¹³C{¹H} NMR spectrum of **5** in acetone-d₆.

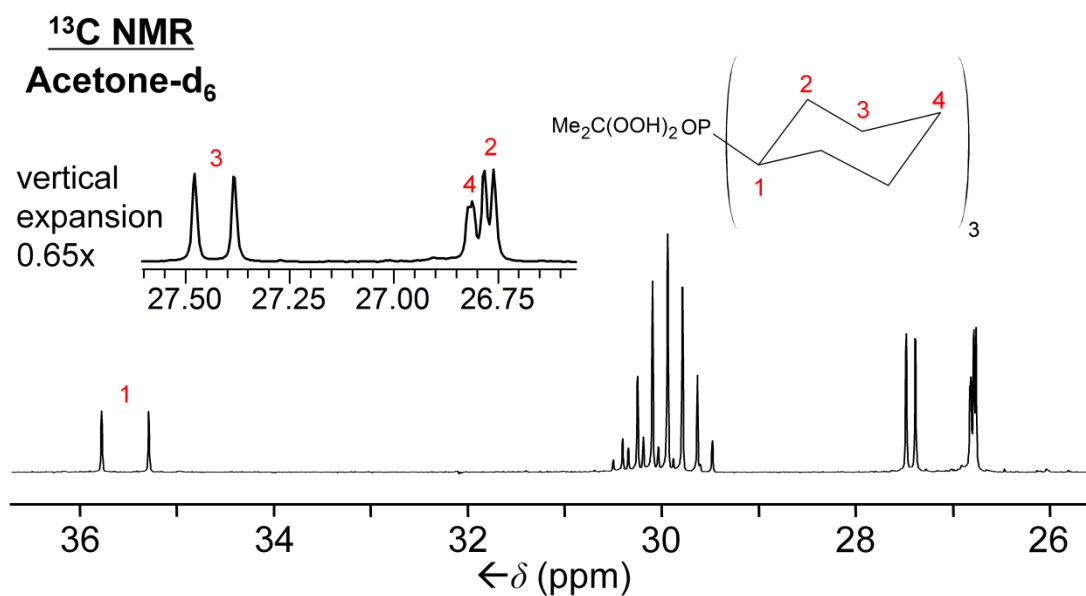


Figure A.23. $^{13}\text{C}\{^1\text{H}\}$ NMR spectrum of **5** in acetone- d_6 , alkyl region expansion.

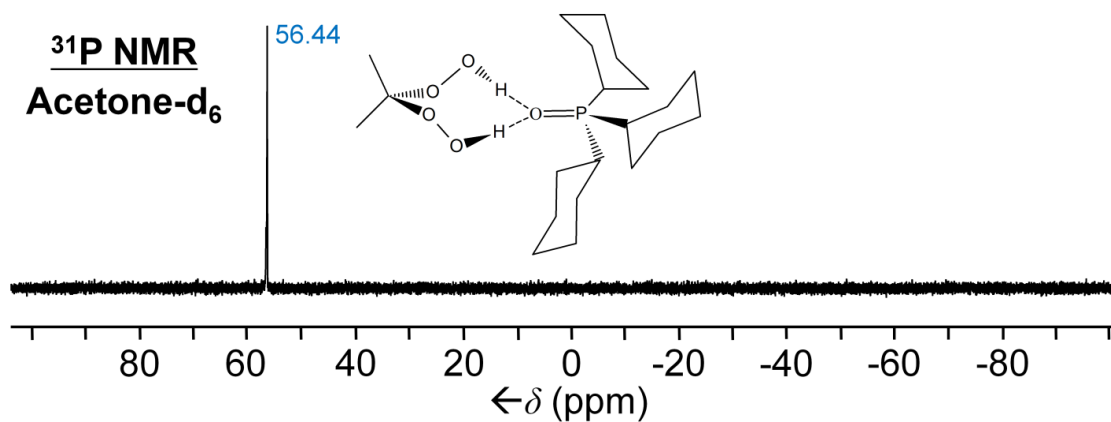


Figure A.24. $^{31}\text{P}\{^1\text{H}\}$ NMR spectrum of **5** in acetone- d_6 .

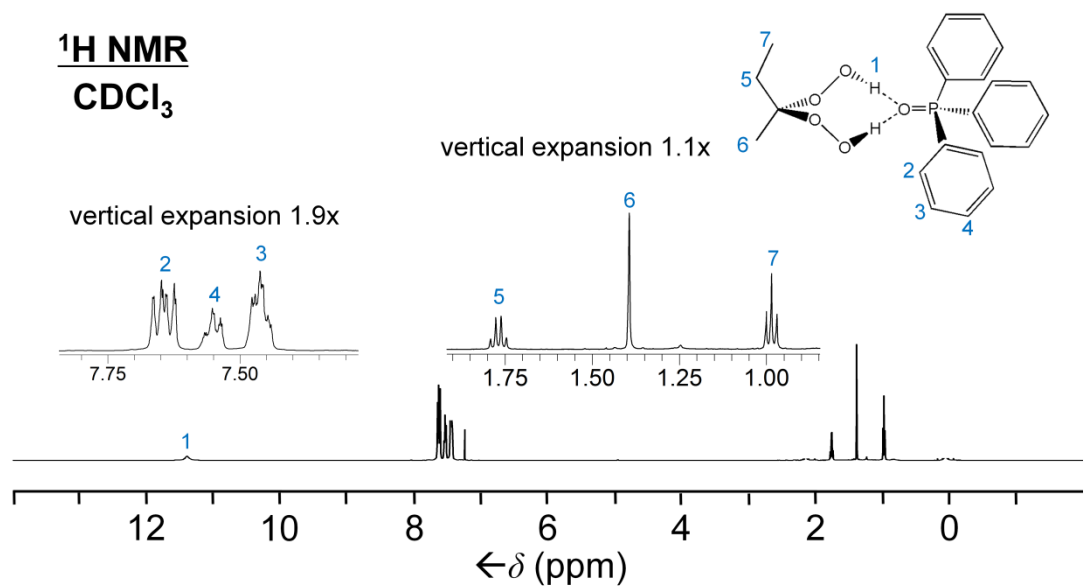


Figure A.25. ^1H NMR spectrum of **6** in CDCl_3 .

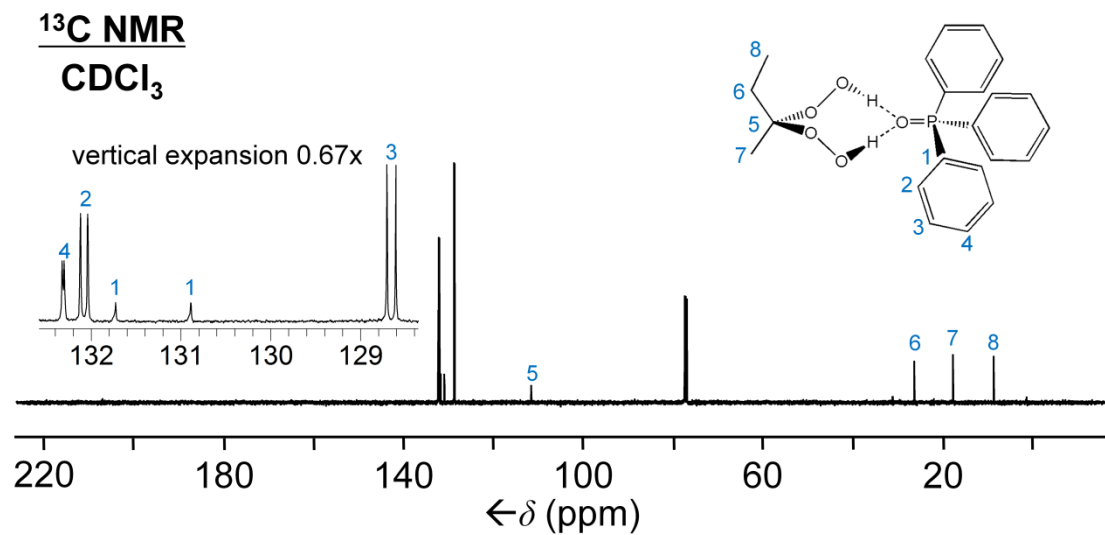


Figure A.26. $^{13}\text{C}\{^1\text{H}\}$ NMR spectrum of **6** in CDCl_3 .

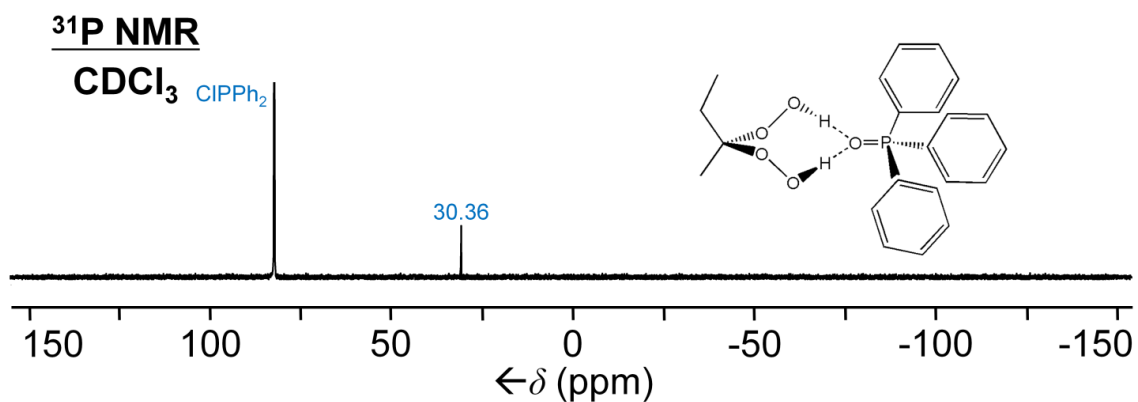


Figure A.27. ³¹P{¹H} NMR spectrum of **6** in CDCl₃.

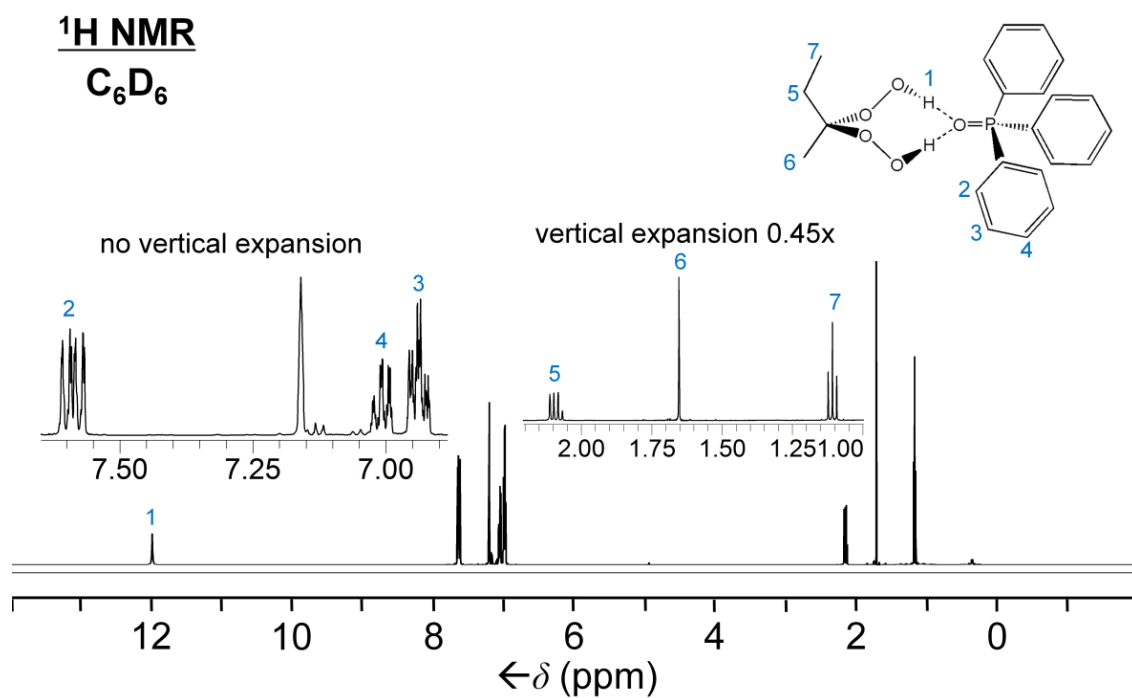


Figure A.28. ¹H NMR spectrum of **6** in C₆D₆.

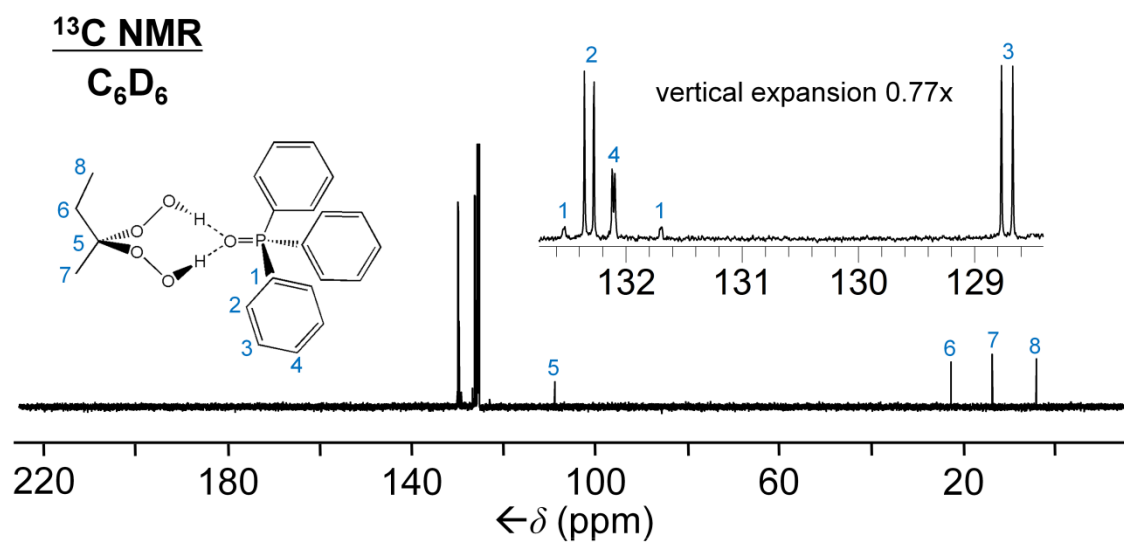


Figure A.29. $^{13}\text{C}\{^1\text{H}\}$ NMR spectrum of **6** in C_6D_6 .

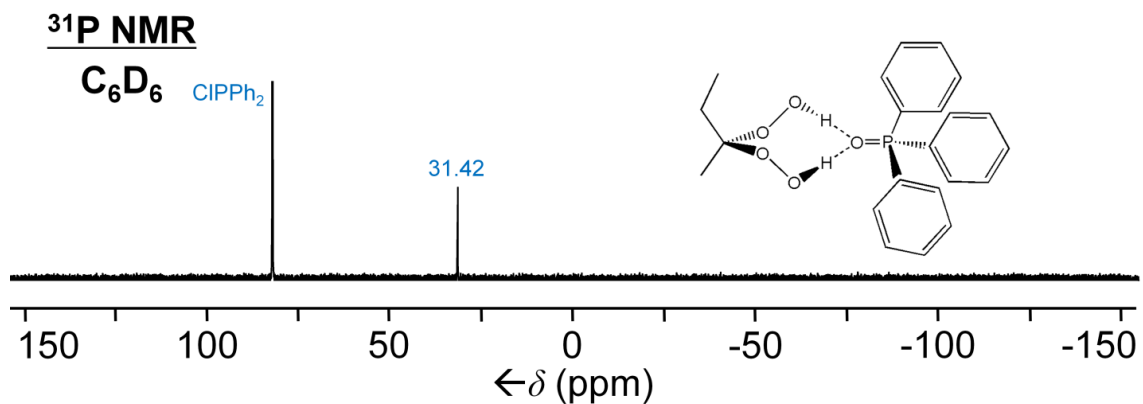


Figure A.30. $^{31}\text{P}\{^1\text{H}\}$ NMR spectrum of **6** in C_6D_6 .

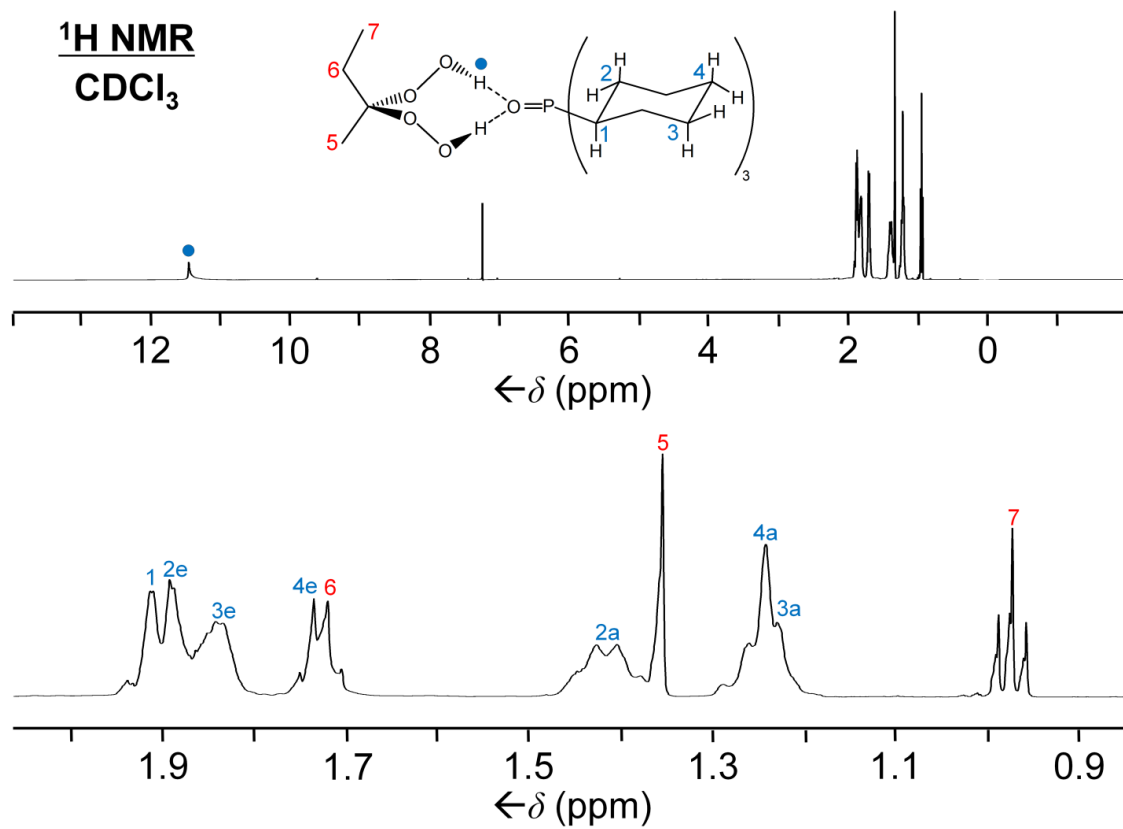


Figure A.31. ¹H NMR spectrum of **7** in CDCl₃ (top), alkyl region expansion (bottom).

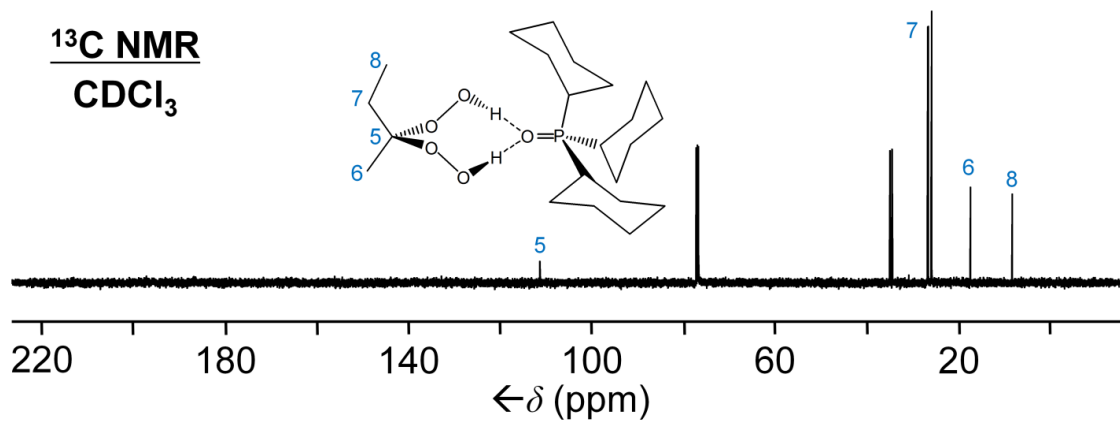


Figure A.32. $^{13}\text{C}\{^1\text{H}\}$ NMR spectrum of **7** in CDCl_3 .

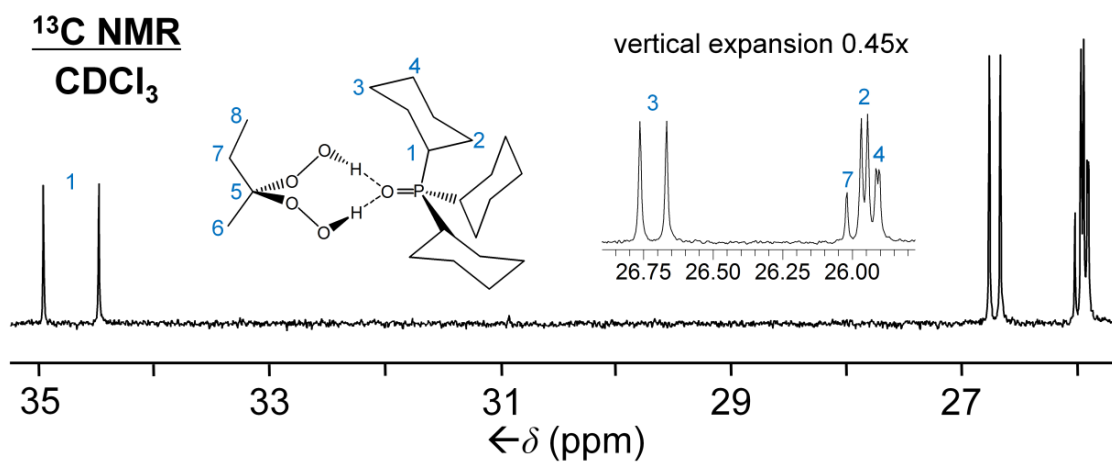


Figure A.33. $^{13}\text{C}\{^1\text{H}\}$ NMR spectrum of **7** in CDCl_3 , alkyl region expansion.

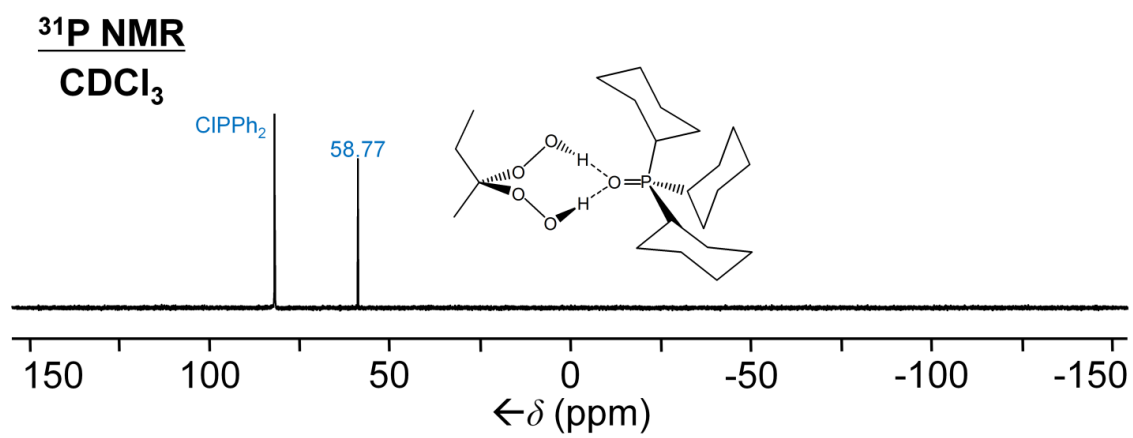


Figure A.34. $^{31}\text{P}\{^1\text{H}\}$ NMR spectrum of **7** in CDCl_3 .

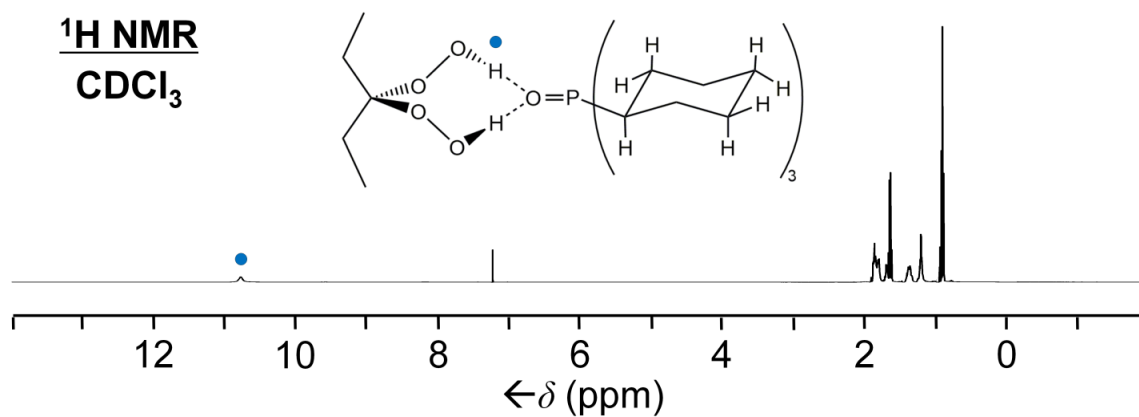


Figure A.35. ¹H NMR spectrum of **8** in CDCl₃.

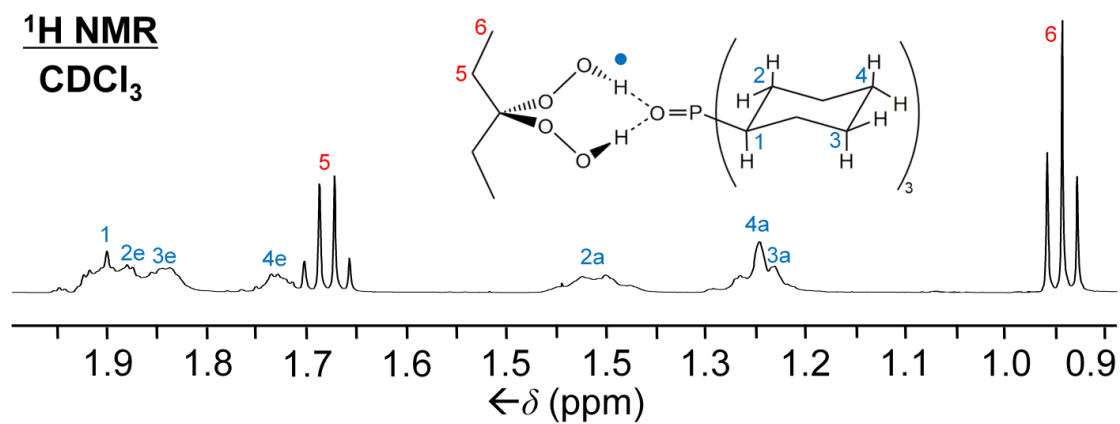


Figure A.36. ¹H NMR spectrum of **8** in CDCl₃, alkyl region expansion.

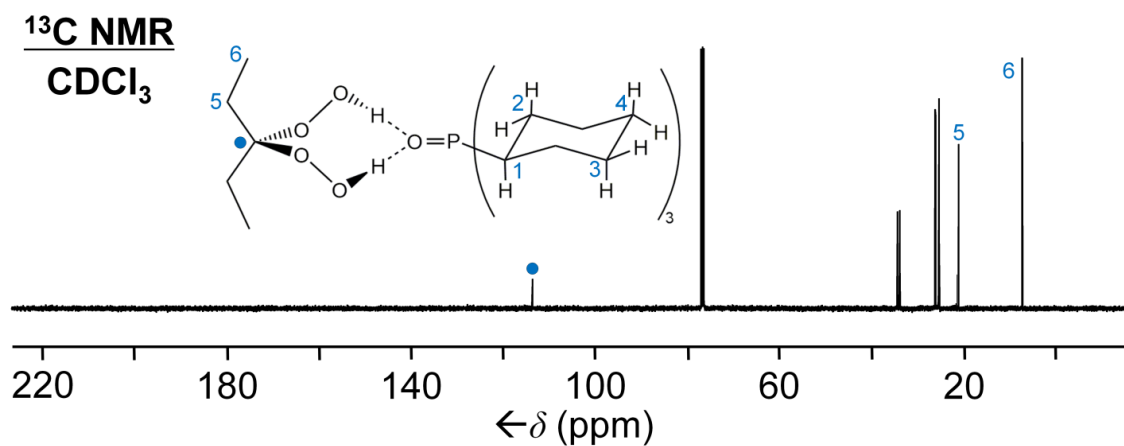


Figure A.37. $^{13}\text{C}\{^1\text{H}\}$ NMR spectrum of **8** in CDCl_3 .

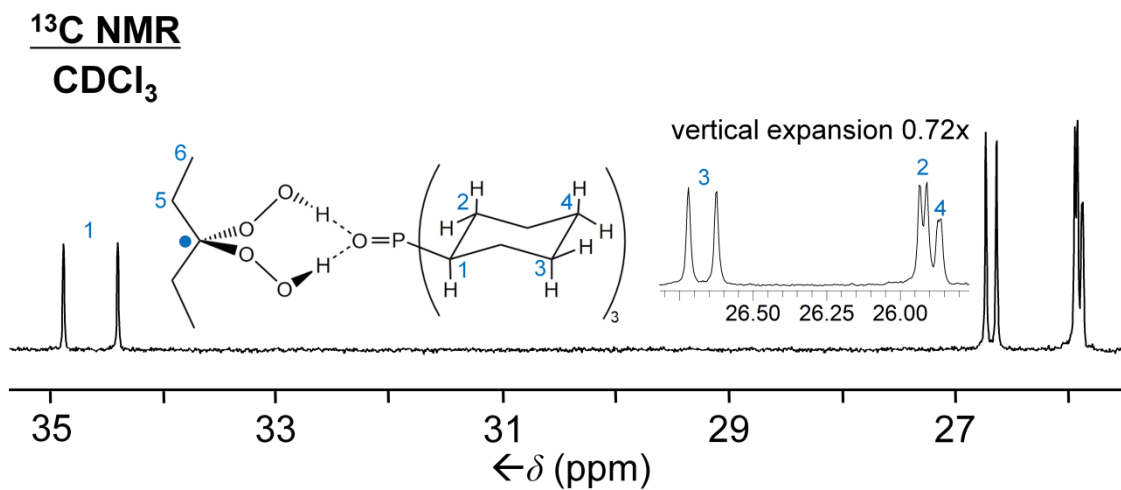


Figure A.38. $^{13}\text{C}\{^1\text{H}\}$ NMR spectrum of **8** in CDCl_3 , alkyl region expansion.

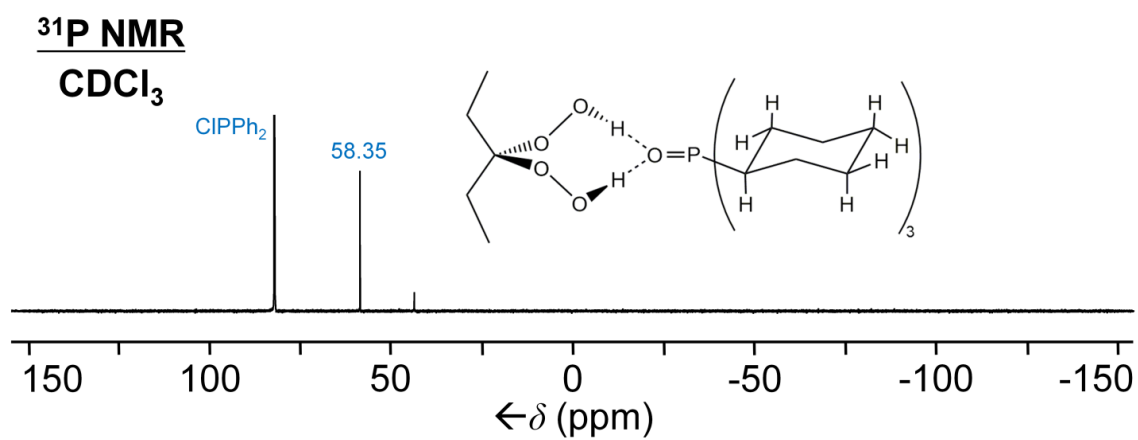


Figure A.39. $^{31}\text{P}\{^1\text{H}\}$ NMR spectrum of **8** in CDCl_3 .

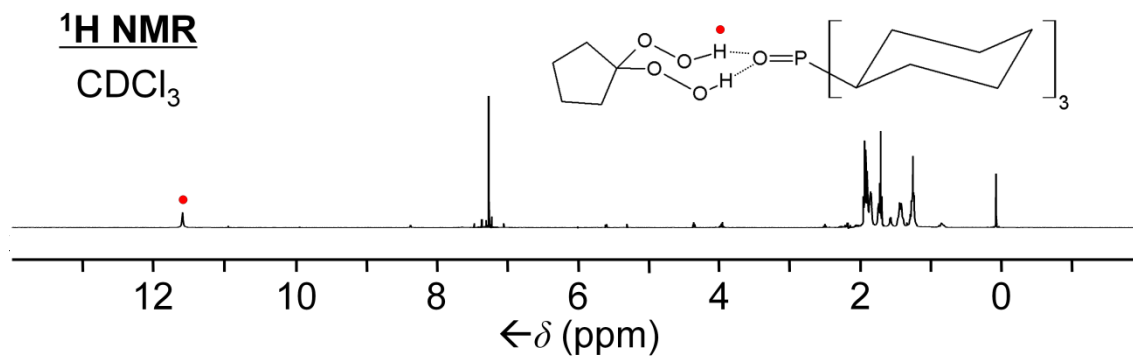


Figure A.40. ¹H NMR spectrum of **9** in CDCl₃.

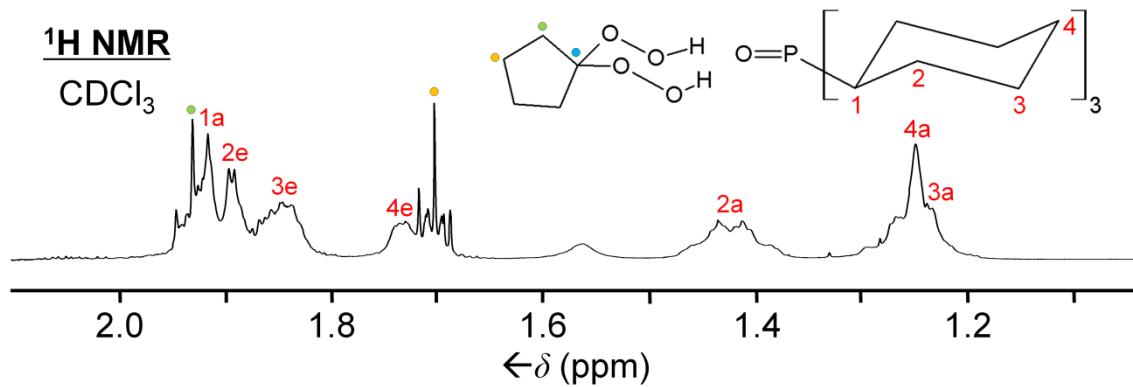


Figure A.41. ¹H NMR spectrum of **9** in CDCl₃, alkyl region expansion.

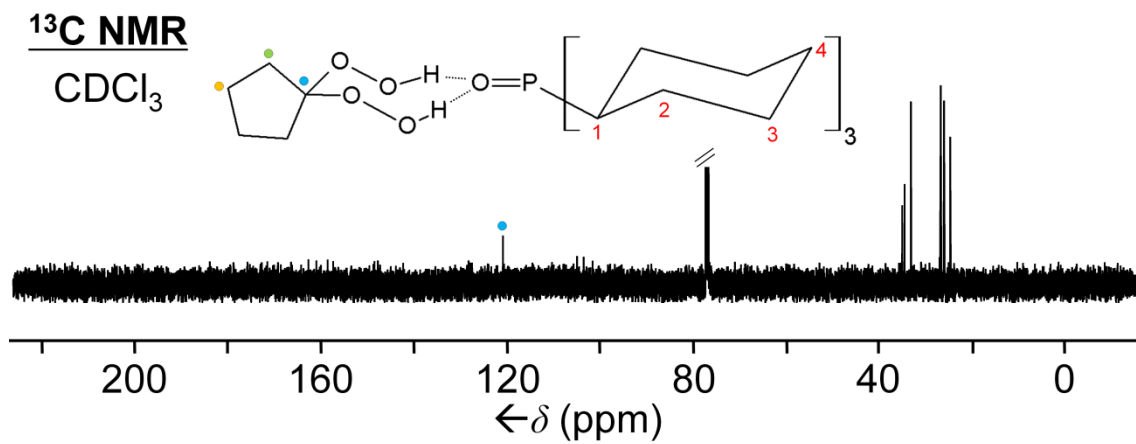


Figure A.42. $^{13}\text{C}\{^1\text{H}\}$ NMR spectrum of **9** in CDCl₃.

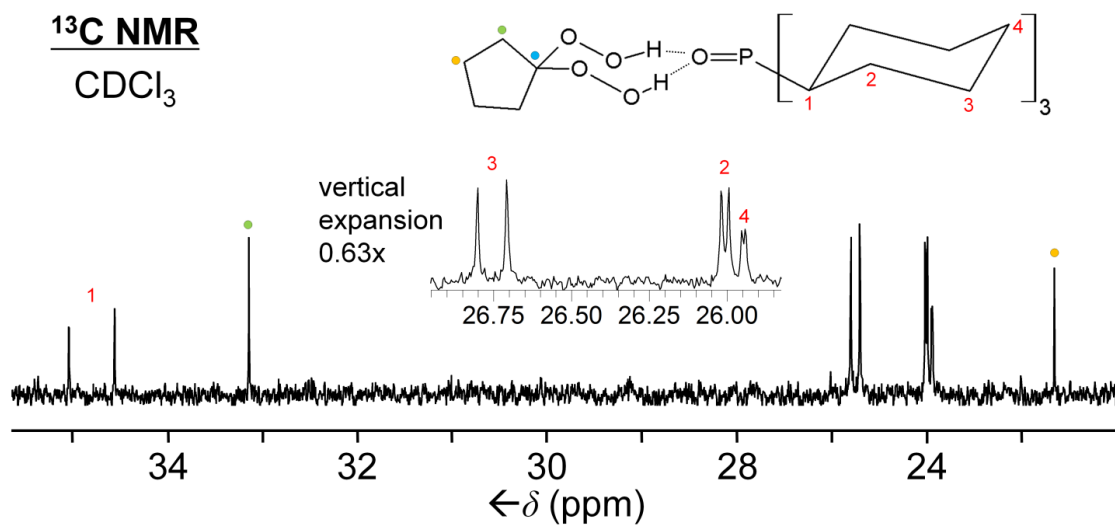


Figure A.43. $^{13}\text{C}\{^1\text{H}\}$ NMR spectrum of **9** in CDCl₃, alkyl region expansion.

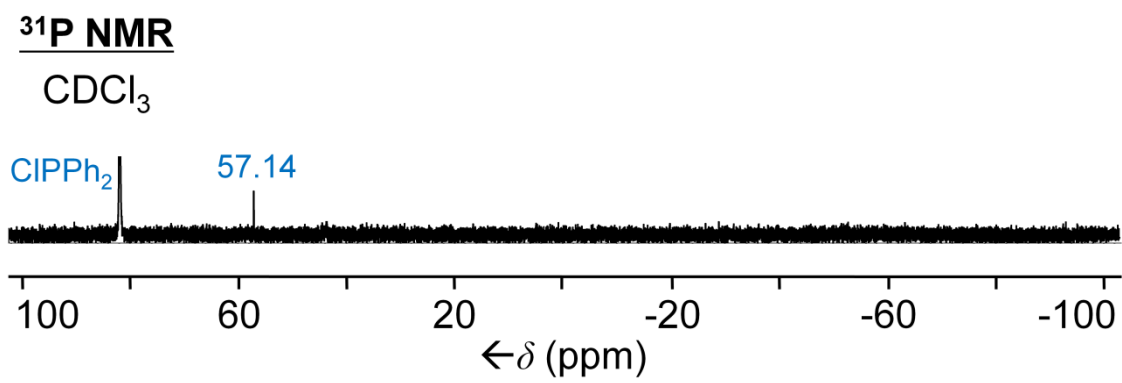


Figure A.44. $^{31}\text{P}\{^1\text{H}\}$ NMR spectrum of **9** in CDCl_3 .

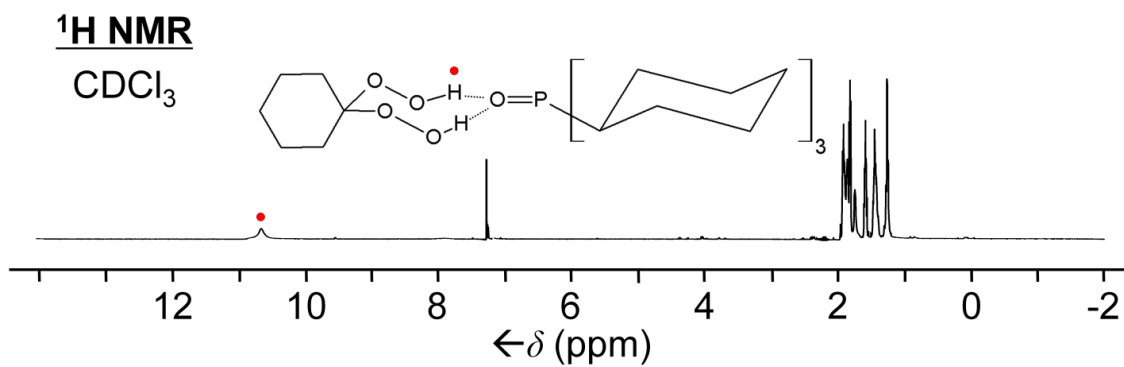


Figure A.45. ¹H NMR spectrum of **10** in CDCl₃.

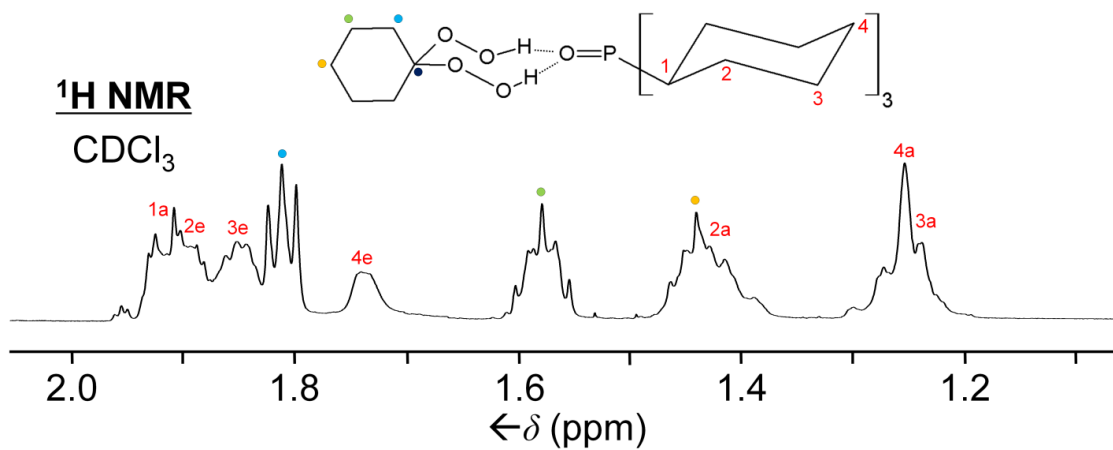


Figure A.46. ¹H NMR spectrum of **10** in CDCl₃, alkyl region expansion.

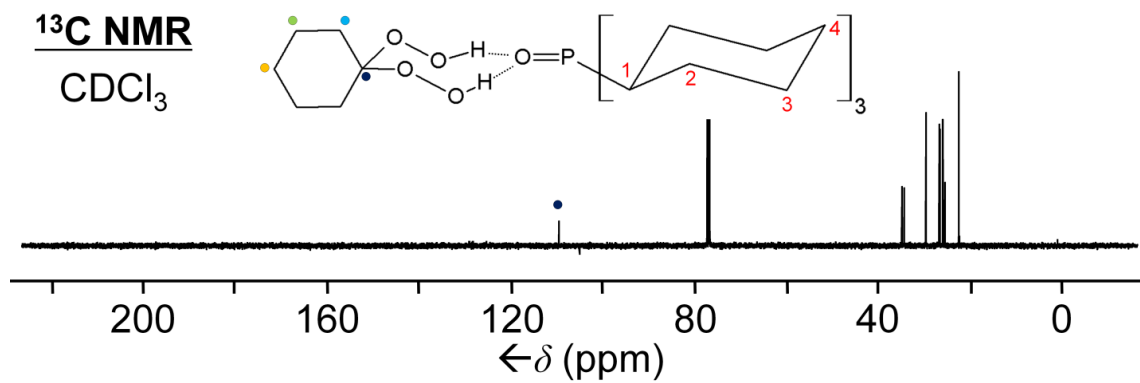


Figure A.47. $^{13}\text{C}\{^1\text{H}\}$ NMR spectrum of **10** in CDCl₃.

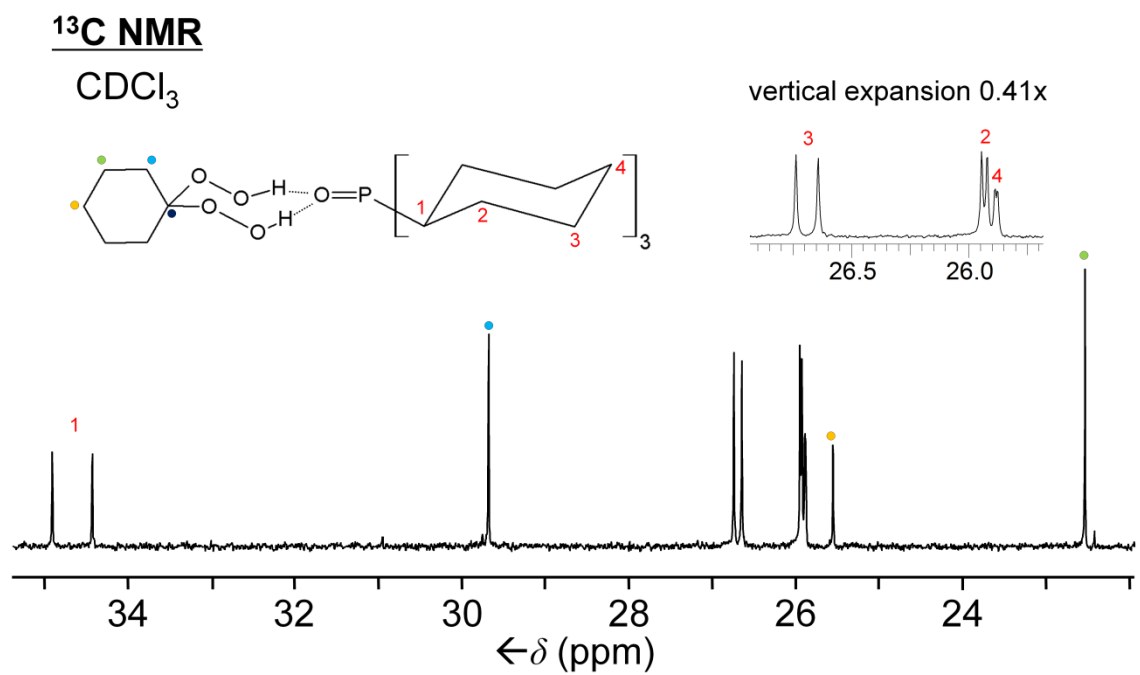


Figure A.48 $^{13}\text{C}\{^1\text{H}\}$ NMR spectrum of **10** in CDCl₃, alkyl region expansion.

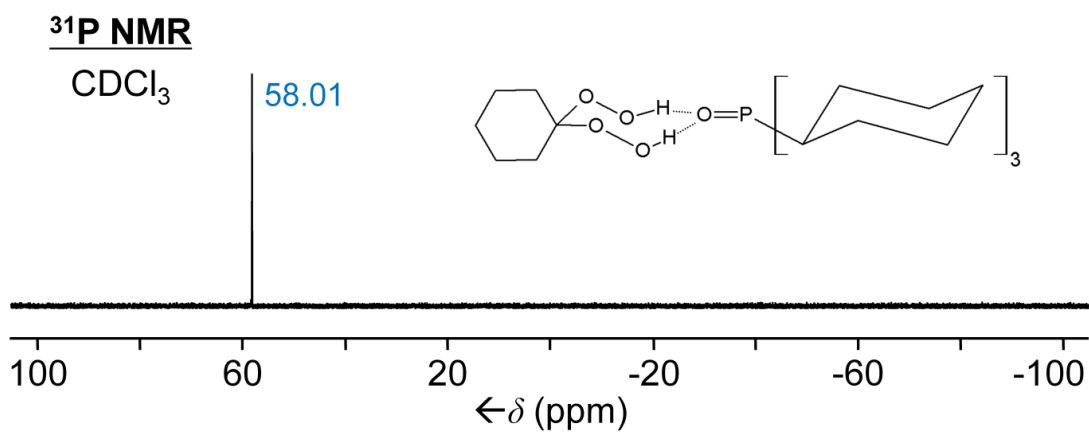


Figure A.49. $^{31}\text{P}\{^1\text{H}\}$ NMR spectrum of **10** in CDCl_3 .

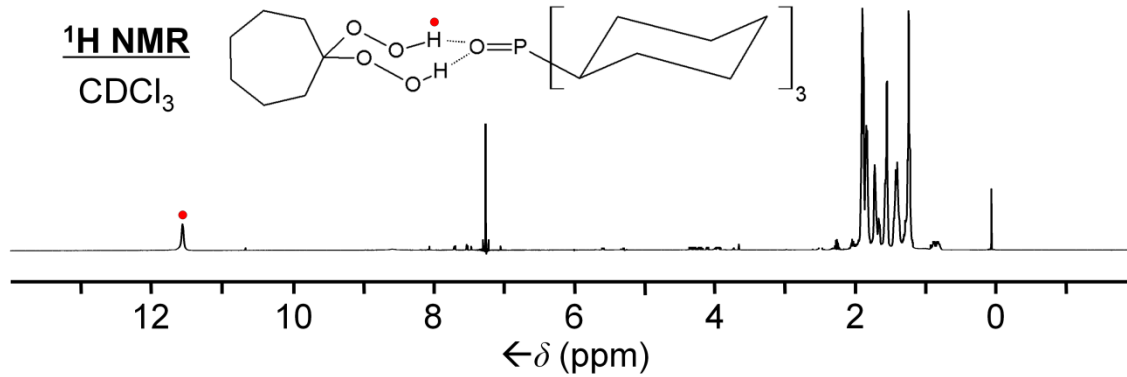


Figure A.50. ¹H NMR spectrum of **11** in CDCl₃.

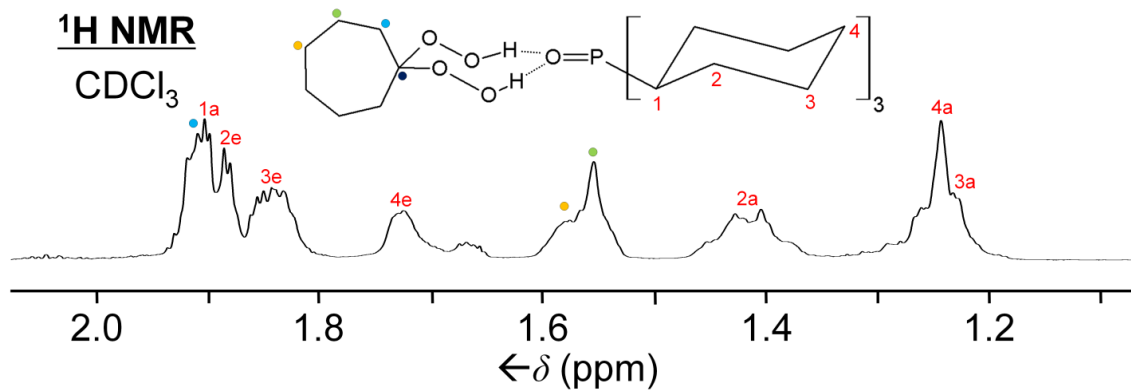


Figure A.51. ¹H NMR spectrum of **11** in CDCl₃, alkyl region expansion.

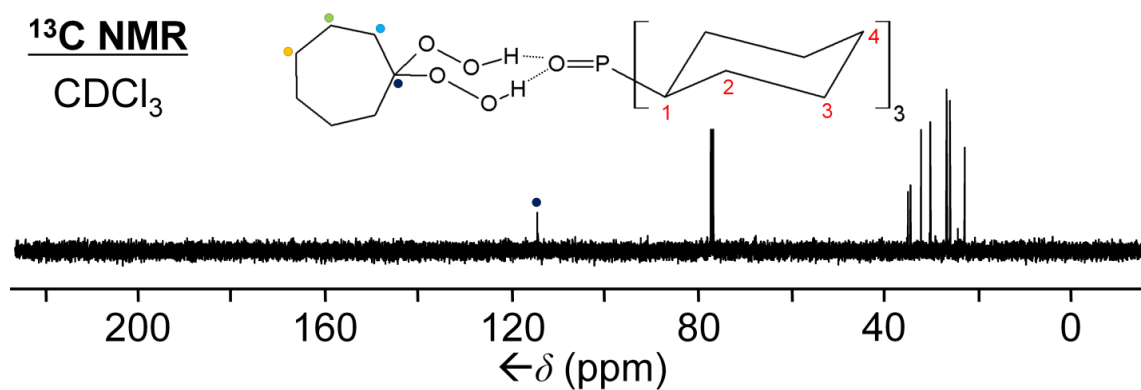


Figure A.52. ¹³C{¹H} NMR spectrum of **11** in CDCl₃.

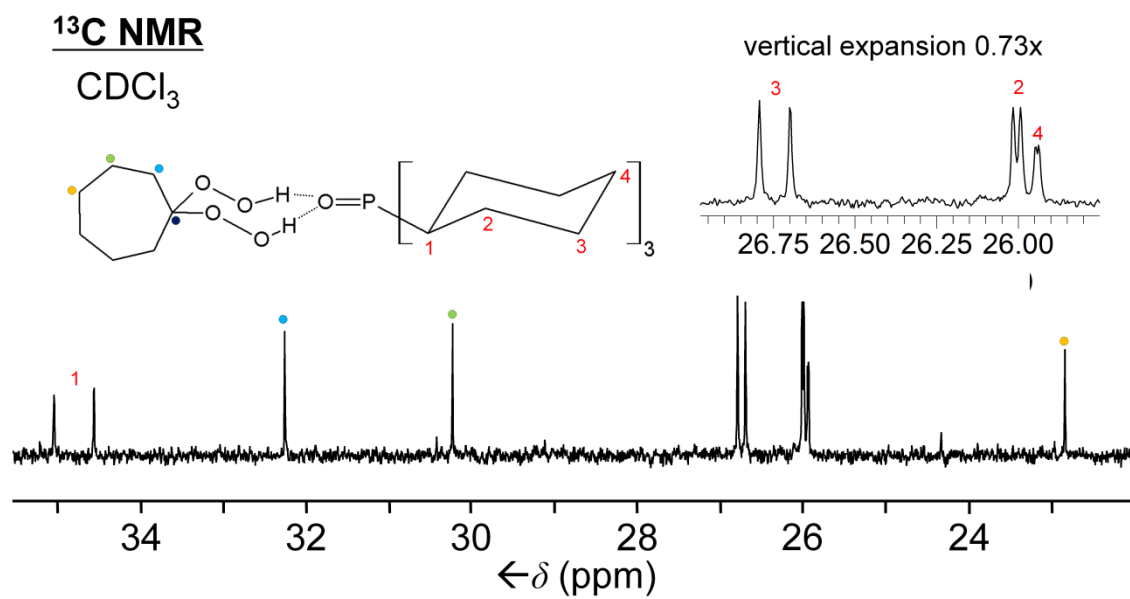


Figure A.53. ¹³C{¹H} NMR spectrum of **11** in CDCl₃, alkyl region expansion.

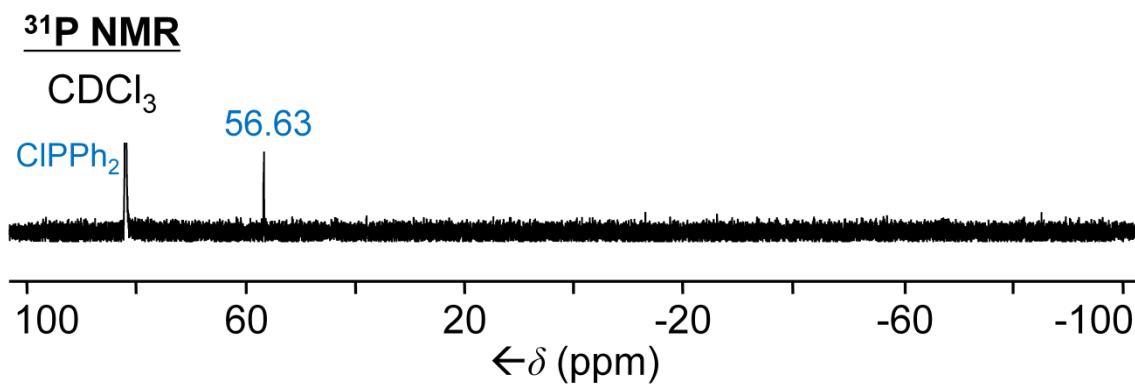


Figure A.54. $^{31}\text{P}\{^1\text{H}\}$ NMR spectrum of **11** in CDCl_3 .

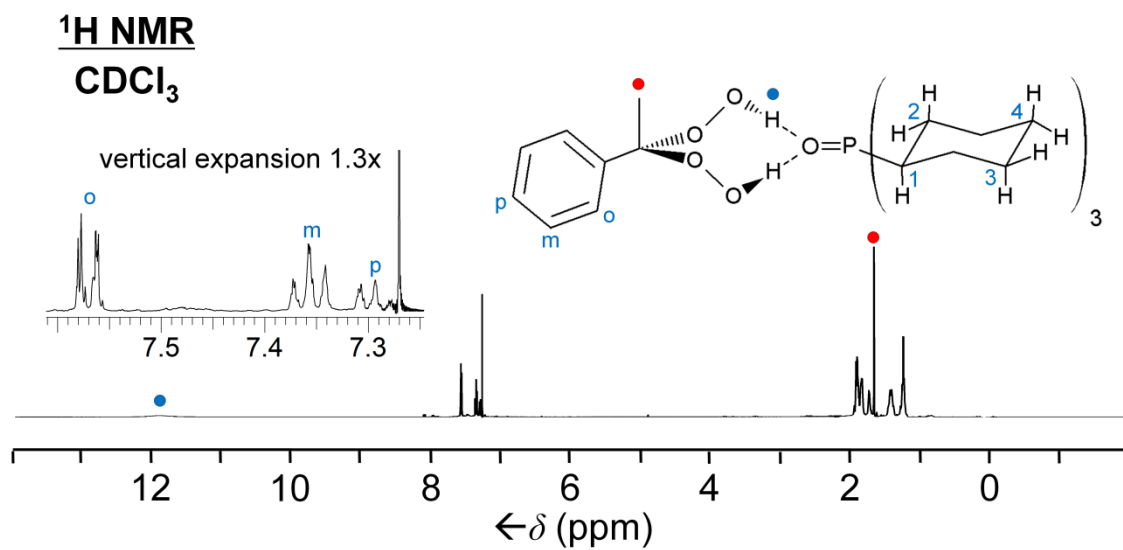


Figure A.55. ¹H NMR spectrum of **12** in CDCl₃.

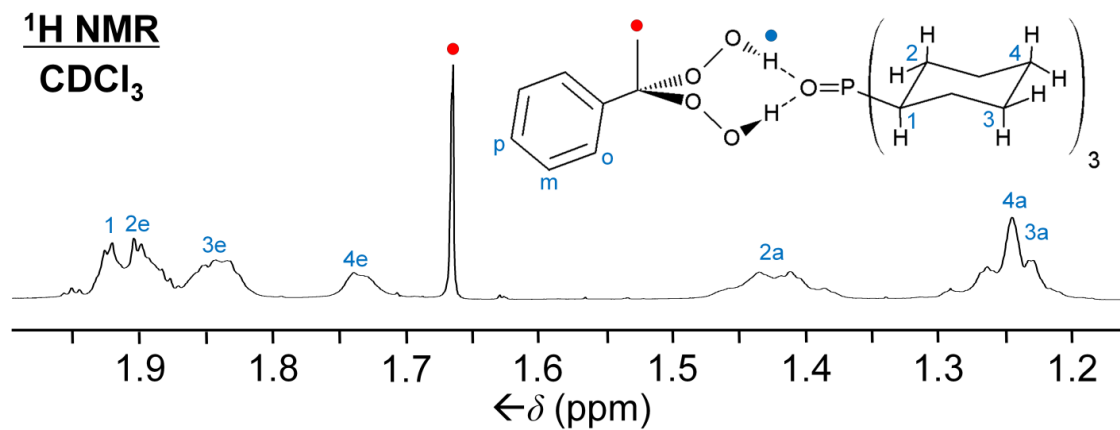


Figure A.56. ¹H NMR spectrum of **12** in CDCl₃, alkyl region expansion.

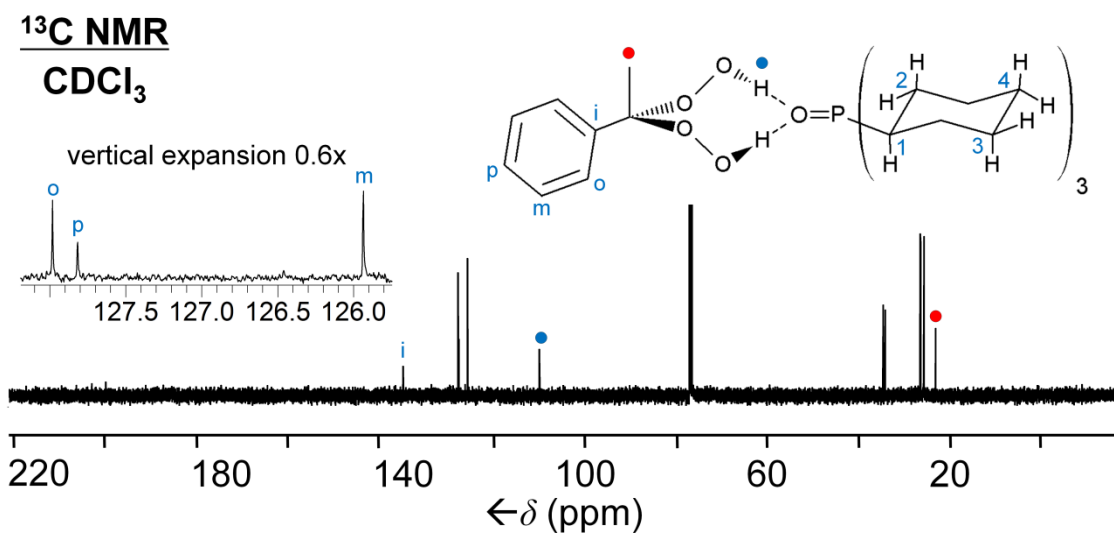


Figure A.57. $^{13}\text{C}\{^1\text{H}\}$ NMR spectrum of **12** in CDCl_3 .

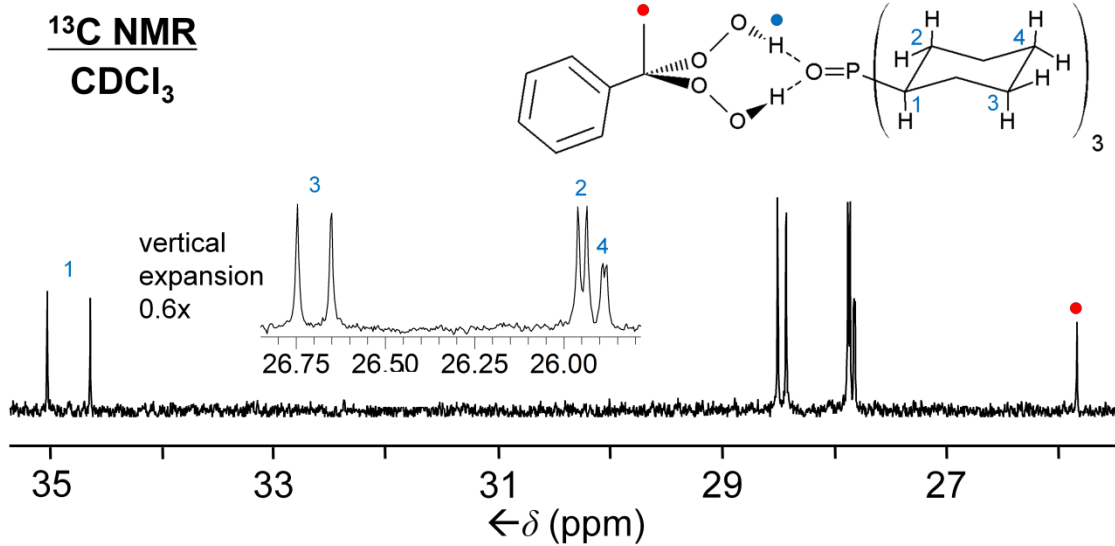


Figure A.58. $^{13}\text{C}\{^1\text{H}\}$ NMR spectrum of **12** in CDCl_3 , alkyl region expansion.

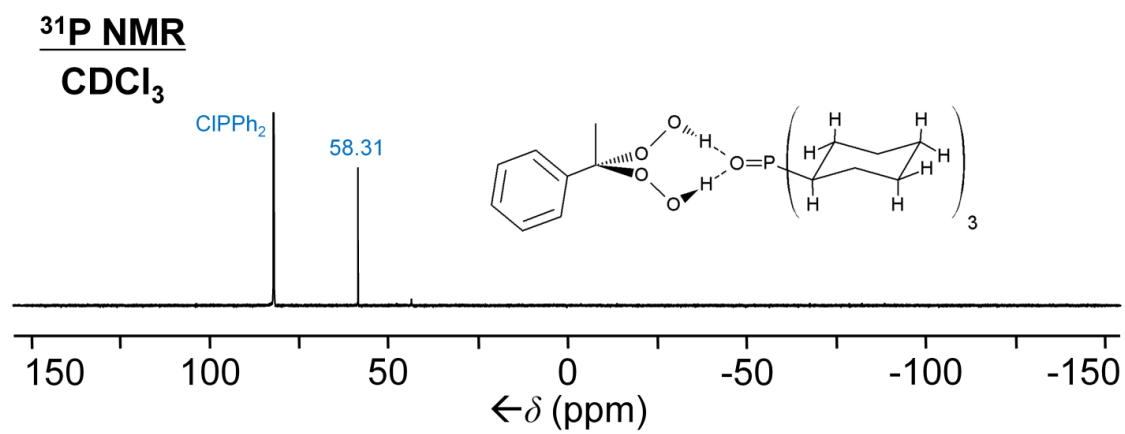


Figure A.59. ³¹P{¹H} NMR spectrum of **12** in CDCl₃.

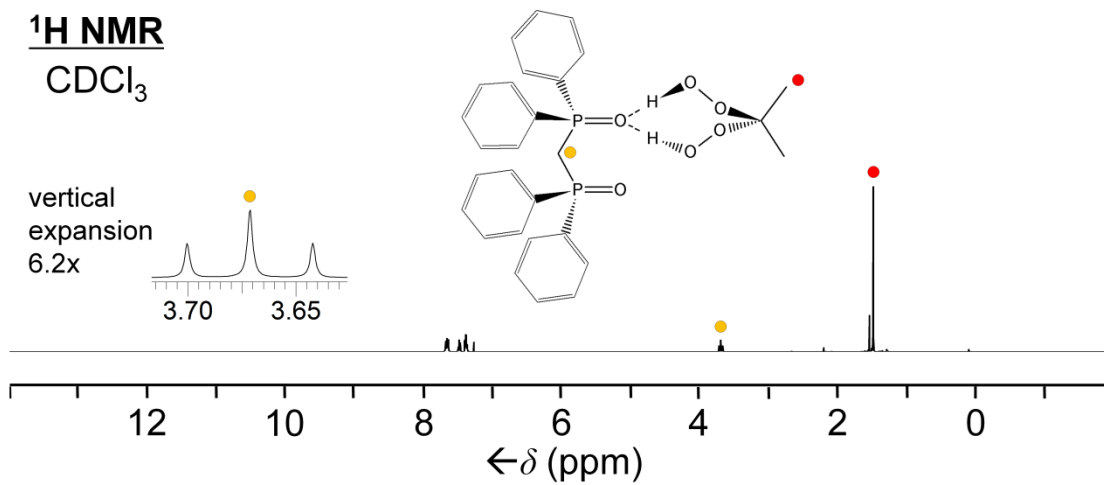


Figure A.60. ¹H NMR spectrum of **13** in CDCl₃.

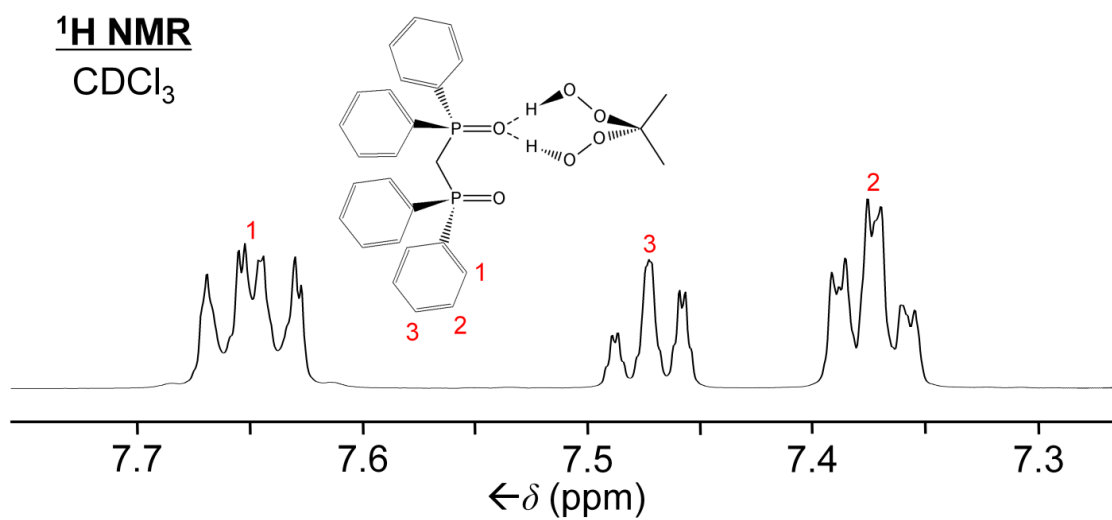


Figure A.61. ¹H NMR spectrum of **13** in CDCl₃, aryl region expansion.

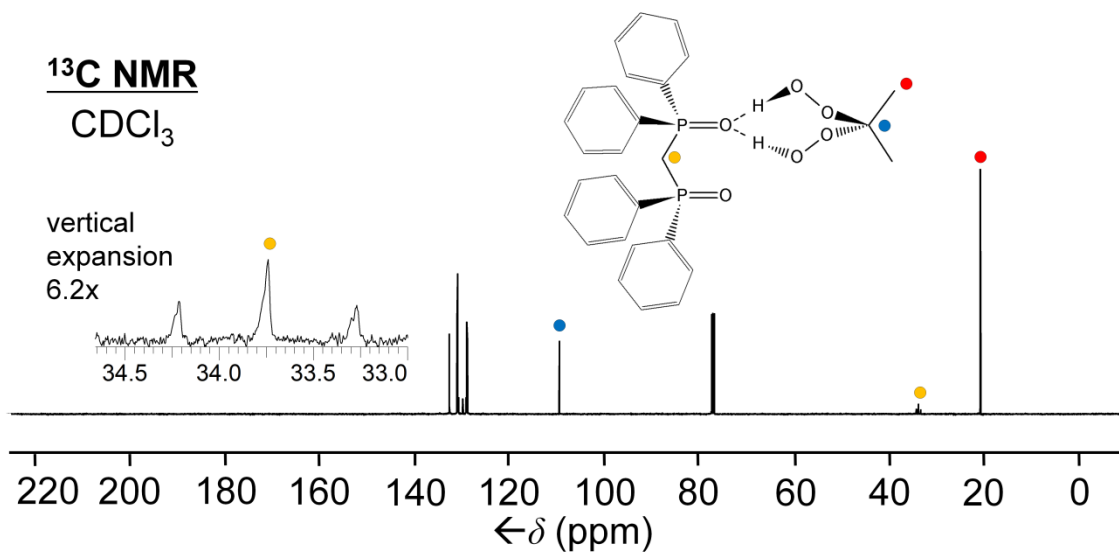


Figure A.62. ¹³C{¹H} NMR spectrum of **13** in CDCl₃.

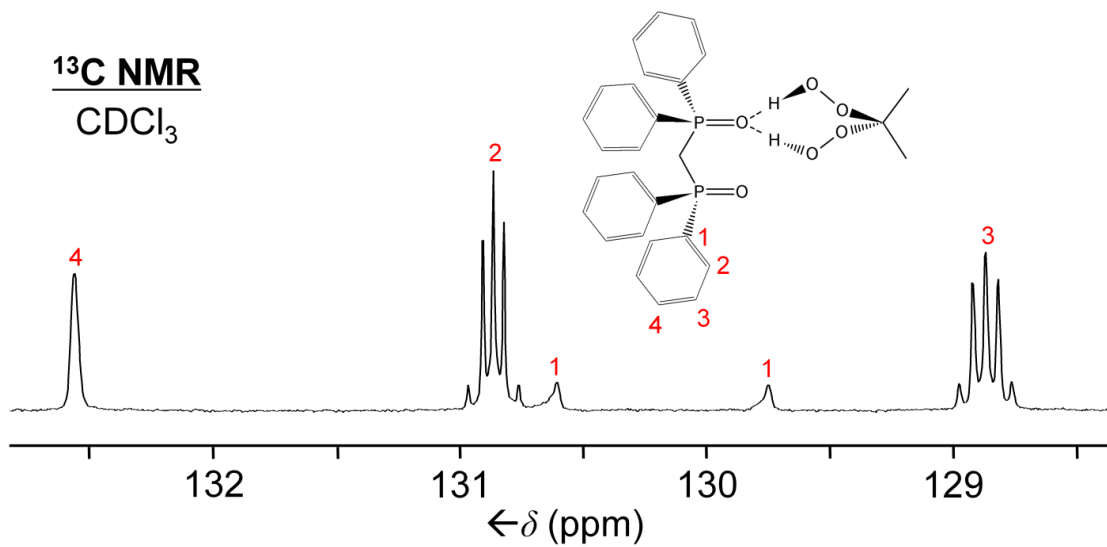


Figure A.63. ¹³C{¹H} NMR spectrum of **13** in CDCl₃, aryl region expansion.

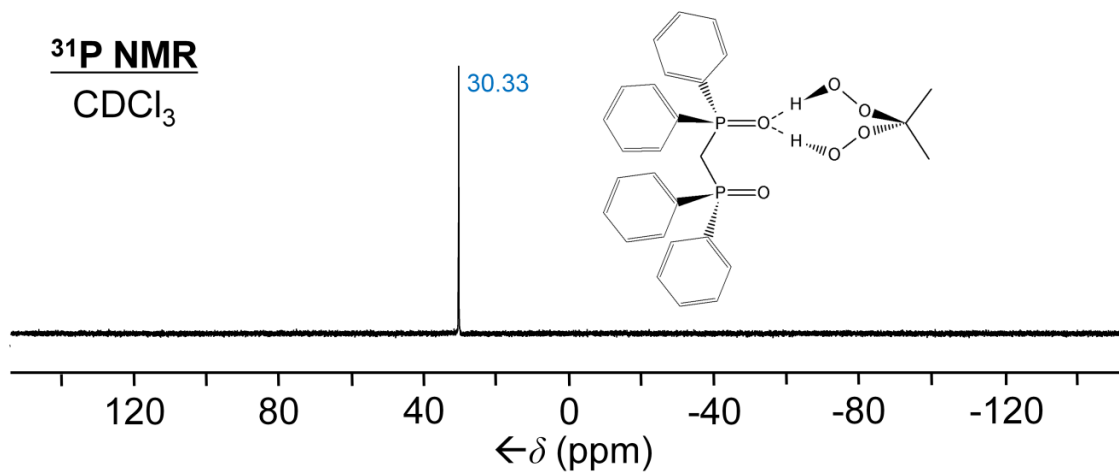


Figure A.64. ³¹P{¹H} NMR spectrum of **13** in CDCl₃.

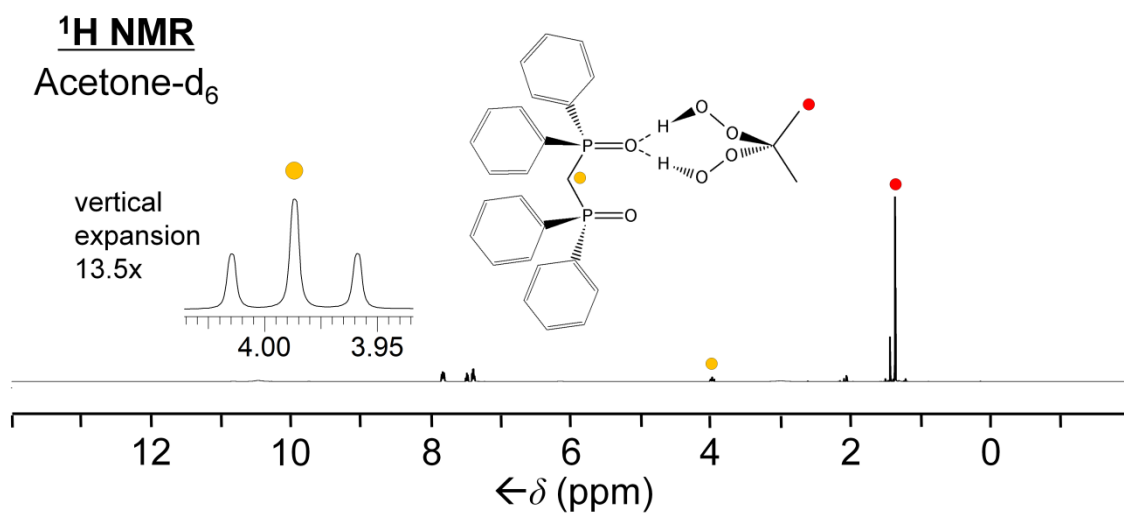


Figure A.65. ¹H NMR spectrum of **13** in acetone-d₆.

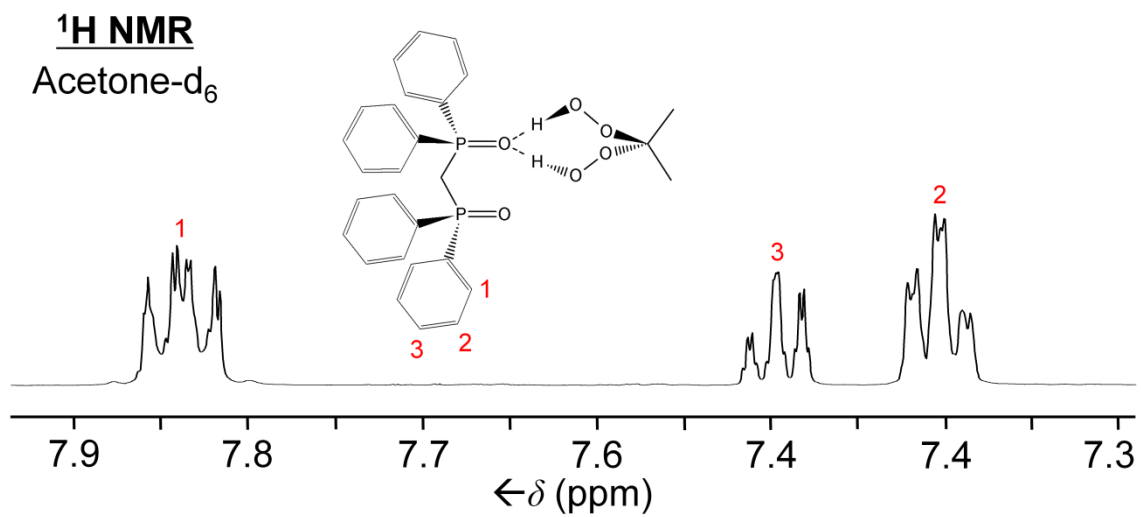


Figure A.66. ¹H NMR spectrum of **13** in acetone-d₆, aryl region expansion.

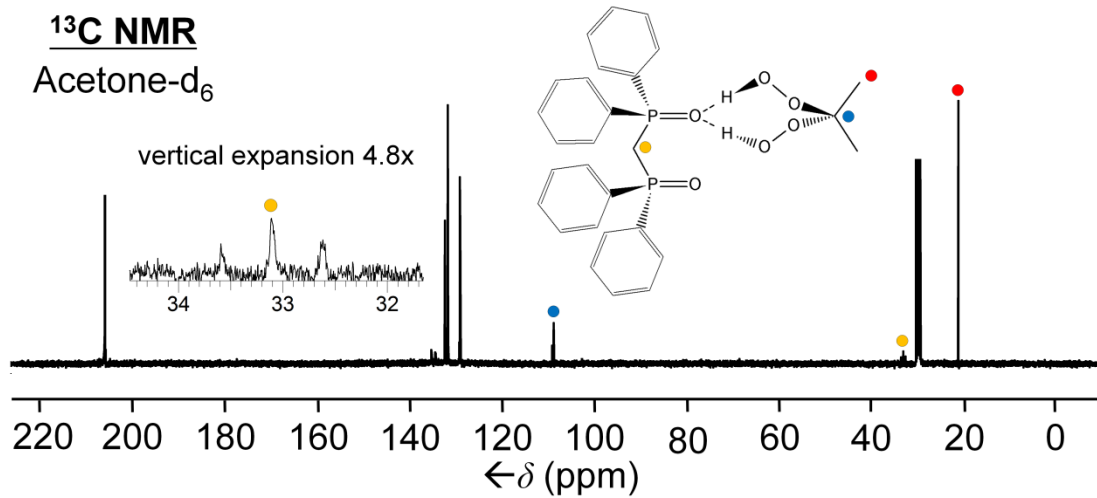


Figure A.67. ¹³C{¹H} NMR spectrum of **13** in acetone-d₆.

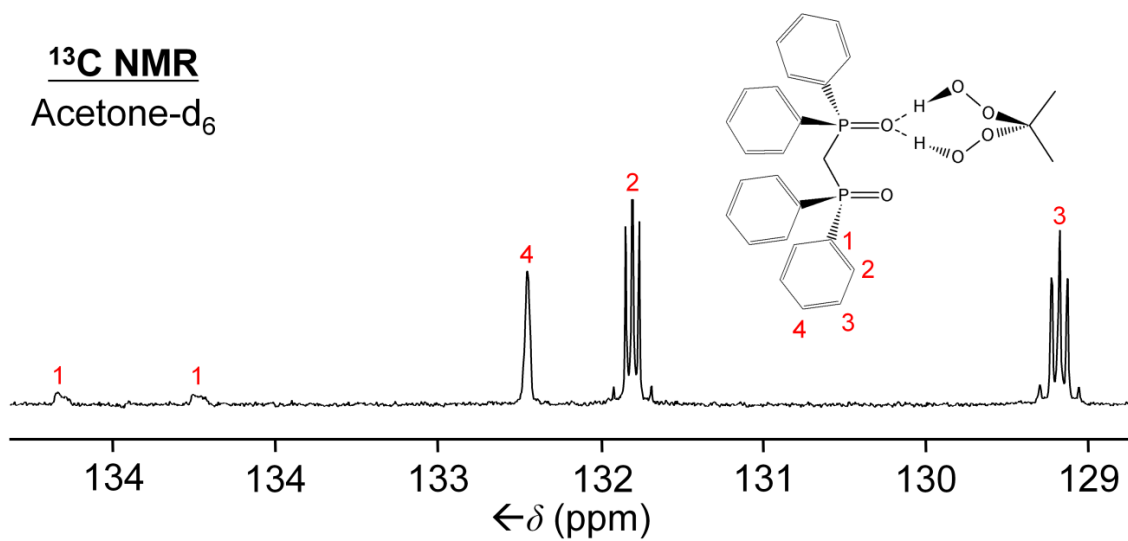


Figure A.68. $^{13}\text{C}\{^1\text{H}\}$ NMR spectrum of **13** in acetone-d₆, aryl region expansion.

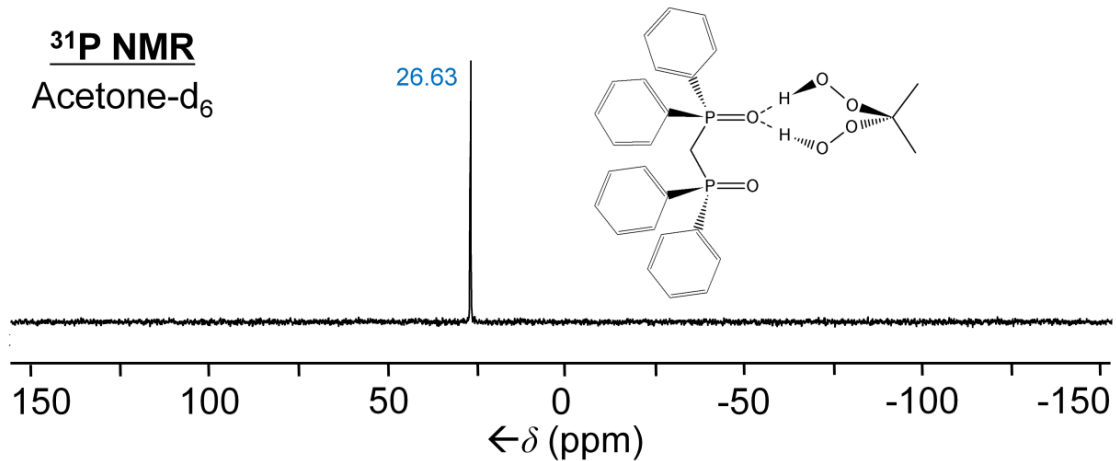


Figure A.69 $^{31}\text{P}\{^1\text{H}\}$ NMR spectrum of **13** in acetone-d₆.

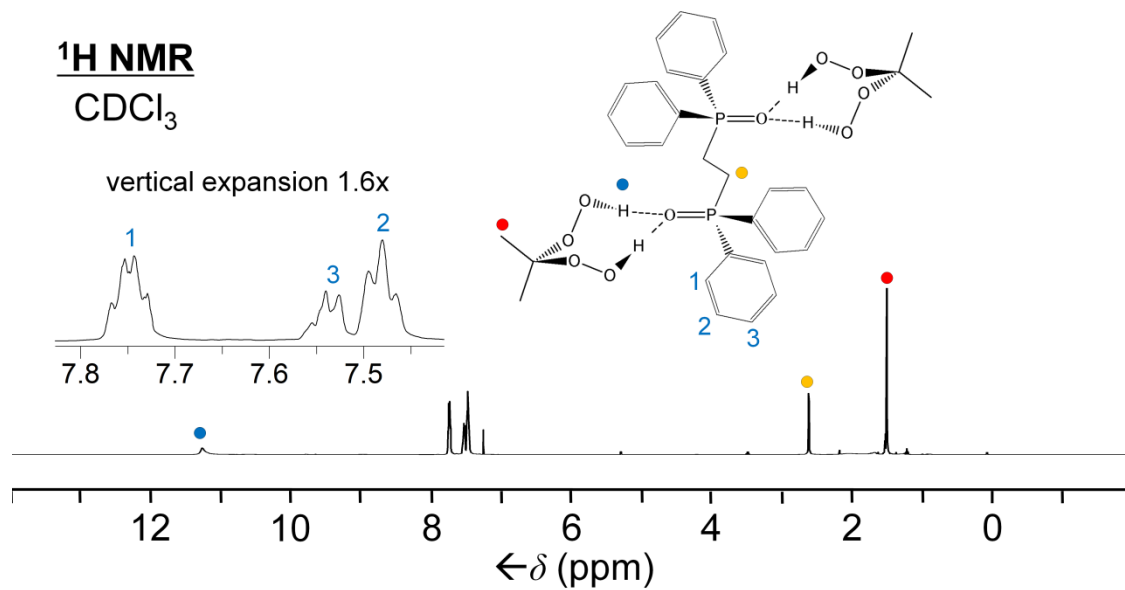


Figure A.70. ¹H NMR spectrum of **14** in CDCl₃.

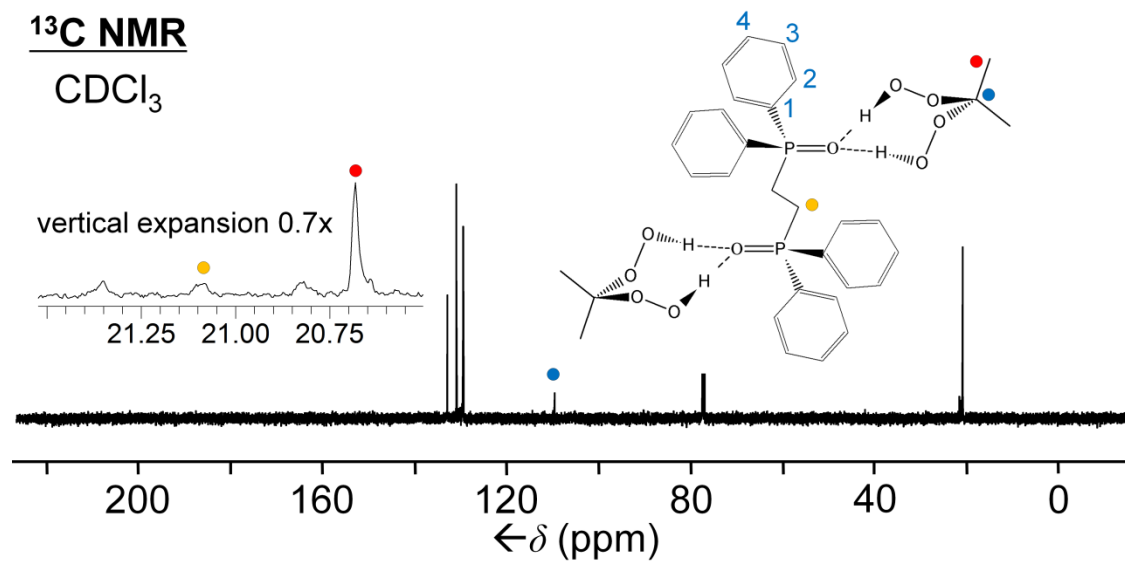


Figure A.71. ¹³C{¹H} NMR spectrum of **14** in CDCl₃.

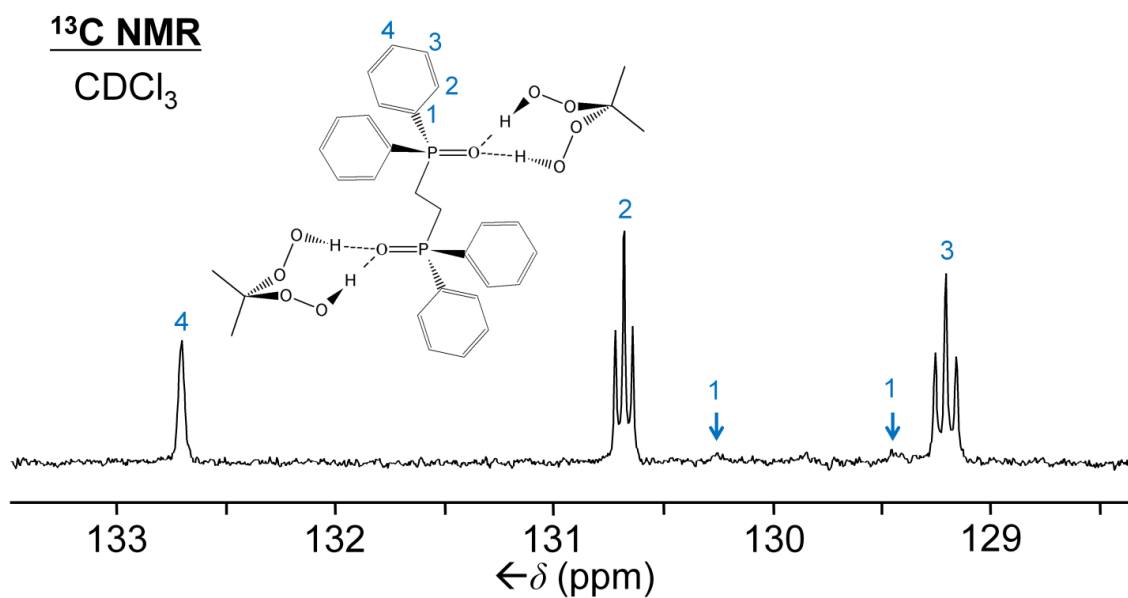


Figure A.72. $^{13}\text{C}\{^1\text{H}\}$ NMR spectrum of **14** in CDCl₃, aryl region expansion.

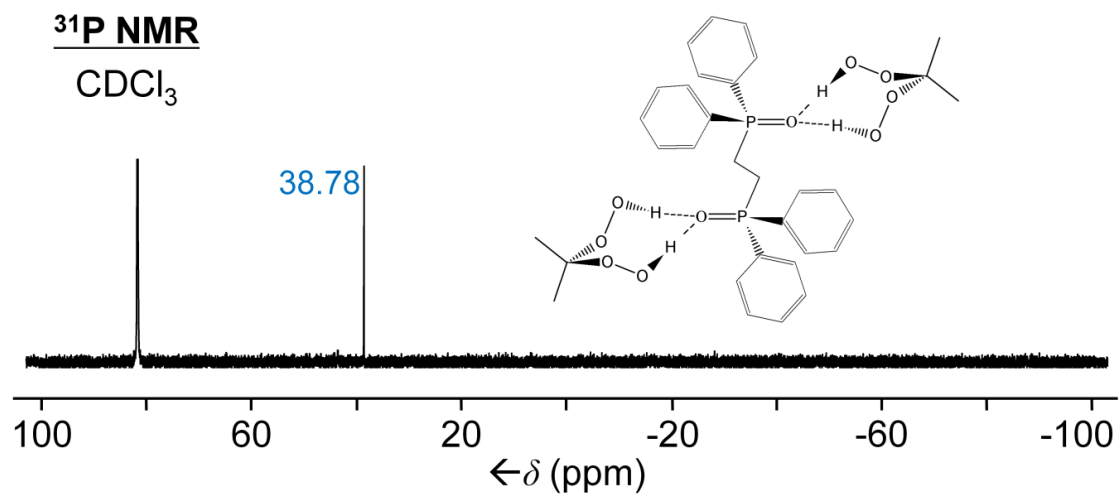


Figure A.73. $^{31}\text{P}\{^1\text{H}\}$ NMR spectrum of **14** in CDCl₃.

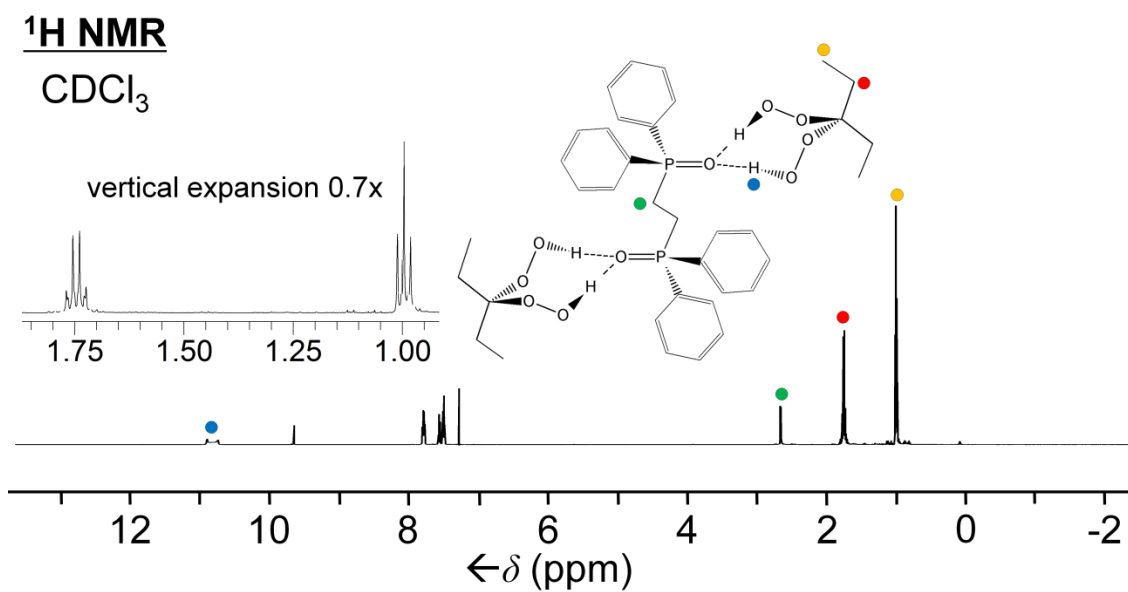


Figure A.74. ¹H NMR spectrum of **15** in CDCl₃.

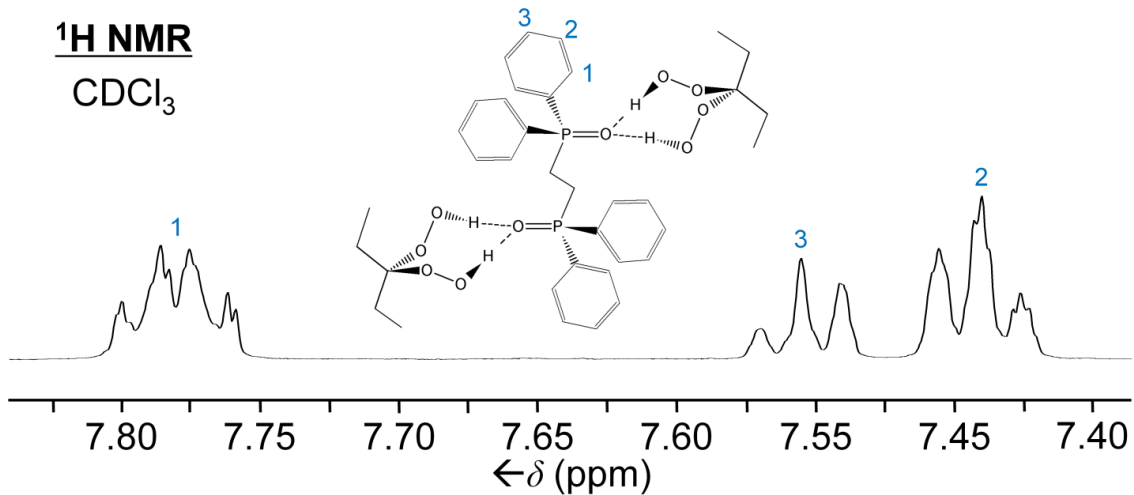


Figure A.75. ¹H NMR spectrum of **15** in CDCl₃, aryl region expansion.

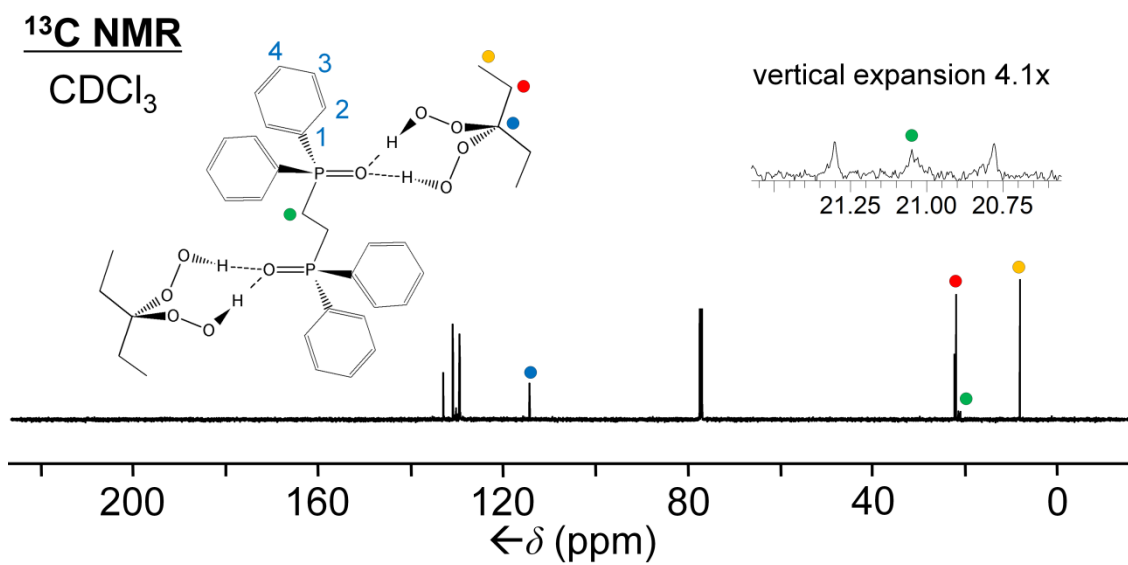


Figure A.76. $^{13}\text{C}\{^1\text{H}\}$ NMR spectrum of **15** in CDCl_3 .

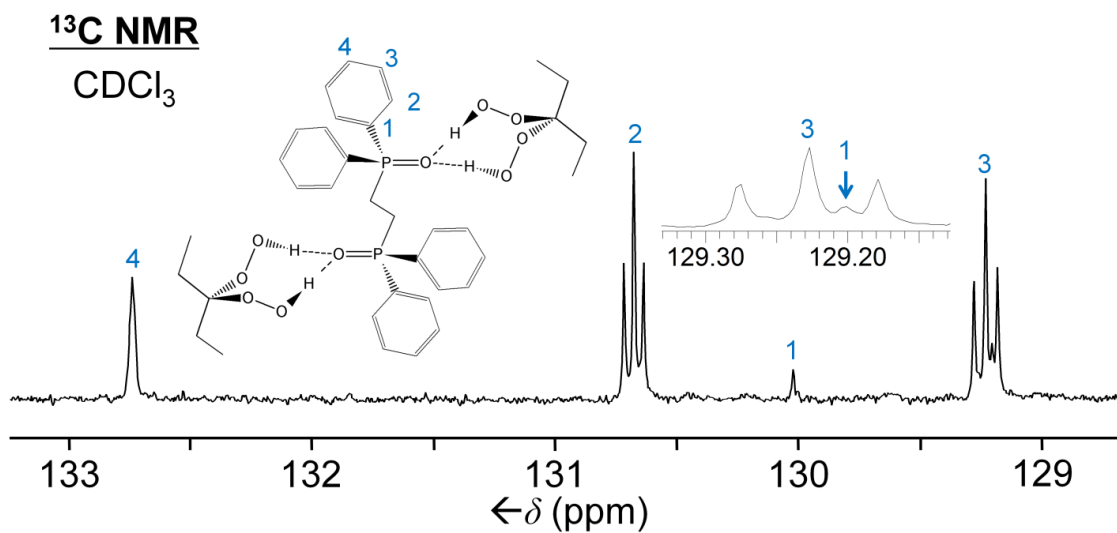


Figure A.77. $^{13}\text{C}\{^1\text{H}\}$ NMR spectrum of **15** in CDCl_3 , aryl region expansion.

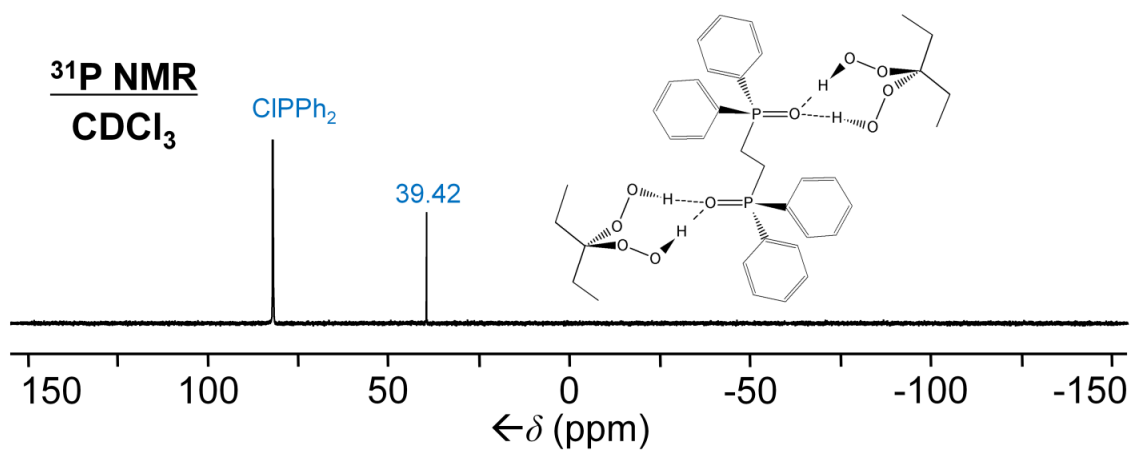


Figure A.78. $^{31}\text{P}\{^1\text{H}\}$ NMR spectrum of **15** in CDCl_3 .

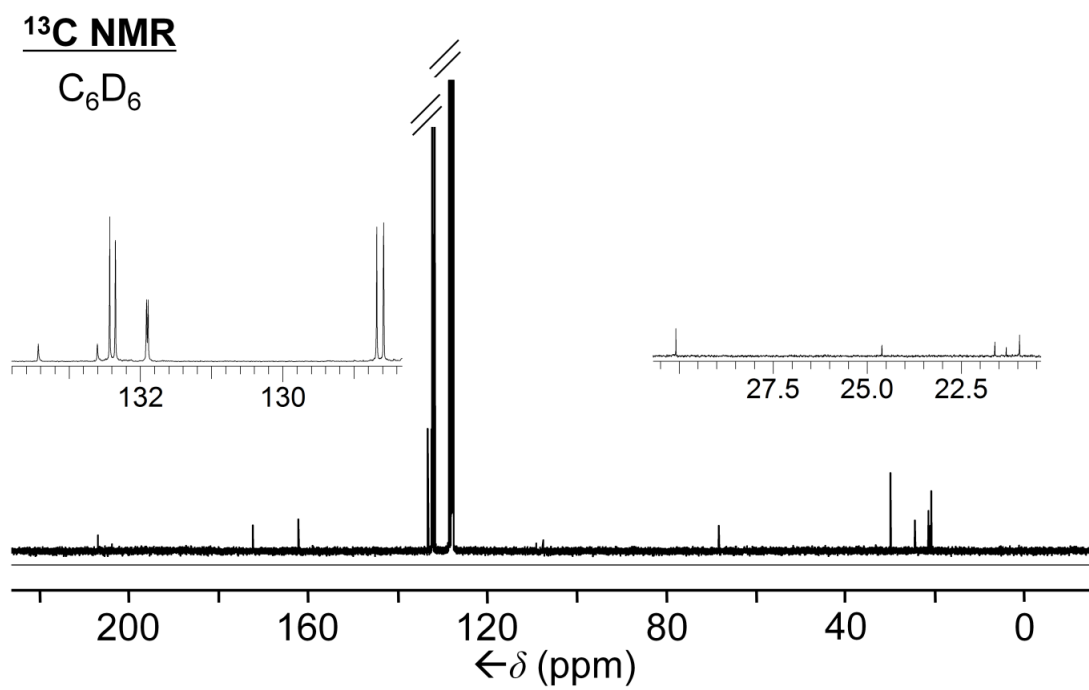


Figure A.79. ¹³C NMR spectrum of **4** in benzene after heating at 90 °C for 3 days.

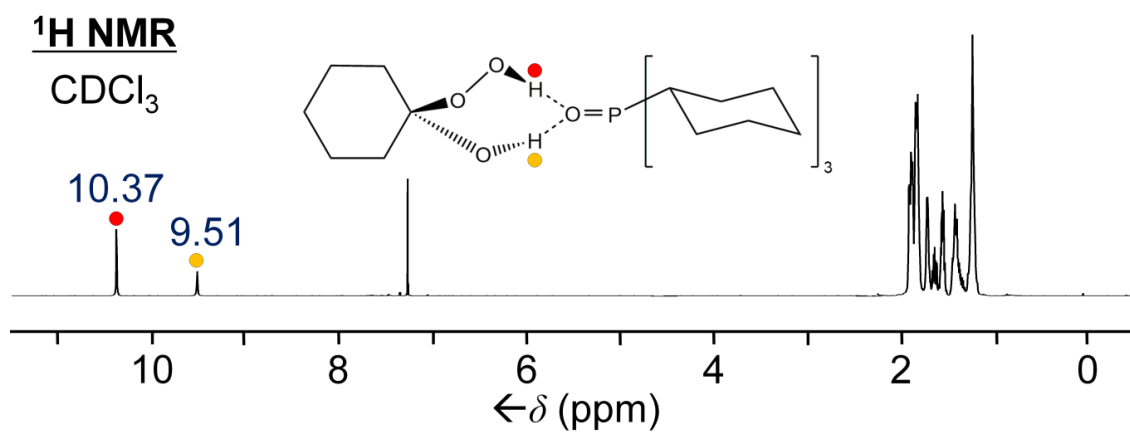


Figure A.80. ¹H NMR spectrum of **16** in CDCl₃.

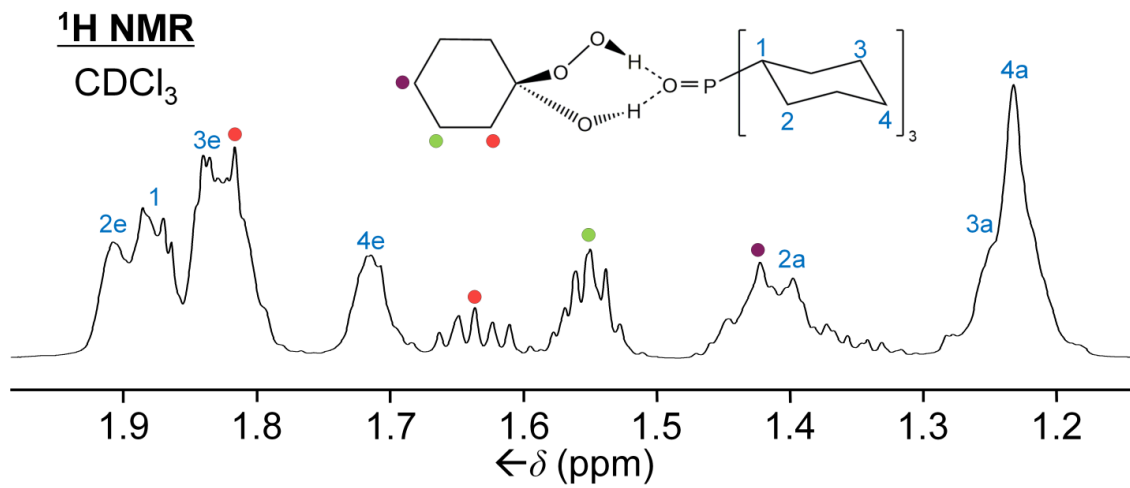


Figure A.81. ¹H NMR spectrum of **16** in CDCl₃, alkyl region expansion.

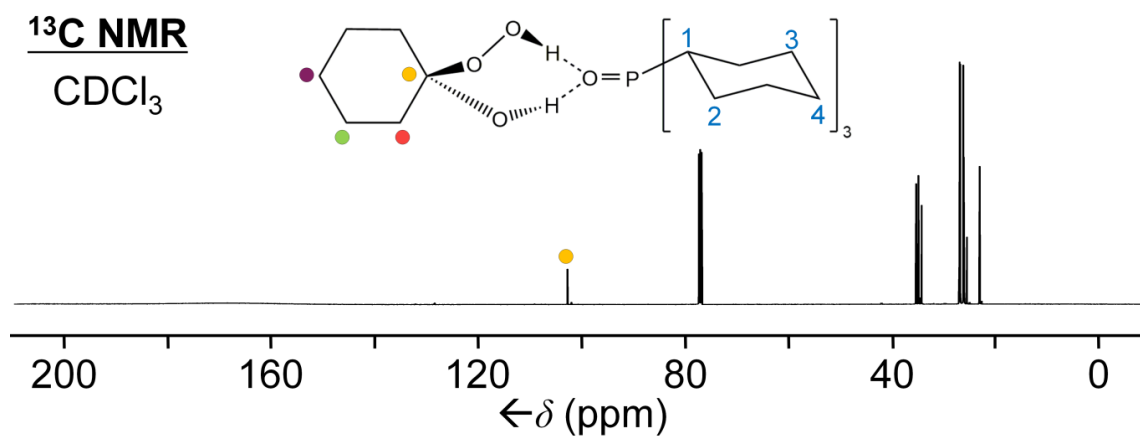


Figure A.82. ¹³C{¹H} NMR spectrum of **16** in CDCl₃.

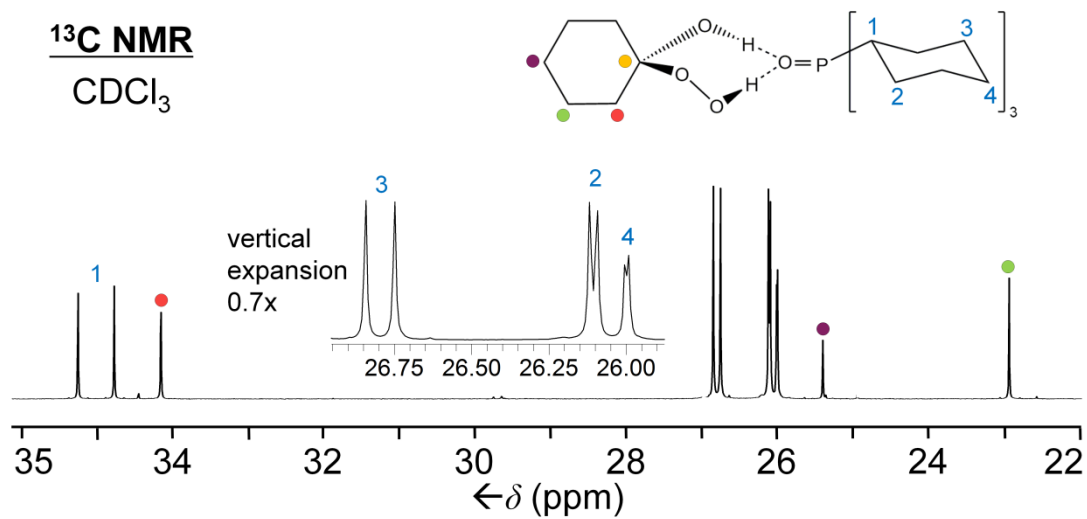


Figure A.83. ¹³C{¹H} NMR spectrum of **16** in CDCl₃, alkyl region expansion.

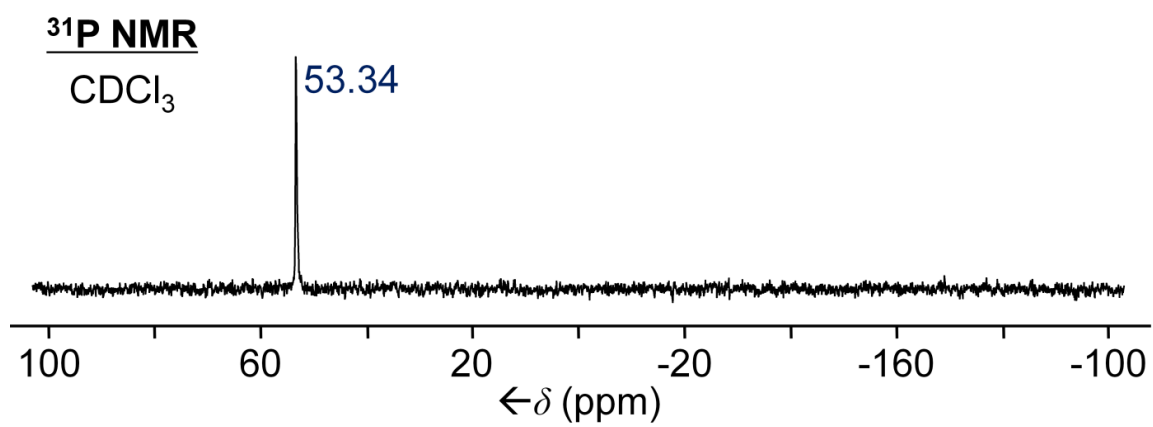


Figure A.84. $^{31}\text{P}\{^1\text{H}\}$ NMR spectrum of **16** in CDCl_3 .

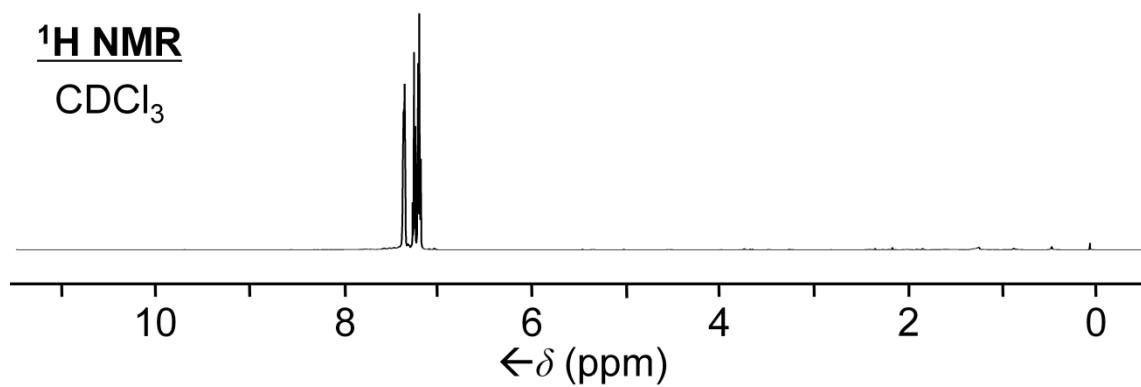


Figure A.85. ¹H NMR spectrum of 1,1,2,2-tetraphenyldiphosphine in CDCl₃.

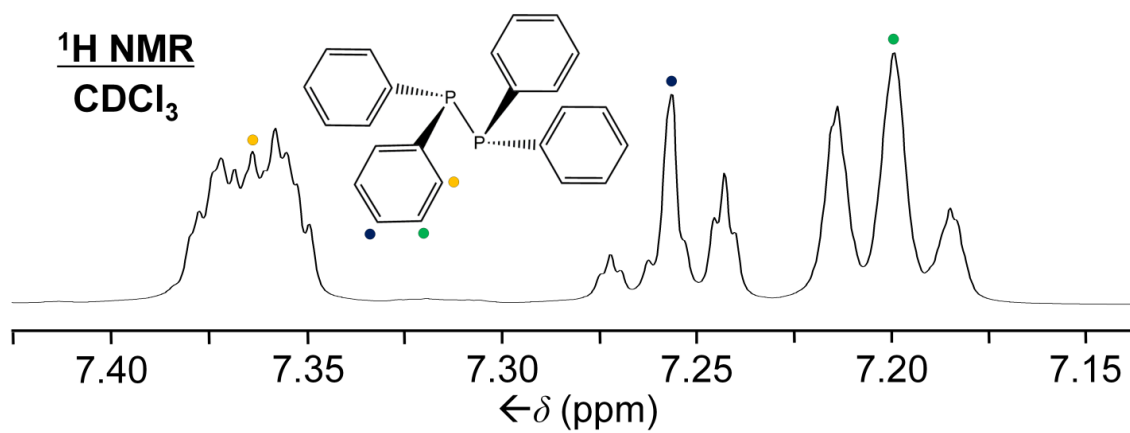


Figure A.86. ¹H NMR spectrum of 1,1,2,2-tetraphenyldiphosphine in CDCl₃, aryl region expansion.

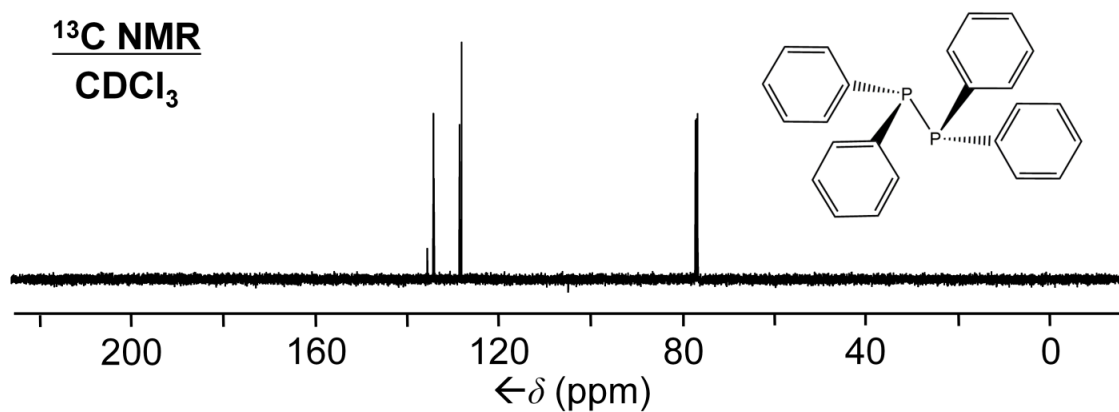


Figure A.87. ¹³C{¹H} NMR spectrum of 1,1,2,2-tetraphenyldiphosphine in CDCl₃.

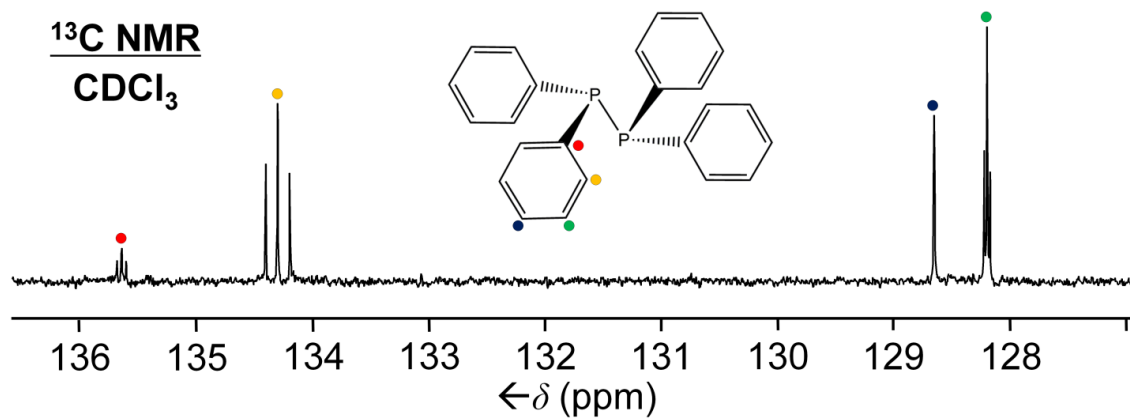


Figure A.88. ¹³C{¹H} NMR spectrum of 1,1,2,2-tetraphenyldiphosphine in CDCl₃, aryl region expansion.

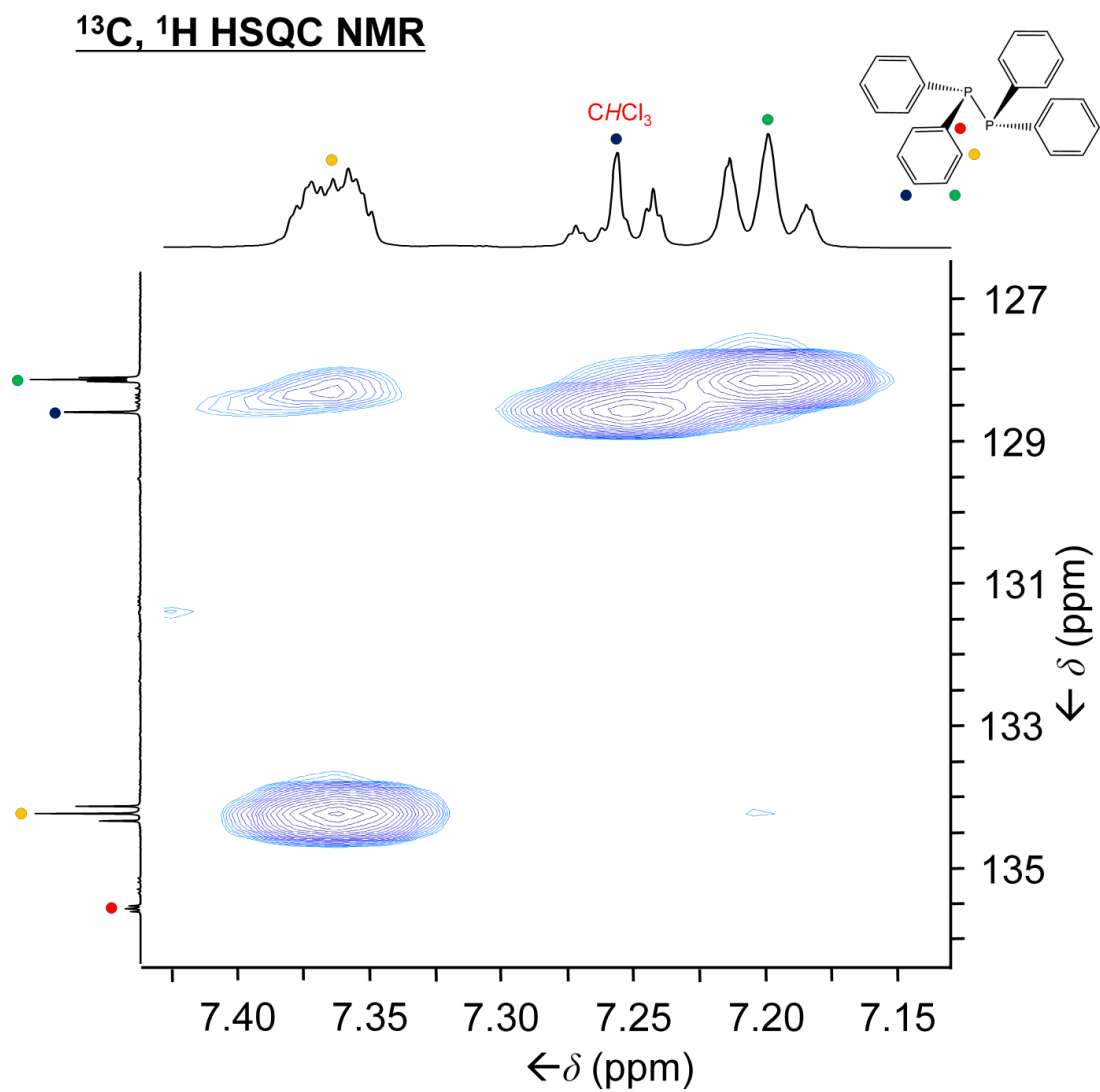


Figure A.89. ^{13}C , ^1H HSQC NMR spectrum of 1,1,2,2-tetraphenyldiphosphine in CDCl_3 .

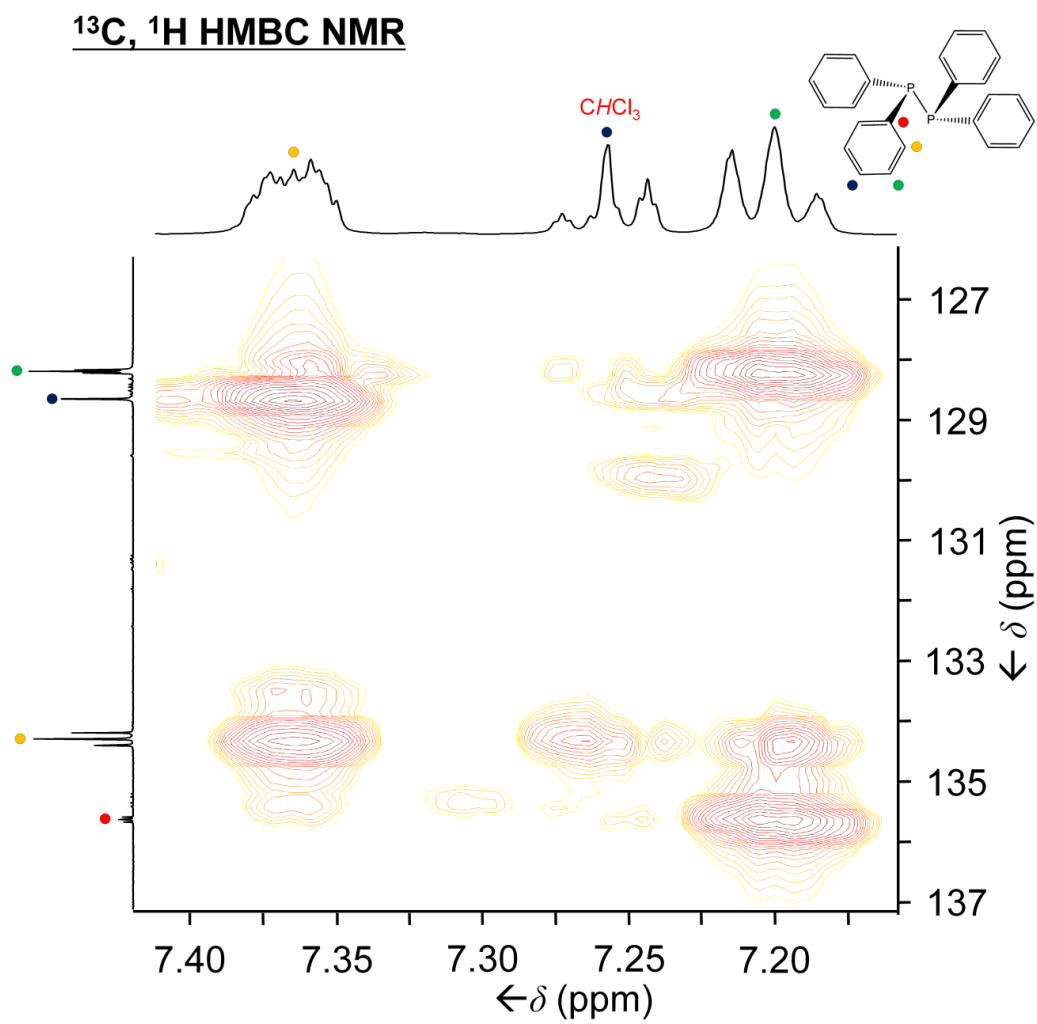


Figure A.90. ^{13}C , ^1H HMBC NMR spectrum of 1,1,2,2-tetraphenyldiphosphine in CDCl_3 .

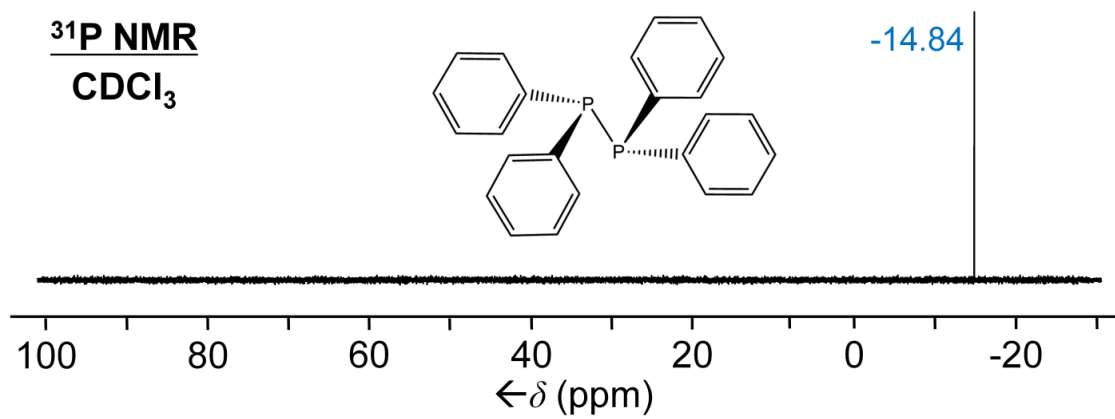


Figure A.91. ³¹P{¹H}NMR spectrum of 1,1,2,2-tetraphenyldiphosphine in CDCl₃.

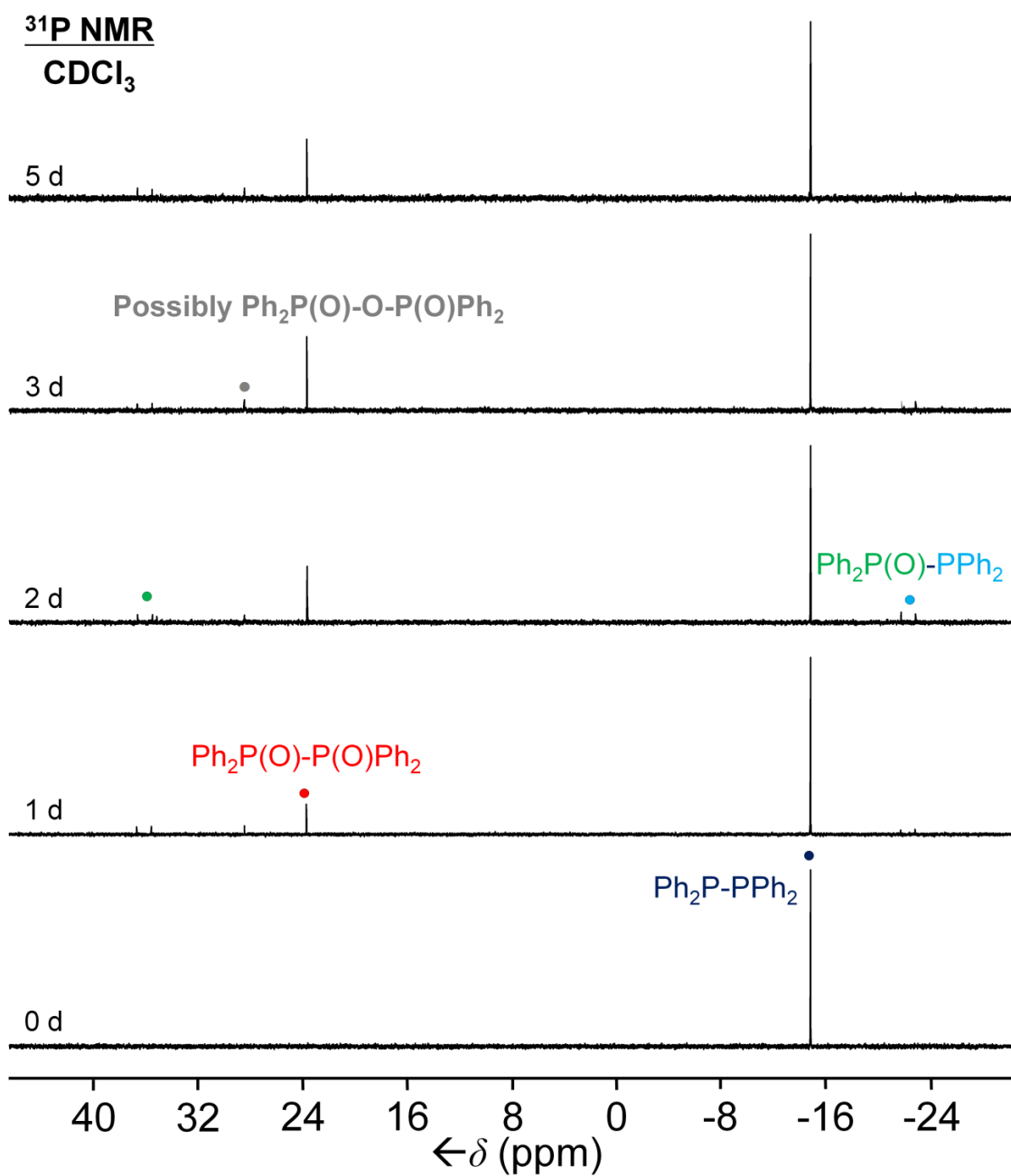


Figure A.92. Oxidation of 1,1,2,2-tetraphenyldiphosphine in air over a period of 5 days.

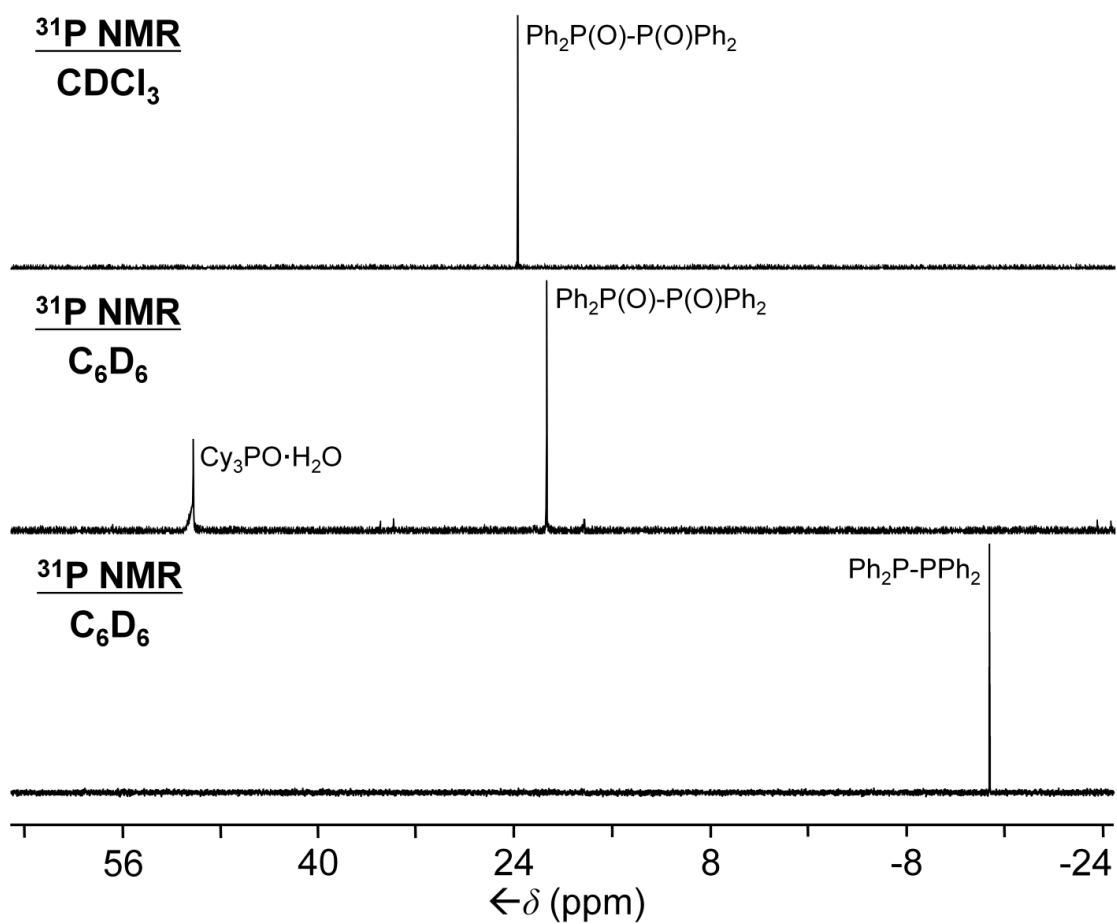


Figure A.93. Stoichiometric oxidation of 1,1,2,2-tetraphenyldiphosphine with **5** as oxidant; starting phosphine in C₆D₆ (bottom), product 1,1,2,2-tetraphenyldiphosphine dioxide and consumed adduct in C₆D₆ (middle), and 1,1,2,2-tetraphenyldiphosphine dioxide isolated via simple filtration and dissolved in CDCl₃ (top).

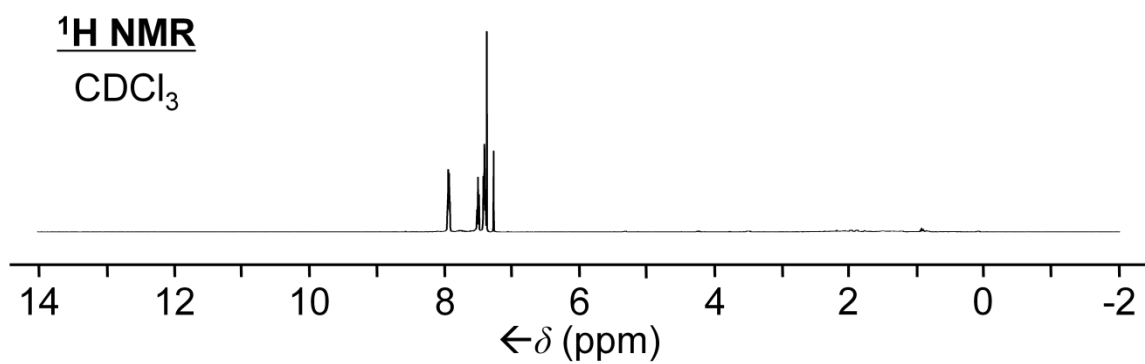


Figure A.94. ¹H NMR spectrum of 1,1,2,2-tetraphenyldiphosphine dioxide (**17**) in CDCl₃.

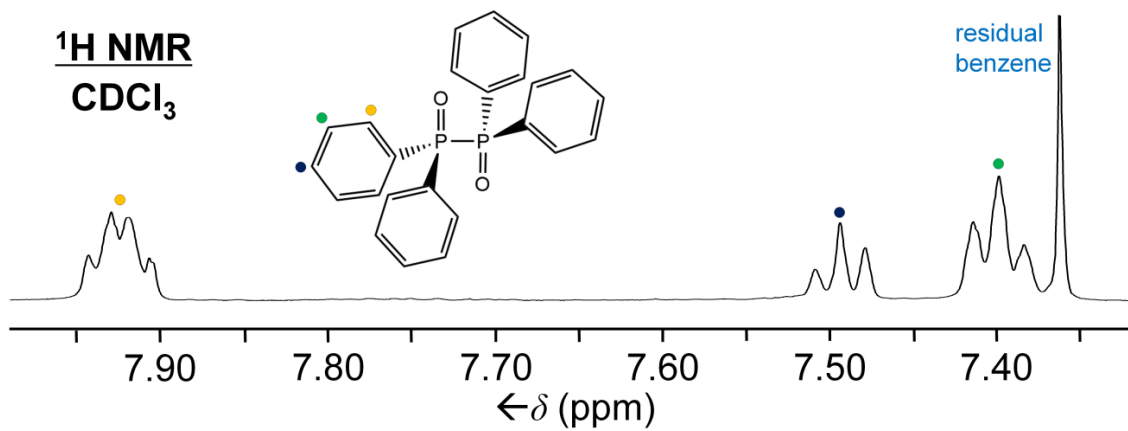


Figure A.95. ¹H NMR spectrum of **17** in CDCl₃, aryl region expansion.

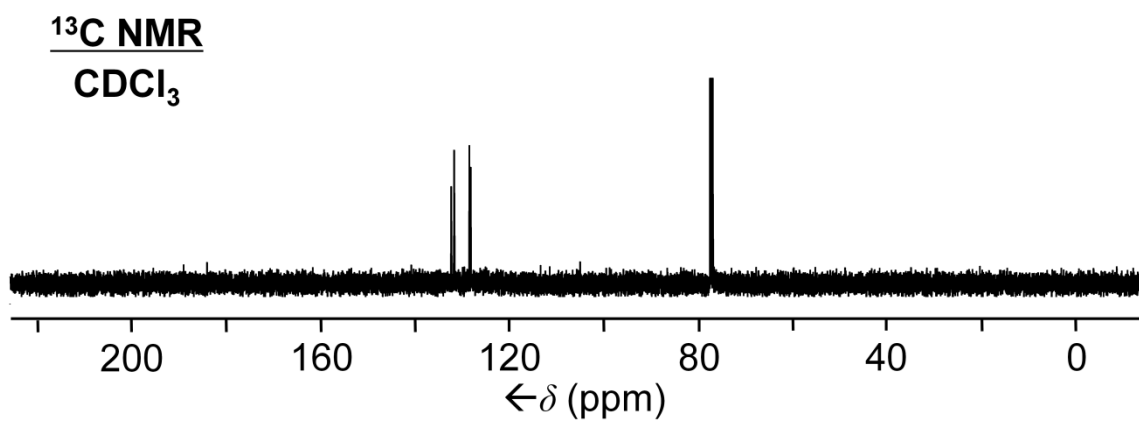


Figure A.96. ¹³C{¹H} NMR spectrum of **17** in CDCl₃.

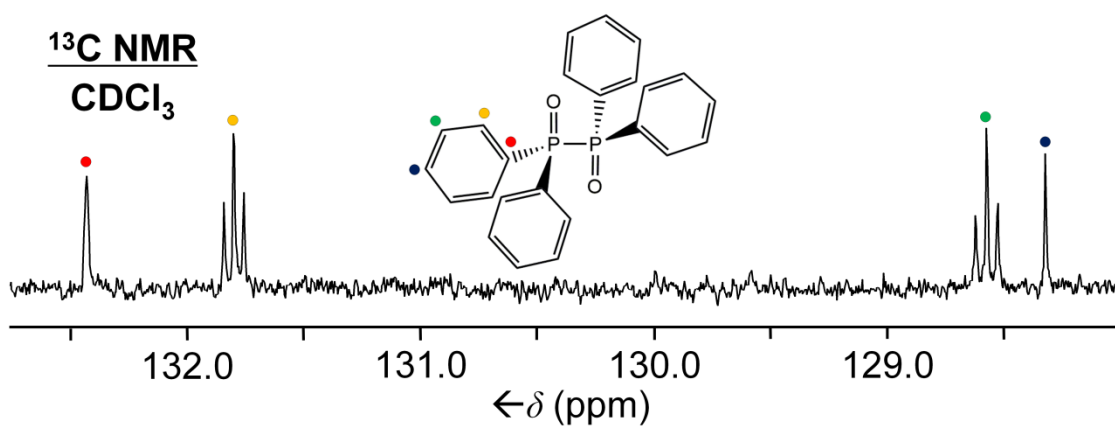


Figure A.97. ¹³C{¹H} NMR spectrum of **17** in CDCl₃, aryl region expansion.

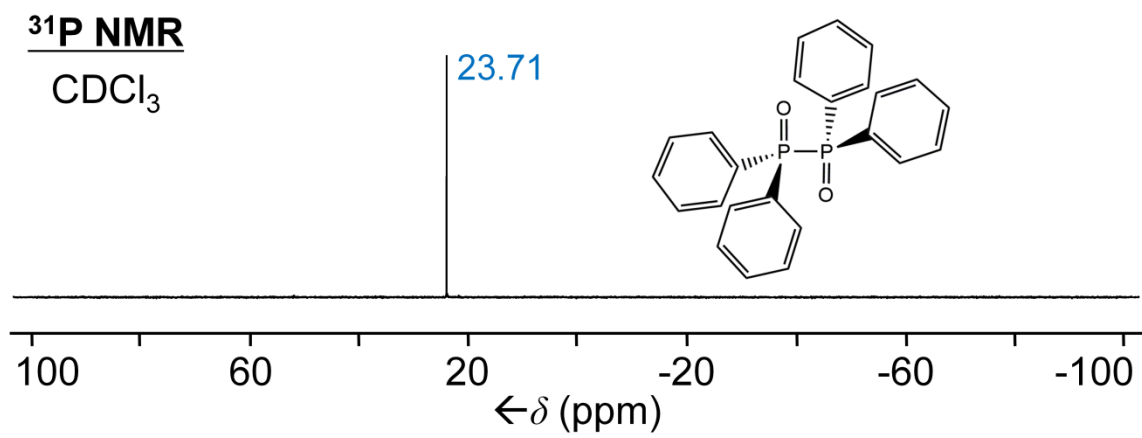


Figure A.98. ³¹P{¹H} NMR spectrum of **17** in CDCl₃.

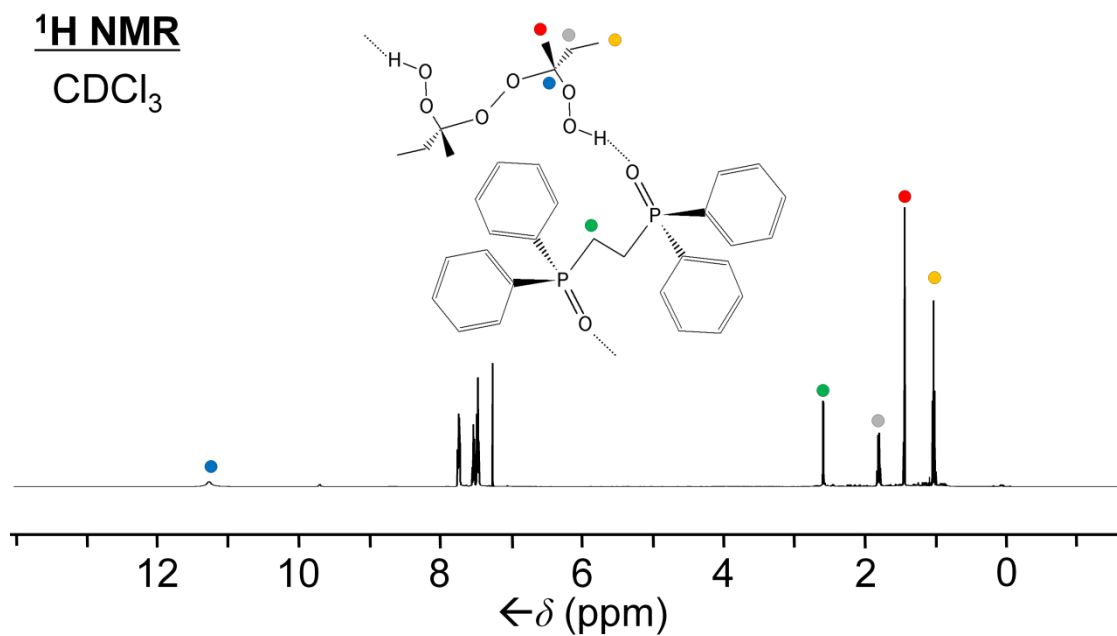


Figure A.99. ¹H NMR spectrum of **18** in CDCl₃.

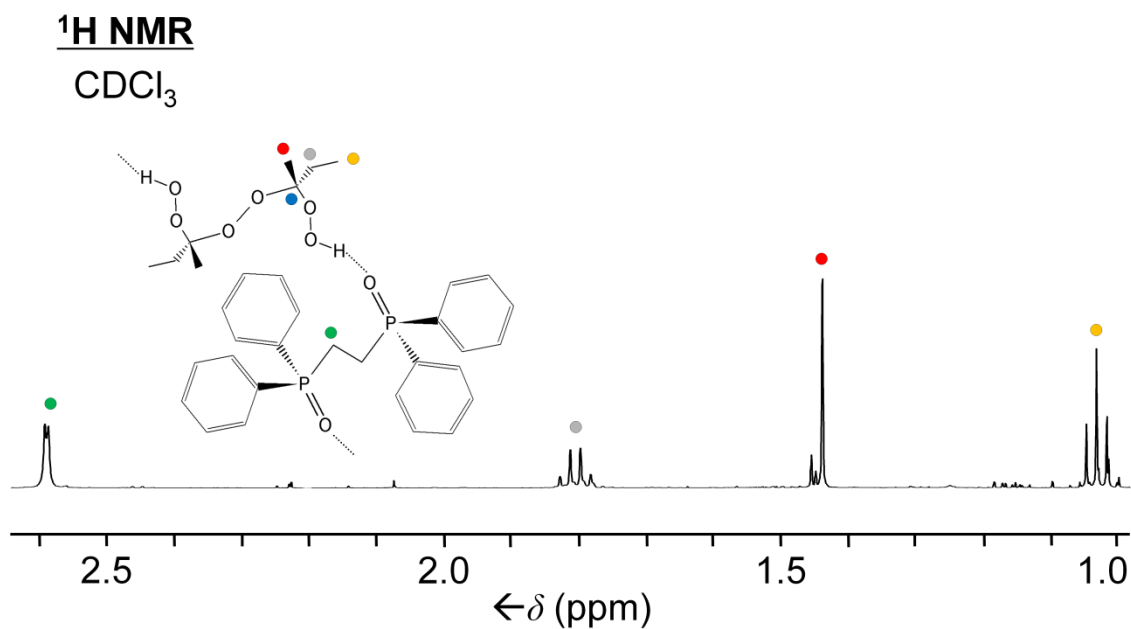


Figure A.100. ¹H NMR spectrum of **18** in CDCl₃, alkyl region expansion.

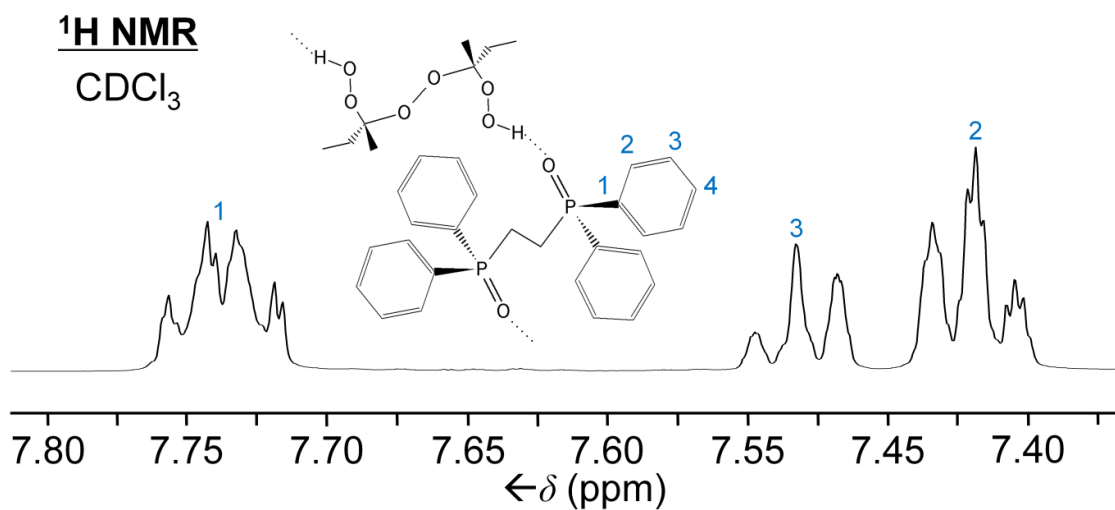


Figure A.101. ¹H NMR spectrum of **18** in CDCl₃, aryl region expansion.

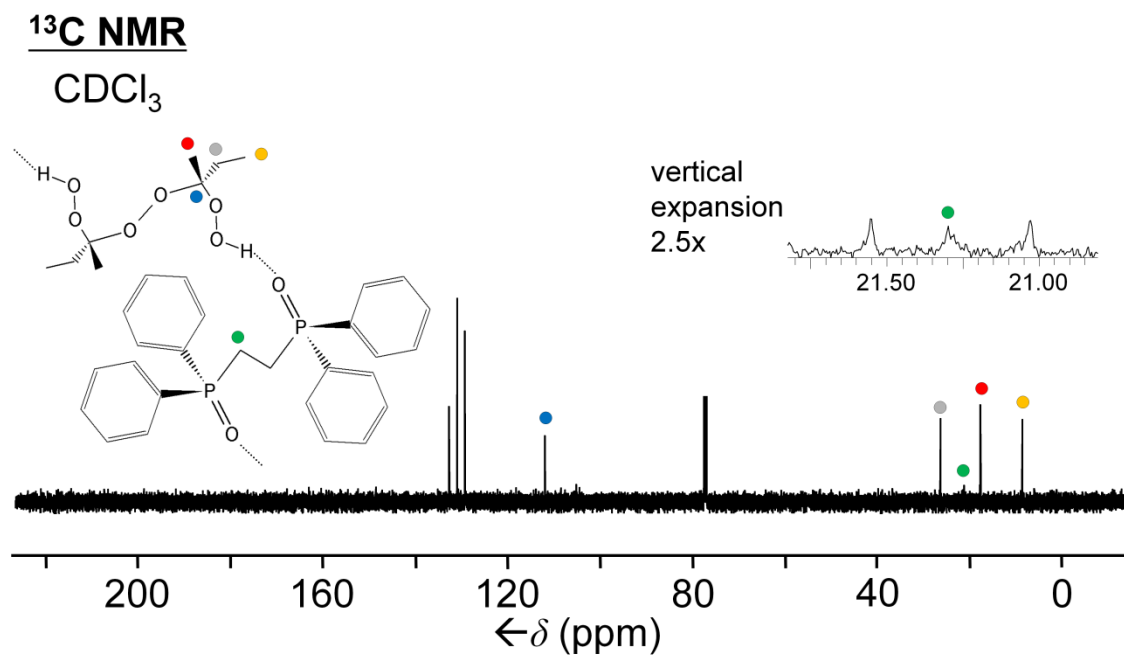


Figure A.102. ¹³C{¹H} NMR spectrum of **18** in CDCl₃.

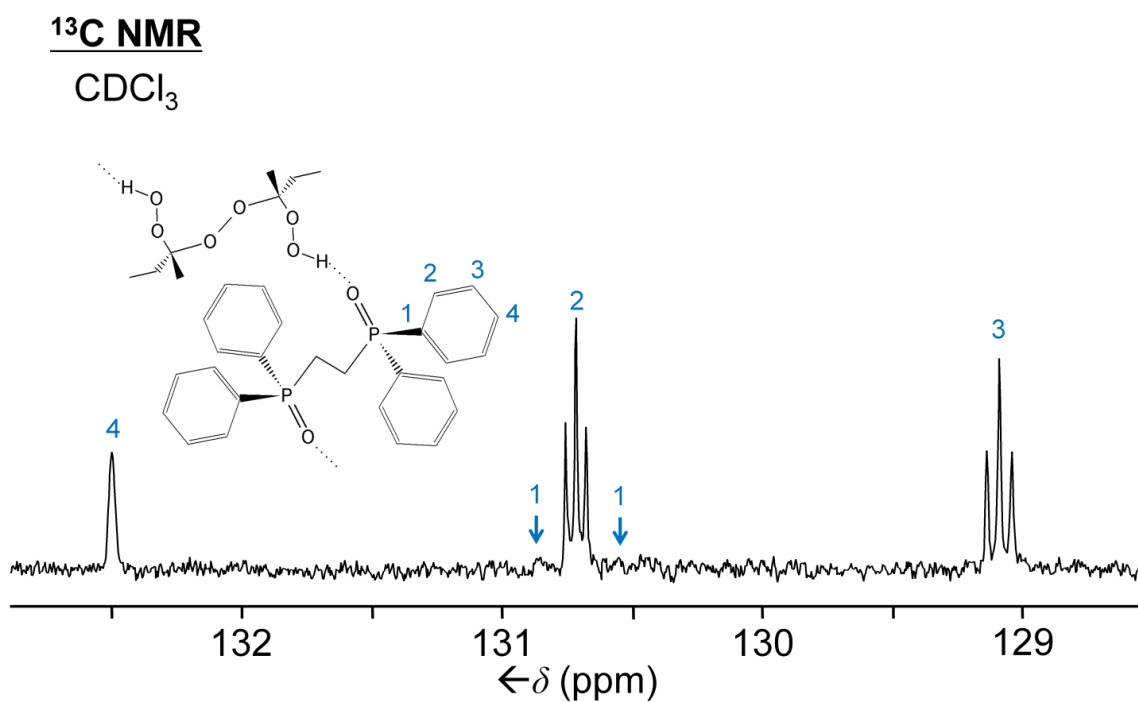


Figure A.103. ¹³C{¹H} NMR spectrum of **18** in CDCl₃, aryl region expansion.

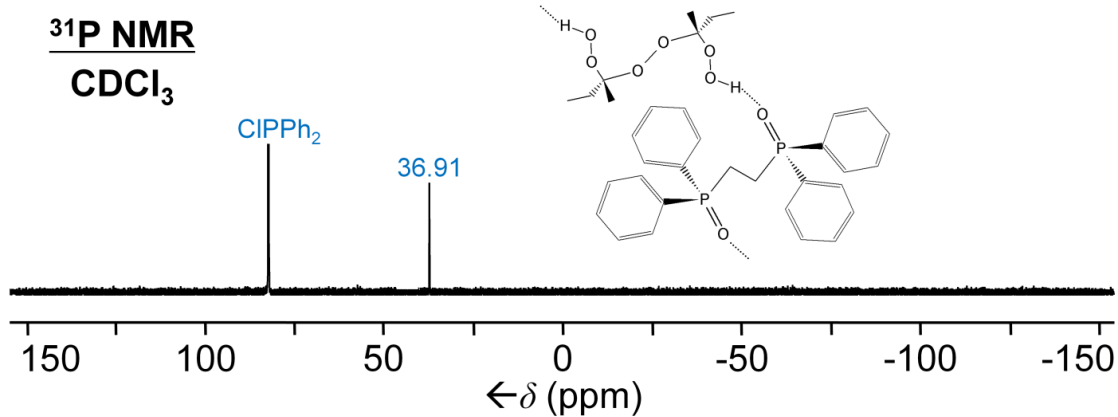


Figure A.104. ³¹P{¹H} NMR spectrum of **18** in CDCl₃.

APPENDIX B
FT-IR SPECTRA

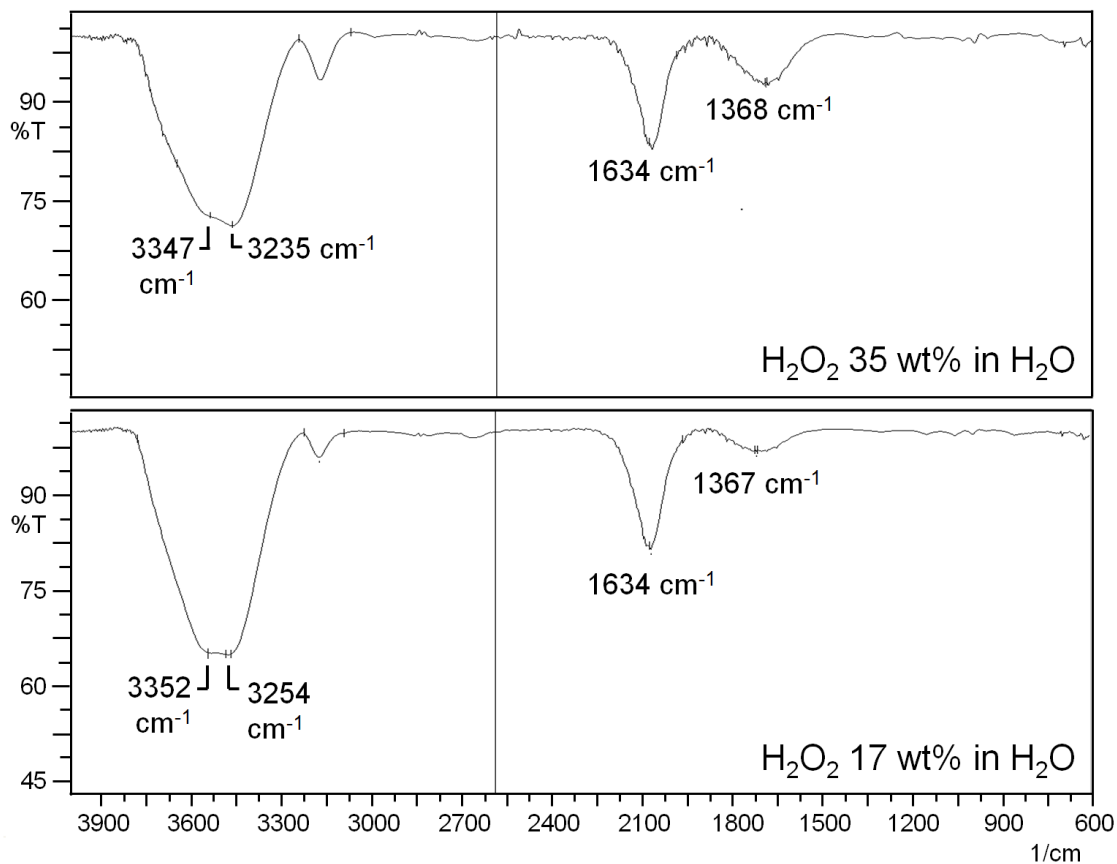


Figure B.1. IR spectra of aqueous H₂O₂ in 35 wt% (top) and 17 wt% (bottom).

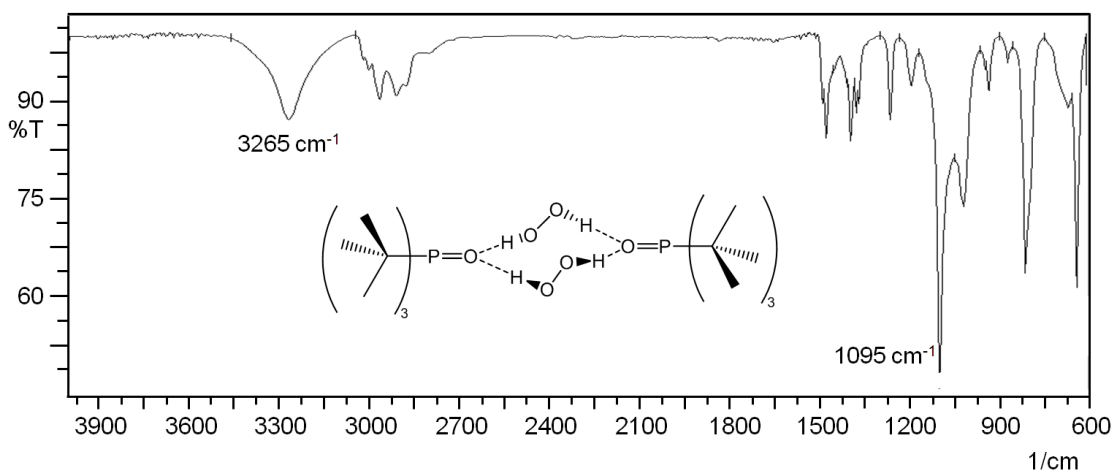


Figure B.2. IR spectrum of **1**.

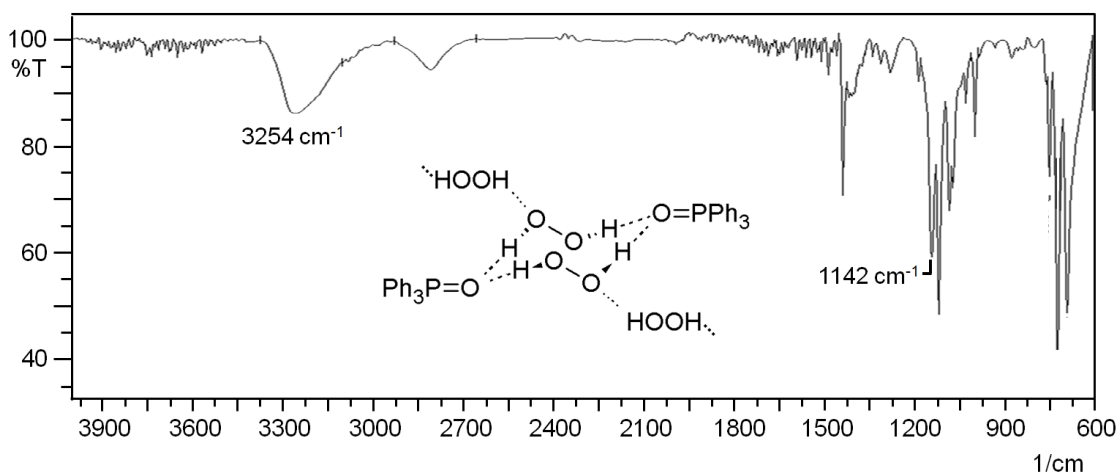


Figure B.3. IR spectrum of **2**.

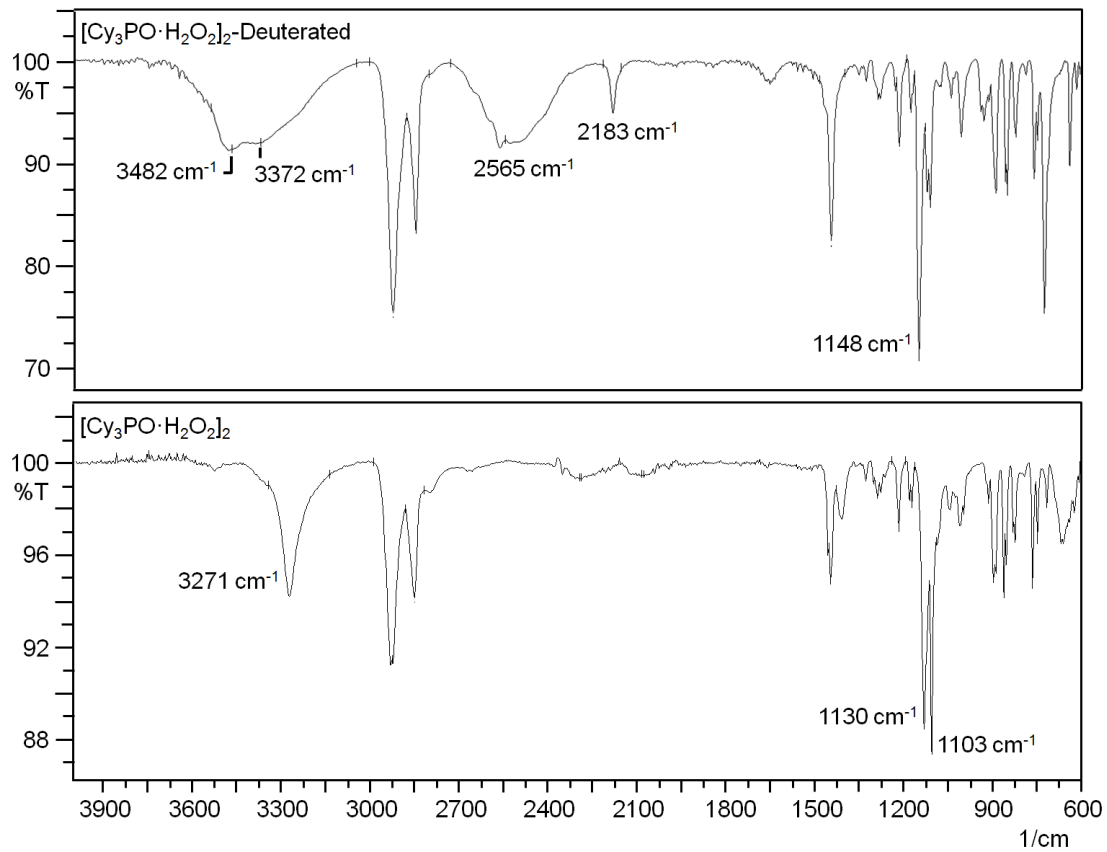


Figure B. 4 IR spectra of **3** before (bottom) and after (top) deuteration.

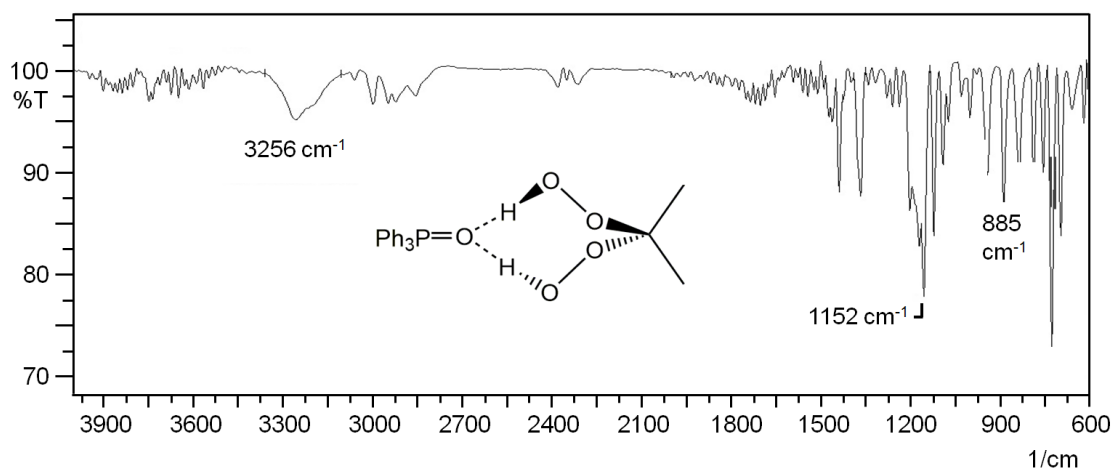


Figure B.5. IR spectrum of **4**.

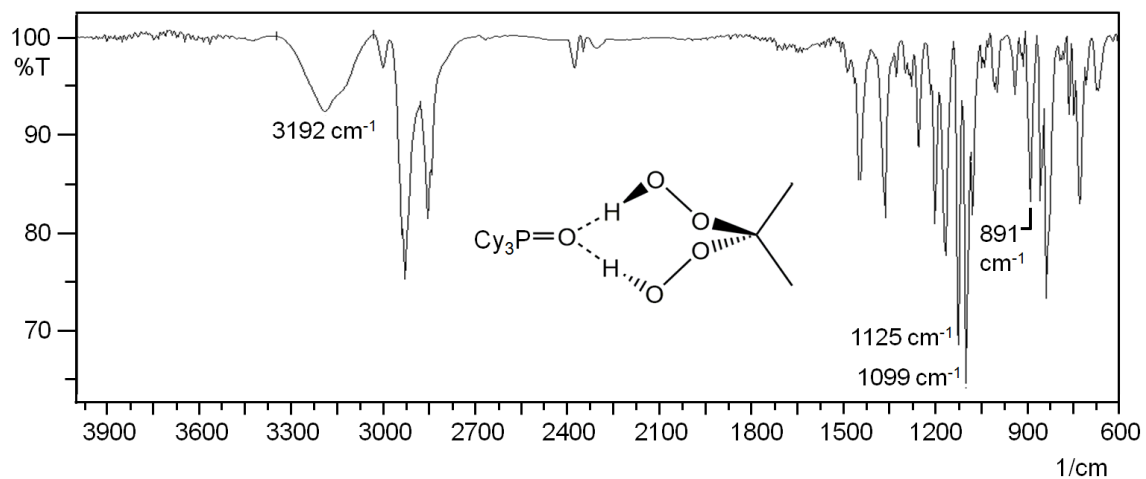


Figure B.6. IR spectrum of **5**.

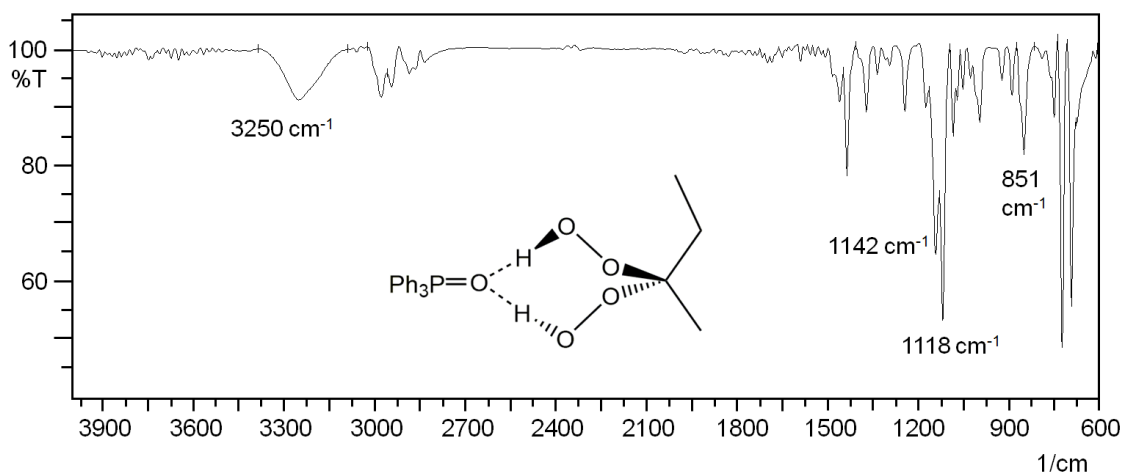


Figure B.7. IR spectrum of **6**.

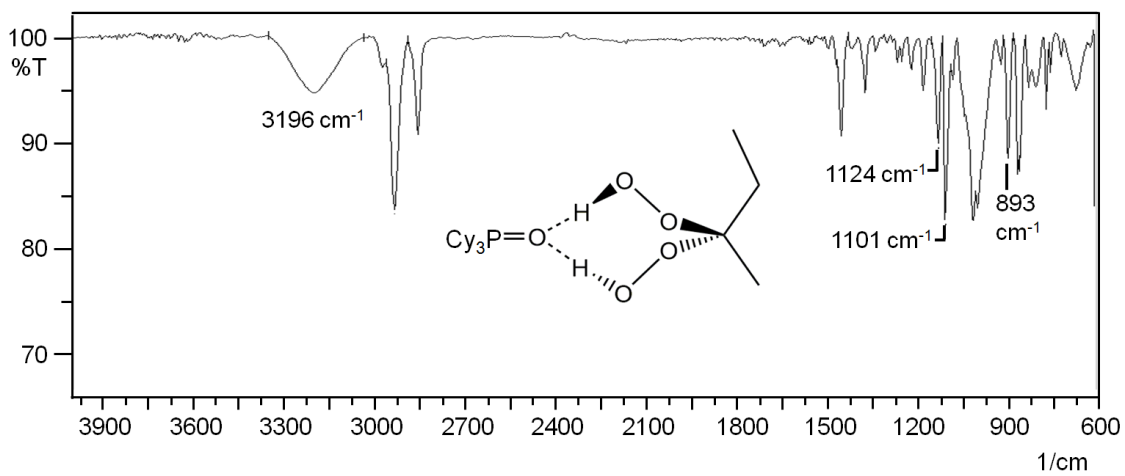


Figure B.8. IR spectrum of **7**.

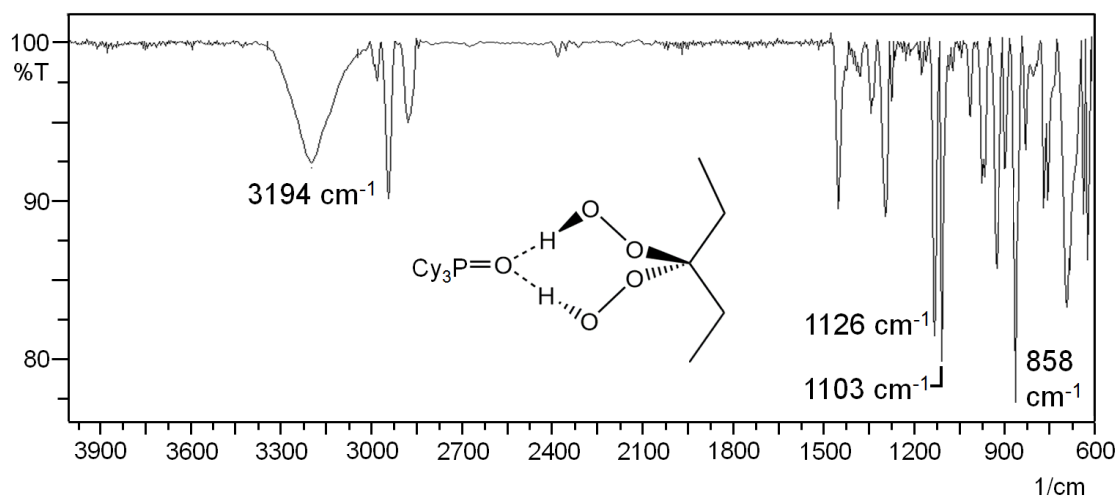


Figure B.9. IR spectrum of **8**.

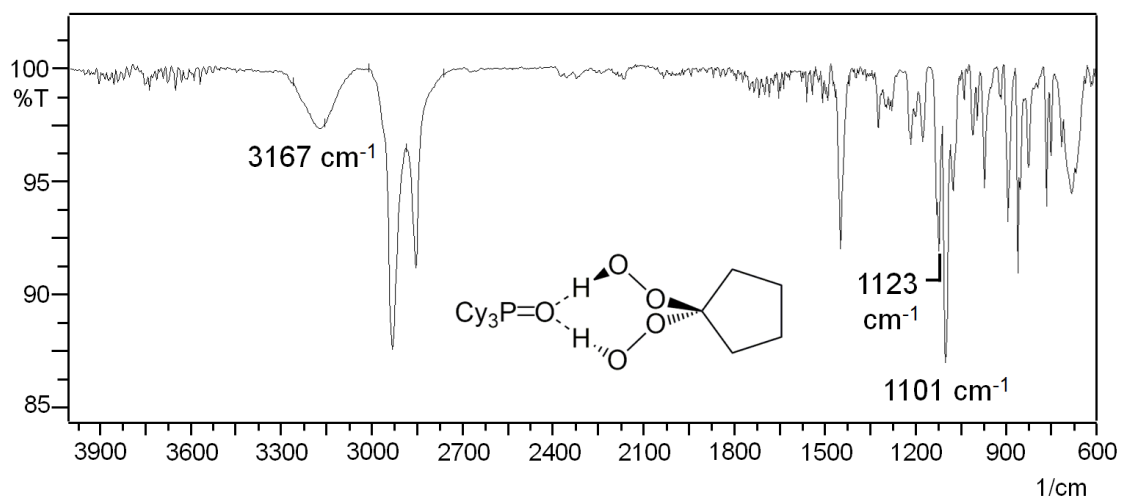


Figure B.10. IR spectrum of **9**.

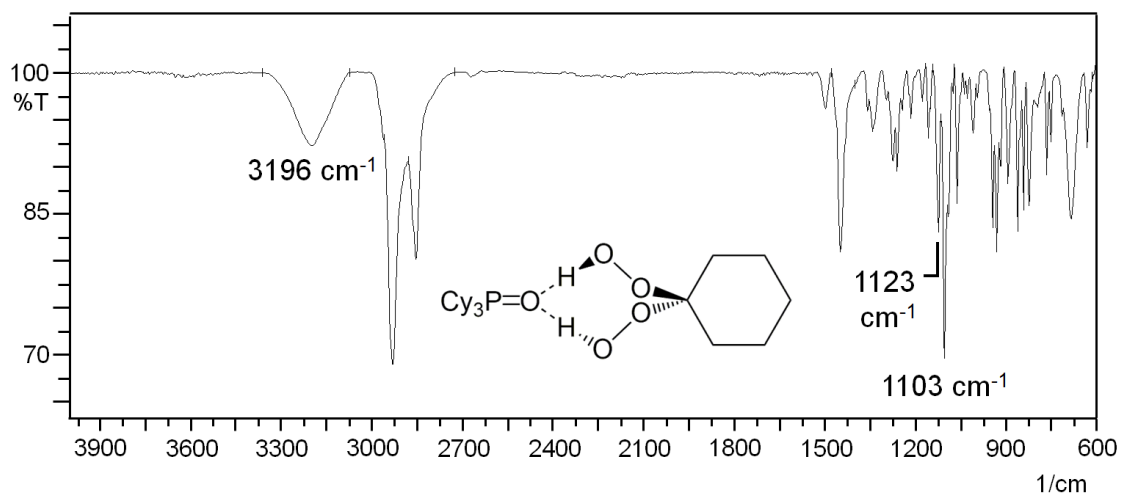


Figure B.11. IR spectrum of **10**.

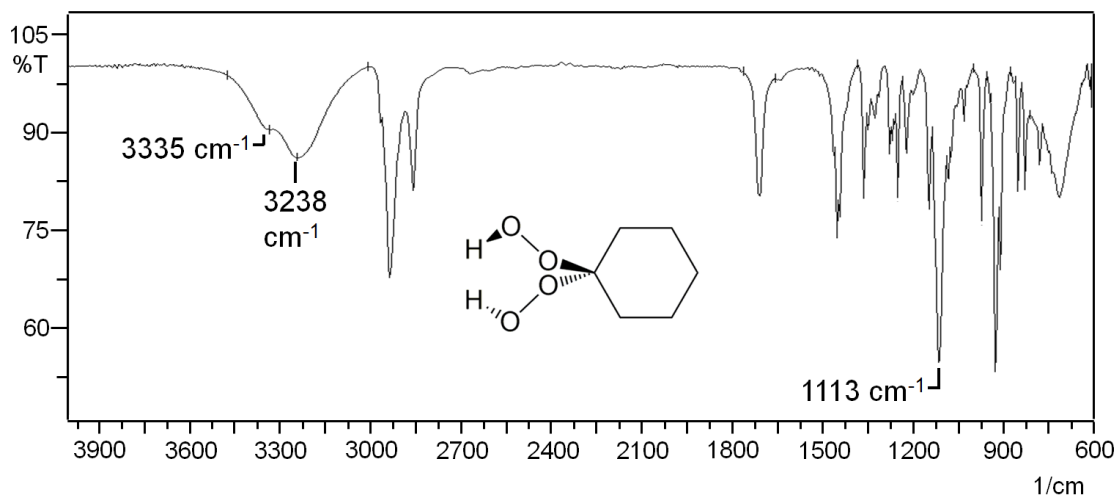


Figure B.12. IR spectrum of 1,1-di(hydroperoxy)cyclohexane.

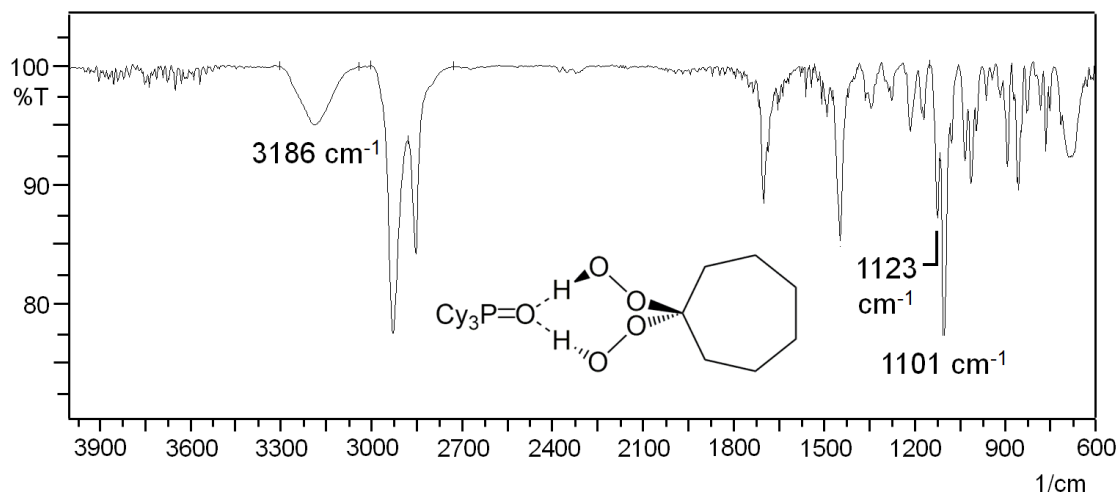


Figure B.13. IR spectrum of **11**.

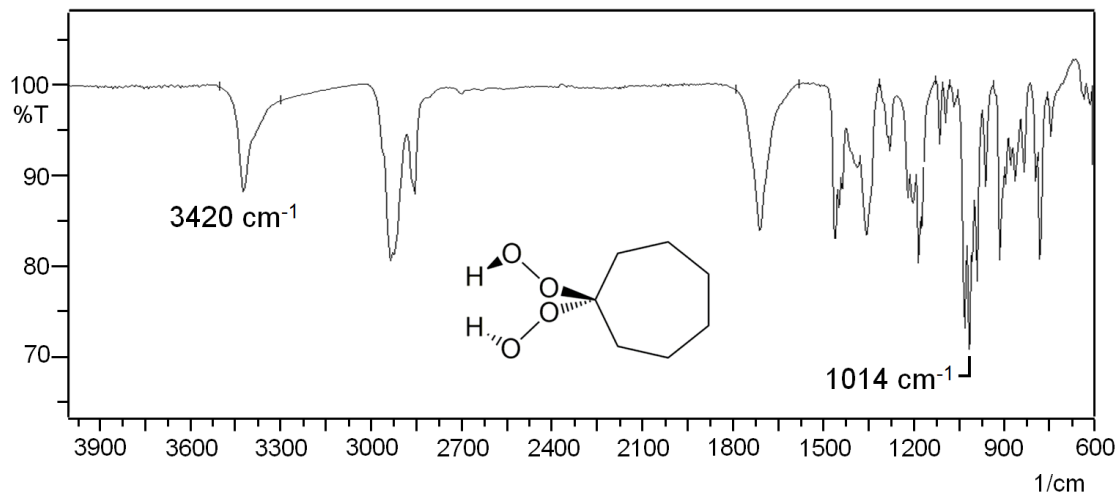


Figure B.14. IR spectrum of 1,1-di(hydroperoxy)heptane.

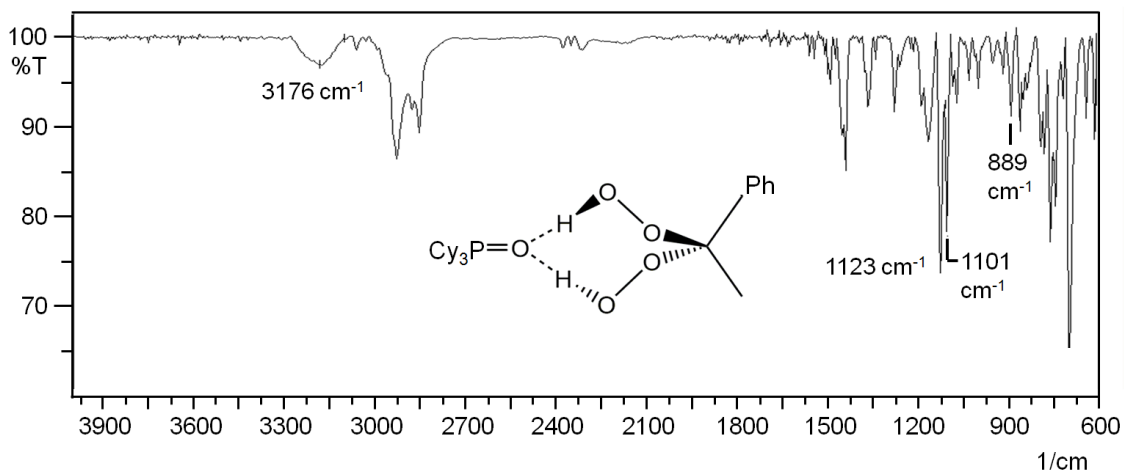


Figure B.15. IR spectrum of **12**.

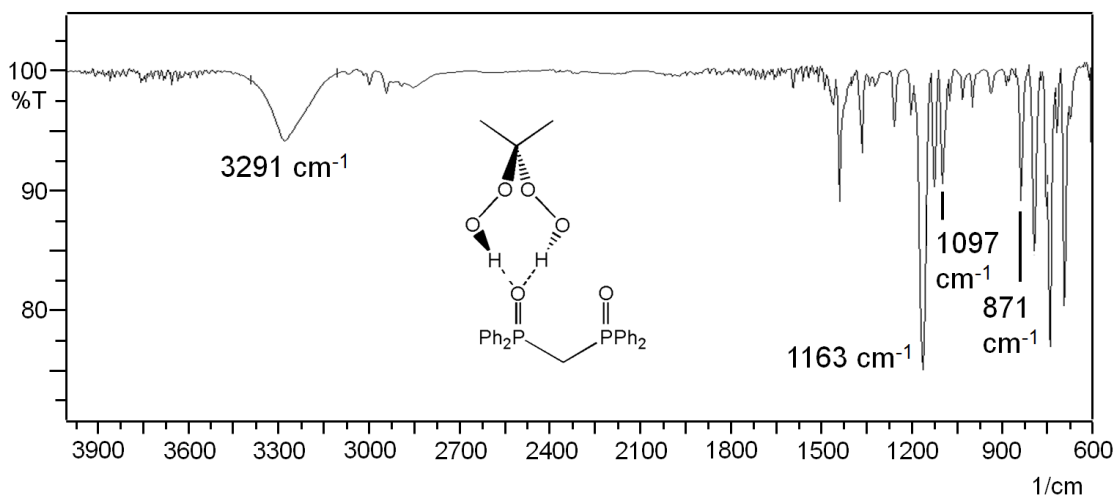


Figure B.16. IR spectrum of **13**.

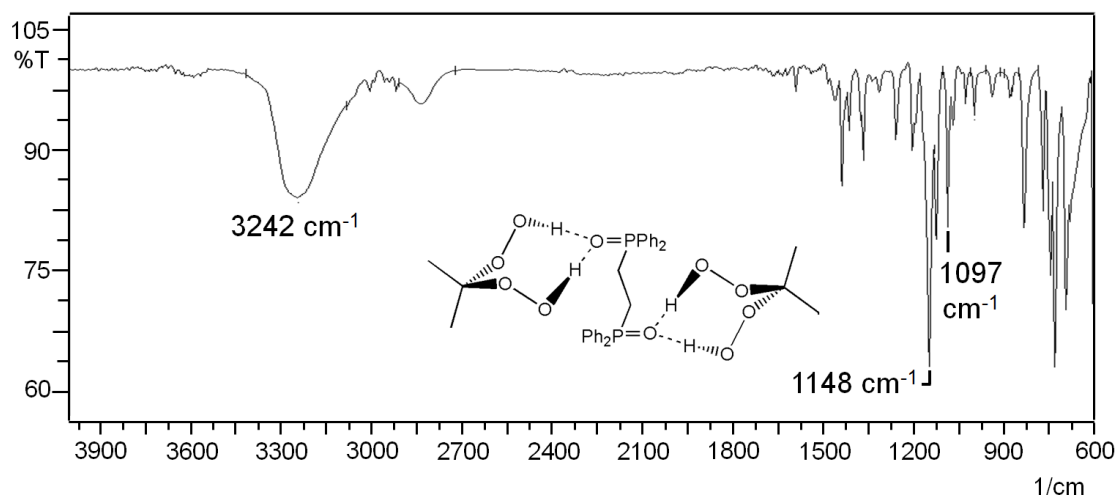


Figure B.17. IR spectrum of **14**.

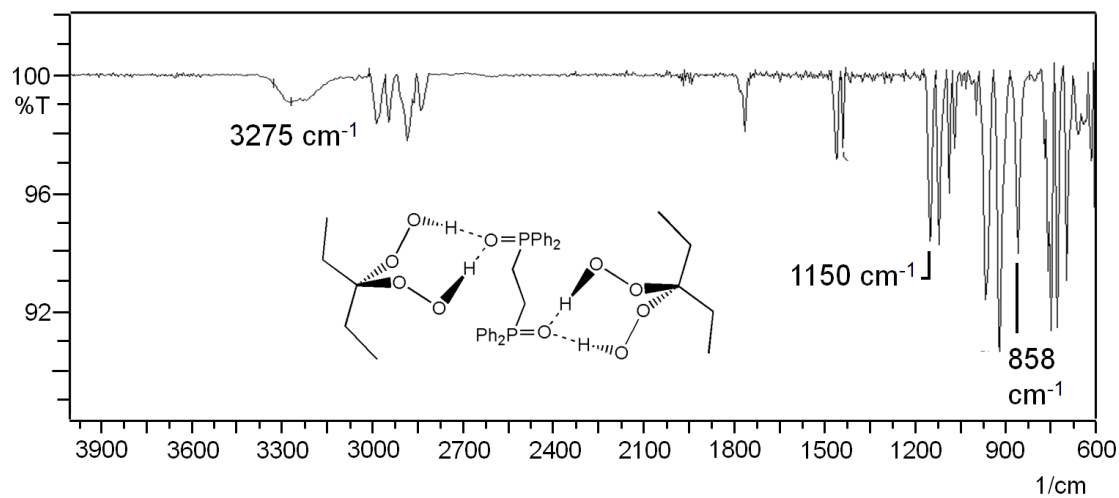


Figure B.18. IR spectrum of **15**.

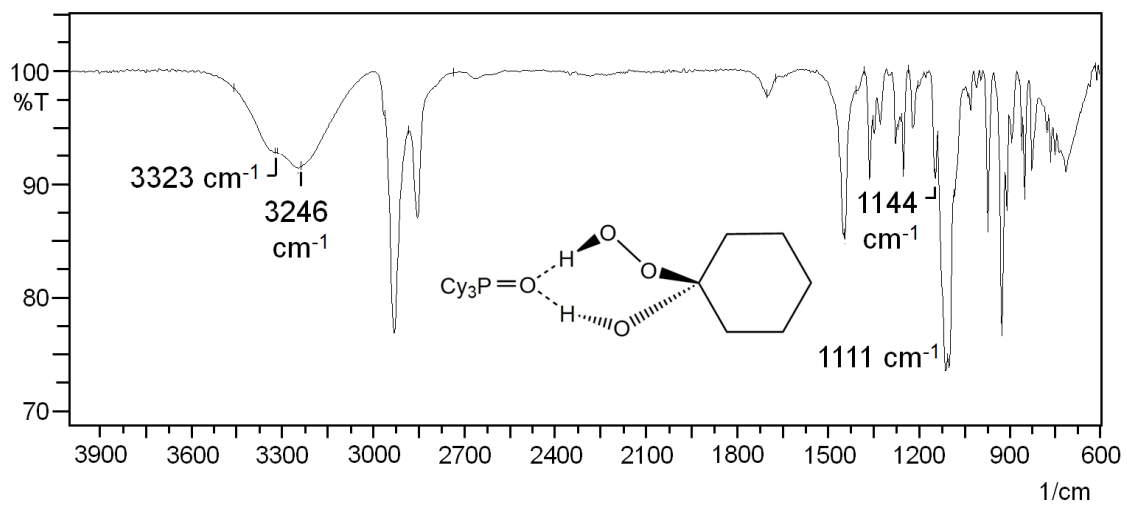


Figure B.19. IR spectrum of 16.

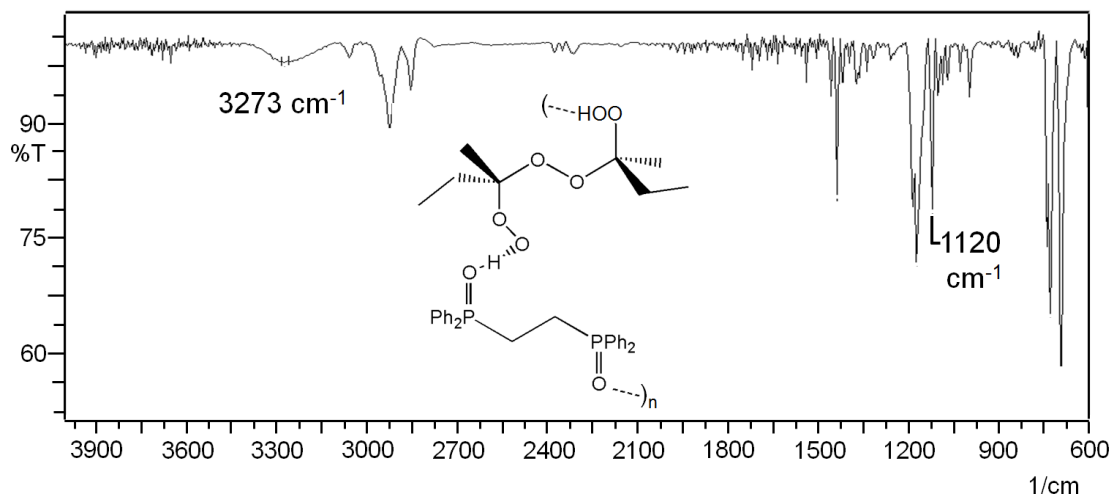


Figure B.20. IR spectrum of 18.

APPENDIX C
DECOMPOSITION DATA

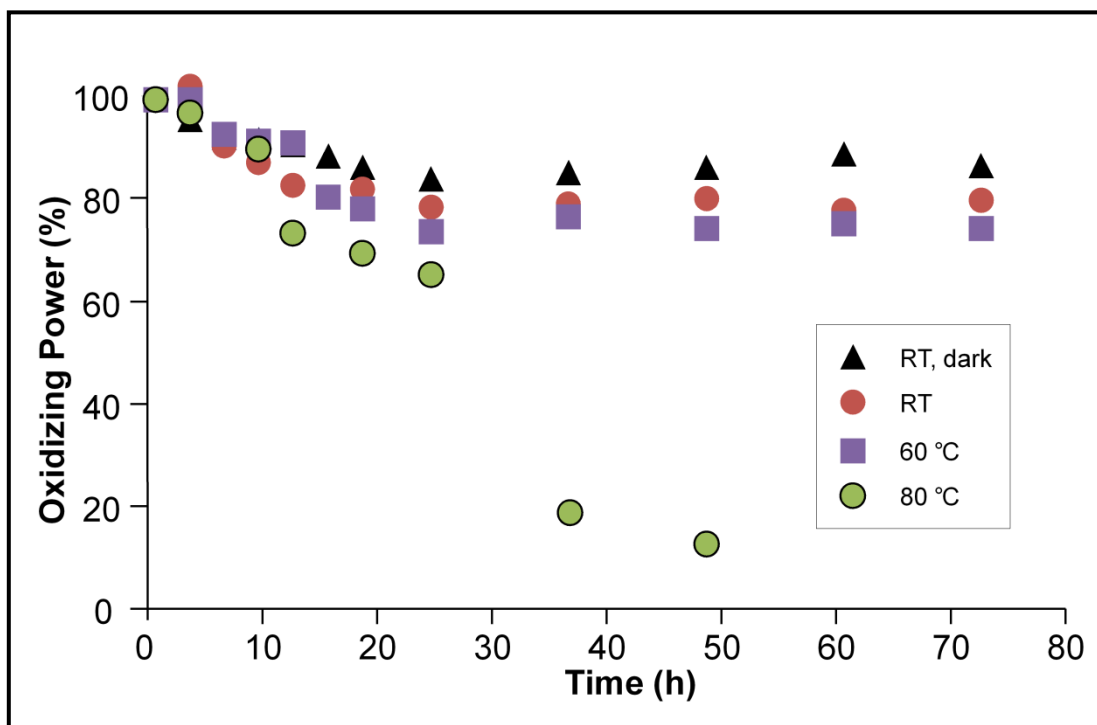


Figure C.1. Oxidizing power of **3** after being stored at the indicated conditions. 100% equals to 2 moles of active oxygen per mole of **3**.

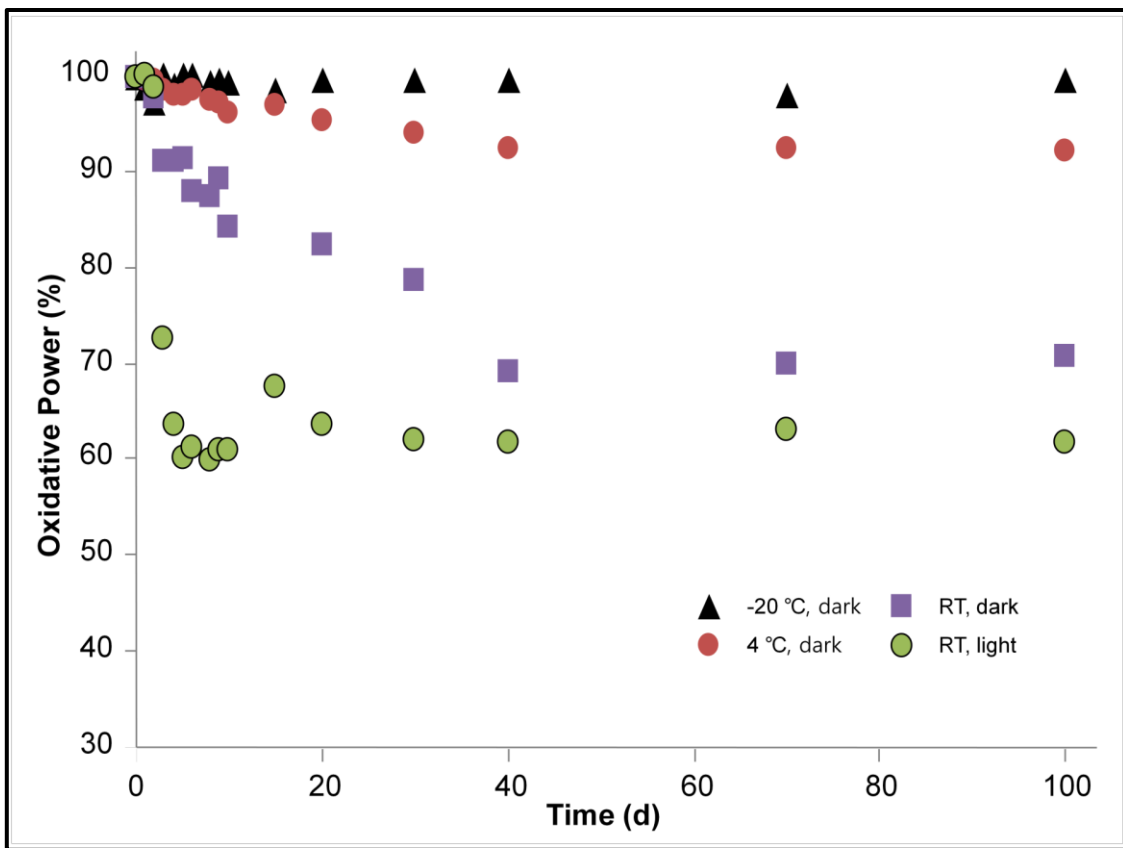


Figure C.2. Oxidizing power of **4** after being stored at the indicated conditions. 100% equals to 2 moles of active oxygen per mole of **4**.

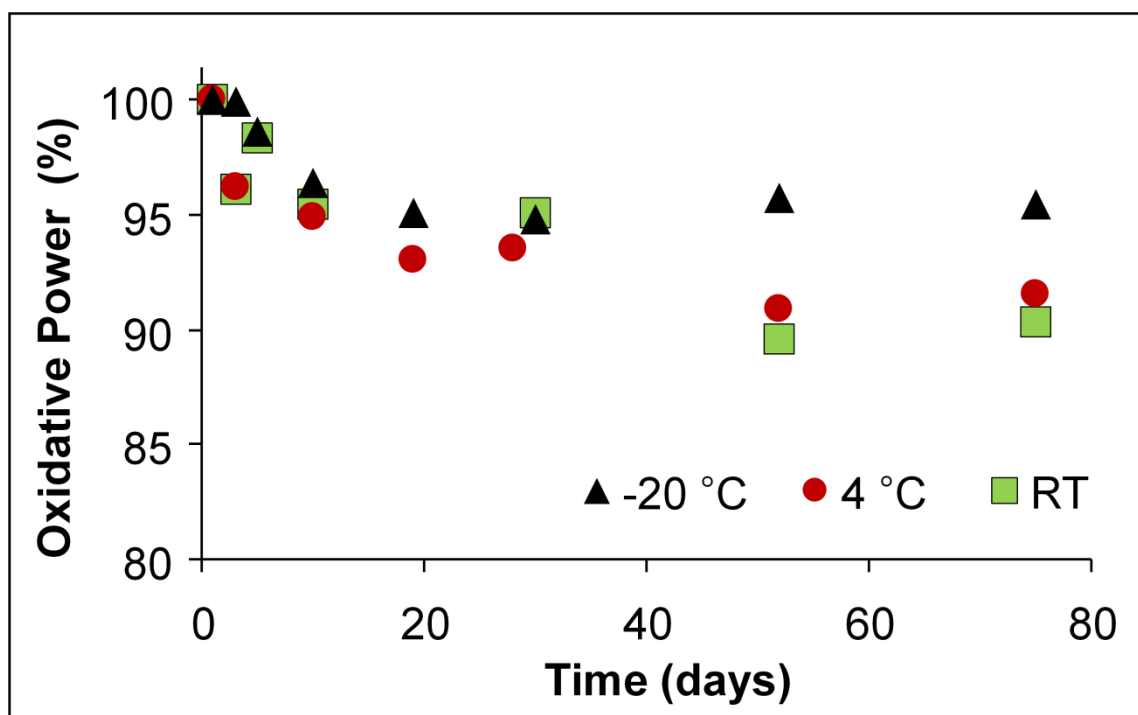


Figure C.3. Oxidizing power of **6** after being stored at the indicated conditions. 100% equals to 2 moles of active oxygen per mole of **6**.

Table C.1. Decomposition temperature of adducts **4-15**.

| Adduct | Decomposition T (°C) | Adduct | Decomposition T (°C) |
|----------|----------------------|-----------|----------------------|
| 4 | 75 | 10 | 121 |
| 5 | 70 | 11 | 138 |
| 6 | 54 | 12 | 100 |
| 7 | 108 | 13 | 120 |
| 8 | 138 | 14 | 105 |
| 9 | 152 | 15 | 110 |